CR 114363

ADVANCEMENT OF PROPROTOR TECHNOLOGY

TASK II - WIND-TUNNEL TEST RESULTS (NASA CONTRACT NAS 2-5386)

REPORT 300-099-004

BELL HELICOPTER COMPANY

A Textron

TABLE OF CONTENTS

TABLE OF CONTENTS - Continued

TABLE OF CONTENTS - Continued

ILLUSTRATIONS

ILLUSTRATIONS - Continued

ILLUSTRATIONS - Continued

ILLUSTRATIONS - Continued

ILLUSTRATIONS - Continued

ILLUSTRATIONS - Continued

ILLUSTRATIONS - Continued

I. SUMMARY

An advanced-design 25-foot-diameter flightworthy proprotor was tested in the NASA-Ames Large-Scale Wind Tunnel under NASA Contract NAS2-5386. Bell Helicopter Company designed and manufactured the proprotor and loaned it to the government for the tests. These tests, Task II of the Advancement of Proprotor Technology Program, have verified and confirmed the theory and design solutions developed as part of the Army Composite Aircraft Program. This report presents the test results and compares them with theoretical predictions. (Reference 1 reports the results of Task I, the design study.)

Figure I-1 shows the proprotor installed in the tunnel in preparation for the July 1970 dynamic tests. This testing (which reached a simulated speed of 408 knots) showed that stability increased with airspeed. The measured damping of the major coupled modes was as predicted from theory and from the results of one-fifth-scale model tests.

During performance tests (Figures I-2 and I-3), conducted in November 1970, the results met or exceeded predictions. Hover thrust 15 percent greater than the predicted maximum was measured. In airplane mode, propulsive efficiencies (some of which exceeded 90 percent) agreed with Theory.

Structurally, the proprotor behaved much as predicted. Blade loads were acceptable in all flight modes, although they exceeded the initially predicted values at intermediate conversion angles. After the tests, however, computational input errors were found in the predicted values. The elimination of these errors put the theoretical (predicted) loads slightly higher than those measured. Blade loads in the airplane flight mode were very low.

These tests took the flightworthy test article through many of the conditions it would encounter in actual flight operations, and found it operationally and structurally satisfactory in all of them. The proprotor is therefore ready for the next logical step in the development of tilt-proprotor technology--flight testing on a research aircraft.

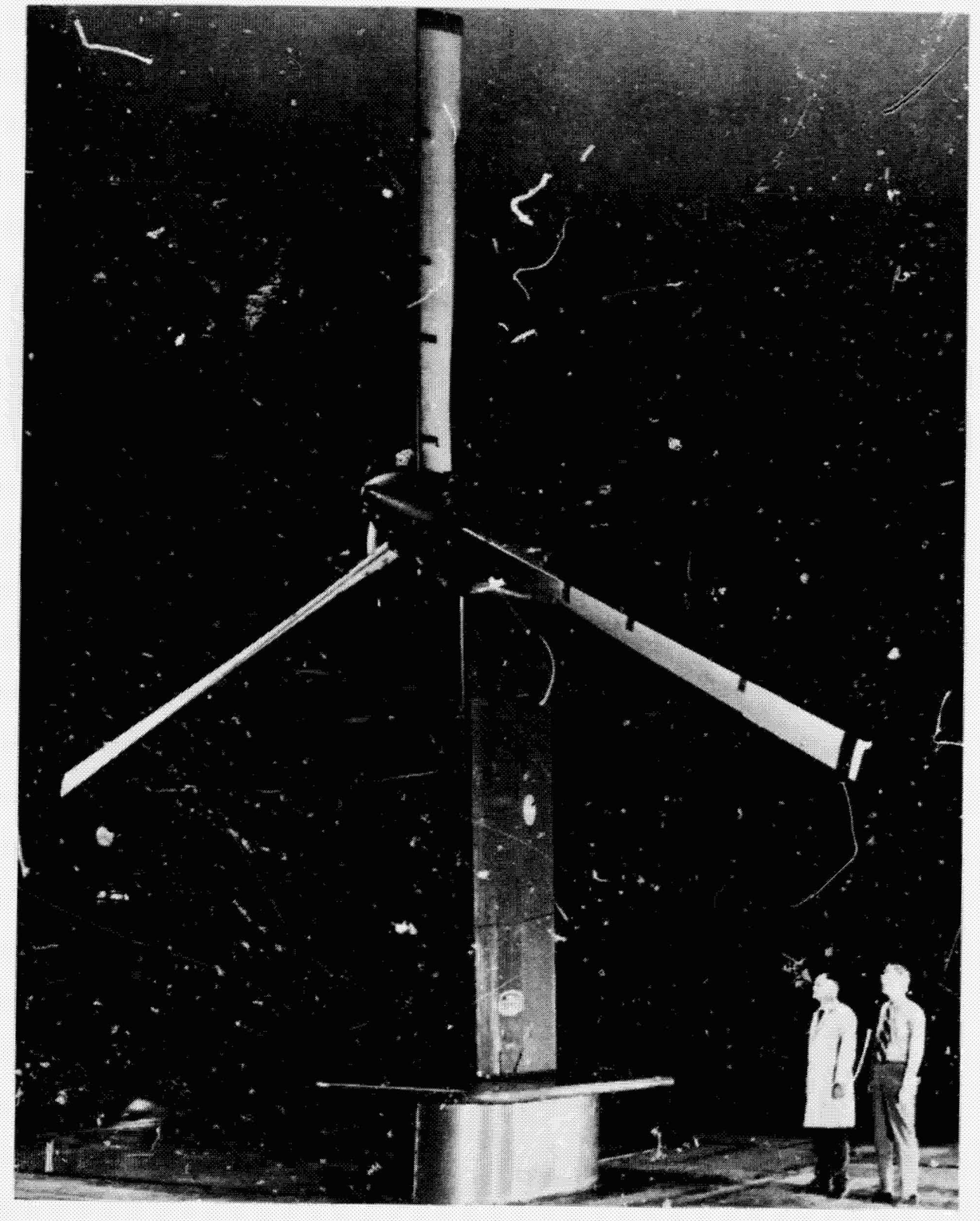

Figure I-1. Proprotor Dynamic Test in NASA-Ames Large-Scale Tunnel.

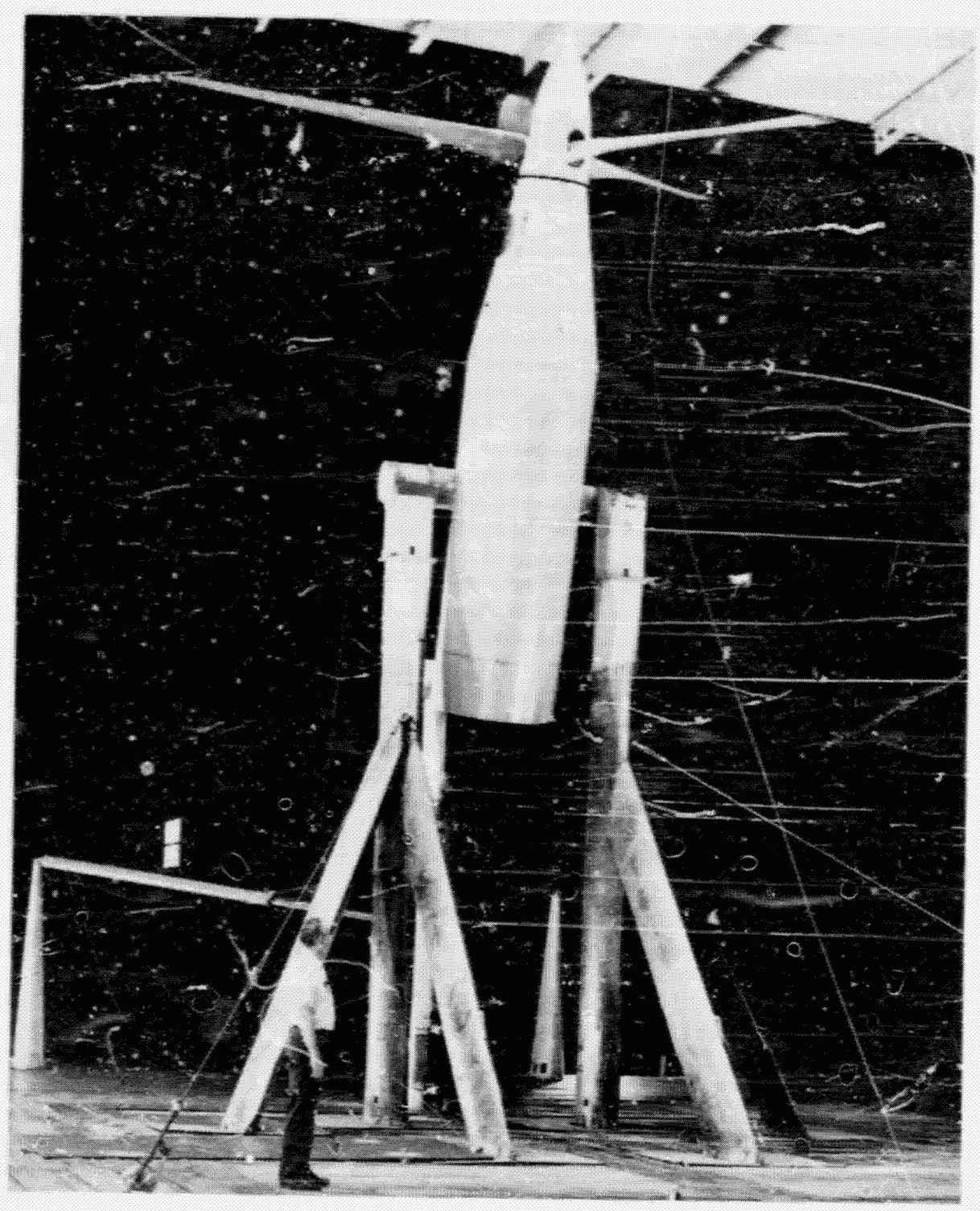

Figure I-2. Proprotor Performance Test in NASA-Ames Large-Scale Tunnel, Helicopter Mode

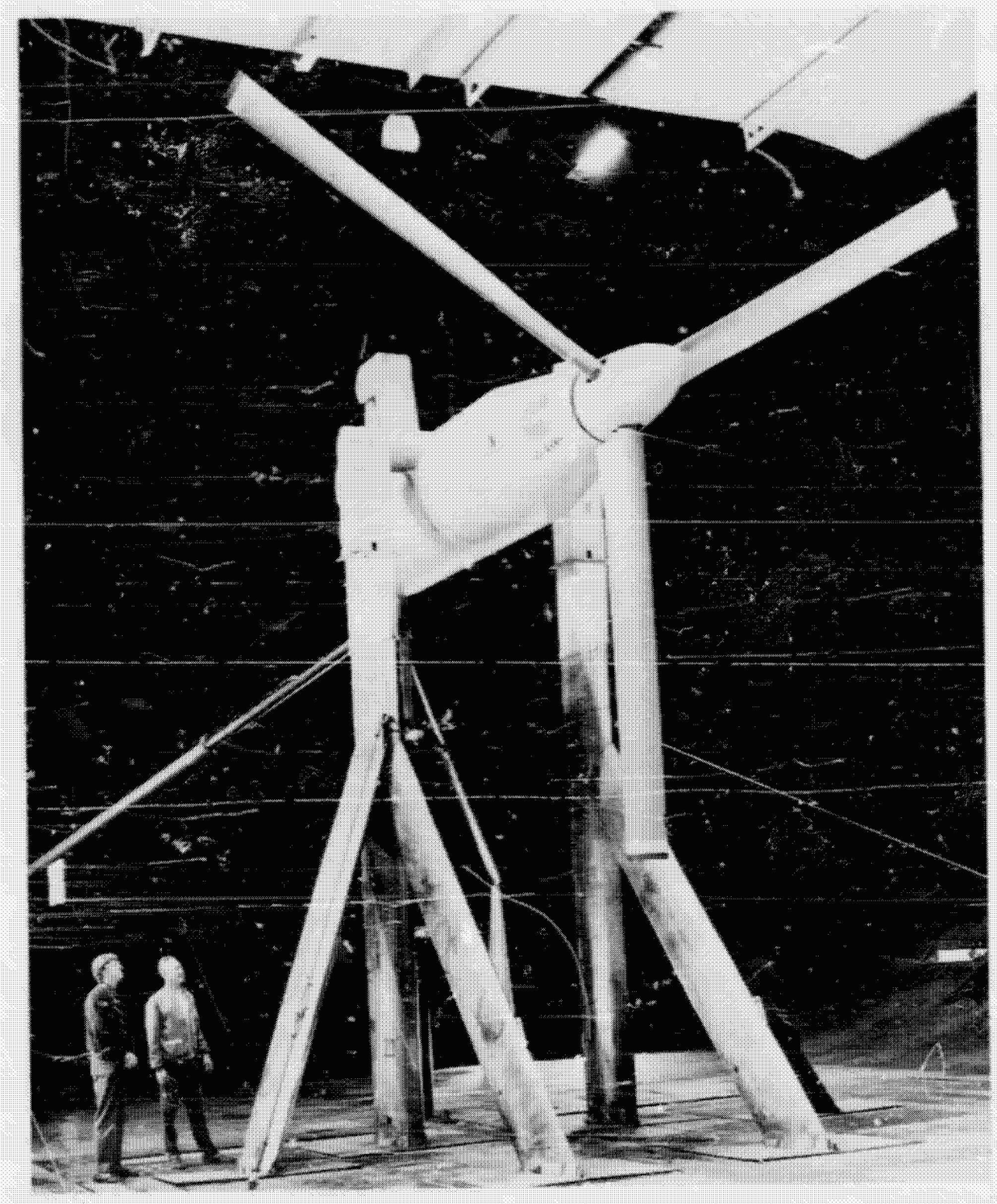

Figure I-3. Proprotor Performance Test in NASA-Ames Large-Scale Tunnel, Airplane Mode.

II. INTRODUCTION

Military and civil planners are becoming aware of the need for VTOL aircraft in a variety of missions and roles. The VTOL concept which appears to offer the greatest promise of filling this need is the tilt-rotor aircraft. It has a high hover payload and causes minimum noise and downwash. It saves weight and complexity by using the same powerplant for both hover and forward flight.

The rotor system, similar to that of the helicopter, gives the pilot the same precise control in the hover and at low flight speeds that a pure helicopter would give him; yet in high-speed flight, this same rotor functions efficiently as a propeller, giving the aircraft the range and endurance of a fixed-wing aircraft. The side-by-side arrangement of the proprotors gives the lift system a large overall span, which in turn gives it exceptionally good STOL characteristics.

Many of the desirable characteristics of the aircraft derive from the low disc loading of the tilt-rotor system. Indeed, studies have shown that low-disc-loading VTOL aircraft, the tilt-rotor in particular, will make the most economical mid-range VTOL transports for either civil or military applications. (Studies by Bell, Westland, Lockheed, Sikorsky, Boeing, and the Marine Corps have supported this prediction. See References 2 through 10.) The low disc loading also minimizes noise and dust; the low downwash velocities contribute to the safety of ground personnel.

The simple conversion process makes the aircraft easy to fly. Conversion may be started, stopped, or reversed at any point, with power on or off. The rotor-lifted speed range overlaps the wing-lifted speed range; therefore the conversion corridor is wide, and airspeed and power need not be programmed with conversion angle. In case of complete power failure, the aircraft converts to helicopter flight and makes an autorotational descent to a helicopter-like flare and low-velocity landing.

The tilt-rotor concept has been under development for two decades. Early work led to the establishment of the joint Army-Air Force XV-3 Convertiplane Program in 1951 (Figure II-1). The evaluation tests were completed in 1961 and reported in References 11 through 13. The program included more than 375 hours of wind-tunnel and ground-run time, and more than 250 test flights in 125 hours of flight time. The test aircraft was flown by ten government test pilots and two Bell pilots, who made a total of more than 110 full conversions. Five of the government test pilots made power-off reconversions from cruise to helicopter autorotation after simulated engine failure. The flight evaluation demonstrated the soundness and safety of the conversion principle and showed that a proprotor could be used equally well for lift and propulsion. It also defined dynamic stability

problems that required further study, problems involving dynamic stability of the proprotors and coupling effects between the proprotors and the aircraft. At that time these phenomena were little understood and there was no theory for predicting them with any degree of accuracy.

Specifically, the problems were high proprotor flapping during airplane maneuvers, proprotor/pylon stability (later found to be closely related to propeller-nacelle whirl flutter), and aircraft dutch roll and short-period longitudinal stability. In the early 1960's Bell Helicopter Company initiated an extensive theory and model research program to resolve these problems and to develop technology for the design of future aircraft. The program yielded a fundamental understanding of proprotor/pylon phenomena and explained the behavior of the XV-3 in flight and in the wind tunnel (Reference 14).

The proprotor/pylon stability behavior of the XV-3 in the 1962 tunnel test was first simulated with a simple model. As theory was further refined and more effects and degrees of freedom were added to the equations, wind-tunnel testing went on to evaluate blade flexibility, airframe aeroelastic modes, and airplane flight degrees of freedom (References 15 and 16). Some of the models used in the dynamic model test program are shown in Figure II-2. Several different design approaches for dynamic stability evolved and were studied in detail. These included positive pitch flap coupling (negative δ_3), high wing stiffness, swashplate/pylon coupling, a focused rotor, and automatic flapping control.

In 1965 the Army established the Composite Aircraft Program to combine in one aircraft the good hover characteristics of the helicopter and the efficient high-speed cruise characteristics of the fixed-wing aircraft. The XV-3 experience and subsequent theory and model work provided a foundation for design effort in that program. The Bell Model 266 aircraft design shown in Figure II-3 resulted from this work. (This work is documented and reviewed in References 17 through 22).

The exploratory definition phase of the Composite Aircraft Program was completed in 1967. The research aircraft program which was planned to follow would have established that the level of technology was adequate for an aircraft system. This program was not begun, however, primarily because of a lack of R&D funding and the absence of a well-defined mission requirement. Recognizing the need for large-scale verification of the technology that had developed from the time of the XV-3, Bell authorized as part of its IR&D program the design and fabrication of a 25-foot-diameter rotor and drive system components suitable for testing in the NASA-Ames Large-Scale Wind Tunnel. This was in 1968.

In 1969 the NASA-Ames Research Center and the Army Aeronautical Laboratory contracted with Bell (Reference 23) for tunnel tests

of the 25-foot rotor and for design studies of a tilt-rotor proof-of-concept aircraft. The Bell Model 300 aircraft design shown in Figure II-4 resulted from the design study (Reference 1).

The 25-foot-diameter proprotor completed its first tunnel test in July 1970 (Figure I-1). The dynamic investigations showed that the system was stable to the maximum tunnel speed of 202 knots with a full stiffness wing structure. Flight was simulated to 408 knots with a one-fourth-stiffness wing structure. Damping of all modes was good and trends were predicted accurately by theory. Control and structural investigations showed low blade, hub, and control stresses. Investigations with an automatic flapping control device were in agreement with theory.

The most recent tests of the 25-foot proprotor took place in the Ames 40- by 80-foot tunnel in November 1970 (Figures I-2 and I-3). During these tests, the rotor was power driven in the helicopter mode, in the airplane mode, and over a range of conversion angles between these modes. Test results correlated well with predictions as is summarized in Reference 24 and shown in detail in the following sections of this report. The dynamic stability of the rotor was excellent in all modes, and blade loads were acceptable. The results of the tests show that the 25-foot-diameter proprotor is ready for testing on a complete aircraft.

Figure II-1. XV-3 Convertiplane.

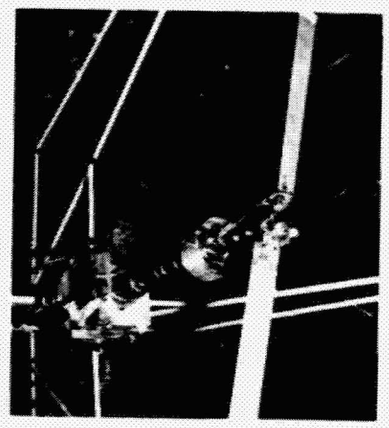

XV-3 on Isotropic Pylon

Blade, Pylon, and Wing Flexibilities

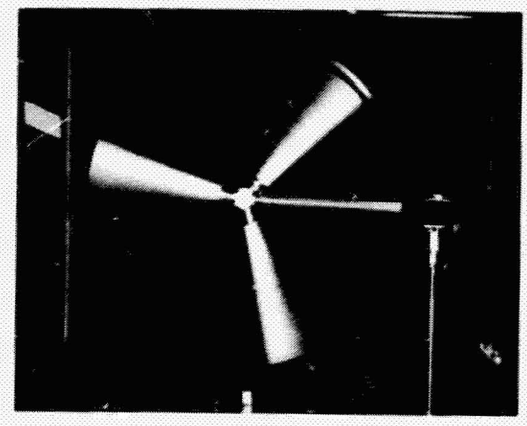

Aeroelastic Proprotor and Wing

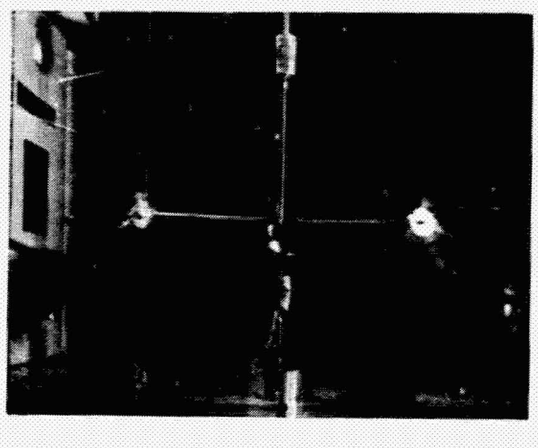

Semi-Freeflight Aerodynamic Model

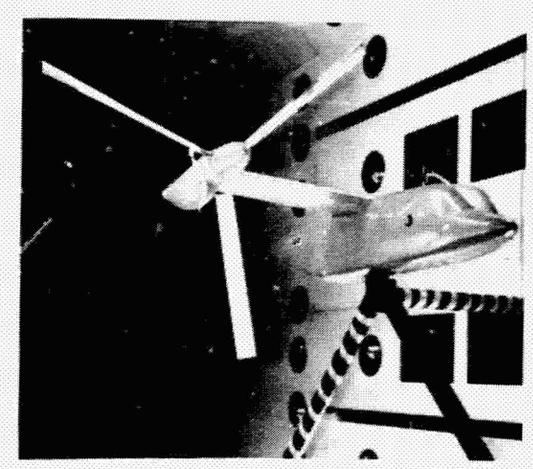

Model 266 Aeroelastic Test in NASA-Langley Dynamics Tunnel

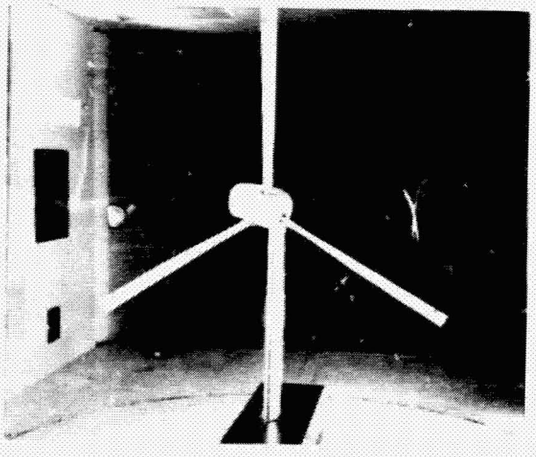

Model 300 Semispan One-Fifth Scale Aeroelastic Model

Figure II-2. Dynamic Model Testing.

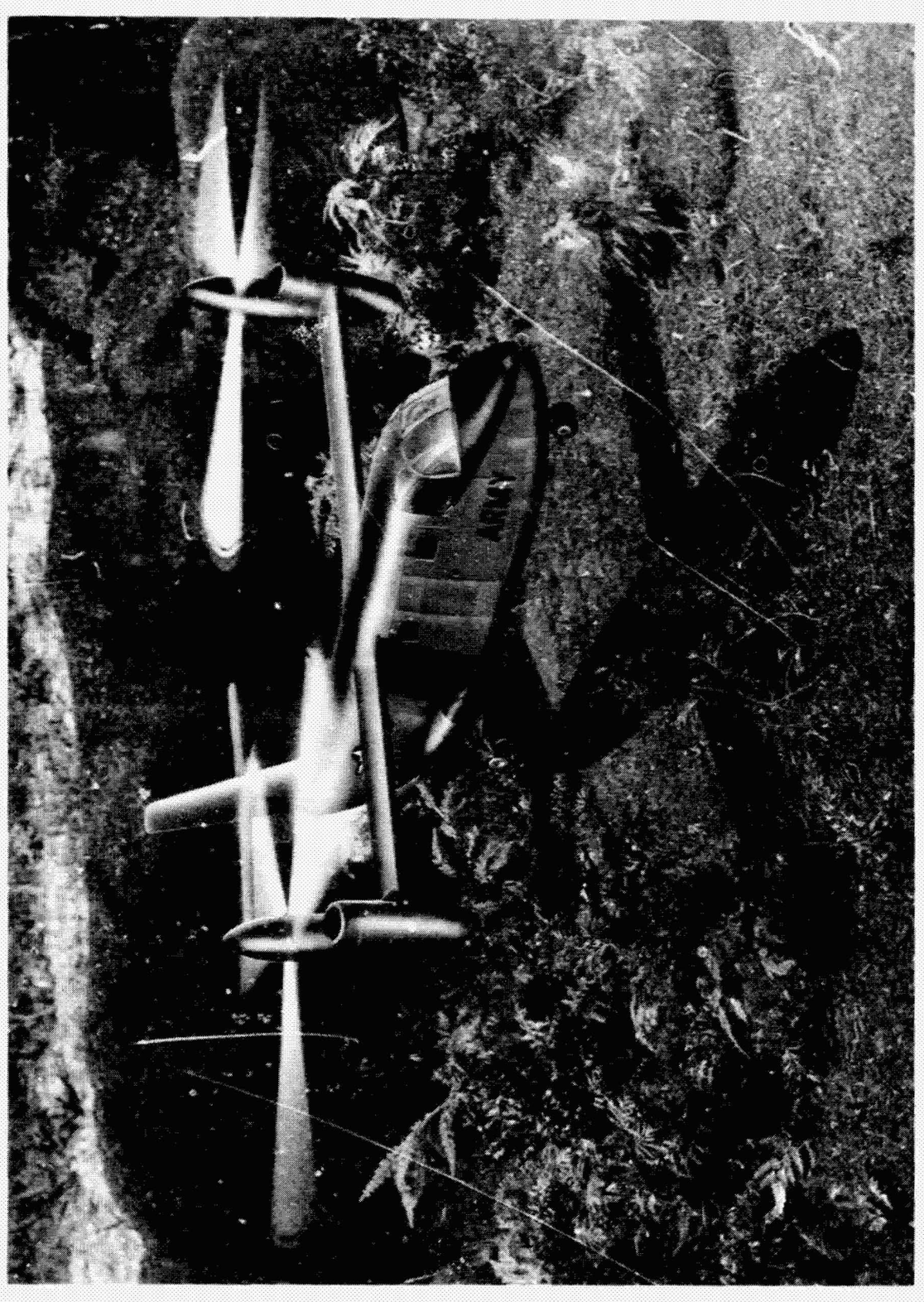

Figure II-3. Bell Model 266 Army Composite Research Aircraft.

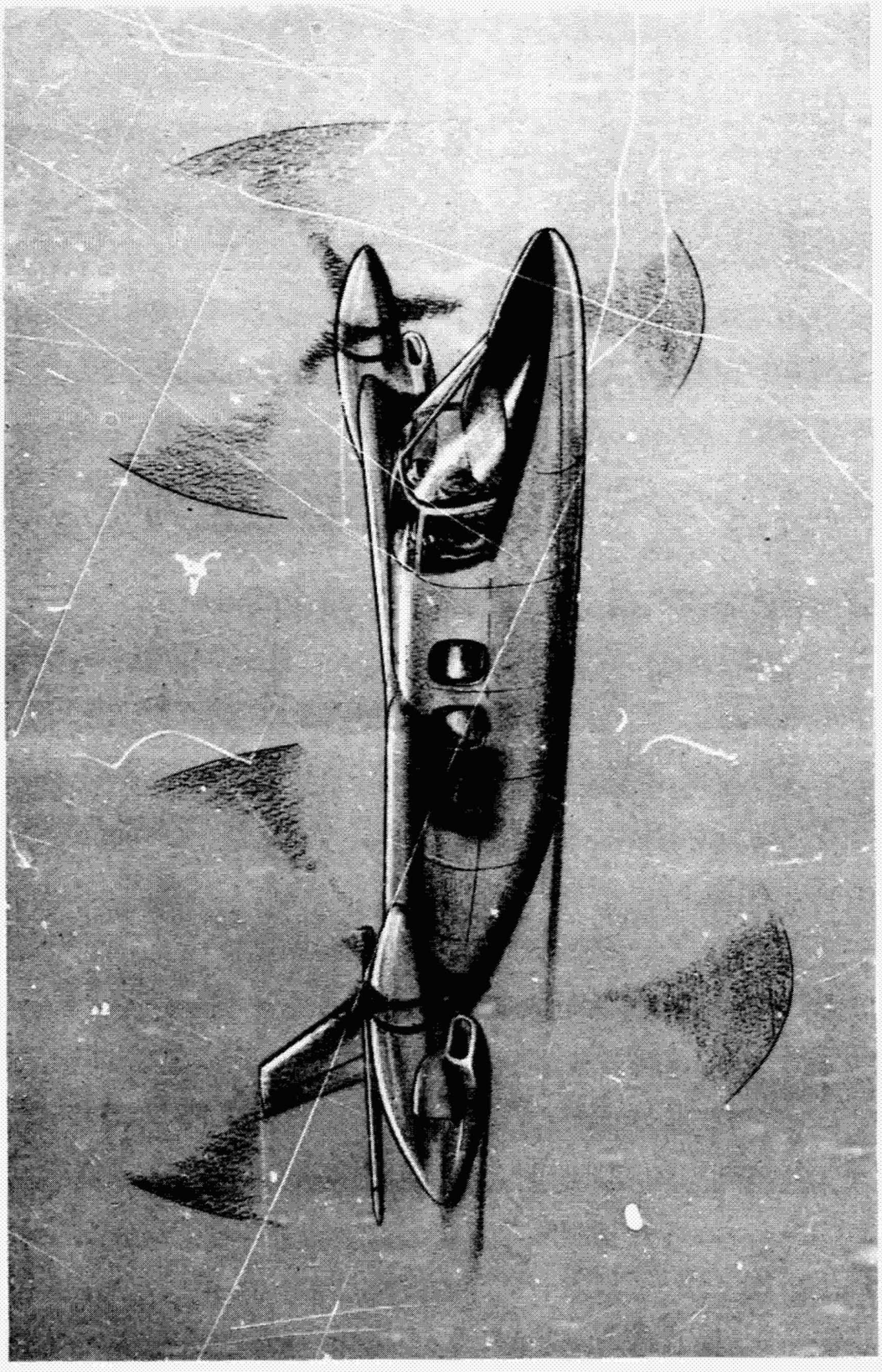

Figure II-4. Bell Model 300 Tilt-Rotor Aircraft.

III. DESCRIPTION OF TEST HARDWARE

A. PROPROTOR AND CONTROLS

1. Description

The 25-foot three-bladed proprotor used for these tests is semi-rigid, with the hub gimbal mounted to the mast to provide blade flapping freedom. The all-bonded blades are made with high-strength, heat-treated stainless steel. Blade pitch motion and retention are provided by needle bearings and wire straps. Stainless steel liners, bonded to the titanium yoke, prevent fretting. The stiff titanium yoke places all blade bending frequencies above rotor speed as is discussed in Subsection III.A.2 of this report.

The geometry of the blades was developed with the help of two-dimensional tests in subsonic and transonic wind tunnels. The blades have an NACA 64-208 airfoil at the tip and a highly cambered, 27-percent thick section at the root. A combination of twist and camber was chosen to meet the aerodynamic requirements for both helicopter and airplane flight, and to permit the blade spar structure to have a uniform twist rate. The integral blade and grip eliminate the need for an aerodynamic cuff at the root of the blade, thereby saving weight and minimizing performance losses.

An elastomeric hub spring is utilized to increase the control and damping moment capability of the proprotor. The hub spring is located in the nonrotating system to eliminate fatigue loading on this component. The spring is attached directly to the top case of the transmission and to the hub yoke through a bearing.

Cyclic control is achieved through a monocyclic (fore and aft) swashplate below the proprotor. A rise-and-fall collective head assembly above the proprotor moves three walking beams thereby providing collective control. Hydraulic actuators position the cyclic and collective controls. The servo valves of the 1500 psi hydraulic actuators were positioned by a 28-volt electro-mechanical actuator to provide remote control for these tests. In the event of hydraulic pressure loss, the electric actuator provided a mechanical back-up to carry the control loads until the tunnel could be shut down.

Table III-I provides a summary of the pertinent data concerning the proprotors. Both aerodynamic and dynamic data are included. Bell drawings 300-960-002, 300-010-001, and 300-010-100 included in the appendix show some of the construction details of the proprotor. Reference 1 provides a complete description of the proprotor including mass and stiffness distributions.

TABLE III-I. PROPROTOR DESCRIPTIVE DATA

Number of Blades per Proprotor	3
Diameter	25.0 ft
Disc Area per Proprotor	491 sq ft
Blade Chord	14 in basic blade 17 in cuff root at 0.0875R Tapering to 14 in at 0.25R
Blade Area (3 Blades)	43.75 sq ft
Solidity	0.089
Blade Airfoil Section	
Root ($\mathcal{C}_L$ Mast)	NACA 64-935 a = 0.3
Tip	NACA 64-208 a = 0.3
Blade Twist (See Figure IV-1 for Distribution)	-45.0 deg
Hub Precone Angle	+2.5 deg
δ_3	-15.0 deg
Underslinging	0 deg
Mast Moment Spring Rate (per Rotor)	2700 in lb/deg
Flapping Design Clearance	±12.0 deg
Blade Flapping Inertia (per Blade)	105 Slug ft^2
Blade Lock Number	3.83

	Tip Speed (fps)	(rpm)
Helicopter	740	565
Conversion	700	534
Airplane	600	458

2. Natural Frequencies

Prior to the wind-tunnel tests the proprotor natural frequencies were measured in a nonrotating vibration survey and their locations confirmed during a whirl test at the contractor facility.

Figures III-1 and III-2 compare the measured nonrotating frequencies with the calculated frequencies. In BHC terminology the collective modes are the symmetric modes of the proprotor, i.e., polar symmetric about the mast. The cyclic modes are the asymmetric modes. For the vibration survey, the proprotor was mounted on a test fixture which was effectively rigid in the direction normal to the plane of the rotor, but which had an inplane mode close to the first cyclic out-of-plane mode. Coupling of the two modes was not included in the calculation but is evident in the measured frequencies.

The first torsional mode of the blade was measured at 80 cps as shown in Figure III-1. The vibration survey test stand provided an extremely stiff torsional restraint, hence this is effectively the torsional natural frequency of a cantilevered blade. The calculated first torsional natural frequency for the cantilevered blade is 87 cps. With the control system flexibility included in the calculations, a mode which is rigid body feathering on the control system is introduced at 36 cps. Coupling with this mode forces the torsion mode up to 122 cps.

When the proprotor was whirl tested on a horizontal test stand, the blade natural frequencies were further established by resonant crossings and harmonic excitation of the swashplate. Figures III-3 and III-4 compare these frequencies' identifications with fan plots based on extrapolation of the frequencies measured during the nonrotating vibration survey. Note that several modes are indicated to be in resonance, namely the third collective mode and the second and third cyclic modes. These resonances were closely monitored during the wind-tunnel tests, but were never a problem.

B. TEST STANDS

1. Performance Stand

a. Description

Performance testing of the Model 300 proprotor was accomplished on the NASA propeller test rig as shown on Figures I-2 and I-3. The power module of this rig consists of two 1500 hp electric motors mounted in tandem on a frame, driving an R-2800 engine reduction gearbox. The power module was mounted at approximately the center of the tunnel test section on struts attached to the tunnel balance frame. Angle of attack could be changed on the module by means of a remotely-actuated tail strut. The angle

range available was from 0 degrees (mast horizontal) to 85 degrees (mast nearly vertical). Bell Drawing 300-018-013, included in the appendix, shows the proprotor mounted on the test rig.

To adapt the Model 300 rotor to the test rig gearbox, a new gearbox front cover was made. A mast support case containing a all thrust bearing and a radial roller bearing was attached to the special front cover. The bearings in the mast case were separated by 13.5 inches to carry moments generated by the rotor. A collective pitch input sleeve was installed between the bearings. This sleeve contained a rotating-to-rotating bearing set, and attached to a collective tube inside the mast. The collective control cylinder, installed below the gearbox, actuated the sleeve through a lever. The upper end of the wind-tunnel mast case was similar to the Model 300 transmission mast case, and had attachment points for the Model 300 swashplate and hub moment spring. An instrumentation slip ring was installed inside the mast case, above the upper bearing.

The mast used during the wind-tunnel tests was identical to that of the Model 300 above the mast case. Inside the mast case, the wind-tunnel mast was slotted to permit operation of the collective sleeve. The mast wall thickness in the area of the slots was increased over that of the Model 300 in order to maintain the mast strength. The lower end of the mast had a drive spline to which a modified R-2800 planetary gear carrier attached. The carrier contained standard R-2800 planetary gears.

The Model 300 proprotor and rotating controls attached to the wind-tunnel mast and mast case without modification. The Model 300 spinner faired the forward portion of the rig; nonstructural fairings, attached to the tunnel floor, faired the remainder of the rig.

b. Natural Frequencies

A vibration analysis of the propeller test stand, with the 25-foot proprotor installed, was made prior to the powered test. The test stand structure was modeled on the NASTRAN structural analysis (Reference 25) and the natural frequencies through eight per rev calculated. Figure III-5 shows the NASTRAN structural model.

A vibration survey of the propeller test stand was conducted with the stand installed in the test section. For the survey the proprotor blades were removed and replaced by equivalent weights. A Lazan eccentric mass vibrator was installed in a blade grip to provide excitation. Surveys were made at nacelle angles of 0 and 60 degrees. The influence of nacelle angle was very small.

The measured stand natural frequencies are compared to the calculated frequencies in Table III-II. While the frequency correlation is reasonable, neglecting the flexibility of the stand torquemeter in the math model caused a considerable error in the

TABLE III-II. PROPELLER TEST STAND NATURAL FREQUENCIES

α_{MAST} = 0 DEGREES

Mode No.	Measured (cps)	Calculated (cps)	Identification
1	1.8	1.66	Strut first lateral bending
2	3.8	2.52	Nacelle yaw
3	3.5	2.73	Strut fore and aft bending
4	5.2[1]	10.47	Cross tube vertical bending
5	16.9[2]	22.3	Mast lateral bending
6	22.1[2]	26.7	Mast vertical bending
7	--	29.7	Nacelle torsion (rear)
8	34.4	35.3	Nacelle lateral bending
9	--	38.2	Stand Torsion (front)
10	--	42.1	Strut
11	42.0	42.4	Nacelle vertical bending

[1]Cross tube stiffness too high in NASTRAN model

[2]Torque meter softness at interface between stand & mast case not represented in NASTRAN model

frequencies of the mast vertical and lateral bending modes. The location of these modes is very important since they are located in the two-per-rev and three-per-rev excitation frequency range. During this test, two-per-rev loads at 535 rpm proved a limitation and prevented extensive operation at that rpm. However, there was no problem in operating at rotor speeds higher or lower than 535 rpm.

2. Dynamic Test Stands

a. Description

The Model 300 pro rotor was tested for dynamic stability on a structure which simulated the Model 300 semispan wing and nacelle. Bell Drawing 300-018-041, included in the appendix, shows the test assembly. This wing was mounted vertically in the wind tunnel, and attached directly to the tunnel balance. The wing angle of attack could be varied remotely; also, the nacelle could be pitched relative to the wing from 0 to 20 degrees manually. Extensive use was made of the remote angle of attack variation capability during the test, however, all dynamic test-stand runs were made with the nacelle in the airplane mode.

The basic wing structure consisted of a beam of rectangular cross section, and equal in bending and torsional stiffness to the actual Model 300 wing design. A second beam, having one-fourth the stiffnesses of the flight wing, was also provided. The wing "airfoil" was a simple aerodynamic fairing complete with light nonstructural components. The fairings would adapt to either wing beam. All components of the beam and fairings were aluminum.

The test stand parameters--wing chord, span, weight, stiffness, and sweep--were held as close to those of the Model 300 as possible. The airfoil section, however, was simplified to reduce manufacturing cost. Its thickness was 13.5 percent as compared to the Model 300 wing's 23 percent.

The basic structure of the nacelle was a steel weldment which attached to the wing tip by means of a conversion spindle. The bending stiffness of the spindle was the same as the Model 300 conversion spindle. The conversion actuator was replaced by a link. A yaw link was also provided to simulate the pylon-to-wing attachment when the pylon is fully converted so that a downstop is engaged. The mast support case used on the power test rig attached to the front of the weldment. Two aluminum bulkheads, attached to the weldment, supported a fiberglass fairing over the structure. The fairing contour was made to the Model 300 nacelle lines.

The collective control mechanism was the same as was used on the power rig. The cyclic hydraulic cylinder was also used, but was controlled by a small hydraulic actuator (SCAS Unit) equipped with an electrically controlled servo valve. The SCAS cylinder was used for the flapping controller input and as a cyclic control system shaker.

In addition to the cyclic shaker, an aerodynamic shaker was also provided. This shaker consisted of a small airfoil mounted on a shaft, attached near the aft end of the nacelle. The shaker was oscillated by another SCAS hydraulic cylinder.

b. Scaling

The scaling factors of the two design stands are given in Table III-III for reference. Note that data from the design stiffness stand may be used directly. Data from the one-fourth design stiffness test stand must be multiplied by the appropriate factor from Table III-III to obtain the full-scale equivalent value.

c. Test Stand Natural Frequencies

The test stand natural frequencies were calculated prior to the dynamic stability test using a finite element structural model of the stands. Figure III-6 shows the layout of the structural model and the element properties and node point masses are given in Tables III-IV and III-V.

A vibration survey of the design-stiffness test stand was conducted first at the contractor's facility and again when the stand was installed in the test section. A vibration survey of the one-fourth-design-stiffness stand was also conducted in the test section.

During these surveys the proprotor blades were removed and replaced by equivalent weights. A Lazan shaker was used to excite the system natural frequencies. Hand excitation of the fundamental modes was used to obtain modal damping ratios.

During the design stiffness stand vibration survey the tunnel balance natural frequencies were identified. Strain gaged beam transducers mounted at the corners of the balance frame were used to determine the balance mode shapes.

The natural frequencies for the Model 300, the calculated stand natural frequencies, and the measured frequencies are tabulated in Table III-VI. The measured damping is also indicated. Also listed in Table III-VI are the frequencies of the balance modes.

The mode shapes for the four lowest modes of the design-stiffness test stand are shown in Figure III-7. These modes are the same for the one-fourth-stiffness stand with the exception of fourth modes, which is a pylon yawing mode. The balance modes were essentially rigid body and uncoupled.

d. Test Stand Dynamic Stability Boundaries

Figure III-8 shows the calculated dynamic stability boundaries for the test stand as a function of proprotor rpm. These are based on the test stand measured natural frequencies. Two

TABLE III-III. DYNAMIC TEST STAND SCALE FACTORS[1]

Parameter	Design Stiffness[2] Test Stand	One-Fourth Stiffness[3] Test Stand
Length	1.0	1.0
Mass	1.0	1.0
Time	1.0	0.5
Velocity	1.0	2.0
Acceleration	1.0	4.0
Frequency	1.0	2.0
Force	1.0	4.0

[1]Multiply model data by scale factor to obtain equivalent full-scale value

[2]Scaling - Mach No. 1:1
Froude No. 1:1
Lock No. 1:1

[3]Scaling - Mach No. 0.5:1
Froude No. 0.25:1
Lock No. 1:1

TABLE III-IV. DYNAMIC TEST STAND MASS PROPERTIES

	Mass and Inertia*					
Node	M_x	M_y	M_z	$I_{\theta x}$	$I_{\theta y}$	$I_{\theta z}$
2	--	0.43	0.43	0.6	--	--
4	--	0.2	0.2	0.6	--	--
6	--	0.2	0.2	0.6	--	--
8	--	0.2	0.2	0.6	--	--
9	--	0.511	0.511	0.6	--	--
12	0.01	0.01	0.01	0.01	0.01	0.01
13	0.01	0.01	0.01	0.01	0.01	0.01
15	1.087	1.087	1.087	772.0	772.0	--
17	2.13	2.13	2.13	800.0	800.0	208.0
21	1.036	1.036	1.036	--	--	--
22	--	--	--	112.96	112.96	--
27	0.01	0.01	--	--	--	--

*See Figure III-6 for element coordinate system.
All units in lb-in-sec system.
-- Indicates coordinate was not retained.

TABLE III-V. DYNAMIC TEST STAND STIFFNESS PROPERTIES

Segment	Length (in)	EI_{BEAM} (lb-in^2) x 10^{-6}	EI_{CHORD} (lb-in^2) x 10^{-1}	GJ (lb-in^2) x 10^{-6}
1	41.0	9202.9	18794.1	16868.0
2*	21.0	2653.0	10410.0	2696.0
3*	21.0	2653.0	10410.0	2696.0
4*	21.0	2653.0	10410.0	2696.0
5*	21.0	2653.0	10410.0	2696.0
6*	21.0	2653.0	10410.0	2696.0
7*	21.0	2653.0	10410.0	2696.1
8*	18.4	2653.0	10410.0	2696.1
9*	8.7	2653.0	10410.0	2696.1
10*	8.7	2653.0	10410.0	2696.1
11	6.8	1659.0	123.9	340.0
12	6.8	1659.0	123.9	340.0
13	18.4	525.0	525.0	310.0
14	8.2	970.0	970.0	808.0
15	6.8	4000.0	4000.0	4200.0
16	16.8	10908.0	16991.0	10293.0
17	5.6	33292.0	23800.0	15277.0
18	1.7	9136.0	9136.0	7613.0
19	13.7	1100.0	790.0	725.0
20	13.7	600.0	600.0	466.0
21	1.8	341.1	341.1	284.3
22	16.3	140.0	140.0	109.0
23	1.0	0.0	0.0	0.2
24	2.0	3000.0	10000.0	3000.0
25	6.3	3000.0	10000.0	3000.0
26	4.0		AE = 15 x 10^6 lb	
27	12.6		AE = 11.68 x 10^6 lb	
28	6.3	3000.0	10000.0	3000.0
29	2.0	3000.0	10000.0	3000.0
30	7.9	2643.0	10000.0	2696.0

*Multiply EI and GJ x 0.25 for one-fourth design stiffness stand.

TABLE III-VI. 25-FOOT PROPROTOR DYNAMIC TEST STAND AND 40- x 80-FOOT FULL-SCALE WIND TUNNEL MEASURED NATURAL FREQUENCIES AND DAMPING

Mode Description	At BHC	At NASA-Ames Installed in 40- x 80-Foot Wind Tunnel			
	Yaw Link In (cps)	Balance Free Yaw Link In (cps)	Balance Locked Yaw Link In (cps)	Balance Locked Yaw Link Out (cps)	Damping Ratio
Design Stiffness Stand					
Wing Beam	3.35	2.75	2.87	--	0.010
Wing Chord	5.95	5.0	5.22	5.19	0.018
Wing Torsion	10.45	10.3	10.75	10.4	--
Pylon Yaw	36.0	--	32.3	14.1	--
Mast Lateral	25.7	--	22.2	>50.0	--
Wing Second Beam	51.2	--	47.2	47.2	--
1/4 Design Stiffness Stand					
Wing Beam	1.6	--	1.39	1.4	0.008
Wing Chord	2.8	--	2.51	2.46	0.006
Wing Torsion	5.3	--	4.70	4.80	0.032
Pylon Yaw	20.0	--	18.6	12.65	--
Mast Lateral	38.4	--	31.2	31.2	--
Wing Second Beam	24.8	--	16.1	16.4	--
Balance Modes					
Fore -Aft	--	1.6	--	--	--
Lateral	--	1.80	--	--	--
Yaw (Torsion)	--	2.40	--	--	--

boundaries are shown for the one-fourth-design-stiffness stand, one when the scaled one-fourth-design-stiffness hub restraint is used, and one when the design-stiffness restraint is employed. Prior to the test it was planned to switch to a one-fourth-design-stiffness hub restraint when the wing spars were switched. However, while the test was in progress a decision was made to retain the design-stiffness hub restraint for the one-fourth design stiffness stand tests, in order to conserve occupancy time. Calculations indicated the stability characteristics were not significantly affected by the hub restraint and that the time required to change to the one-fourth-design-stiffness restraint would not be justified. The difference in one-fourth stiffness test stand dynamic characteristics with hub restraint is discussed further in Section V.

C. INSTRUMENTATION

Conventional instrumentation was used to measure loads, deflection, vibrations, and pressures during both tests. The transducers included strain gages, potentiometers, accelerometers and pressure sensors. Proprotor rotating system instrumentation channels utilized a 52-ring slip ring to provide 2 excitation power channels and 24 data channels. Table III-VII is a summary of the data channels for the dynamic and the powered tests. There were 27 channels available during the dynamic test and 41 channels available during the powered test. The channel frequency range is shown for reference. System accuracy is estimated to be within ± 3 percent (based on channel full-scale with errors being the square root of the sum of the square of the individual errors).

Data were recorded using direct-write oscillographs, and during the dynamic tests magnetic tape records were also made. Two 18-channel oscillographs were used during the dynamic tests and four of the same type oscillographs were used during the powered tests.

TABLE III-VII. INSTRUMENTATION SUMMARY

Dynamic Stability Test Item	Transducer	Channel Frequency Range (cps)
Mast parallel bending (in red blade flapping sense)	Strain gage	0-60
Yoke beam bending	Strain gage	0-60
Red pitch link axial load	Strain gage	0-135
Red blade spindle chord bending	Strain gage	0-60
Blade beam Sta 52.5 (35 percent R) bending	Strain gage	0-135
Blade beam Sta 75 (50 percent R) bending	Strain gage	0-135
Blade chord Sta 52.5 (35 percent R) bending	Strain gage	0-135
Red blade flapping	Rotating pot	0-135
Fore and aft flapping	Stationary pot	0-190
Lateral flapping	Stationary pot	0-190
Wing beam inboard bending	Strain gage	0-160
Wing chord inboard bending	Strain gage	0-60
Wing torsion inboard bending	Strain gage	0-60
Wing chord outboard bending	Strain gage	0-60
Cyclic tube axial load	Strain gage	0-60
Collective tube axial load	Strain gage	0-60
Conversion link axial load	Strain gage	0-60
Yaw link axial load	Strain gage	0-60
Shaker beam	Strain gage	0-60
Pylon internal static pressure	Pressure	0-60
Inlet total head pressure	Pressure	0-60
Hydraulic pressure	Pressure	0-60
Fore and aft acceleration	Accelerometer	0-60
Pylon Sta 0 beam acceleration	Accelerometer	0-60
Pylon Sta 0 yaw acceleration	Accelerometer	0-60
Pylon Sta 36.0 beam acceleration	Accelerometer	0-60
Pylon Sta 36.0 yaw acceleration	Accelerometer	0-60

TABLE III-VII. CONTINUED

Powered Test Item	Transducer	Channel Frequency Range (cps)
Mast parallel bending (in red blade flapping sense)	Strain gage	0-60
Mast perpendicular bending (normal to red blade flapping sense)	Strain gage	0-60
Red pitch link axial load	Strain gage	0-60
White pitch link axial load	Strain gage	0-60
Green pitch link axial load	Strain gage	0-60
Red blade spindle beam bending	Strain gage	0-60
Red blade spindle chord bending	Strain gage	0-60
White blade spindle beam bending	Strain gage	0-60
White blade spindle chord bending	Strain gage	0-60
Blade beam Sta 22.8 (15 percent R) bending	Strain gage	0-60
Blade beam Sta 75 (50 percent R) bending	Strain gage	0-60
Blade beam Sta 112.5 (75 percent R) bending	Strain gage	0-60
Blade chord Sta 52.5 (35 percent R) bending	Strain gage	0-60
Blade chord Sta 75 (50 percent R) bending	Strain gage	0-60
Blade chord Sta 112.5 (75 percent R) bending	Strain gage	0-60
Blade torsion Sta 112.5 (75 percent R) bending	Strain gage	0-60
Red blade flapping	Rotating pot	0-60
Red blade feathering	Strain gage	0-60
Fore and aft flapping	Stationary pot	0-60
Lateral flapping	Stationary pot	0-60
Red blade trailing edge stress	Strain gage	
Cyclic tube axial load	Strain gage	0-60
Collective tube axial load	Strain gage	0-60
Collective sleeve perpendicular bending	Strain gage	0-60

TABLE III-VII. CONCLUDED

Item	Transducer	Channel Frequency Range (cps)
Collective sleeve parallel bending	Strain gage	0-60
Collective position	Linear pot	0-60
Cyclic position	Linear pot	0-60
Spinner upper support arm bending	Strain gage	0-60
Spinner lower support arm bending	Strain gage	0-60
Driver load	Strain gage	0-60
Mast torque	Strain gage	0-60
Test stand internal static pressure	Pressure	0-60
Hydraulic pressure	Pressure	0-60
Tunnel airspeed	Pressure	0-60
Mast case axial acceleration	Accelerometer	0-60
Mast case beam acceleration	Accelerometer	0-60
Mast case yaw acceleration	Accelerometer	0-60
Test stand aft vertical acceleration	Accelerometer	0-135
Test stand aft lateral acceleration	Accelerometer	0-135
Test stand forward vertical acceleration	Accelerometer	0-60
Test stand forward lateral accelerometer	Accelerometer	0-60

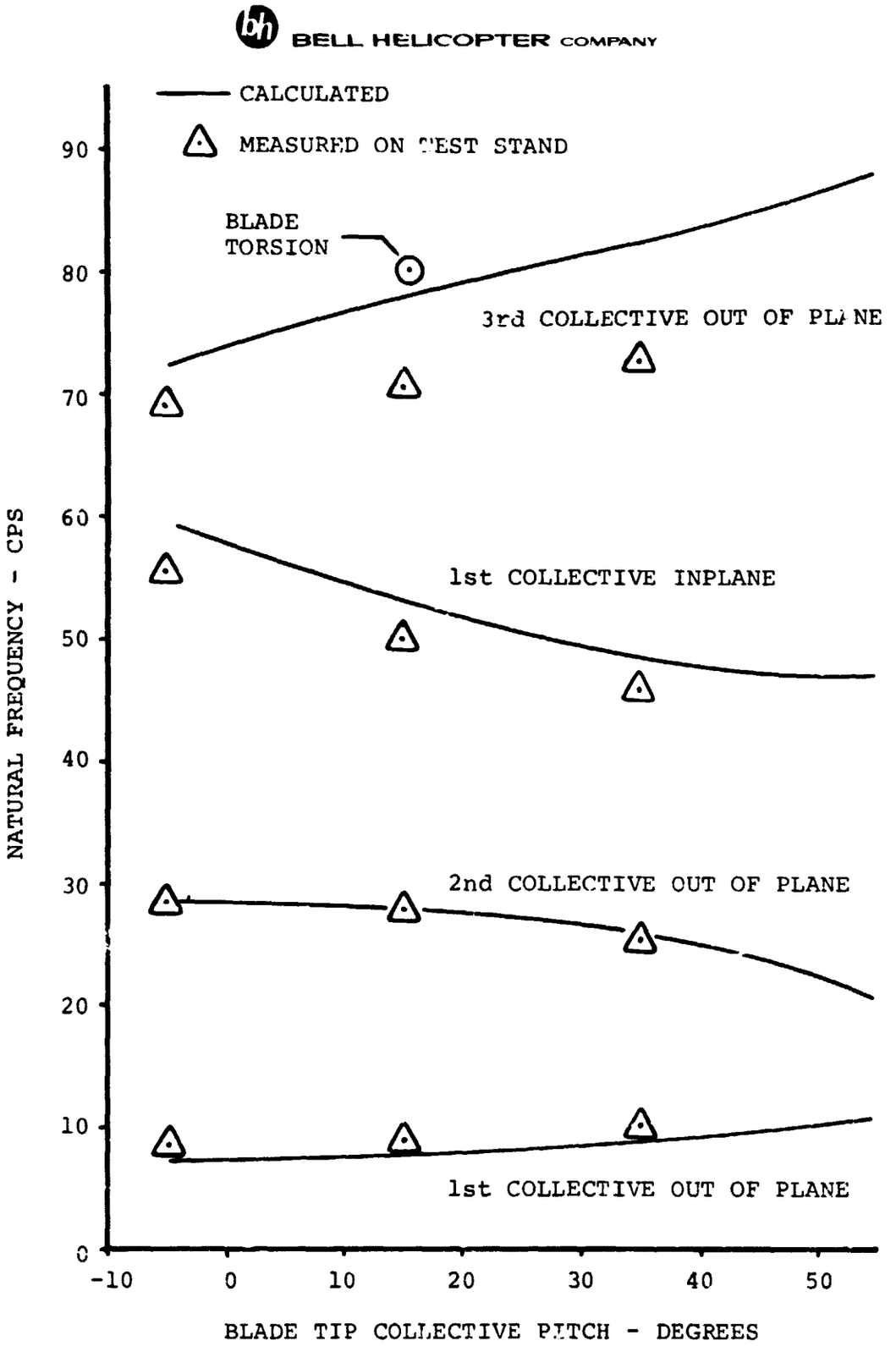

Figure III-1. Proprotor Collective Mode Natural Frequencies, Nonrotating.

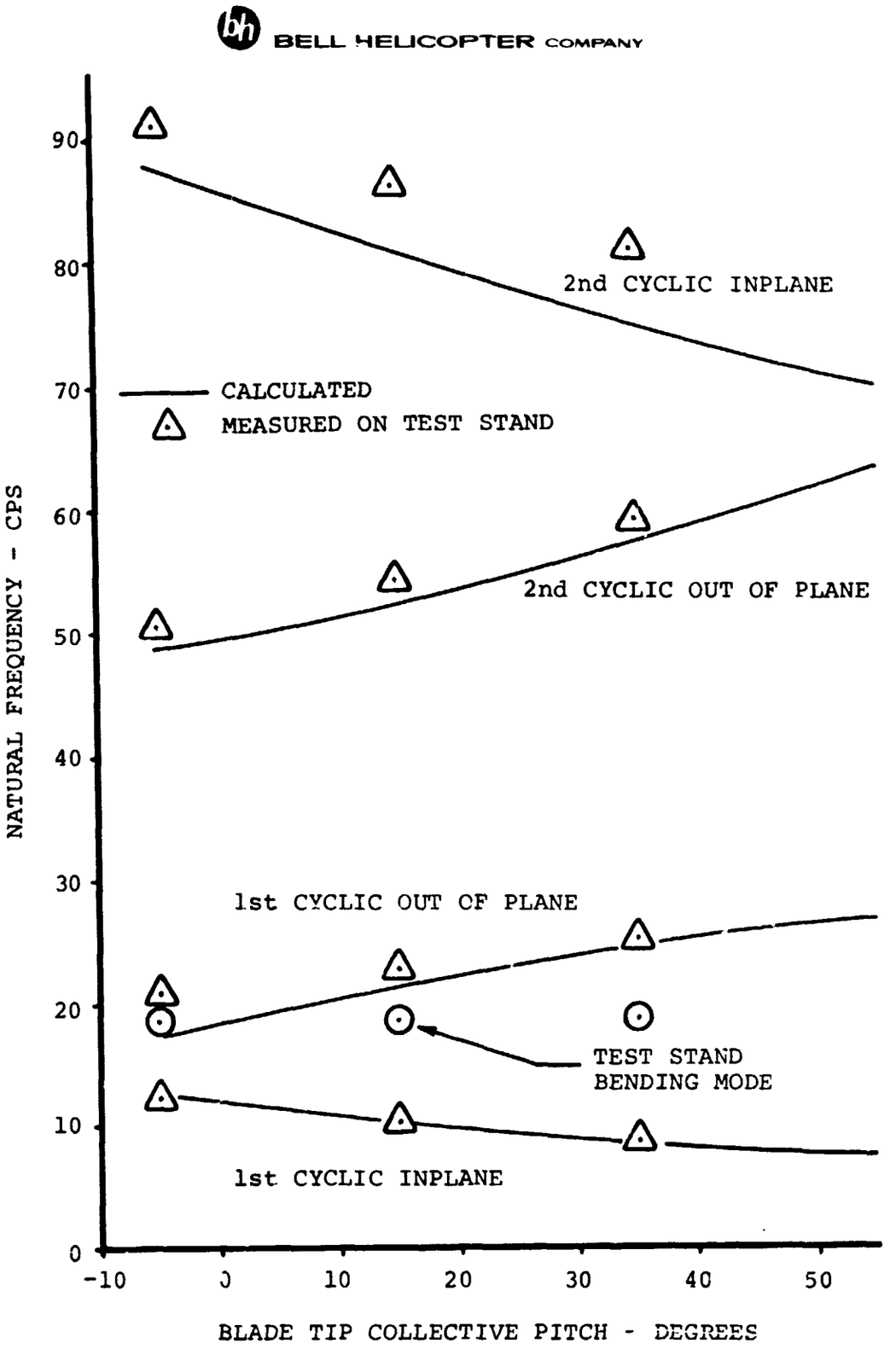

Figure III- 2. Proprotor Cyclic Mode Natural Frequencies, Nonrotating.

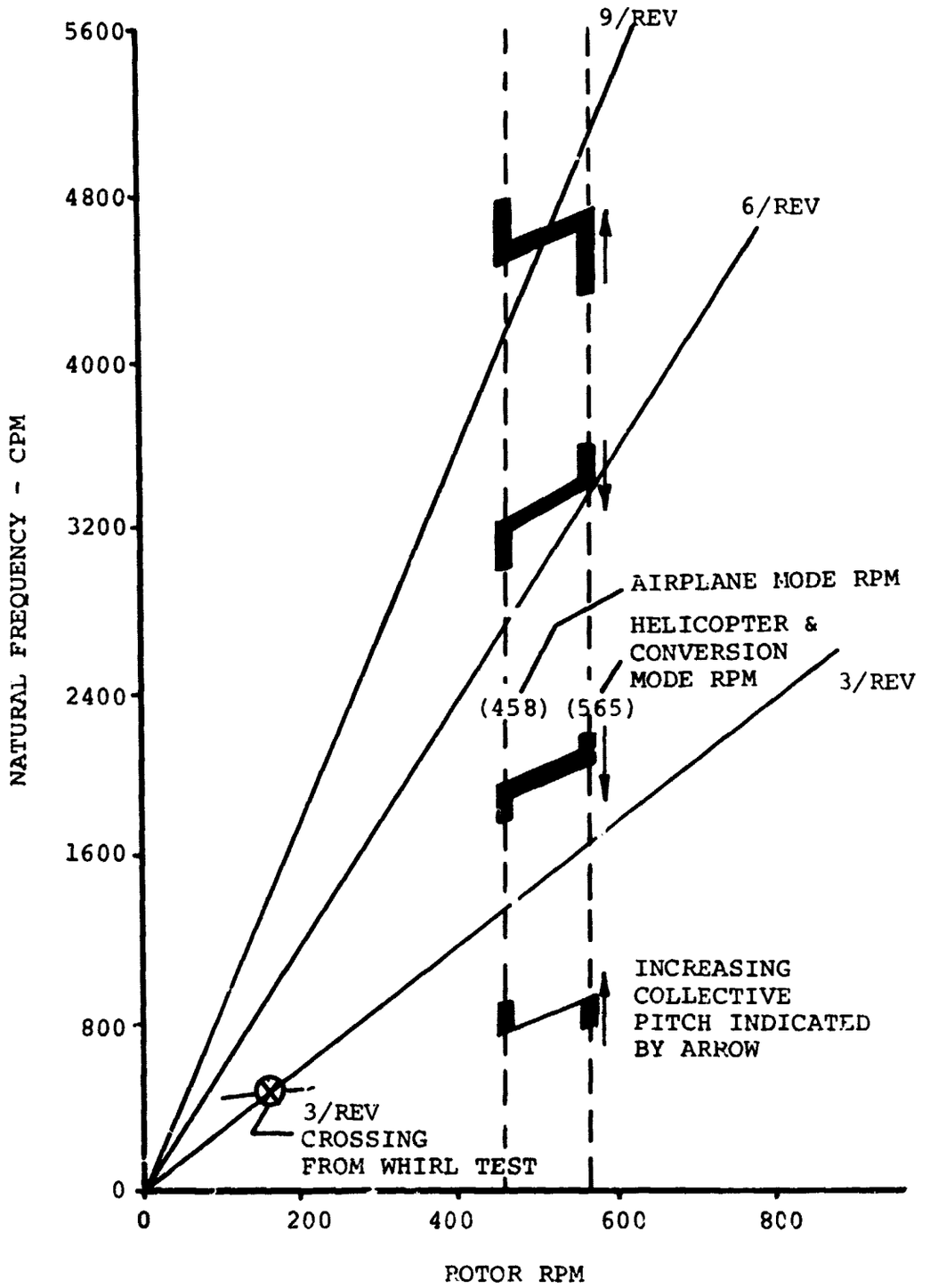

Figure III-3. Proprotor Collective Mode Natural Frequencies, Rotating.

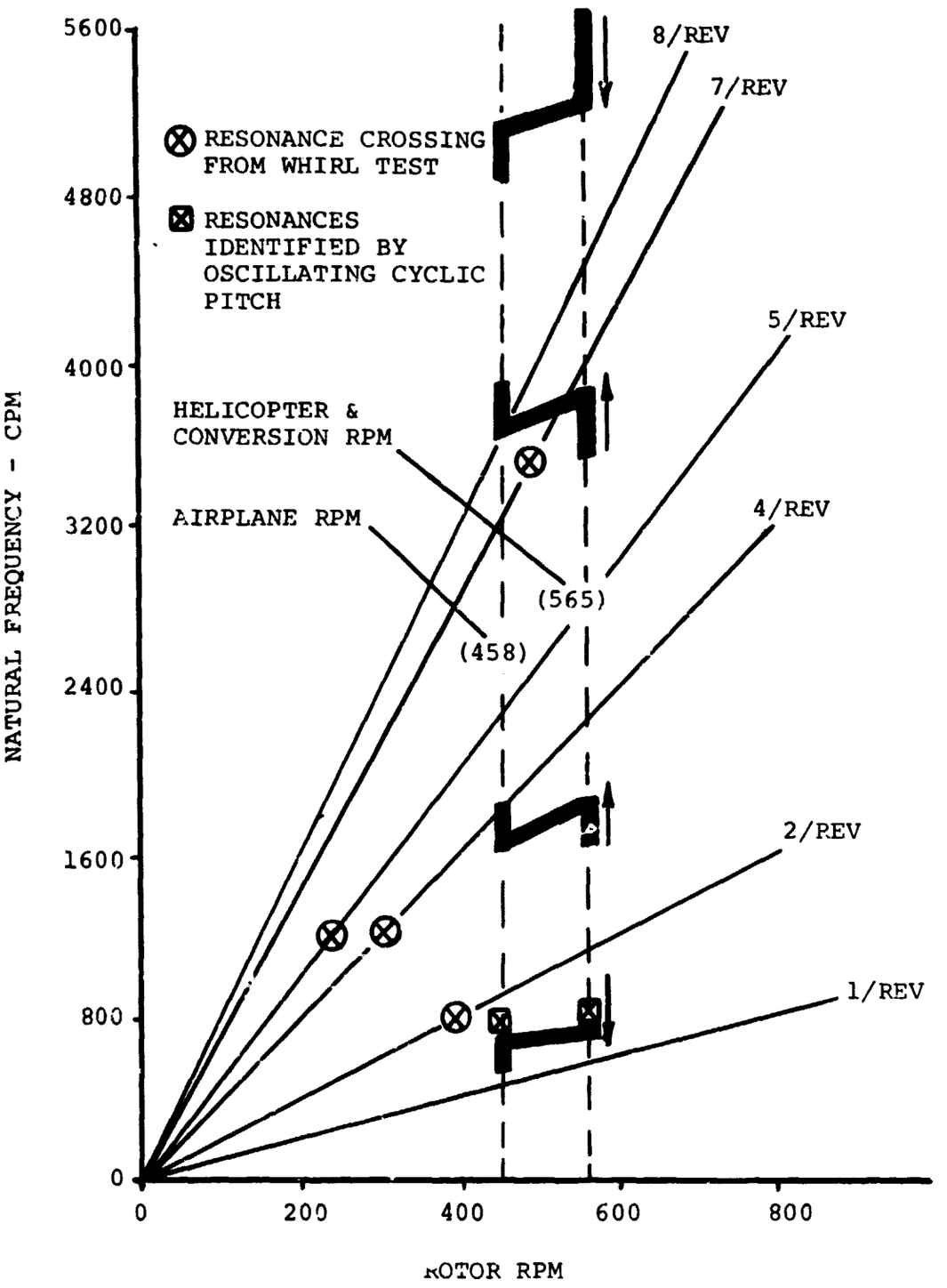

Figure III-4. Proprotor Cyclic Mode Natural Frequencies, Rotating.

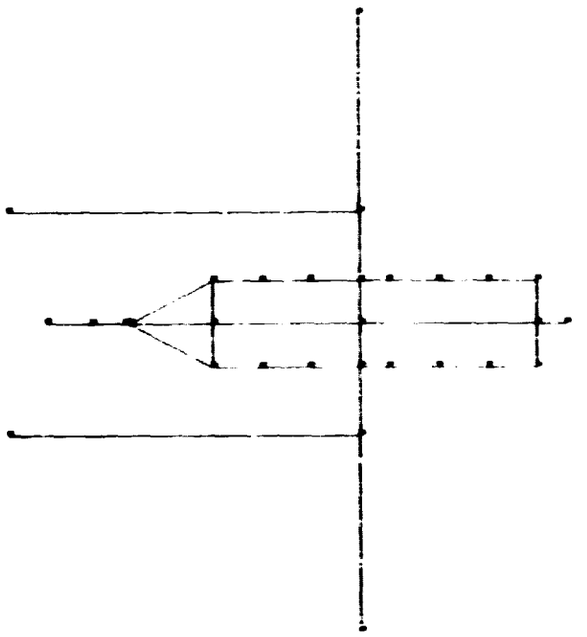

(a) TOP VIEW

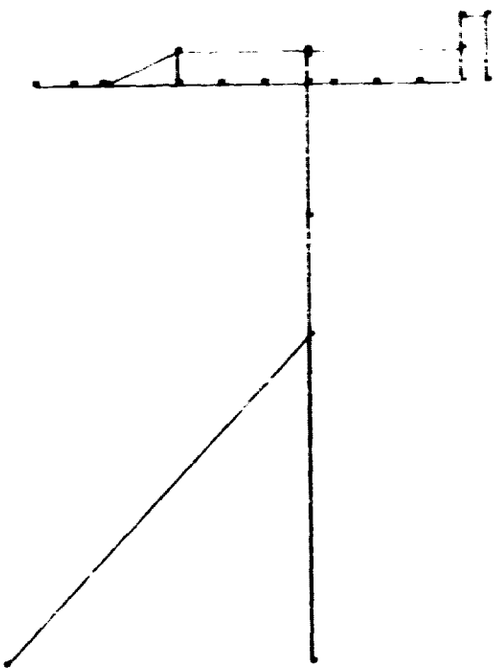

(b) SIDE VIEW

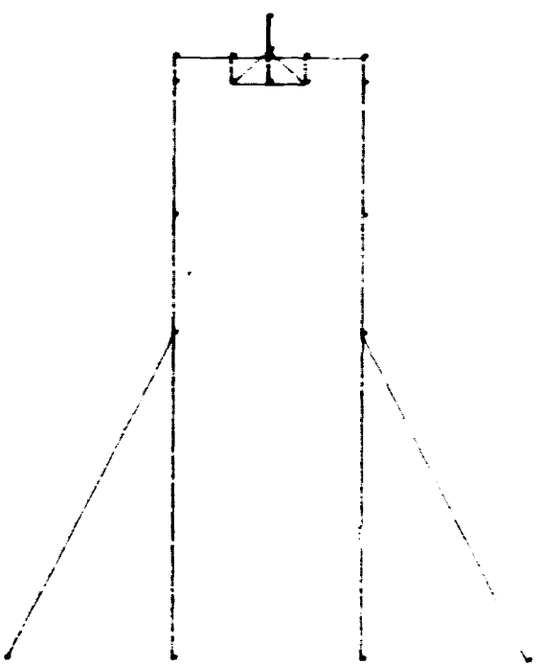

(c) FRONT VIEW

Figure III- 5. NASTRAN Structural Model of Powered Test Stand.

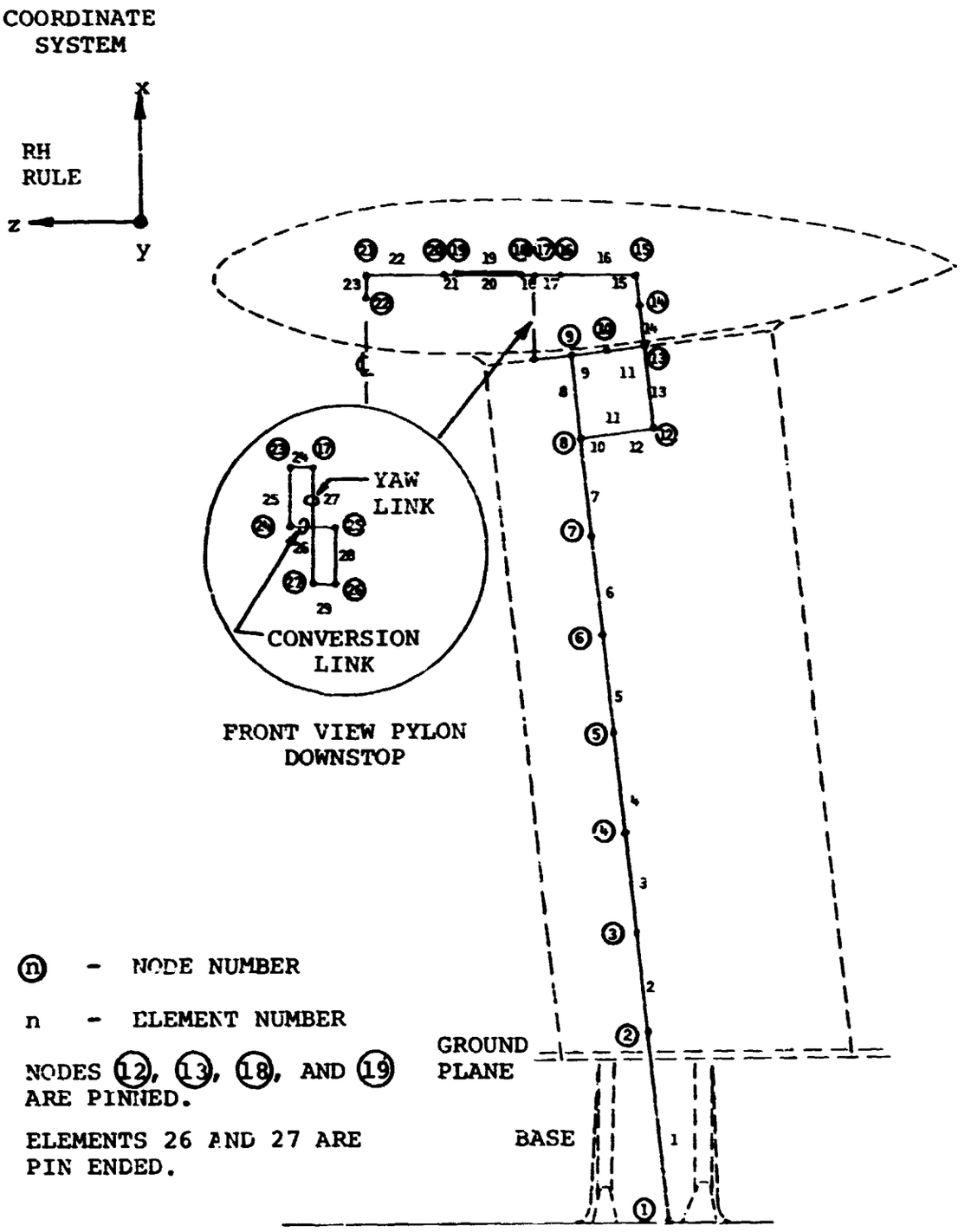

Figure III-6. NASTRAN Structural Model of Dynamic Test Stand.

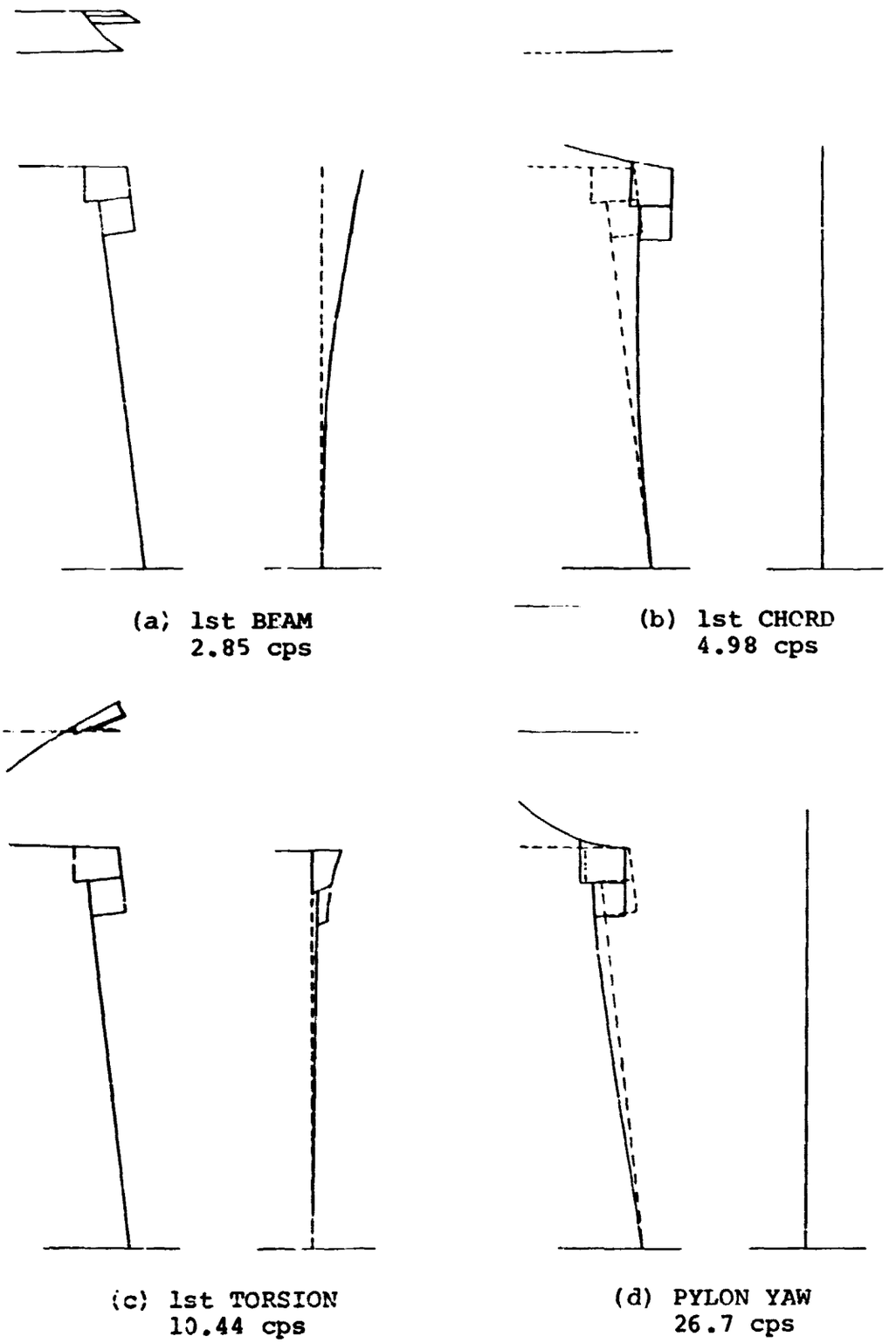

(a) 1st BEAM
2.85 cps

(b) 1st CHORD
4.98 cps

(c) 1st TORSION
10.44 cps

(d) PYLON YAW
26.7 cps

Figure III-7. Mode Shapes - Dynamic Test Stand.

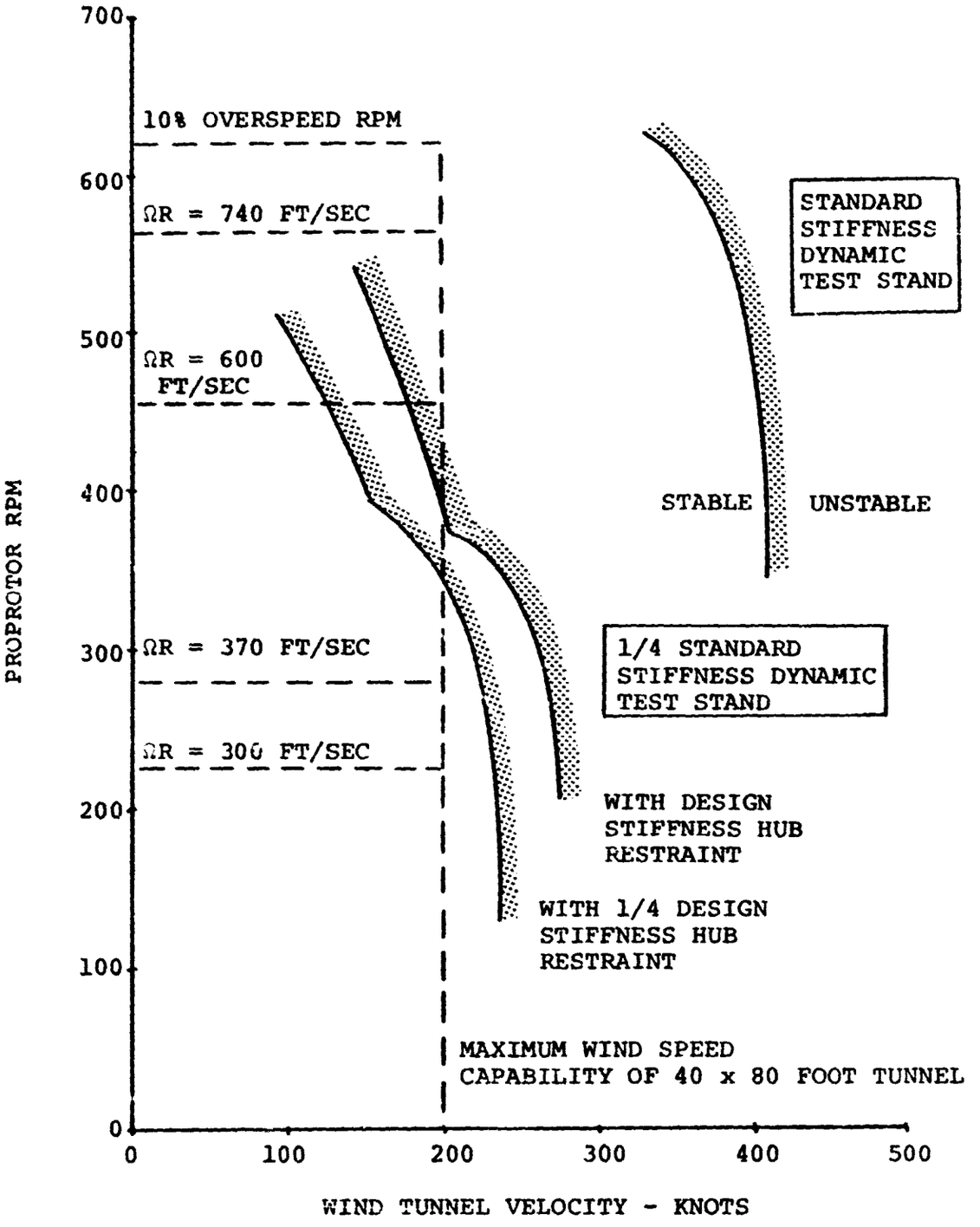

Figure III-8. Dynamic Test Stand Stability Boundaries.

IV. PERFORMANCE

A. GENERAL

The BHC 25-foot-diameter proprotor was tested in the NASA-Ames 40- by 80-foot wind tunnel to evaluate proprotor performance and loads in all three modes of flight: hover, helicopter-conversion, and airplane. The test results correlated well with predictions.

The tests showed that this proprotor maintains good propulsive efficiency in airplane flight mode with no compromise of its performance in the hover or in the helicopter flight mode. The propulsive efficiencies calculated for the cruise conditions are approximately 75 percent. These predictions were verified by the test data. Efficiencies in excess of 90 percent were obtained for the higher thrust requirements. The highest measured rotor mean lift coefficient in hover (as indicated by the value of C_{T_H}/σ) was 18 percent higher than the predicted maximum. Furthermore, the helicopter-conversion flight data were slightly better than predicted.

Predictions of performance were calculated prior to the tests, using BHC's standard prediction techniques. Where test results and predicted performance disagree, the test performance is usually better. For example, the power required for a given lift was not as high during the tests as was predicted.

Data are presented here by flight mode. Where applicable, i.e., for the proper operating tip speeds, data are shown for the typical operating requirements of a 10,300-pound-gross weight vehicle. Because engineers with diverse backgrounds will be using them, the data have been nondimensionalized in accordance with the two different conventions of airplane and helicopter analysis. The appendix defines the nomenclature.

B. TEST DESCRIPTION

The wind tunnel had equipment for measuring pertinent parameters during powered tests. BHC supplied some additional instrumentation. The six-component balance provided data which were converted to rotor thrust, H-force, and torque. There was also a load cell on the test stand for measuring torque. The rotor mast (shaft) was also strain-gaged to give yet another means of measuring torque. Generally, this report uses torque and power figures obtained by means of the strain gages because they seemed to be more accurate and were, furthermore, conservative in that they showed the rotor to be consuming more power than the other instrumentation showed. In addition to these measurements, the proprotor rpm, collective pitch, cyclic pitch, and flapping were measured. For a more detailed description of the proprotor instrumentation and force/angle relationships, see Subsection III.C and the appendix respectively.

The major test variables were tip speed, tunnel speed, and shaft angle. Table IV-I shows the ranges tested for each of the three flight modes. For the majority of test conditions, the collective pitch was varied while the other variables were held approximately constant (cyclic was adjusted to hold fore and aft flapping constant at zero).

TABLE IV-I. RANGE OF VARIABLES FOR POWERED TEST

	Tunnel Speed (knots)	Tip Speed (fps)	Mast Angle (deg)
Hover	0 - 20	600 - 740	0 - 75
Helicopter-Conversion	80 - 140	700 - 740	15 - 75
Airplane	120 - 185	400 - 740	0

C. CALCULATIONS

Complete predictions of performance for the test conditions were computed and supplied to NASA prior to tunnel entry. These predictions used Bell Helicopter Company program F35. This program employs blade-element-momentum theory with non-uniform inflow for hover and axial flight and uniform inflow for the other flight conditions. It uses two-dimensional airfoil data in conjunction with the blade geometric characteristics. Reference 26 provides further discussion of the theory. Blade geometry is defined in Figure IV-1.

As shown, the blade has been divided into four major segments, the maximum number of divisions allowed by the program for the input of geometric and airfoil sections properties. For calculation purposes, each of the major segments is subdivided in such a way that each blade is represented by 22 elements. The program limitation of four segments resulted in an inability to match exactly the inboard twist and chord.

The airfoil section data for each of the four segments are shown in Figures IV-2 through IV-5. Also shown are modifications made to these data in an attempt to obtain better correlation with the hover data, as discussed in Subsection IV.E.1. The unmodified section data are used throughout this report except as noted for hover. The airfoil data for the first section were obtained from two-dimensional tests conducted in the General Dynamics-Convair low-speed wind tunnel. The data for the outboard three sections were obtained from tests conducted in the United Aircraft Research Laboratories high-speed wind tunnel.

In addition to the geometric properties of the rotor and the airfoil section data, other inputs include the number of blades, tip speed, speed of sound, freestream velocity, air density ratio, mast angle, and collective pitch or thrust.

Tip loss is normally calculated by equating to zero the lift of the blade segment outboard of the spanwise station determined by the relation

$$B = 1 - \frac{\sqrt{2C_T}}{b}$$

The program also allows the user to enter any arbitrary constant tip loss factor. The program then utilizes this factor as explained above; i.e., no lift is produced on the blade outboard of the station set by the tip loss factor.

D. SPINNER TARE DATA

Figures IV-6 through IV-8 show the lift and drag tares used during the test. Approximate tare data were obtained initially with the blade spindles protruding from the spinner. After the test was completed, these spindles were removed and data obtained for both a smooth spinner and one with the blade holes open. In general, curves are faired through all of the data since neither case is truly representative of the actual test conditions. Figure IV-6 shows the effect of the spinner base pressure on the drag tare when the proprotor is in the axial flight mode. Most of the spinner drag was due to skin friction rather than base pressure since during the test the measured $\Delta P/q$ value never exceeded 0.1. These low base pressures were probably a result of the one- to one-and-one-half-inch gap between the spinner and test stand shroud. Also shown in this figure are the tare data previously measured on a one-fifth-scale proprotor model.

Figures IV-7 and IV-8 show the lift and drag tare data used in reducing the helicopter-conversion data. During the spindle-off tare tests, the lift balance data become questionable. In order to obtain the proper lift tare for this condition, the incremental values determined from the one-fifth-scale tests were applied to the full-scale data.

E. RESULTS AND CORRELATION

Figures IV-9 through IV-36 show the calculated data and powered test results. The data are separated into the hover, helicopter-conversion, and axial or airplane flight modes for clarity of presentation. These data are shown in both dimensional and nondimensional form. Nondimensional data have been shown in both airplane and helicopter nomenclature where applicable. All

coefficients are in airplane terms unless noted. Definitions for all coefficients and parameters are found in the appendix. Also in the appendix is a computer listing of all dimensional test data.

All correlation was made in terms of forces and horsepower because they are of primary interest. Correlation with respect to mast angle has been shown by stating the value of mast angle where applicable (helicopter-conversion mode). As the data indicate, good correlation was obtained when the flapping angle was less than ±0.5 degree. The correlation between the calculated and measured data becomes less accurate as the shaft angle is increased, especially beyond 60 degrees. It should be noted, however, that the disagreement is one of conservatism, i.e., more lift and/or propulsive force was produced for a given horsepower. Two contributing factors are (1) the difficulty of determining the absolute mast angle under loaded and dynamic conditions, and (2) the effects of the proximity of the tunnel ceiling for the higher mast angles.

No tunnel angularity corrections have been made to the test data. Such corrections might have some significance for the conditions where the proprotor was at large mast angle positions (60-75 degrees) and the blade tips approached the tunnel roof. To put in perspective all the variables, including the tip-path-plane angle (α_{TPP}) and the tip collective angle (θ_{TIP}), maps of calculated data are shown in Figures IV-20 and IV-21 for the helicopter-conversion flight modes at 80- and 140-knot tunnel speeds.

1. Hover Flight Mode

Figures IV-9 and IV-12 show the results of the hover tests. Data were taken for proprotor tip speeds of 600 and 740 feet per second and for mast angle settings of 0, 30, 60, and 75 degrees. Overall correlation between the test and predicted data is good. For the lower mast angle settings, the induced flow in the tunnel is responsible for the increase in power relative to the calculated data. The tunnel fans were operated in reverse to minimize flow through the test section, but were not entirely effective. The data for the higher mast angle settings may be slightly optimistic from a power standpoint due to the recirculation in the test section, although test section top doors were partially opened to minimize that effect. The rotor plane was more than one rotor diameter above the tunnel floor, which would ordinarily exclude ground effect; however, since the tunnel is rounded on the sides, other recirculation effects may have been present.

The prediction of hover performance and (to a lesser extent) potential maneuvering performance of a new rotor depends upon the accuracy of predictions of the maximum thrust of the rotor. Predictions of the maximum thrust of this rotor have been more conservative as they should have been, with the predicted maximum values falling well below that measured. On the assumption that

the prediction methods were primarily responsible for the non-exact correlation, not the test procedures or data reduction, the prediction methods were examined.

Of special interest was the degree to which some of the input variables affected the predictions. This was investigated by modifying the inputs as follows:

- Tip loss factor = 0.97
- Tip loss factor = 1.00
- Tip loss factor = 0.97 and modified blade element characteristics

This was a departure from the use of the expression given in IV.C for calculating the tip loss factor. The 0.97 factor has been used in the past to improve the correlation between the predicted and the actual performance of helicopter tail rotors. Like the tail rotor, the proprotor has a comparatively high disc loading, and therefore the tip loss factor which is applicable for one should be correct for the other.

The 0.97 tip loss factor did improve the correlation, but not sufficiently. The 1.00 factor was also inadequate, and furthermore was rather unrealistic. Therefore, the tip loss factor was returned to 0.97 and the blade element data modified slightly as shown in Figures IV-2 through IV-5. This combined adjustment put the calculated performance in good agreement with the measured performance.

2. Helicopter-Conversion Flight Mode

Figures IV-14 through IV-19 show (nondimensionally) the variation of horsepower as a function of proprotor lift and propulsive force for mast angles of 15, 30, 60, and 75 degrees, a tunnel speed range of 80 to 140 knots, and tip speeds of 700 and 740 feet per second.

Generally, correlation is best at the lower mast angles, with some deviations occurring with increasing mast angle. The deviations at the higher mast angles may be attributed to an inability to determine the tip-path-plane angle with sufficient accuracy and to the fact that a constant mast angle does not insure a constant tip-path-plane angle as shown by the following relation:

$$\alpha_{TPP} = \alpha_{MAST} + a_{1_S} - 90^\circ$$

An arbitrary limit of ±0.5 degrees has been placed on the value of flapping angle, and all data outside this limit have been flagged. At the higher mast angles this angle range limit could show the sensitivity of the other variables to the tip-path-plane and tip-collective angles.

Figure IV-22 shows the correlation between measured and calculated horsepower for all of the helicopter-conversion data. The data were calculated for the measured lift and propulsive force for this correlation. The figure shows a conservative trend for the calculated data.

3. Airplane Flight Mode

Figures IV-23 through IV-36 contain airplane mode (axial) data. Figures IV-23 through IV-32 show the propulsive force and efficiency data as a function of horsepower. Data are presented for tunnel speeds of 120, 1960, and 185 knots and tip speeds ranging from 400 to 740 feed per second. Correlation for this data is good and where a deviation exists, the calculated data are usually conservative.

Figures IV-33 through IV-35 show the above-mentioned data in the nondimensional form of propulsive efficiency as a function of power coefficient.

Figure IV-36 show a correlation between calculated and measured horsepower for all test conditions. The calculated horsepower data were evaluated for the measured values of propulsive force. This figure shows the trend of the calculated data to be more conservative at the higher values of horsepower.

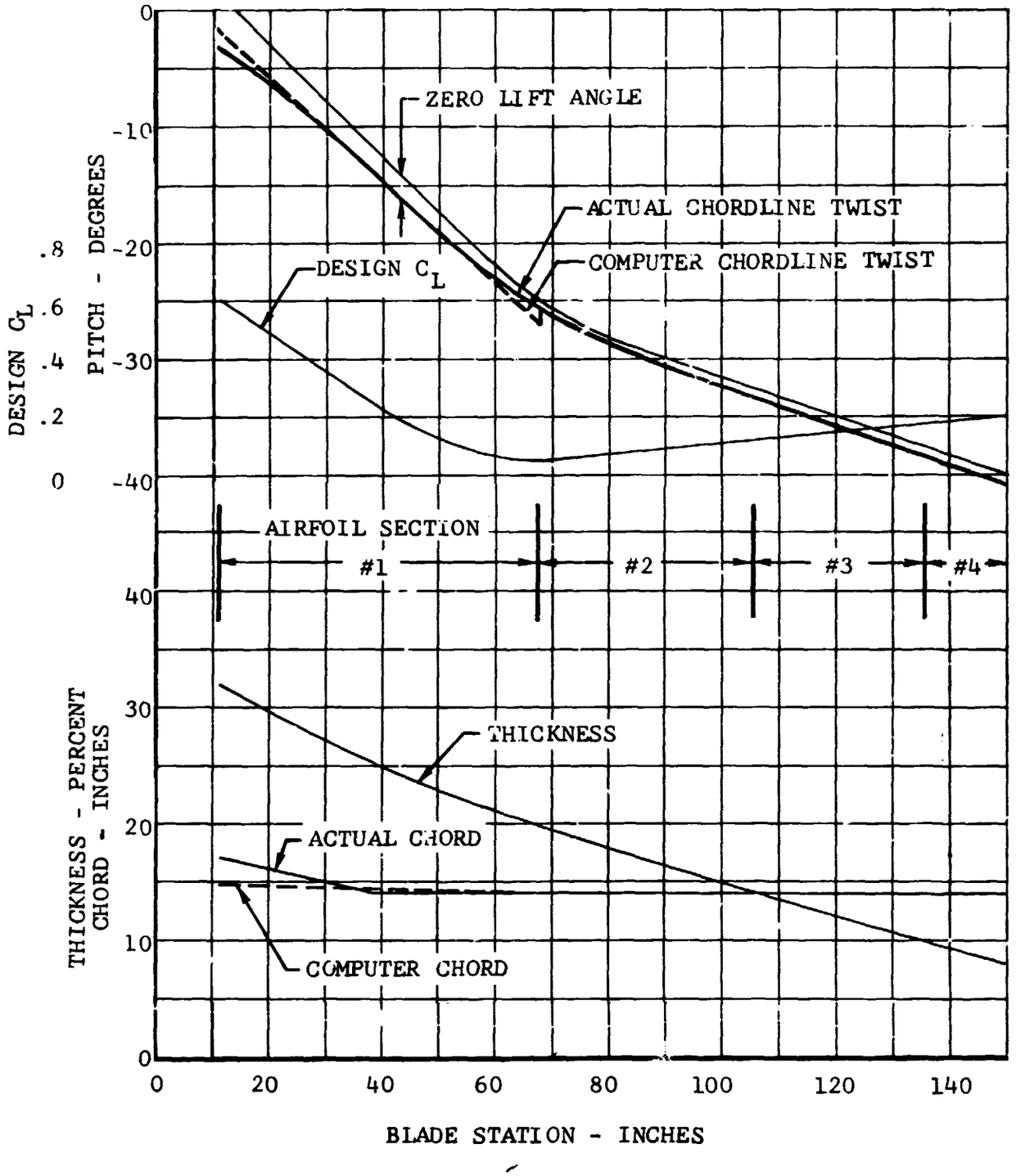

Figure IV-1. Computer Representation of the 25-Foot Proprotor Blade.

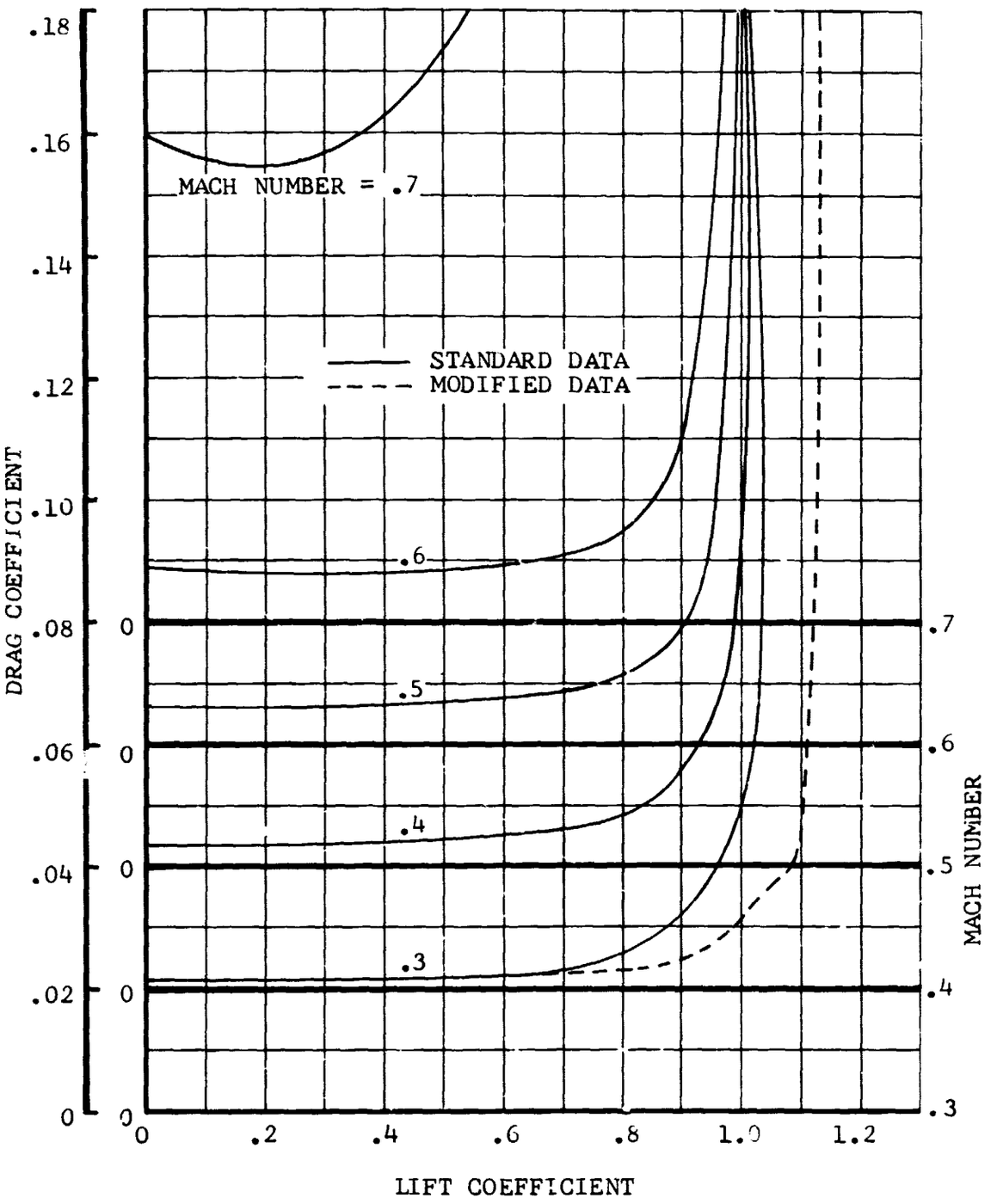

Figure IV-2. Proprotor Blade Section Data, Airfoil Section No. 1, Blade Station 0.075 to 0.45.

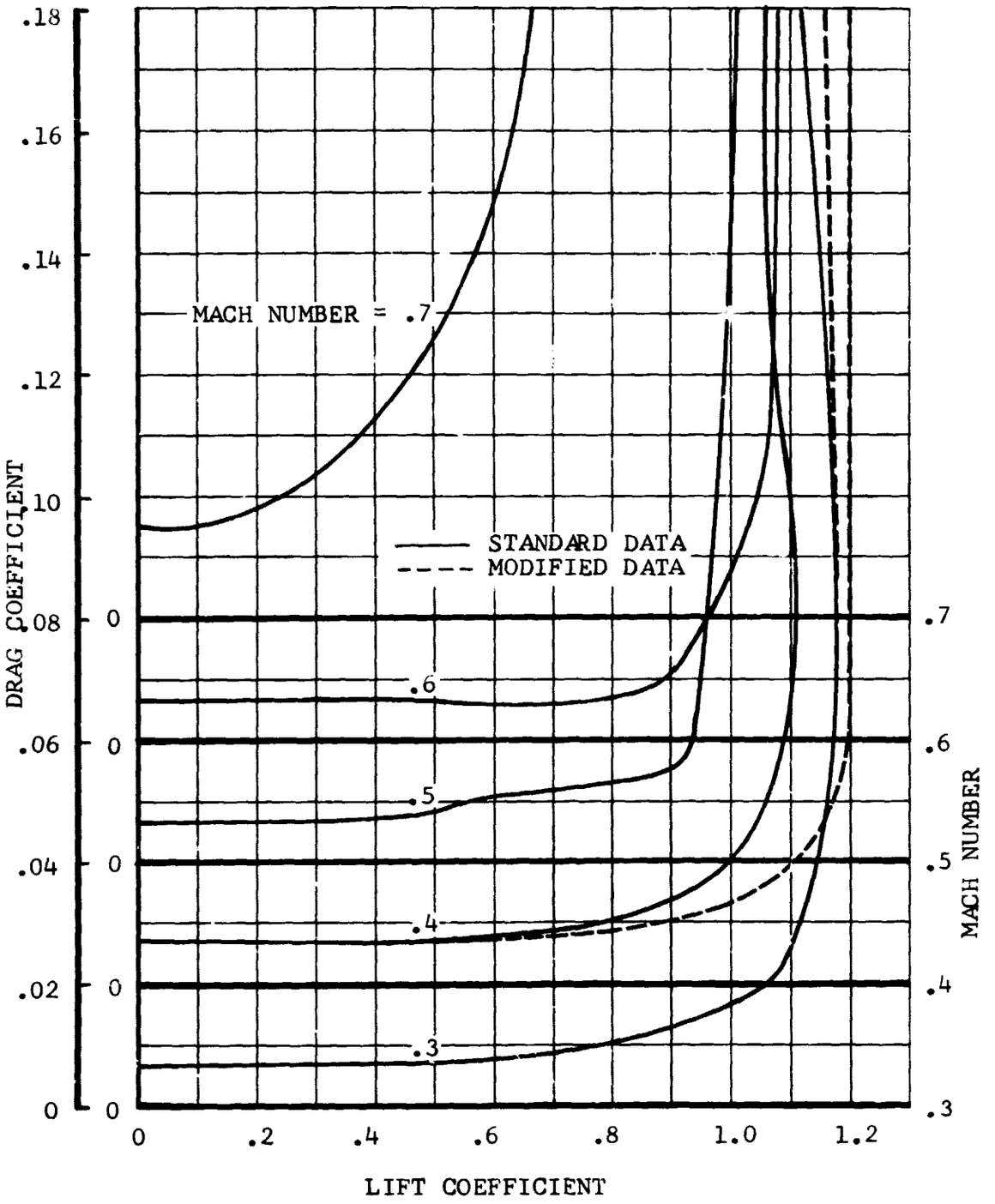

Figure IV-3. Proprotor Blade Section Data, Airfoil Section No. 2, Blade Station 0.45 to 0.70.

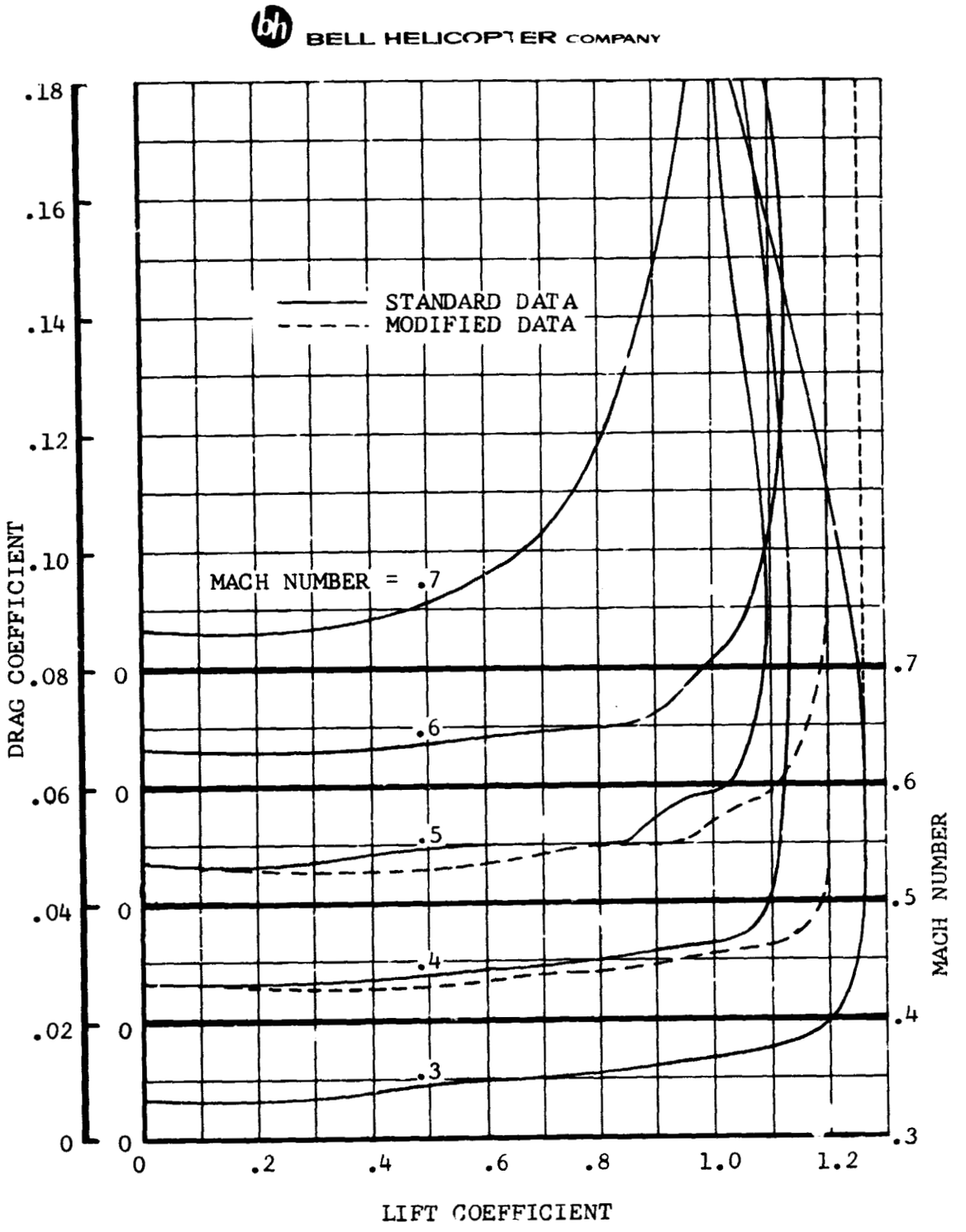

Figure IV-4. Proprotor Blade Section Data, Airfoil Section No. 3, Blade Station 0.70 to 0.90.

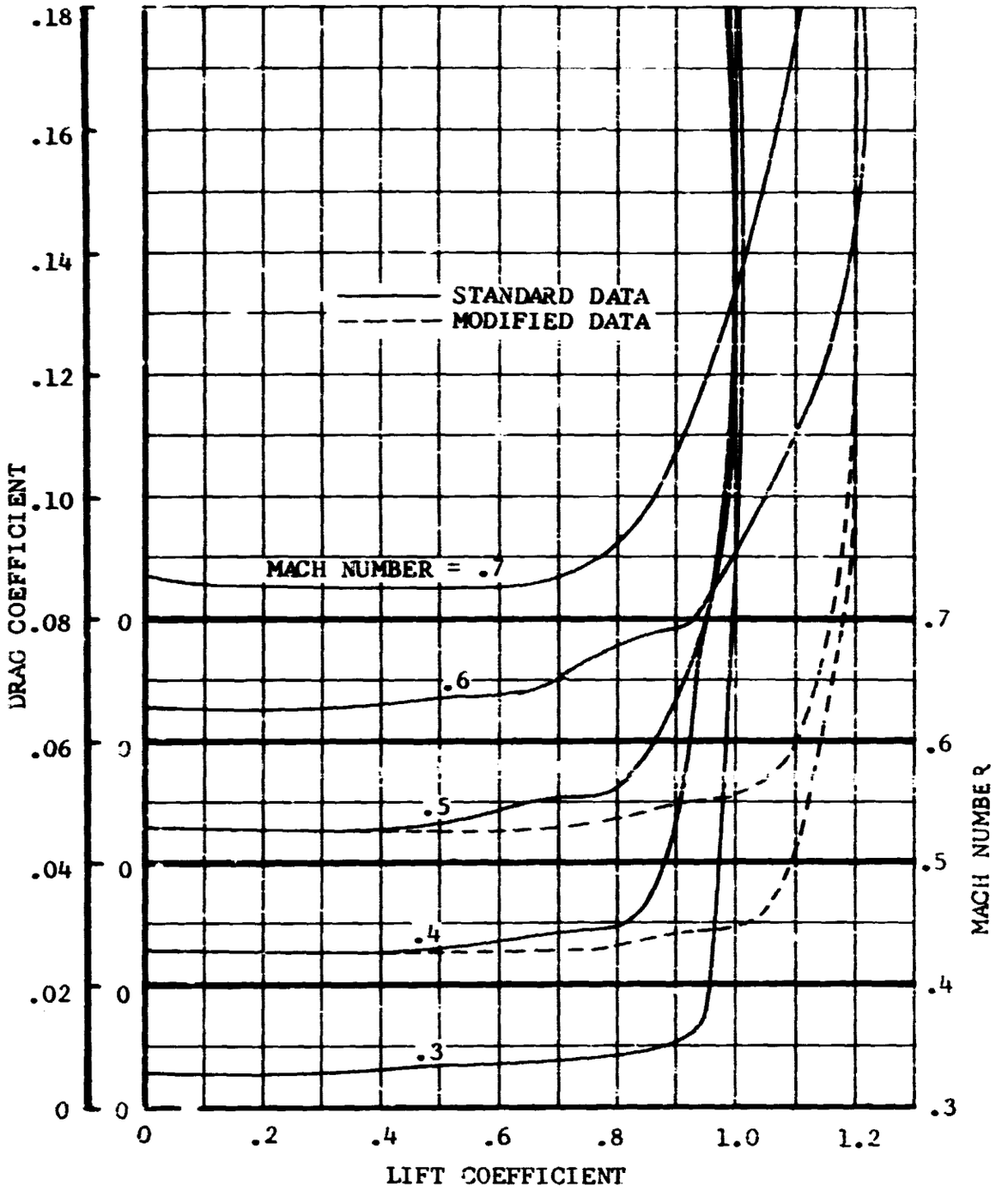

Figure IV-5. Proprotor Blade Section Data, Airfoil Section No. 4, Blade Station 0.90 to 1.00.

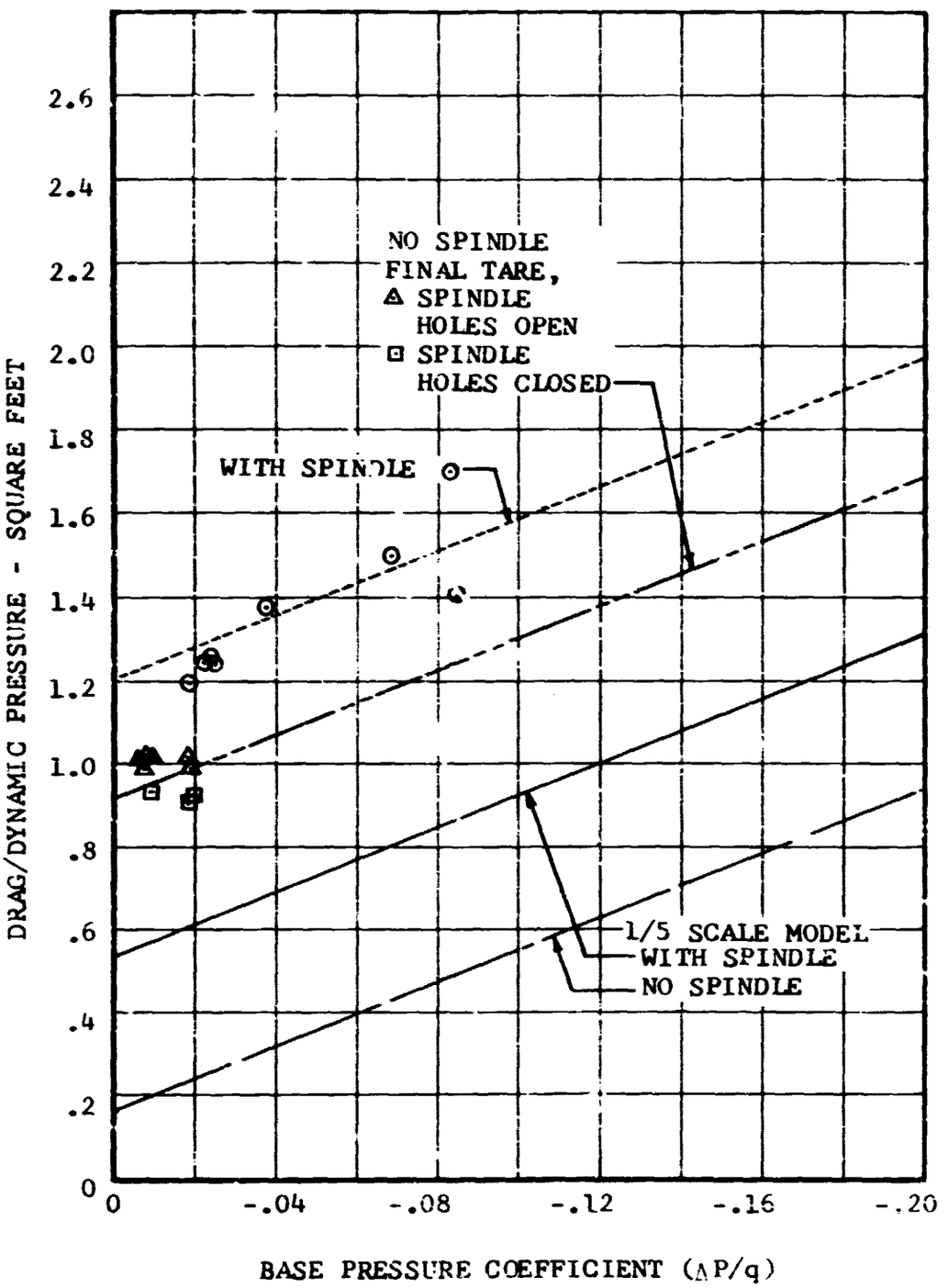

Figure IV-6. Spinner Drag Tare, Airplane Flight Mode.

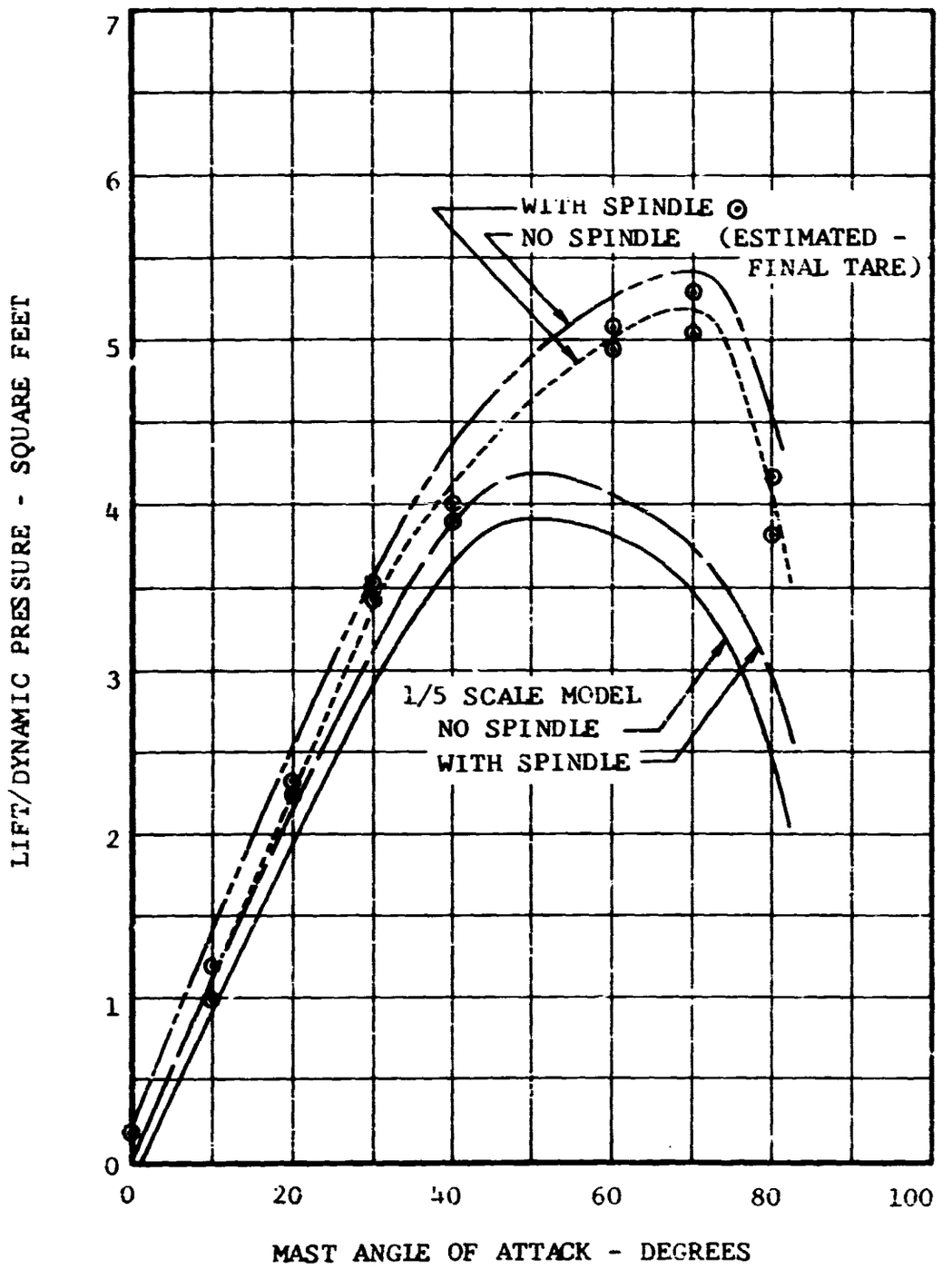

Figure IV-7. Spinner Lift Tare Versus Mast Angle of Attack, Helicopter-Conversion Mode.

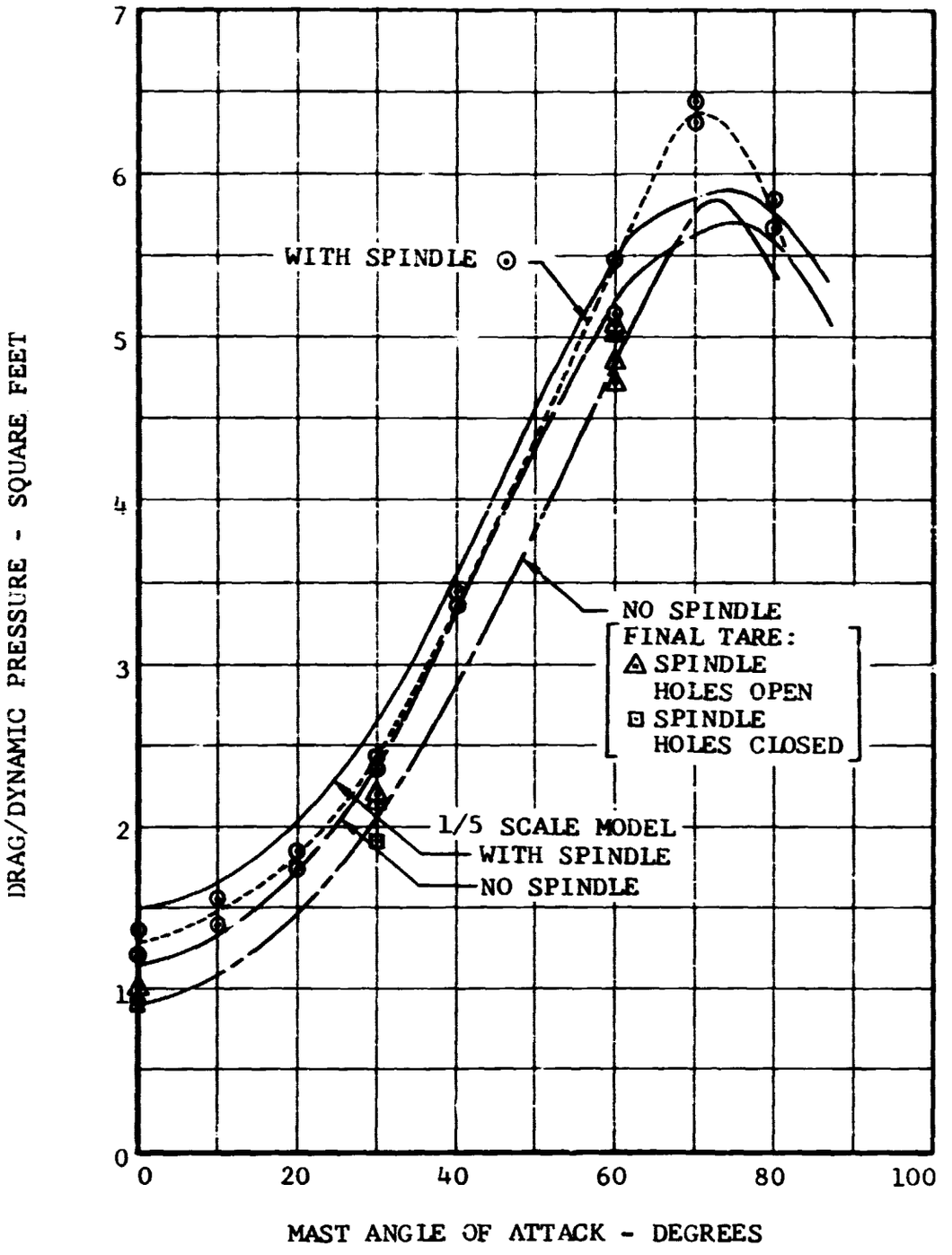

Figure IV.8 Spinner Drag Tare Versus Mast Angle of Attack, Helicopter-Conversion Mode.

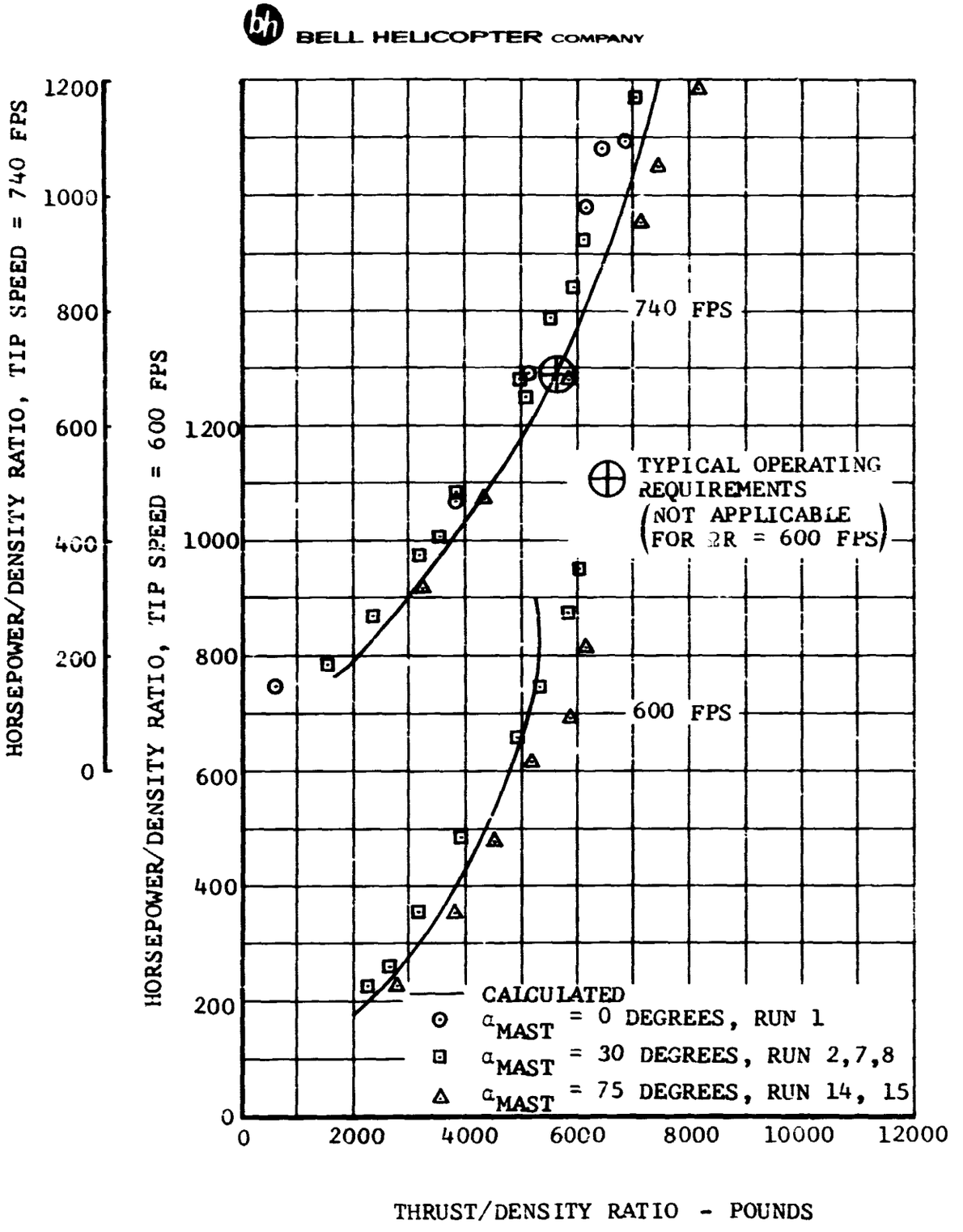

Figure IV-9. Dimensional Hover Power Required.

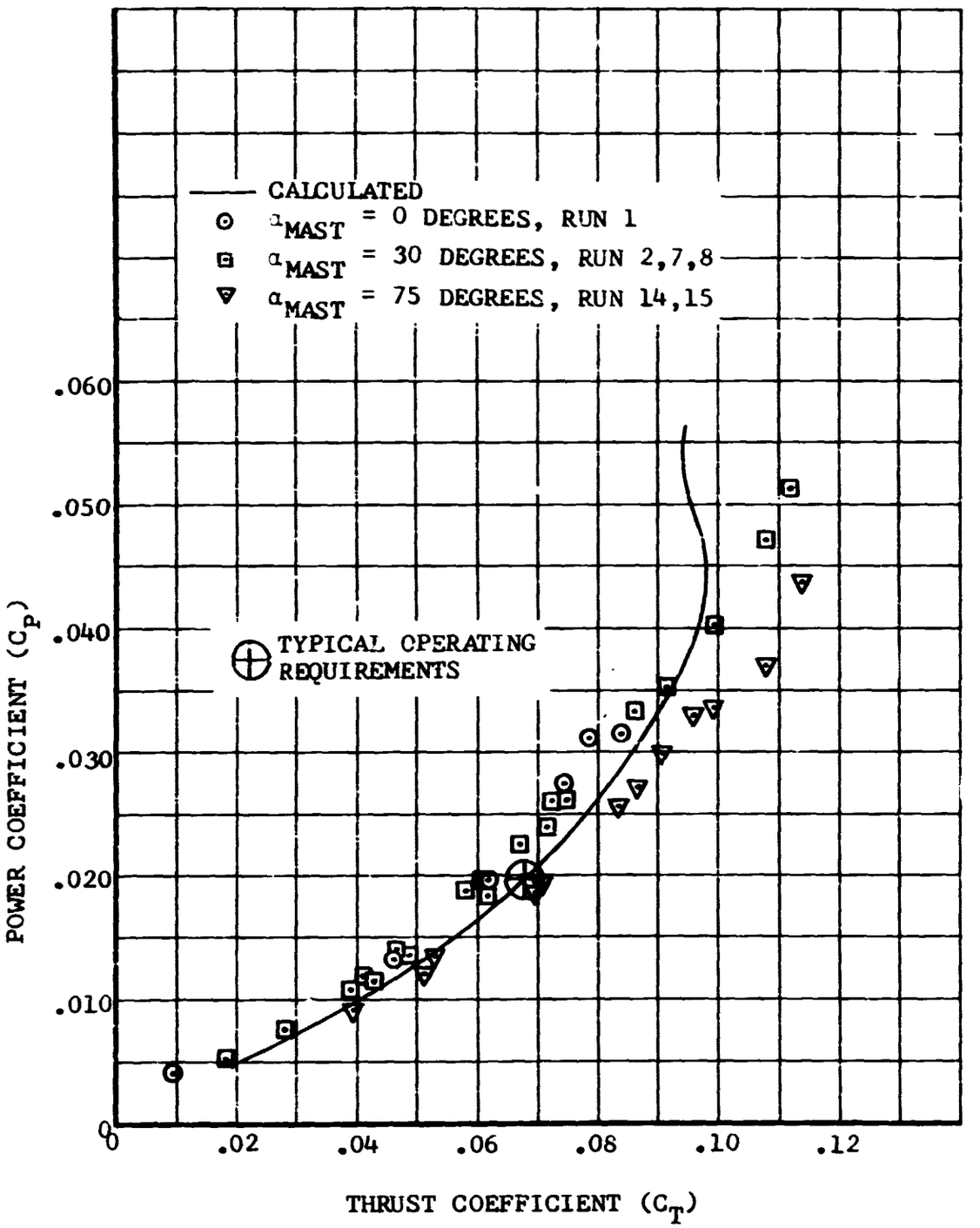

Figure IV-10. Nondimensional Hover Power Required.

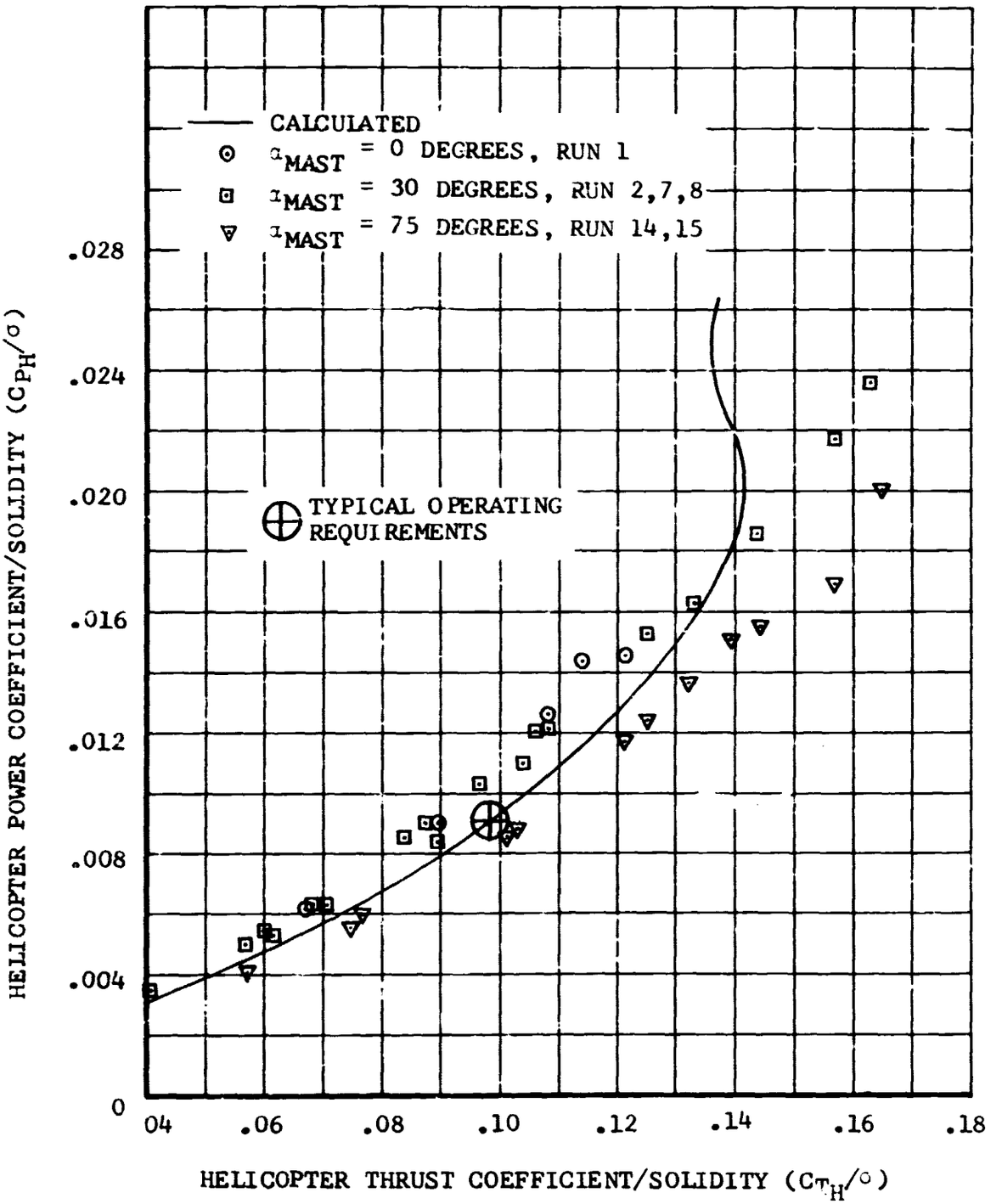

Figure IV-11. Nondimensional Hover Power Required.

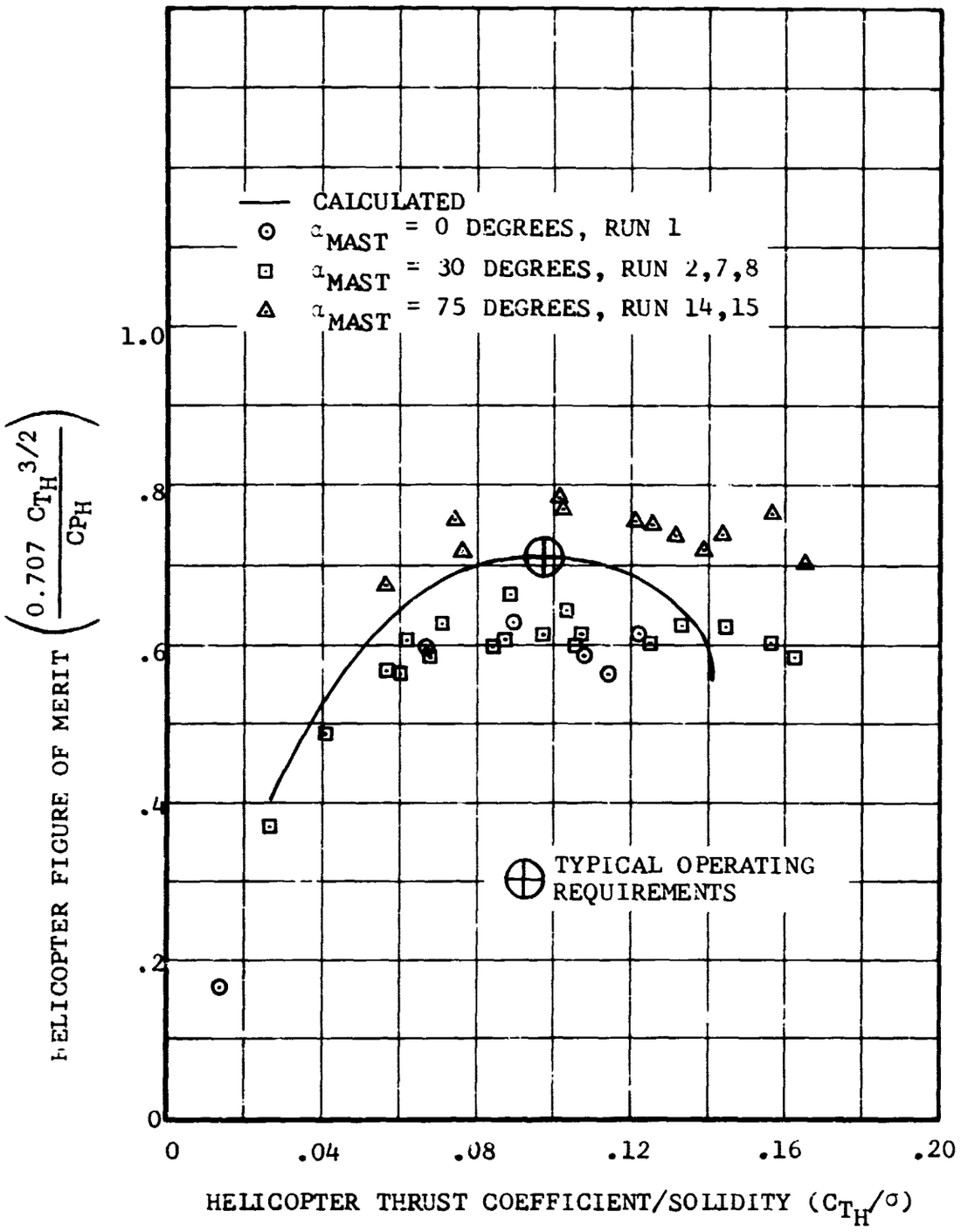

Figure IV-12. Hovering Figure of Merit Versus Helicopter Thrust Coefficient/Solidity.

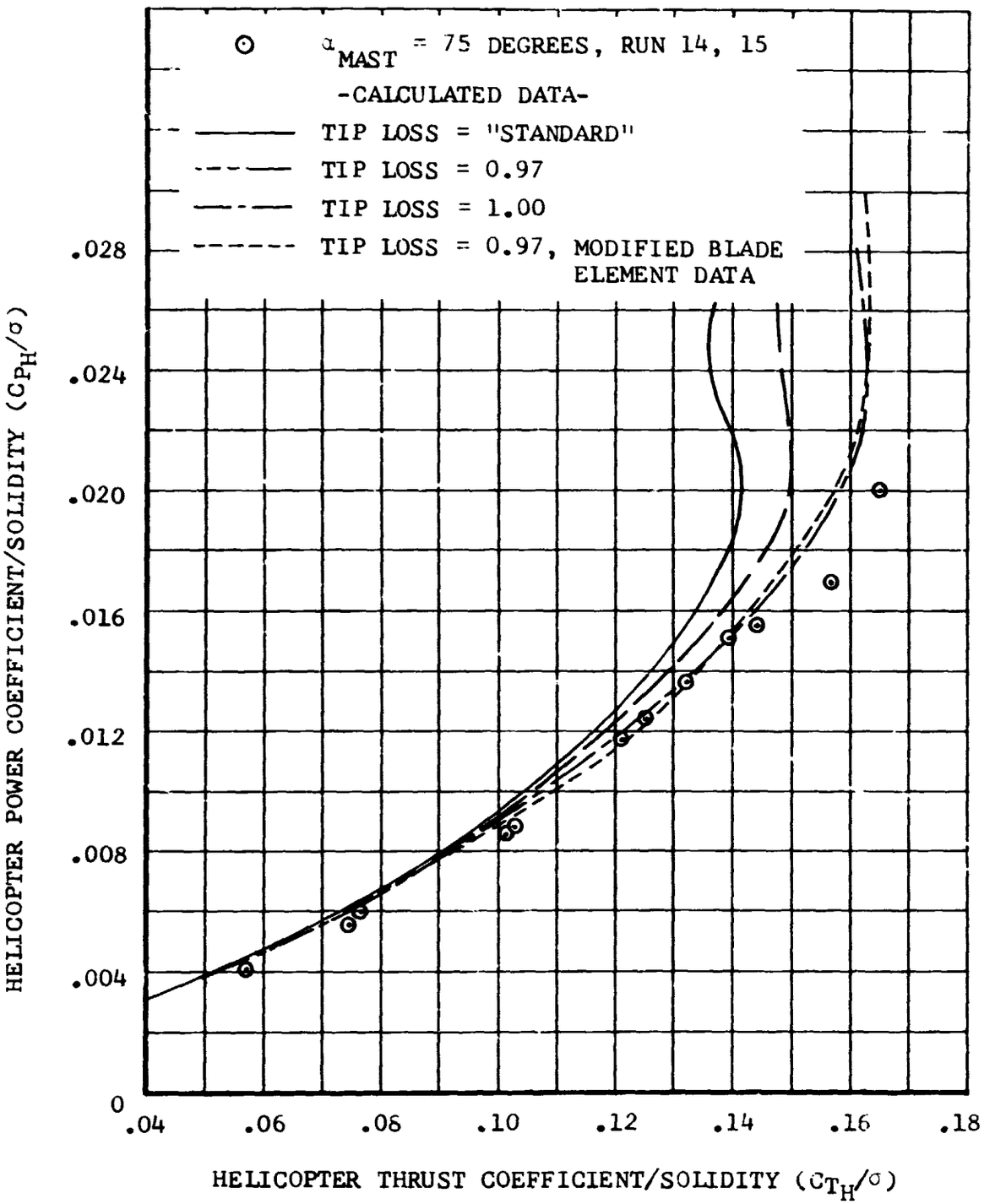

Figure IV-13. Correlation of Nondimensional Hover Power Required.

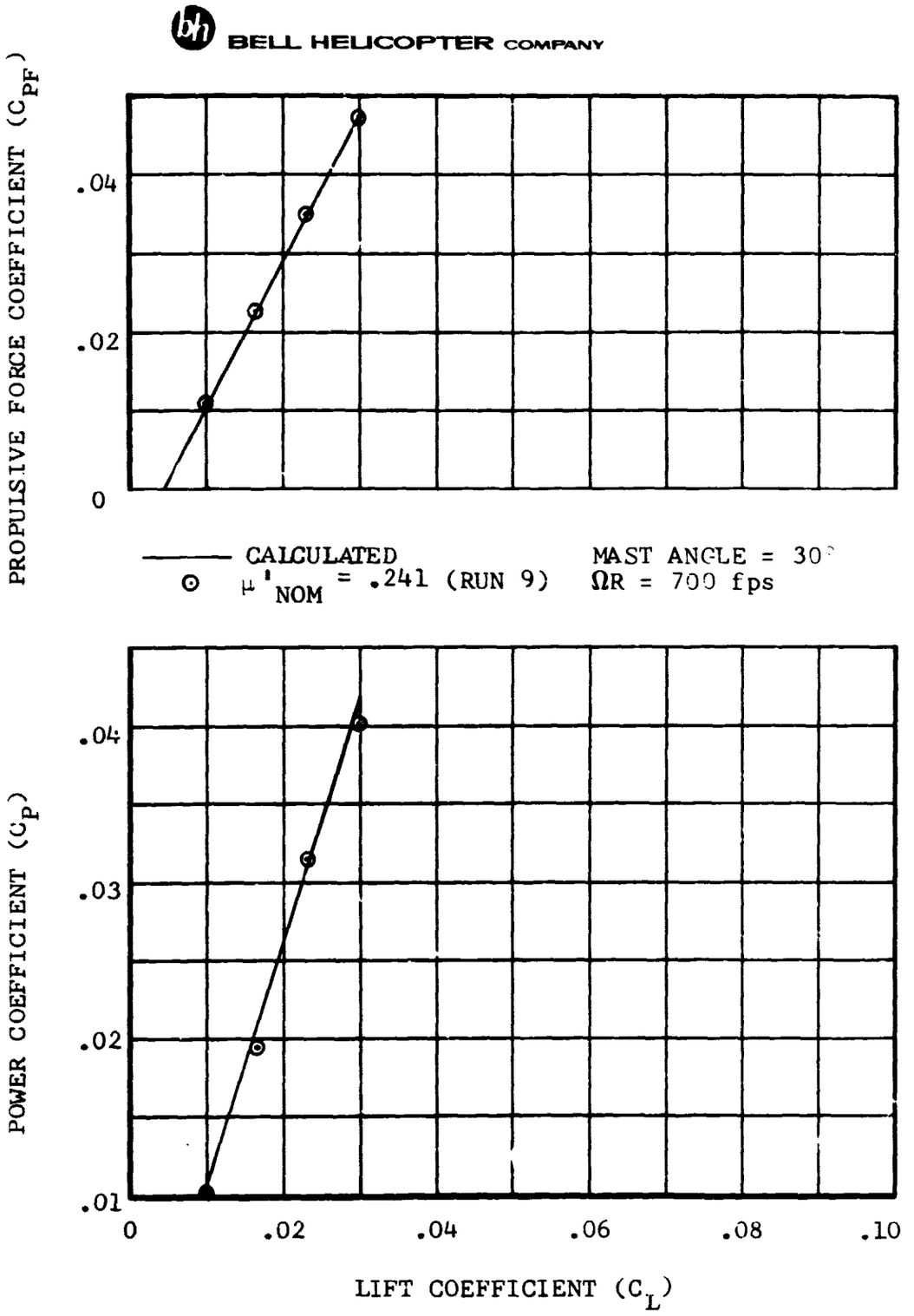

Figure IV-14. Nondimensional Helicopter-Conversion Performance.

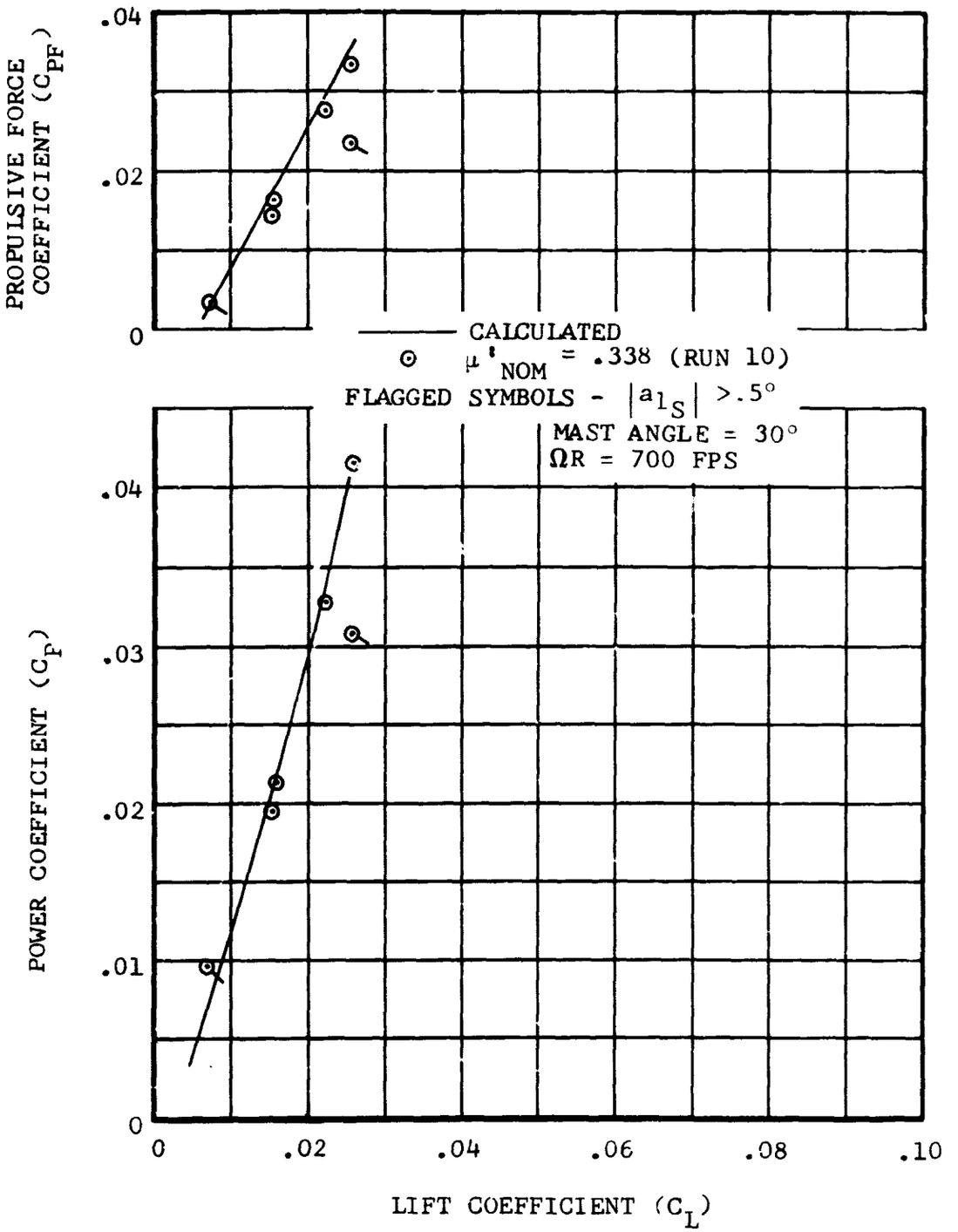

Figure IV-15. Nondimensional Helicopter-Conversion Performance.

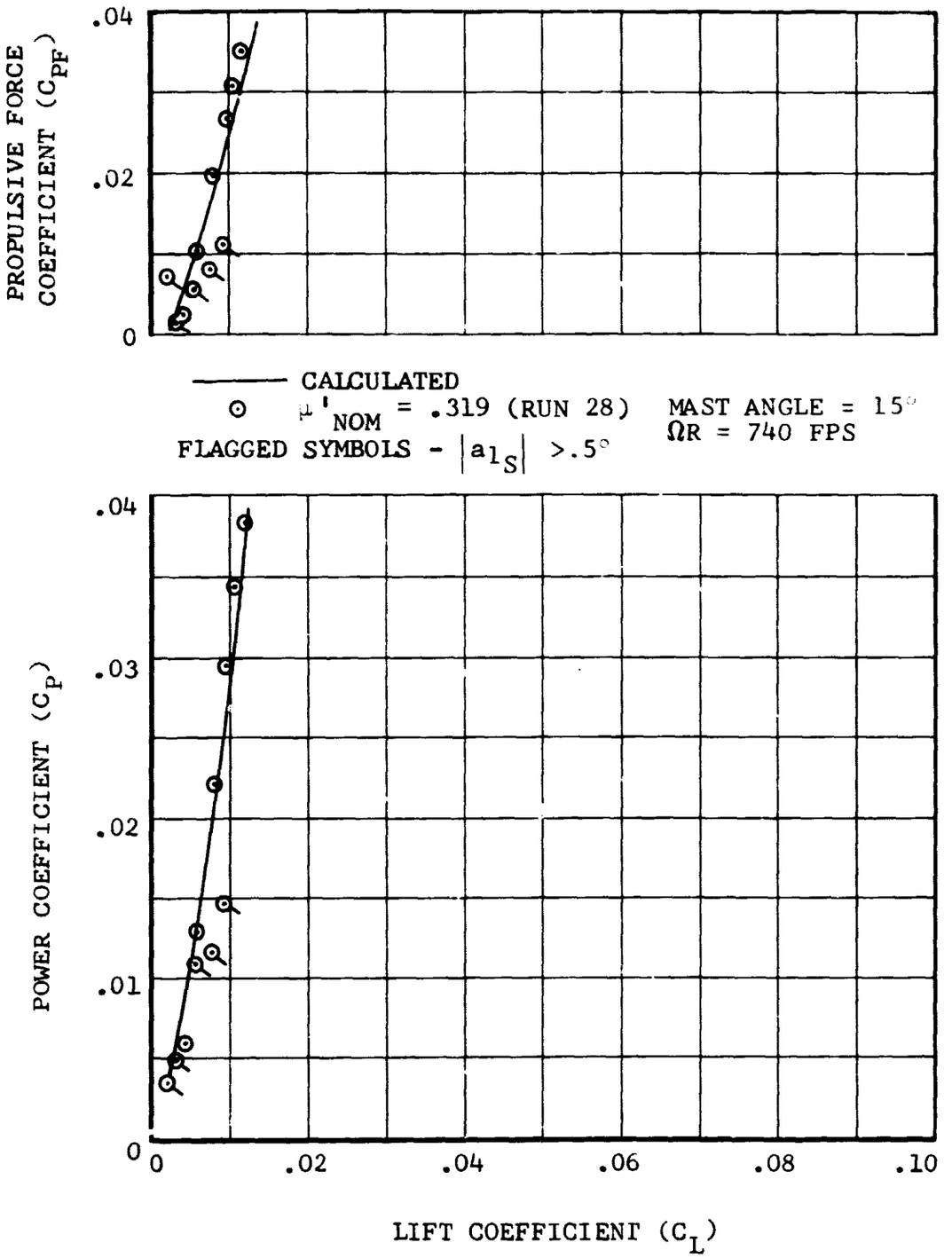

Figure IV-16. Nondimensional Helicopter-Conversion Performance.

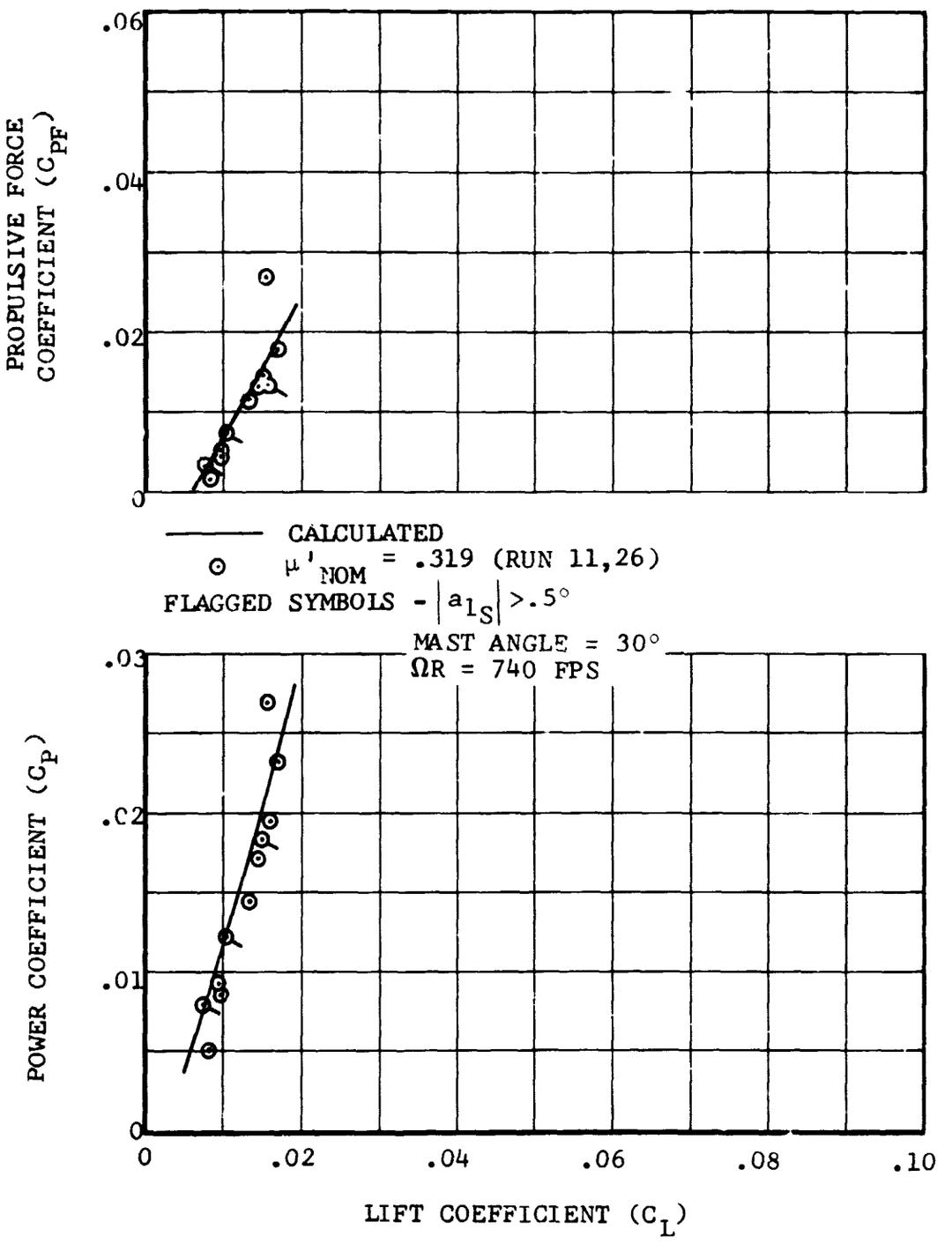

Figure IV-17. Nondimensional Helicopter-Conversion Performance.

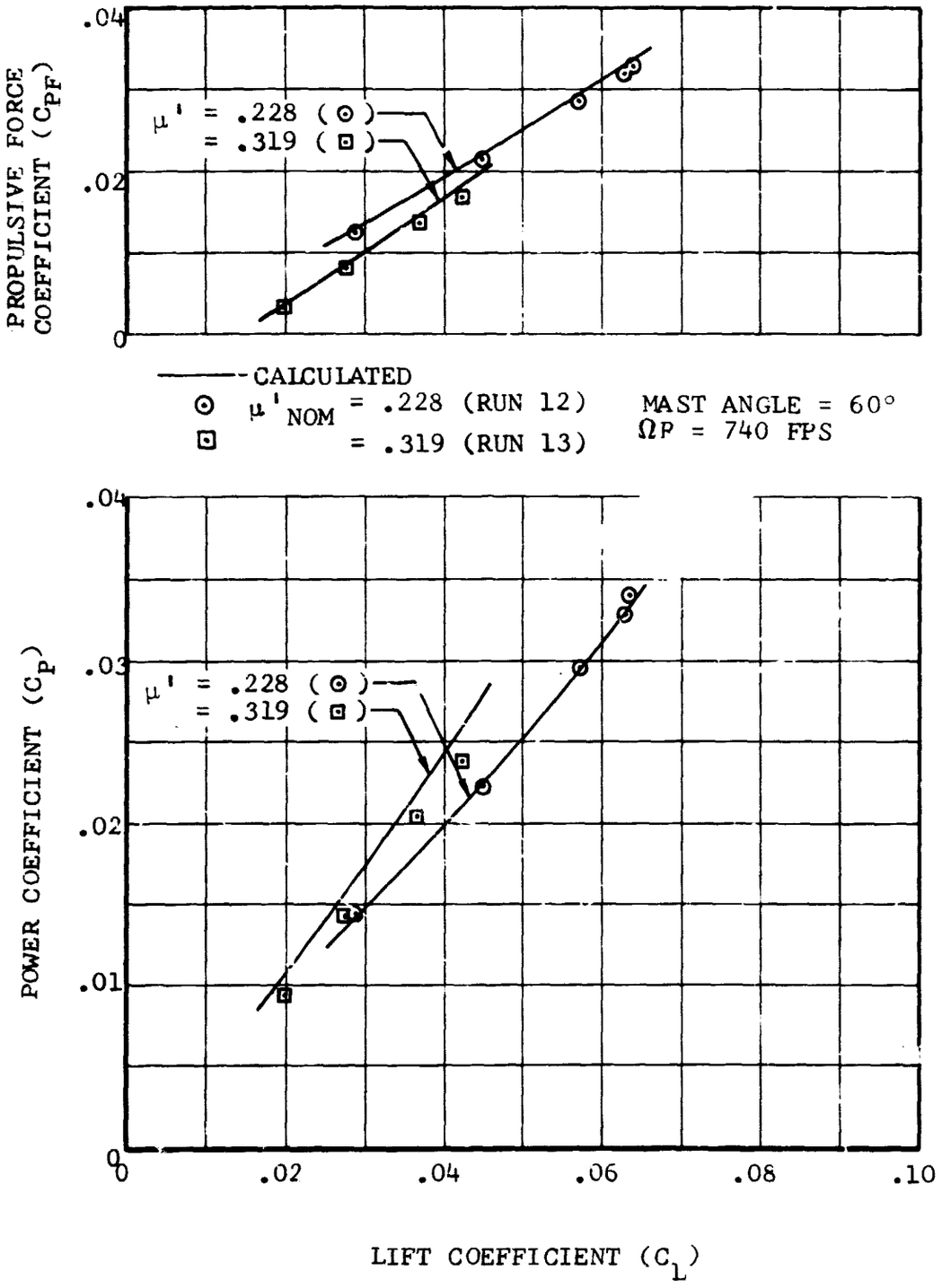

Figure IV-18. Nondimensional Helicopter-Conversion Performance.

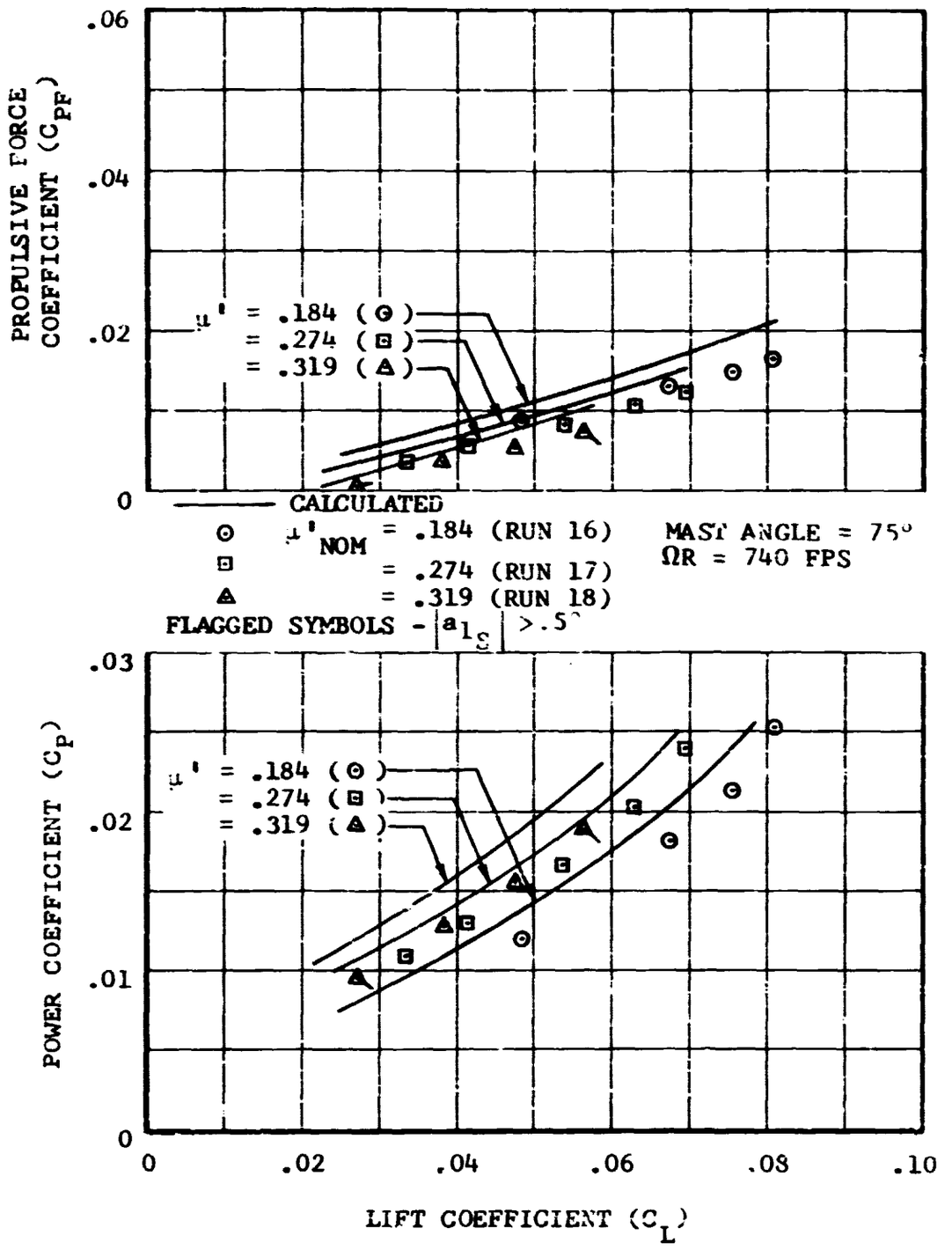

Figure IV-19. Nondimensional Helicopter-Conversion Performance.

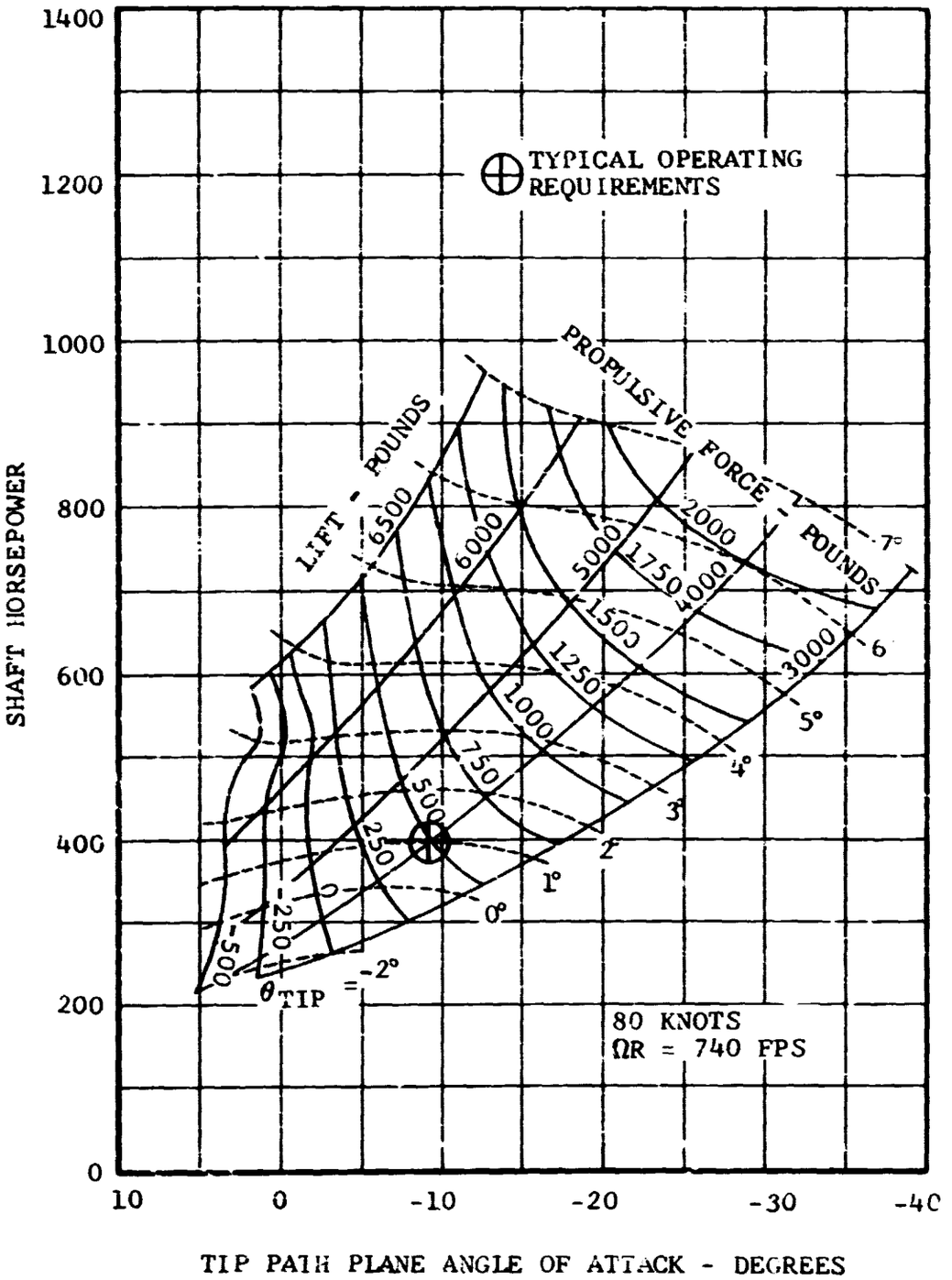

Figure IV-20. Calculated Shaft Horsepower Versus Tip Path Plane Angle of Attack, Helicopter-Conversion Mode, 80 Knots.

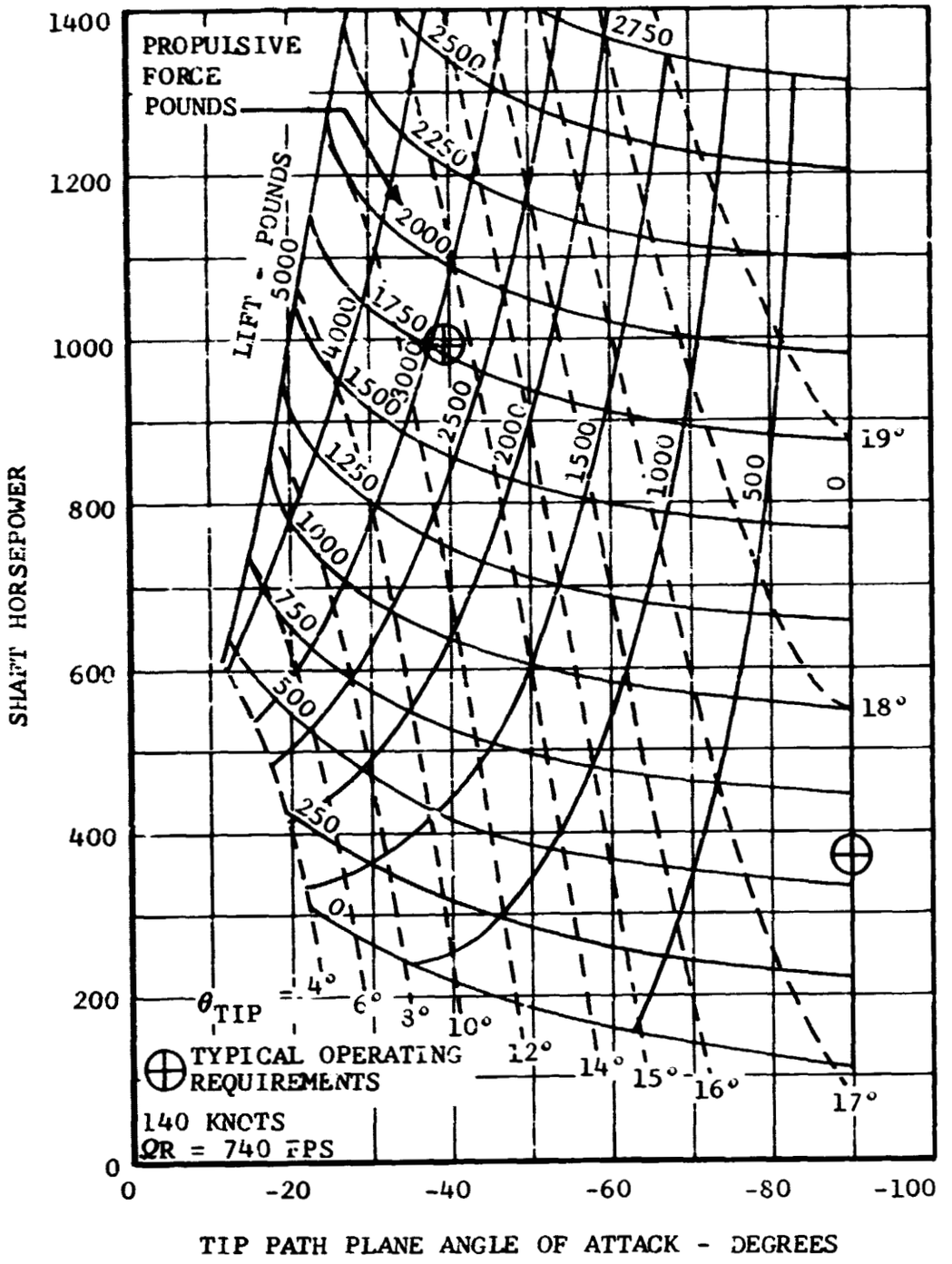

Figure IV-21. Calculated Shaft Horsepower Versus Tip Path Plane Angle of Attack, Helicopter-Conversion Mode, 140 Knots.

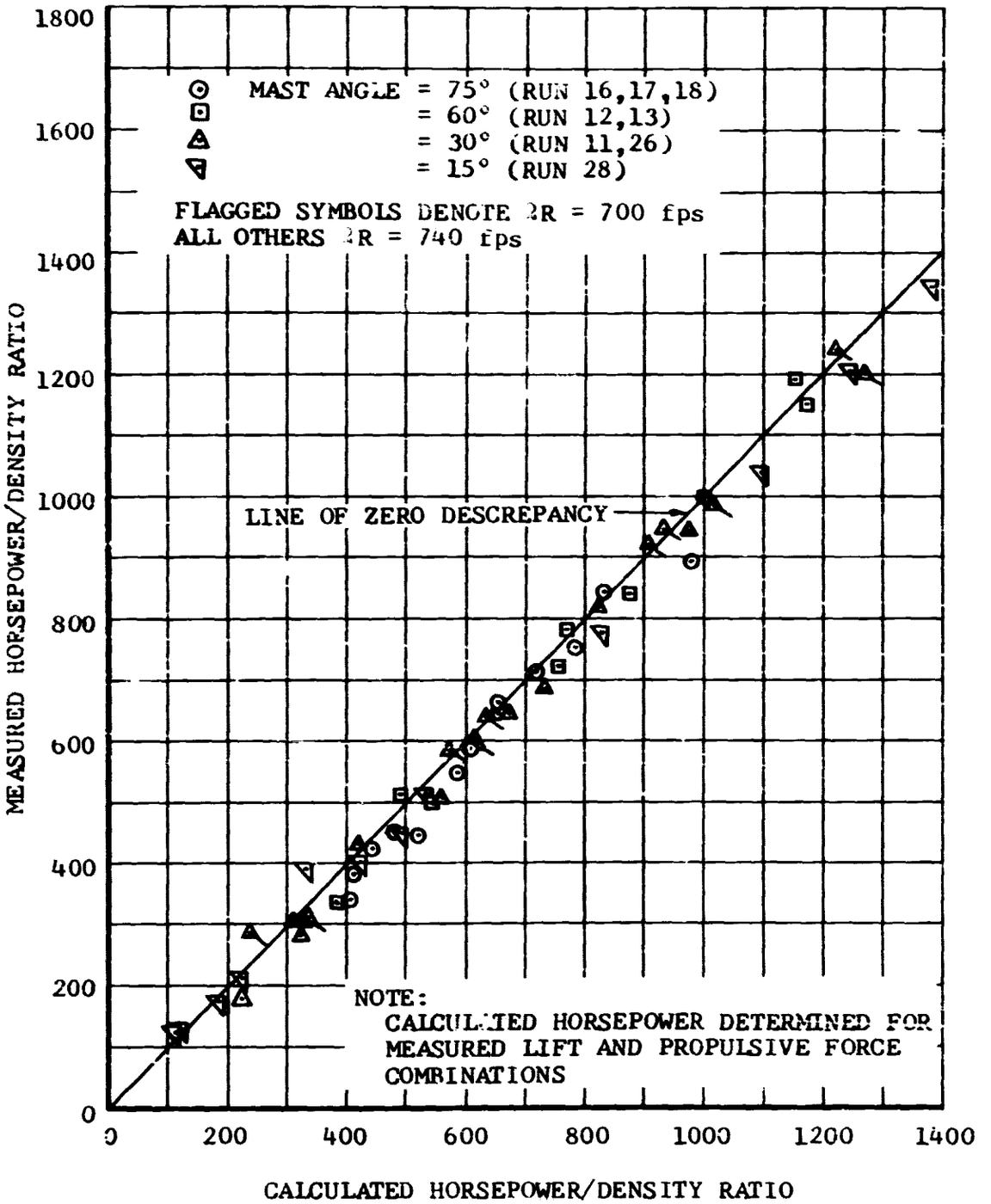

Figure IV-22. Comparison of Measured Horsepower with Calculated Horsepower, Helicopter-Conversion Mode.

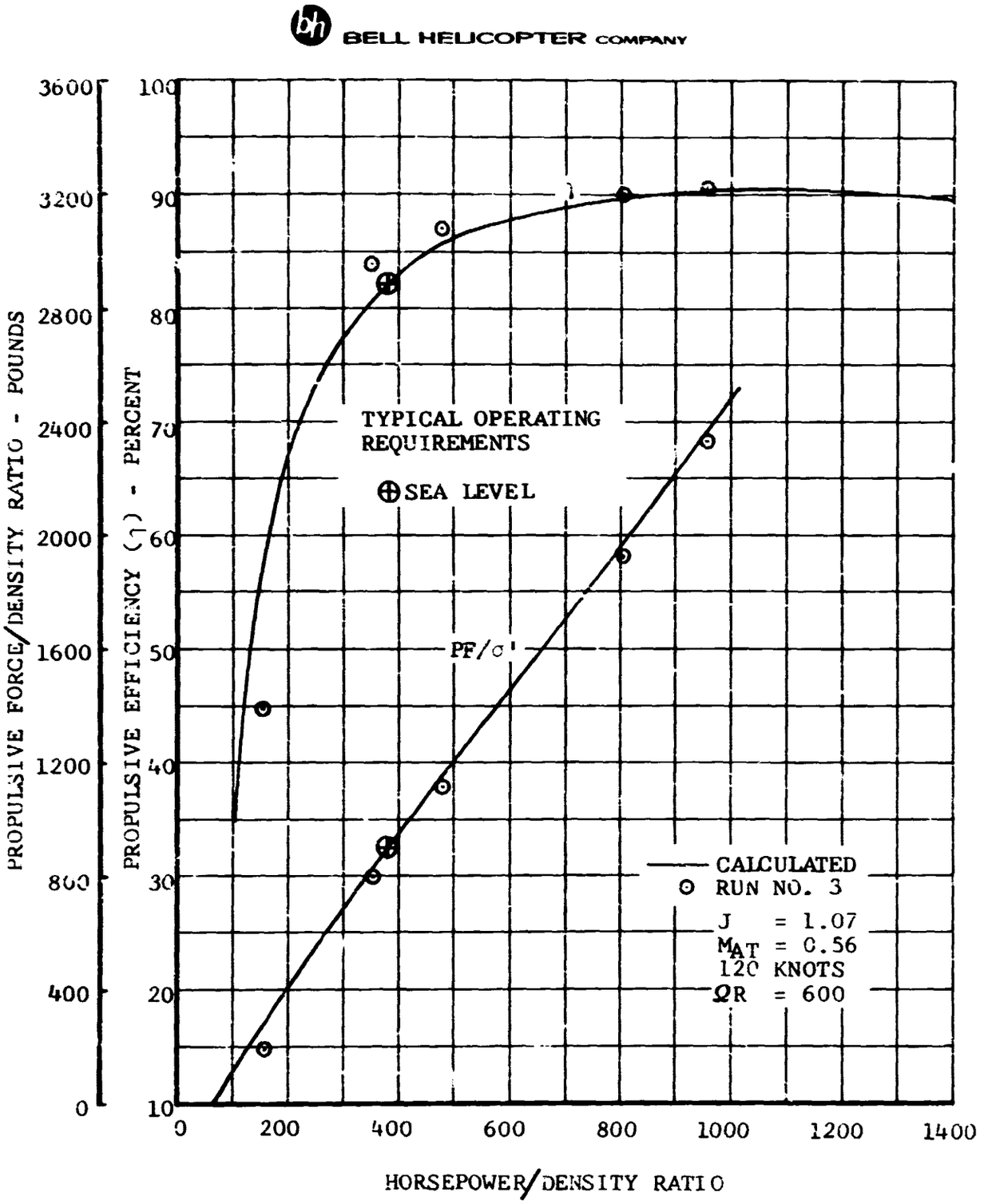

Figure IV-23. Propulsive Force and Efficiency Versus Horsepower, Airplane Mode.

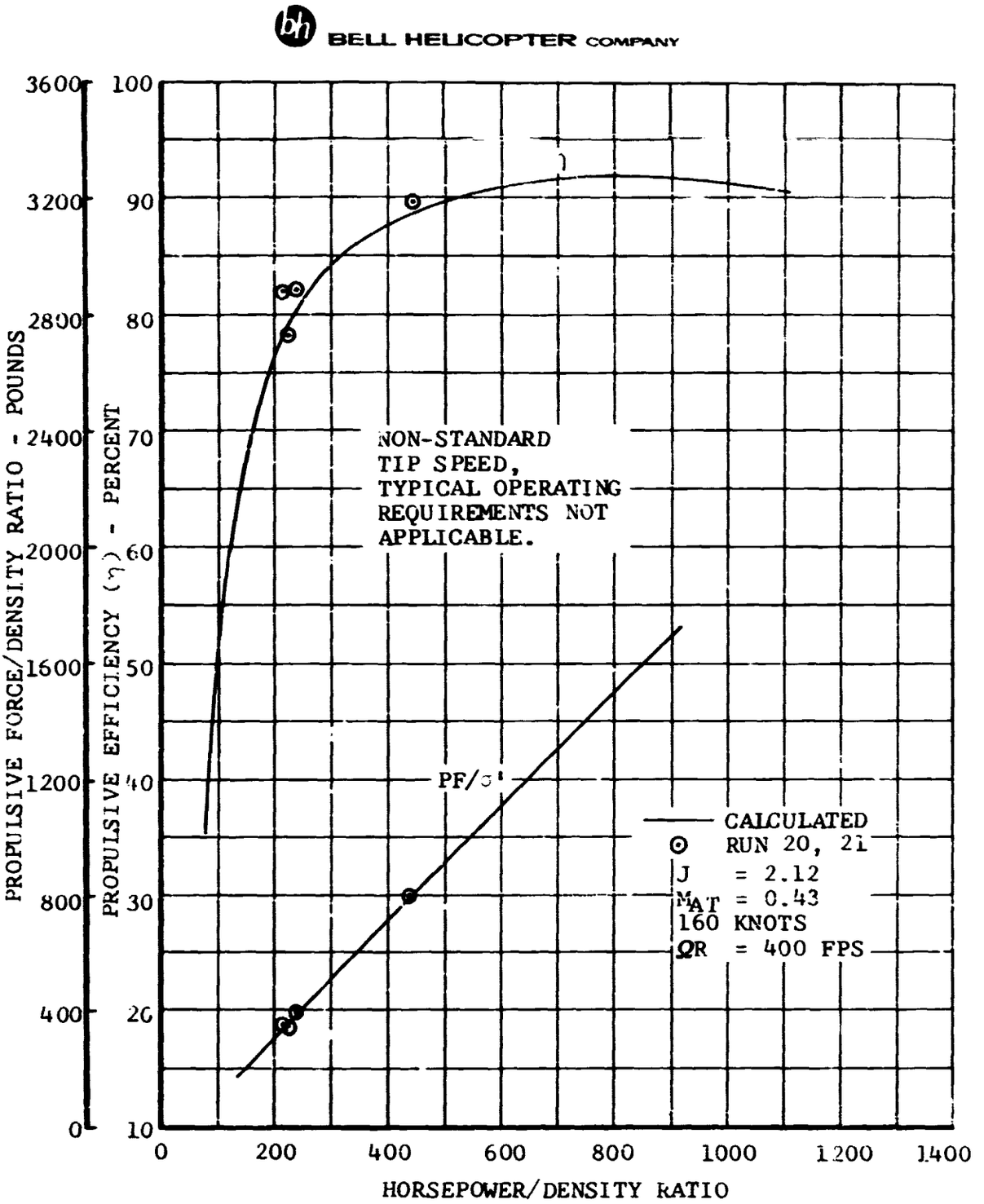

Figure IV-24. Propulsive Force and Efficiency Versus Horsepower, Airplane Mode.

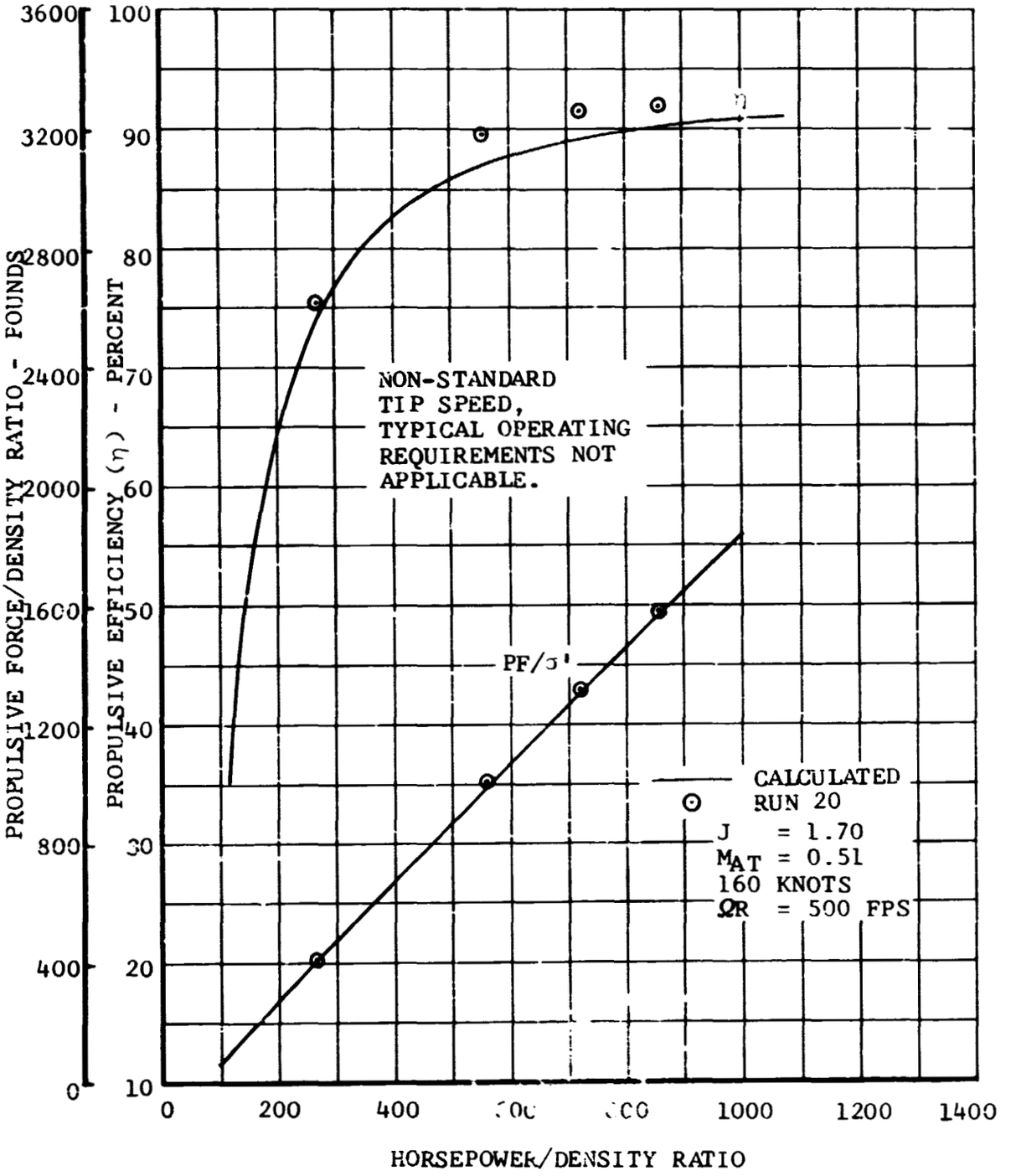

Figure IV-25. Propulsive Force and Efficiency Versus Horsepower, Airplane Mode.

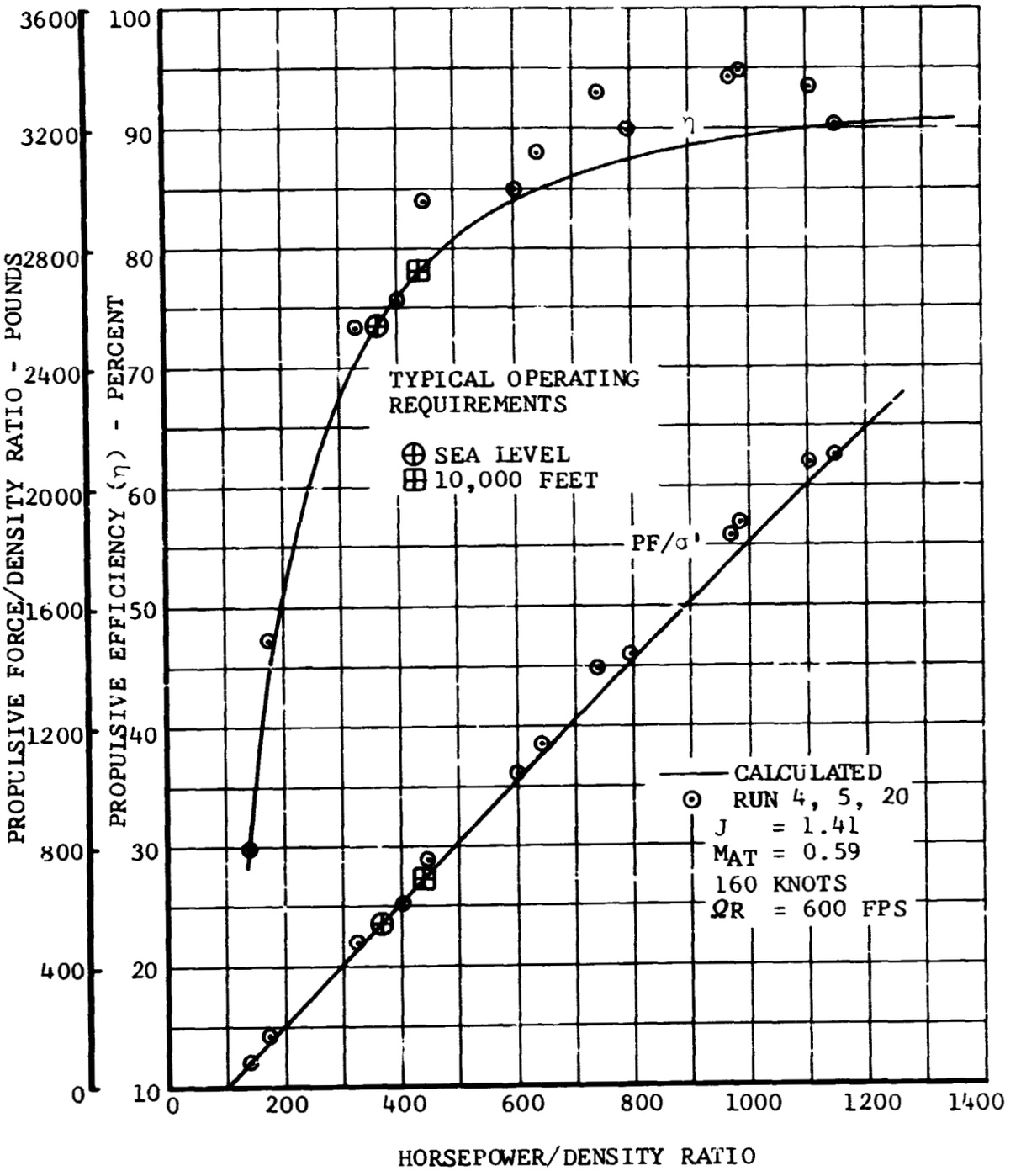

Figure IV-26. Propulsive Force and Efficiency Versus Horsepower, Airplane Mode.

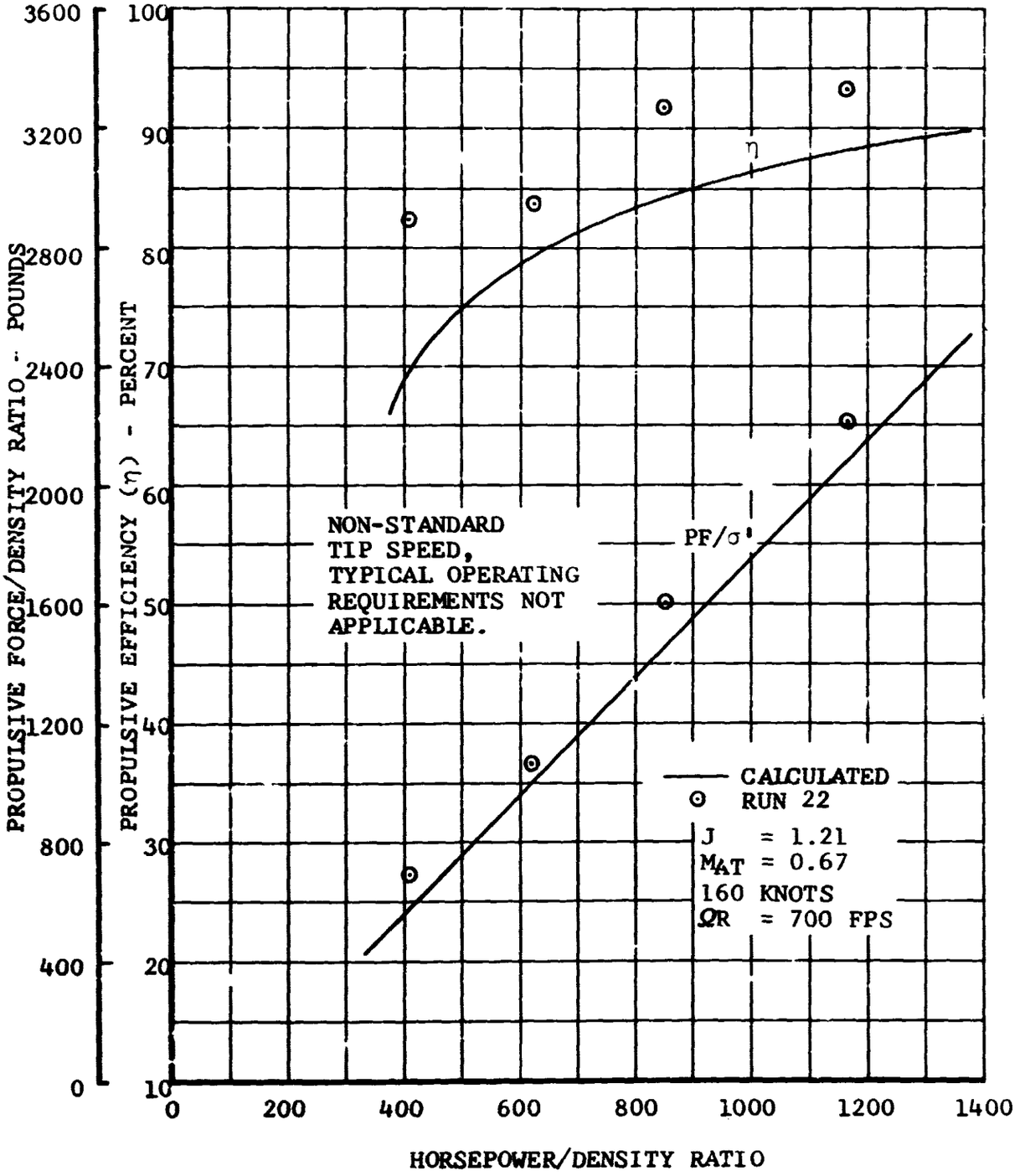

Figure IV-27. Propulsive Force and Efficiency Versus Horsepower, Airplane Mode.

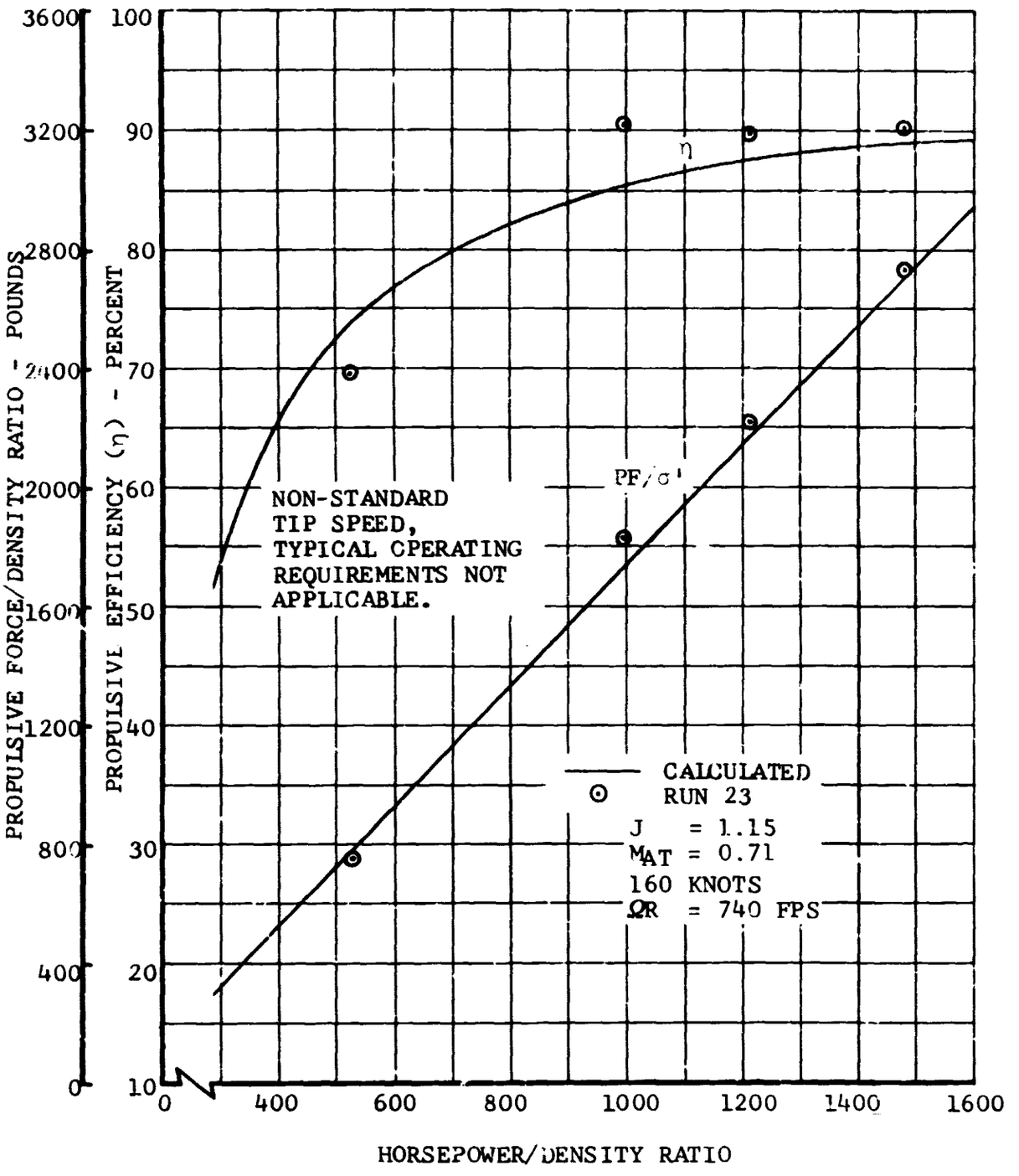

Figure IV-28. Propulsive Force and Efficiency Versus Horsepower, Airplane Mode.

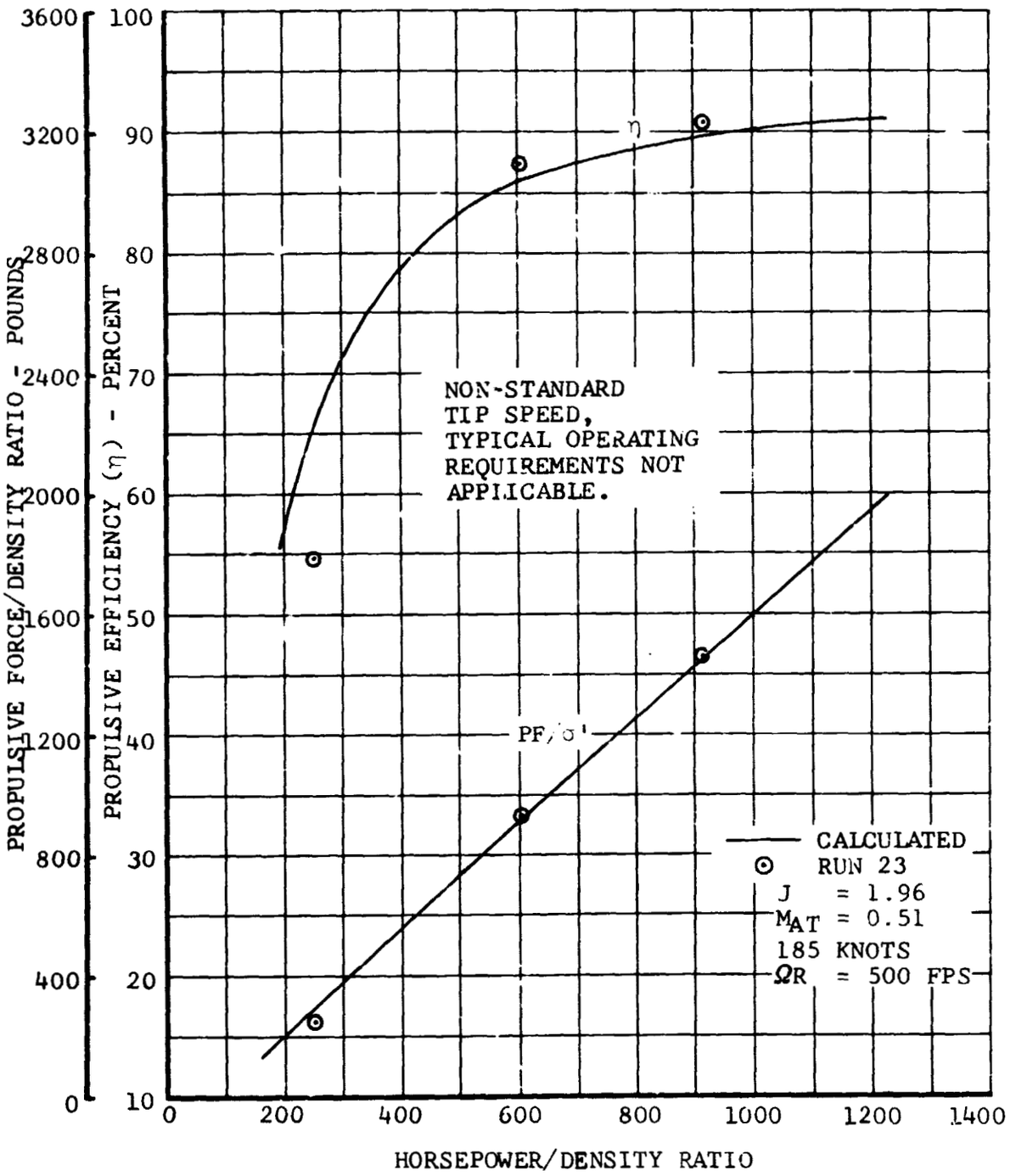

Figure IV-29. Propulsive Force and Efficiency Versus Horsepower, Airplane Mode.

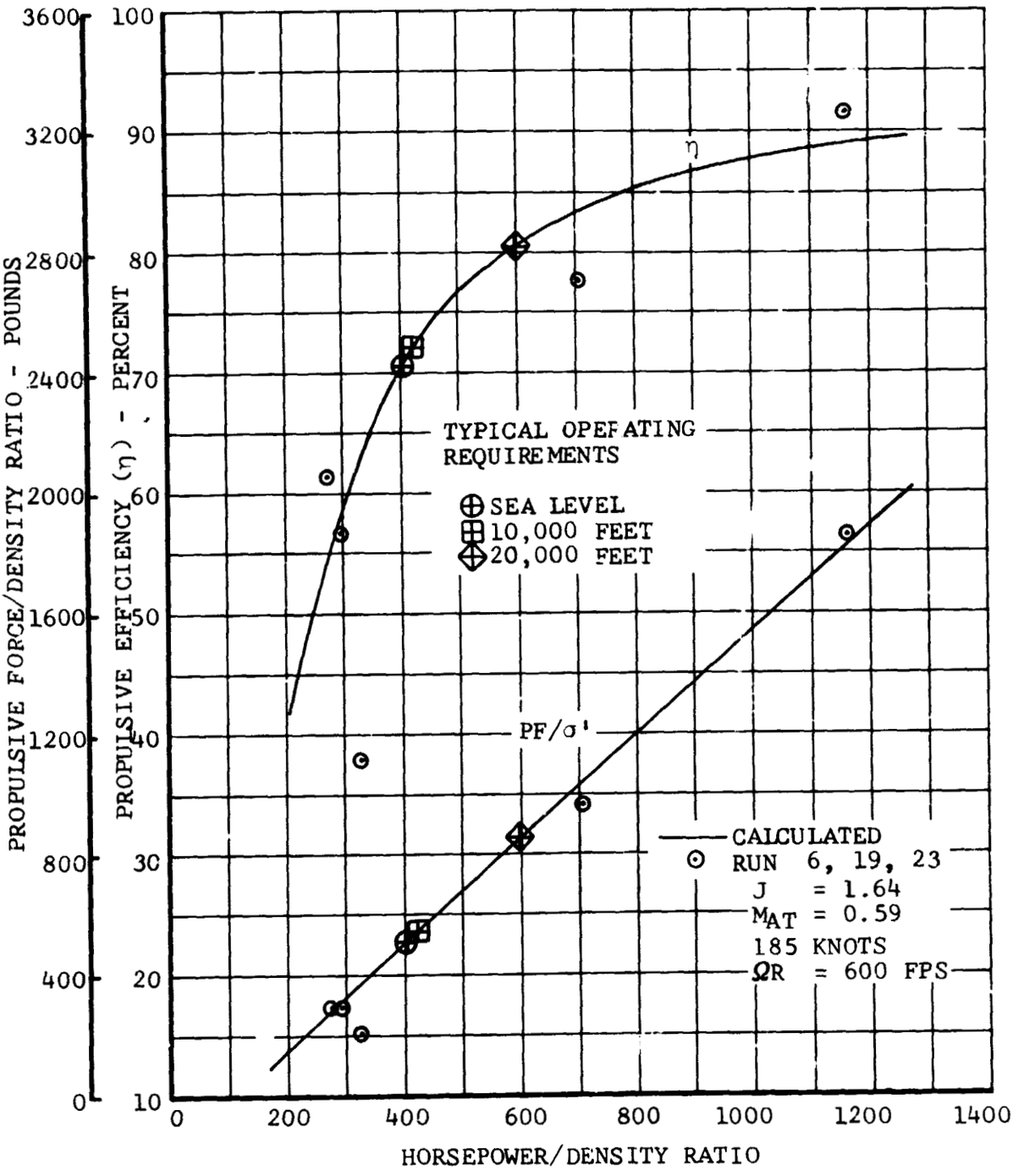

Figure IV-30. Propulsive Force and Efficiency Versus Horsepower, Airplane Mode.

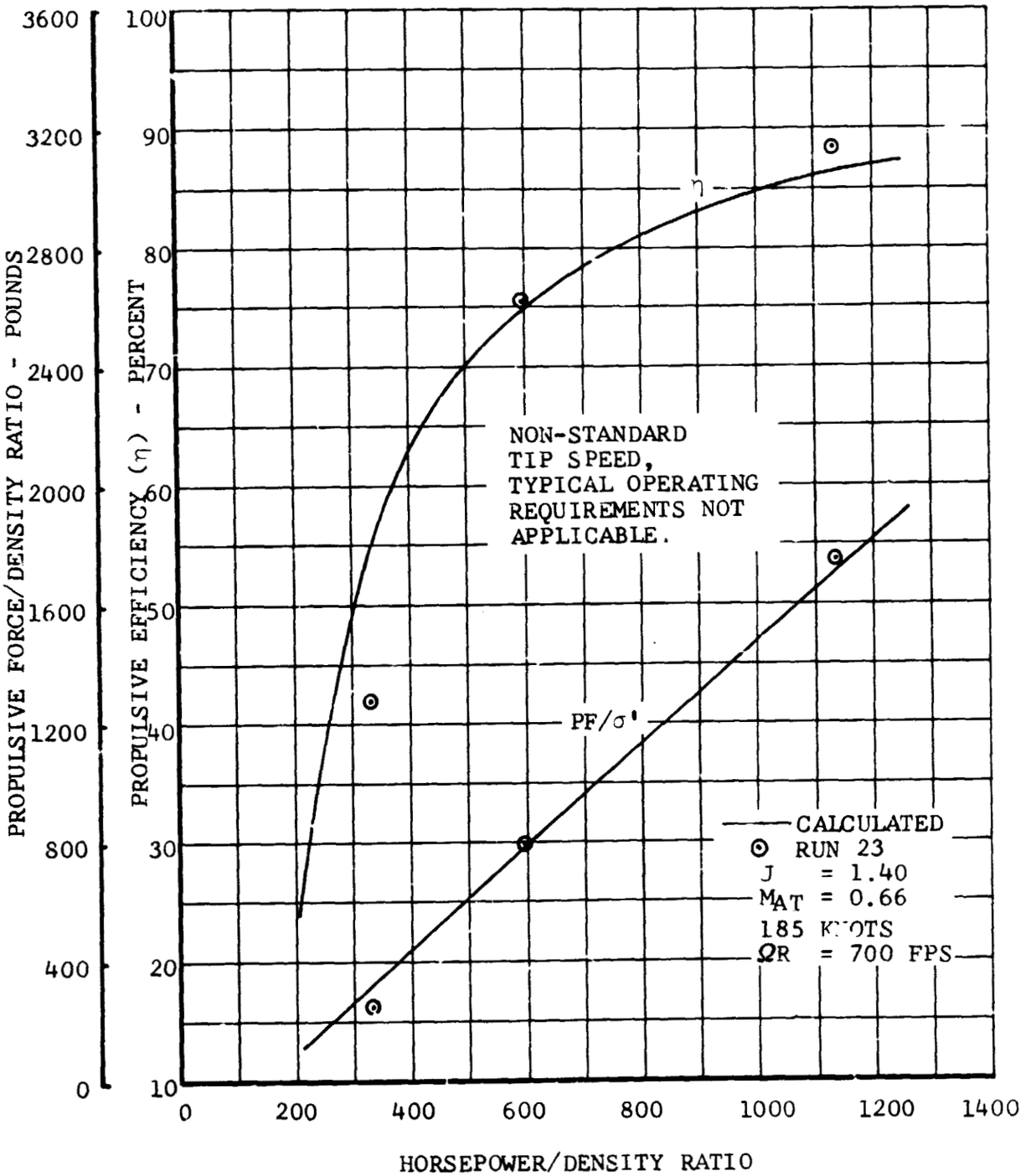

Figure IV-31. Propulsive Force and Efficiency Versus Horsepower, Airplane Mode.

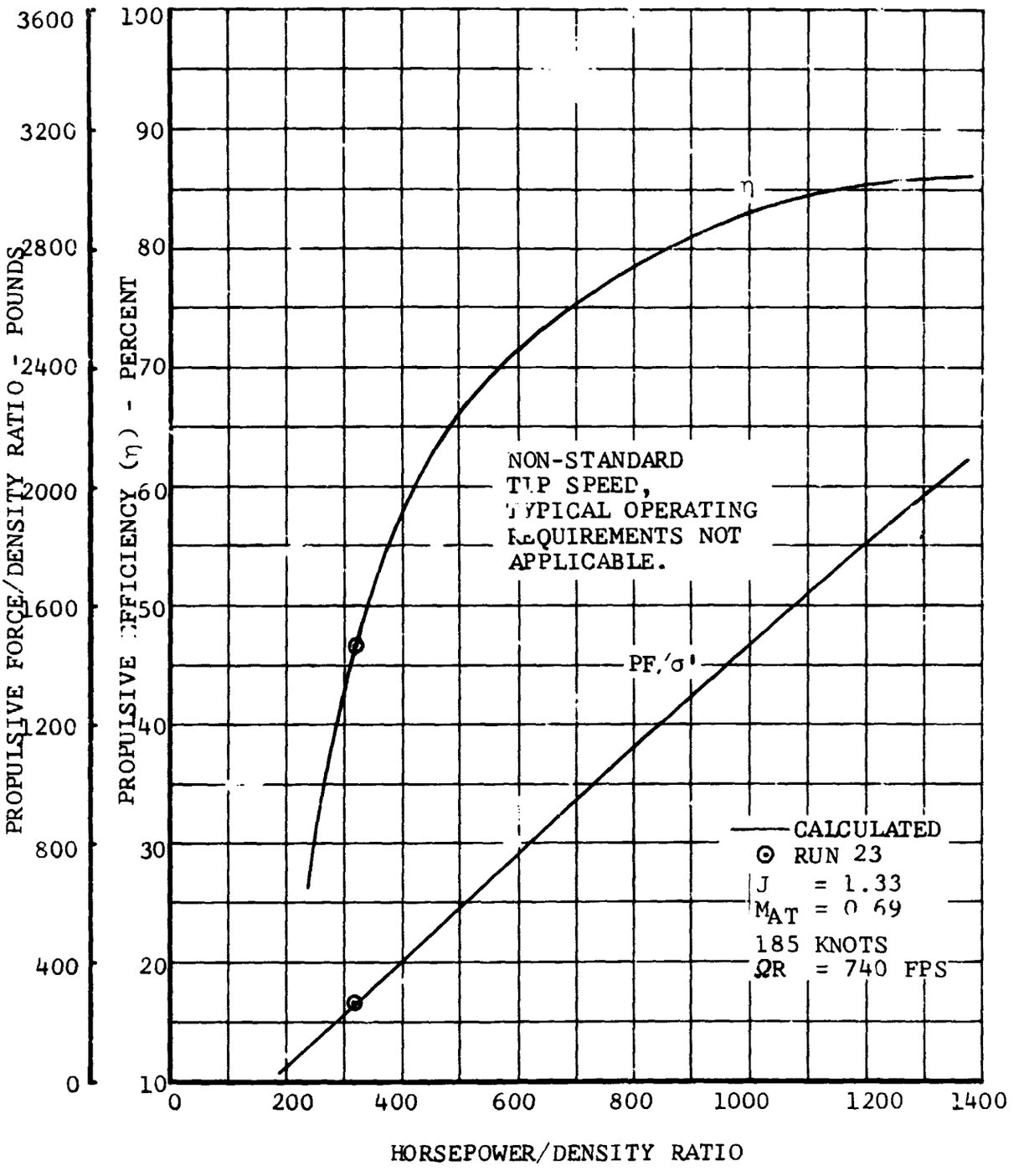

Figure IV-32. Propulsive Force and Efficiency Versus Horsepower, Airplane Mode.

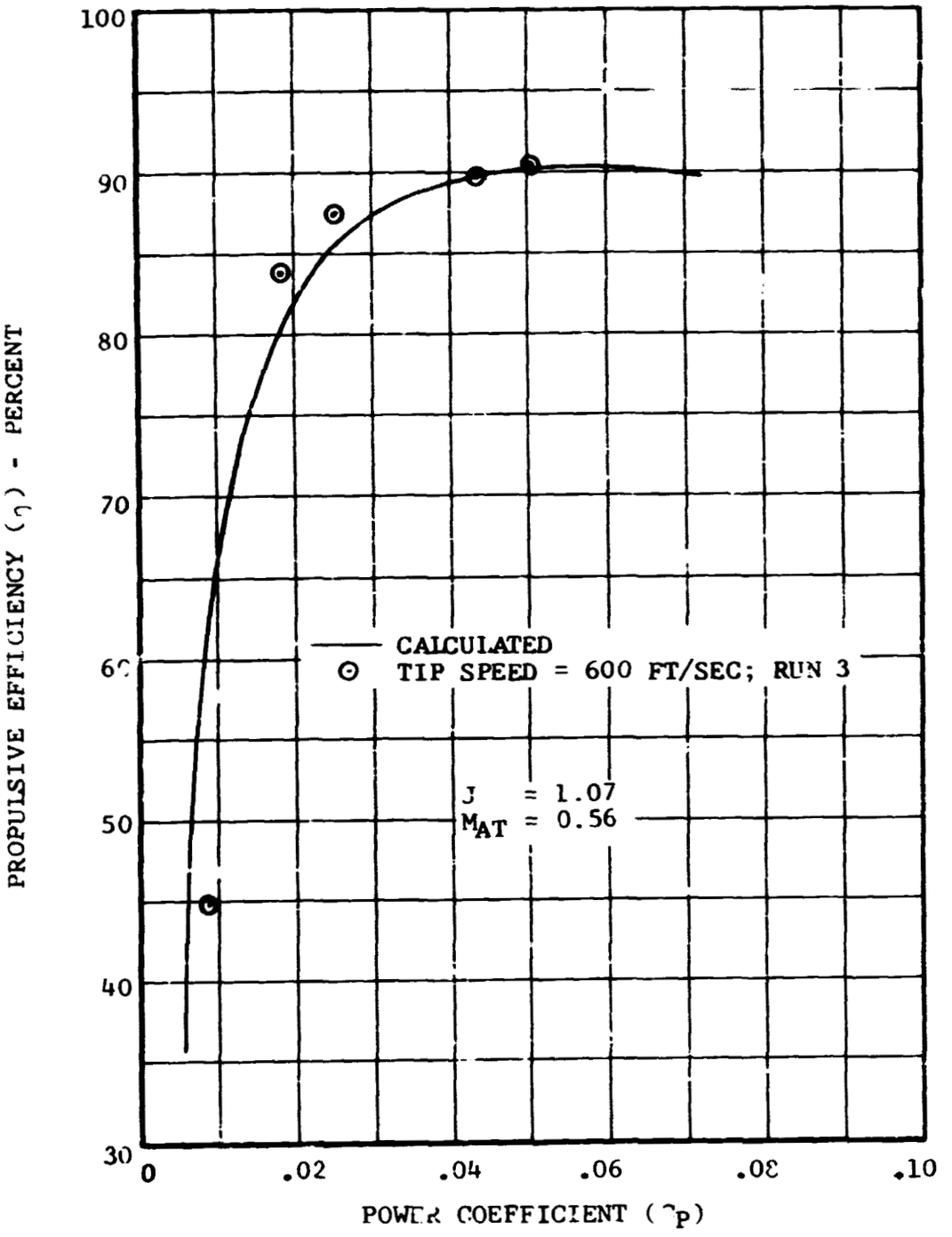

Figure IV-33 Propulsive Efficiency Versus Power Coefficient, 120 Knots, Airplane Mode.

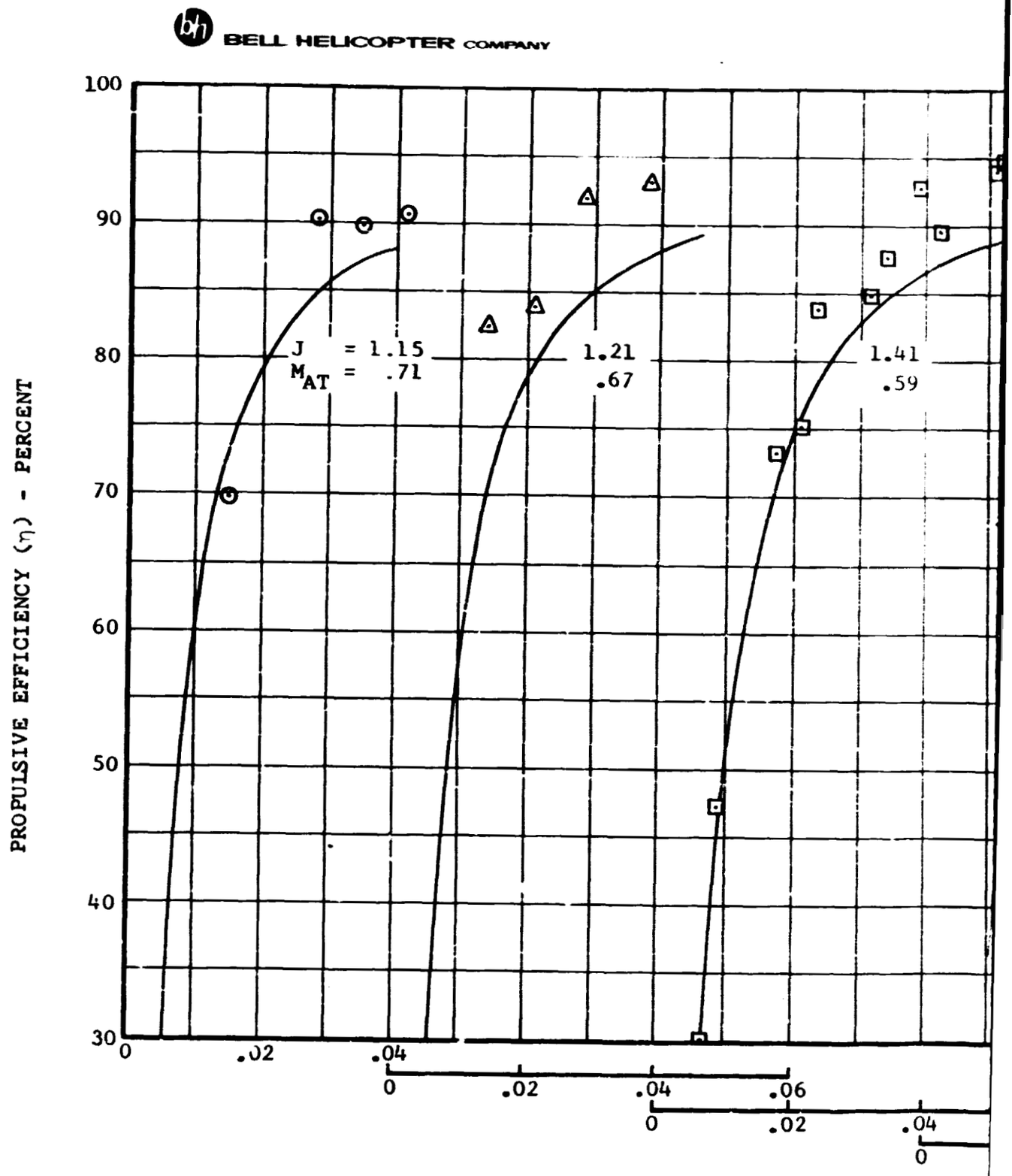

Figure IV-34. Propulsive Efficiency Versus Pow

FOLDOUT FRAME

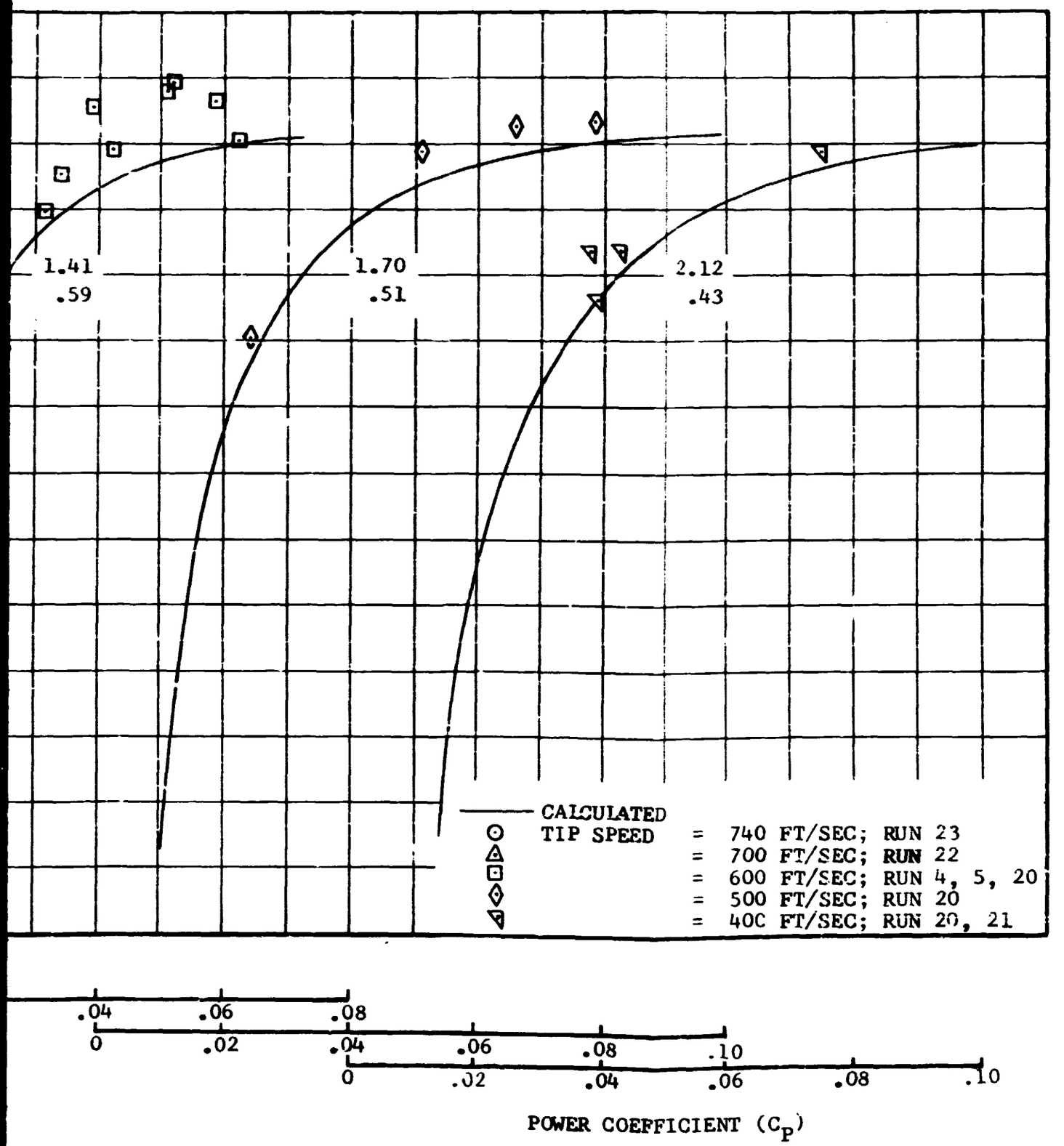

y Versus Power Coefficient and Advance Ratio, 160 Knots, Airplane Mode.

FOLDOUT FRA...

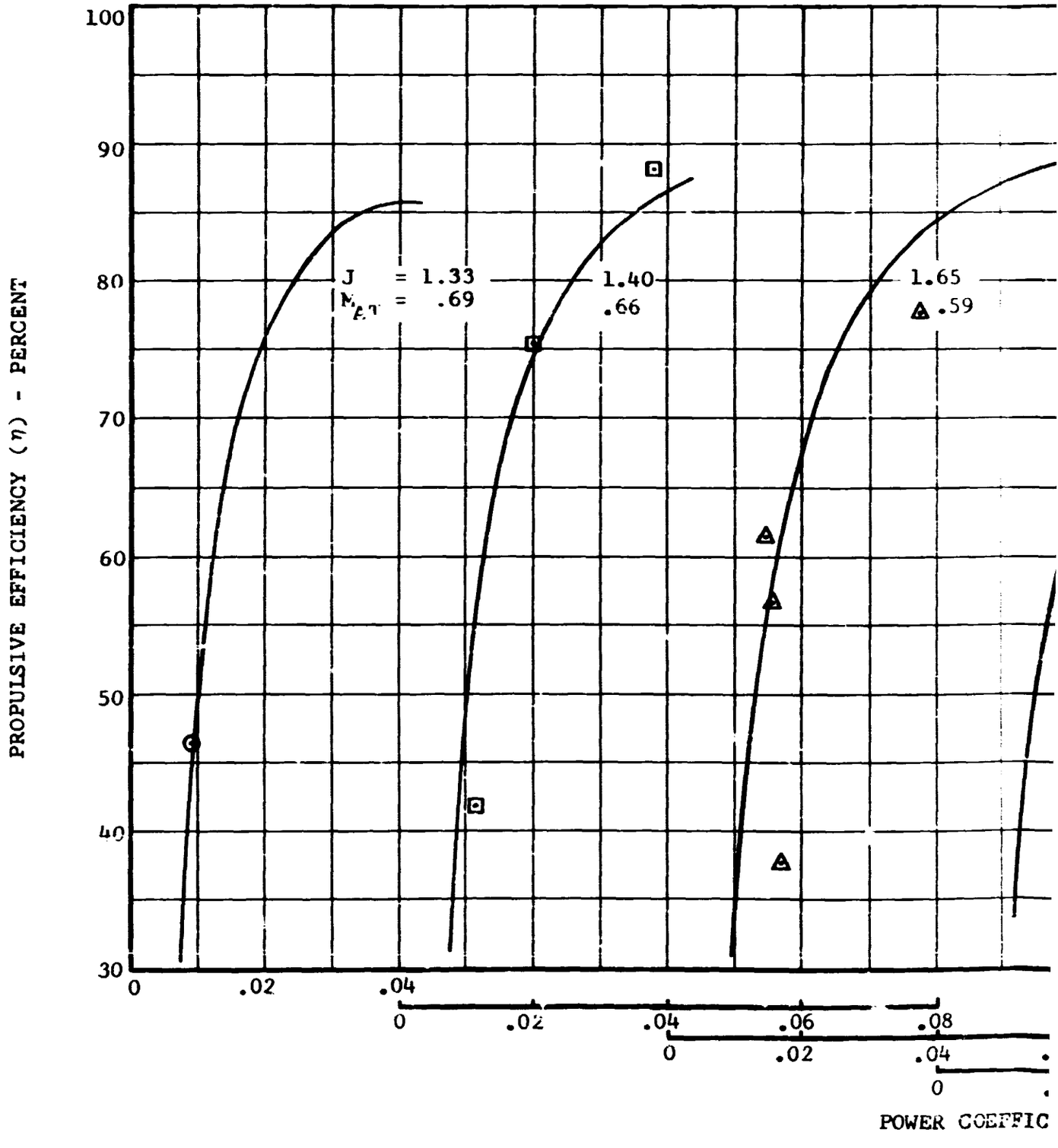

FOLDOUT FRAME

Figure IV-35. Propulsive Efficiency Versus Power C

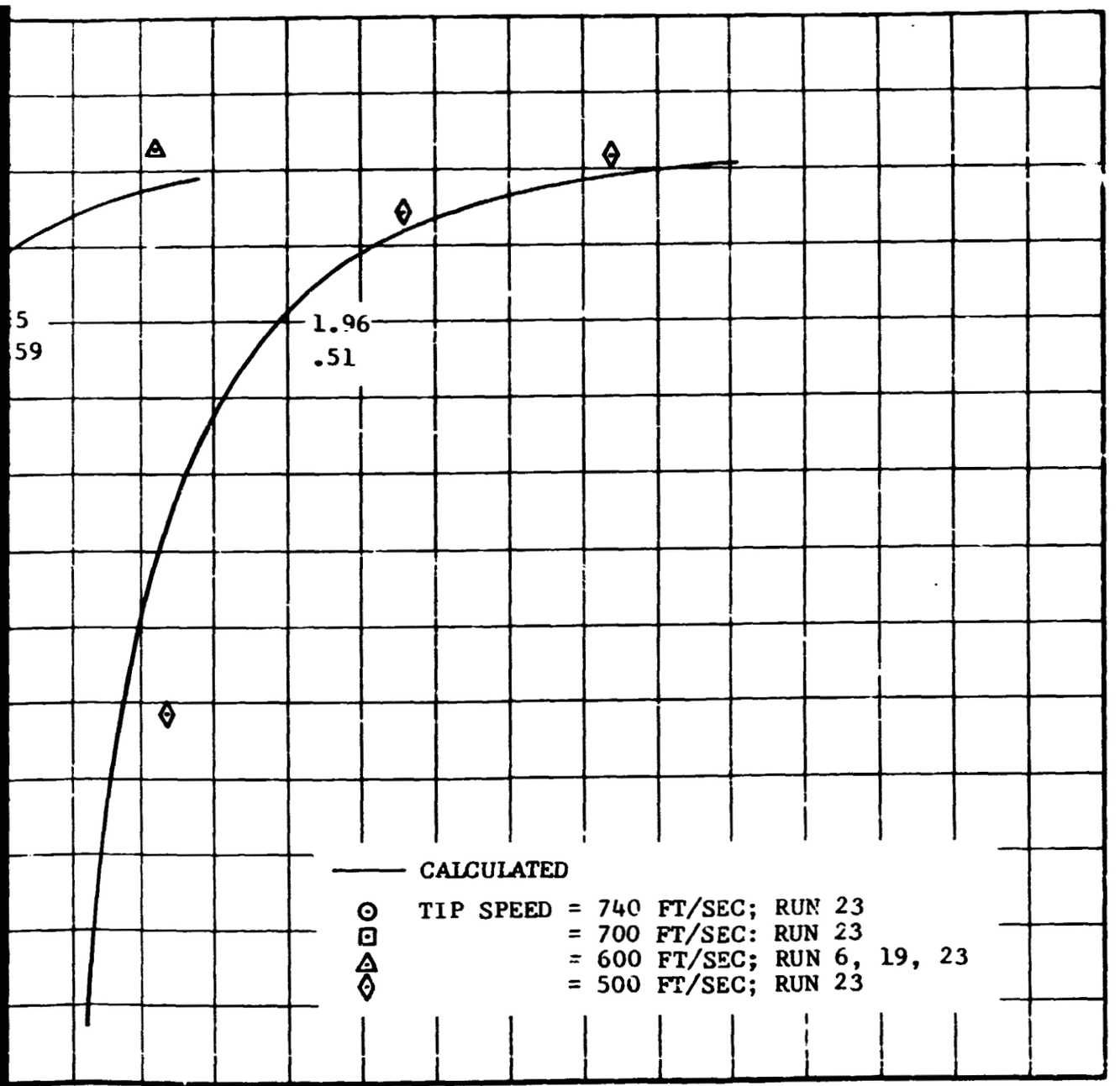

8
4 .06 .08
.02 .04 .06 .08 .10

COEFFICIENT (C_P)

Power Coefficient and Advance Ratio, 185 Knots, Airplane Mode.

FOLDOUT FRAME

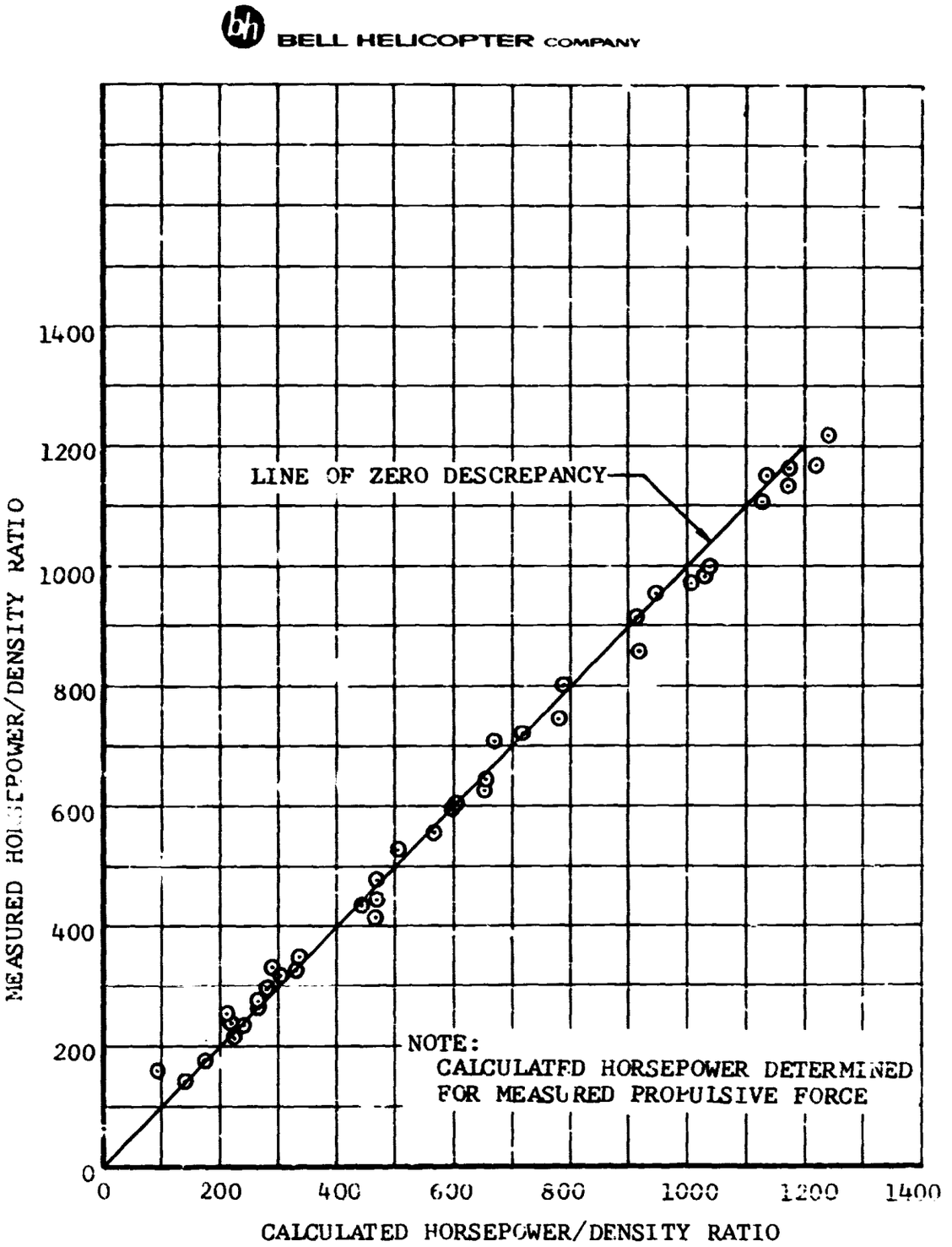

Figure IV-36. Comparison of Measured Horsepower with Calculated Horsepower, Airplane Mode.

V. DYNAMIC STABILITY

A. MODELING TECHNIQUES

1. Justification of Semispan Cantilever Model

Semispan cantilever models are often used in the study of fixed-wing aeroelastic problems. One reason for this is that the aeroelastic characteristics of the cantilever model are generally conservative (for example, flutter can be triggered at lower speeds on the cantilever model than on the free-free wing). Theory indicates that this is also true for proprotor/pylon dynamic stability (sometimes called whirl flutter). Figure V-1 compares the calculated variation of the characteristic roots of a semispan cantilever wing with airspeed with those of the complete aircraft. The modes are identified as being symmetric or asymmetric for clarity. The math model used for theory includes the fundamental beam, chord, and torsion modes of the wing, the proprotor flapping and first inplane bending modes. For the complete aircraft, the six rigid-body degrees of freedom and associated airframe aerodynamics are included, together with the drive system (including engine and interconnect shafting). The proprotor and airframe aerodynamics have been corrected for compressibility.

The most noteworthy difference between root loci of the cantilever wing and those of the complete aircraft is the lower frequency and damping of the wing beam, chord, and torsion modes of the cantilever wing. This indicates that the flutter characteristics of the cantilever wing will be conservative (as References 20 and 22 explain in some detail).

2. Reduced Stiffness Test Stand

For a portion of the dynamic tests, a test stand was used having a stiffness of one-fourth that of the normal design stiffness. The use of this stand and operation at one half the standard proprotor rpm preserves the frequency relationships between the blade flapping and wing modes and the proprotor inflow angles but not the blade elastic mode frequency relationships and compressibility effects on the proprotor aerodynamics. However, calculations indicate that the latter effects are not significant for proprotors where the lowest blade elastic mode is above one per rev and for airspeeds up to 400 knots. Figure V-2 compares the root variation with airspeed of the one-fourth-design-stiffness test stand with that for the cantilever wing of Figure V-1. The characteristics of the wing fundamental beam and chord mode roots are nearly identical, while those of the wing torsion mode are more heavily damped. The root characteristics of the blade flapping and inplane elastic modes are different, but the principal modes of interest are those of the wing beam and chord since they are the most lightly damped.

The damping of the wing fundamental beam and chord modes is compared further in Figure V-3. Note that the damping of modes on the one-fourth-stiffness stand is only slightly higher than that of the cantilever wing at airspeeds above 300 knots. This is due to compressibility effects not being fully represented in the one-fourth-stiffness stand. (Also shown in Figure V-3 is the small difference in damping when the standard stiffness hub restraint is used instead of the scaled one-quarter stiffness hub restraint, as was the case in the dynamic stability test.)

Clearly, the dynamic stability data from the one-fourth-design-stiffness test stand, along with that of the design-stiffness stand, can be used to forecast the dynamic stability characteristics of the complete aircraft.

Figure V-4 is a summary of the measured damping of the wing beam mode for both test stands up to a simulated airspeed of 408 knots. Note that the data for the one-fourth-design-stiffness stand are not at constant rpm; the collective pitch encountered its mechanical limit at a simulated 310 knots, hence rpm increased with increasing airspeed (constant inflow angle). The apparent fall-off in damping above 320 knots is due to the increasing rpm. For reference, the predicted damping is shown for constant rpm and for the test rpm range. Also shown in Figure V-4 are data from tests of a one-fifth-scale semispan aeroelastic model. These data confirm the high level of proprotor pylon stability predicted for the Model 300 aircraft.

B. TEST PROCEDURES

Most of the dynamic stability data were taken with the wind tunnel balance frame locked out. This was done because it had become apparent during the vibration survey of the design-stiffness test stand installation that there was relatively strong coupling between the stand modes and the balance modes. The frequencies of the fundamental beamwise, chordwise, and torsion modes were slightly lower with the balance free. Also, the damping of the wing chord mode was lower with the balance free. For the one-fourth-design-stiffness stand the lateral translation frequency of the balance (1.8 cps) was predicted to have strong coupling with the beamwise bending frequency of the stand (1.4 cps) and to influence the dynamic stability characteristics.

The frequency and damping of the test stand modes were determined at each data point by means of the two-square-foot aerodynamic vane located on the nacelle fairing (mounted vertically in the tunnel sense). The frequency of oscillation of the vane in pitch was adjusted at each point so as to force the selected mode at resonance. (A lissajous figure was generated on a dual-axis oscilloscope to locate resonant frequencies.) When the response was sufficiently high the vane excitation was turned off and the resulting decay of the test stand motion analyzed to determine

the mode frequency and damping. Figure V-5 shows a typical decay history and illustrates the method used to calculate frequency and damping.

This method proved highly satisfactory for the stand fundamental beam and torsion modes, but did not permit ready determination of the stand chordwise bending mode characteristics. In the case of the chordwise mode the excitation was low compared to the beamwise and torsion modes. However, it was also evident from the absence of any transient response in the chordwise bending mode that its damping was relatively high. (With the proprotor blades removed and replaced by equivalent weights, the chord mode damping was low and frequency and damping were measured.)

The system natural frequencies were also excited by oscillating the swashplate. This method was satisfactory, but had the same limitations as the aerodynamic vane insofar as the wing chord mode was concerned.

A frequency sweep in the frequency range of the proprotor flapping and blade inplane modes confirmed that these modes were heavily damped. Frequency sweeps up to 45 cycles per second showed little response in any modes other than the wing fundamental beam, chord, and torsion modes.

C. MEASURED STABILITY CHARACTERISTICS

1. Design-Stiffness Test Stand

The contribution of the wing and pylon airloads to the test stand stability characteristics was determined by removing the proprotor blades and replacing them with equivalent lumped weights. Frequency and damping were determined for wind speeds up to the tunnel maximum speed (204 knots) and for angles of attack up to 18 degrees at 100 knots and 8 degrees at 185 knots.

With the proprotor blades installed, wind speed and angle of attack sweeps were made, as well as proprotor rpm sweeps up to the overspeed rpm. Two pylon configurations were tested: (1) a configuration simulating the pylon-to-wing attachment when the pylon is fully converted so that a downstop is engaged (the yaw link in configuration), and (2) a configuration simulating a condition where the pylon is almost fully converted, but the downstop is not yet engaged (the yaw link out configuration). The dynamic stability was found to be essentially the same for both configurations.

Figures V-6 through V-8 summarize the measured variation in test stand beamwise, chordwise, and torsion mode damping with airspeed. The static frequency and damping are shown for each mode.

The influence of wing/mast angle of attack on the dynamic stability was measured at two airspeeds. The beam mode frequency

and damping variation with angle of attack at the higher airspeed, 185 knots, is shown in Figure V-9. The variation is negligible. Wing chord and torsion mode excitations were not made. The influence of proprotor rpm on beam mode stability is shown in Figure V-10.

2. One-Fourth-Design-Stiffness Test Stand

The contribution of the wing-pylon aerodynamics to the system frequency and damping was established by removing the blades and replacing them with equivalent weights. The wind speed was varied up to the tunnel maximum speed and mast angle of attack sweeps made at 92.5 knots (proprotor inflow equivalent to the 185 knot data from the design stiffness test) and 132.5 knots (simulated 265 knots).

The airspeed and mast angle of attack sweeps were repeated with the proprotor blades installed. In addition, proprotor rpm sweeps up to a simulated 1200 rpm were made at 150 and 170 knots, simulating 300 and 340 knots respectively. The pylon configuration tested simulated the pylon fully converted and on a downstop.

The variation in frequency and damping of the stand beam, chord, and torsion modes with wind speed is shown in Figures V-11 through V-13. Data from BHC tests of a one-fifth-scale dynamic model are shown, as well as the predicted frequency and damping. Note that the one-fourth-design-stiffness data are not for a constant rpm; the upper limit on the collective pitch was reached at a wind speed of 150 knots and the rpm therefore increased as wind speed increased (time considerations precluded reindexing the blade pitch horns to achieve the collective required for operation at 229 rpm up to the maximum tunnel speed). The downward trend in stability at wind speeds above 150 knots is associated with the increasing rpm. At a constant 229 rpm the stability would increase monotonically with wind speed as shown by the predicted damping at constant rpm. The limited data on the chord mode frequency and damping are due to the inability to excite the chord mode with the aerodynamic vane.

Figure V-14 shows the variation in frequency and damping of the wing beam mode with angle of attack at a simulated airspeed of 265 knots. The angle of attack data taken at 92.5 knots were in good agreement with the 185-knot design-stiffness stand data.

The measured variation in frequency and damping of the wing beam mode with proprotor rpm at 150 knots and 170 knots is shown in Figures V-15 and V-16, respectively. The damping trend with rpm for the 170-knot (340 knots simulated) condition indicated that neutral stability would occur at a somewhat higher rpm than the maximum tested. The maximum tested was 420 rpm and simulated 840 rpm, or 180 percent of the normal operating rpm. Damping of the wing torsion mode showed a similar reaction to rpm, as shown in Figure V-17.

D. CORRELATION OF THEORY WITH MEASURED DYNAMIC STABILITY CHARACTERISTICS

For each test condition the frequency and damping of the test stand modes were predicted by means of two independent analyses. These predicted characteristics are shown in Figures V-6 through V-17. The linear analysis, BHC Proprotor Stability Analysis, DYN4 (computer program DRAL06), is based upon perturbation theory. The nonlinear analysis, BHC Proprotor Aeroelastic Analysis, DYN5 (computer program ARAP08), is based on nonlinear open-form theory. A brief description of each analysis is given in the paragraphs below. Complete detail, including the equations of motion, is contained in References 27 and 28.

- Proprotor Stability Analysis, DYN4

  Program DYN4 is a linear, twenty-one-degree-of-freedom proprotor stability analysis. It can determine the proprotor/pylon, blade motion, and flight mode stability characteristics of a tilt-rotor vehicle. A tip-path-plane representation is used for the proprotor, and linear aerodynamic functions are assumed. Details such as pitch-axis preconing, underslinging, pitch-flap coupling, and flapping restraint are included. The first inplane blade mode is represented. Control system flexibility may also be simulated. Five coupled wing/pylon elastic modes are represented: wing beam, chord, and torsion, and pylon pitch and yaw. Six rigid body degrees of freedom are included to allow simulation of free-free body conditions and the aircraft short period flight modes.

  Inputs to DYN4 are lumped parameters describing the dimensions, inertia, stiffness, and kinematics of the aircraft being simulated. Standard aircraft stability derivatives are used to study the influence of the proprotors and the wing/pylon dynamics on the stability of the flight modes. Outputs are system eigenvalues and eigenvectors. Root loci can be plotted automatically.

- Proprotor Aerolastic Analysis, DYN5

  Program DYN5 is a nonlinear, open-form proprotor aeroelastic analysis that uses the same basic mathematical model as DYN4. This program calculates proprotor loads, vibration, and stability in helicopter, conversion, and high-speed modes. A special version of the program was developed for the Air Force under Contract F33615-69-C-1339, "Vibration in V/STOL Aircraft," Reference 28.

  The dynamic equations of motion were derived using the Lagrangian method. Provisions for large flapping and feathering motion are included in DYN5. Small angle

assumptions are made on the wing-pylon and blade elastic degrees of freedom. The aerodynamic functions used in DYN5 are the same as those used in the Bell Rotor Performance Analysis, F35. C_l, C_d, and C_m are input in tabular form for a 180-degree range of angle of attack and for Mach numbers up to 0.9. Tables for different profiles may be input to account for differences in the blade section from root to tip, thereby properly accounting for blade stall and compressibility effects.

DYN5 is programmed for solution by digital computer. A predictor-corrector integration technique is used in the solution of the simultaneous equations of motion; integration interval may be varied as a function of azimuth. Input to the program consists of lumped parameters and the coupled normal modes of the wing, pylon, and proprotor. The output consists of a time history of the wing and pylon motions, and the blade flapping and elastic deflection. Generally, initial conditions are input to minimize the time required for convergence to steady state trim. For stability investigations, the transient response to external inputs or to initial conditions can be calculated.

Figures V-11 through V-16 show frequency and damping data from BHC tests of a one-fifth-scale aeroelastic model. These data justify the hypothesis that proprotor dynamic behavior can be predicted by means of smaller scale models or a minimum-sized research aircraft.

In general the correlation is excellent. The nonlinear analysis is in better agreement with the actual damping than is the linear analysis, but both analyses are conservative. While few measured data on the wing chord mode were obtained, the excellent correlation with regard to the wing beam mode indicates that the stability of the chord mode can be predicted. Furthermore, the one-fifth-scale model chord mode characteristics are in good agreement with theory.

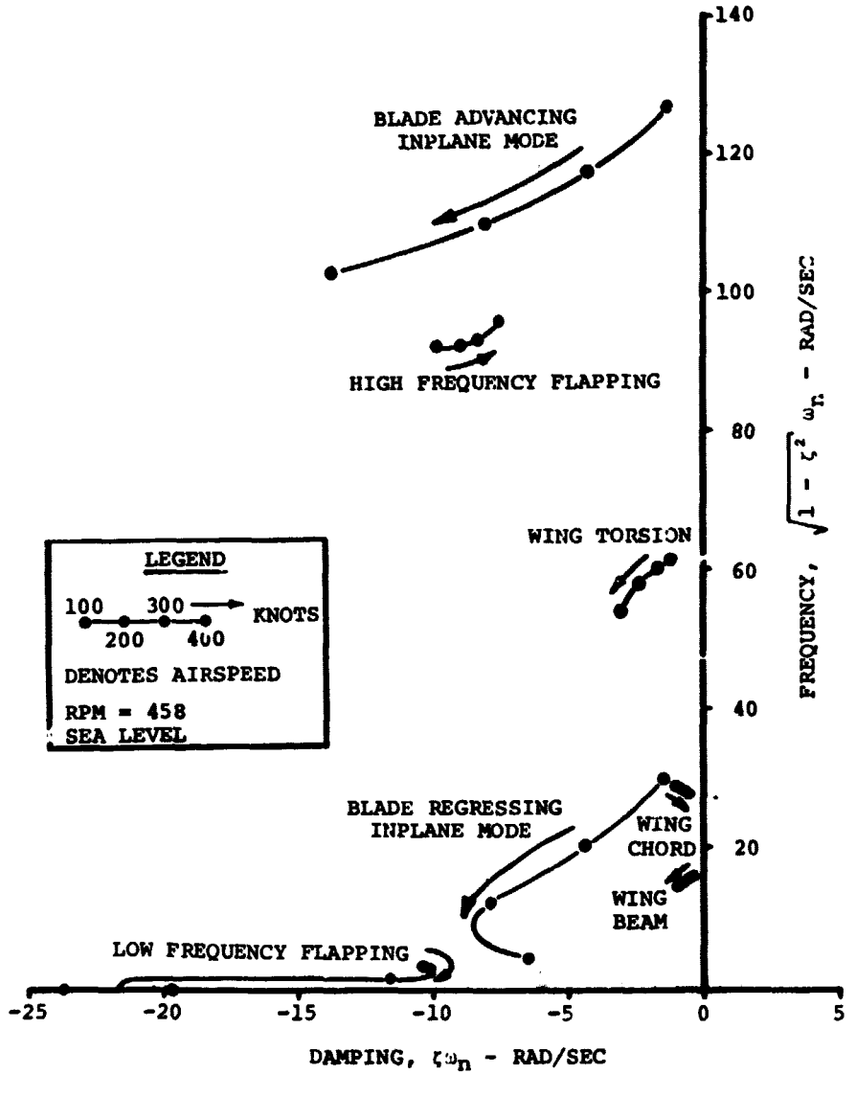

(a) CANTILEVER WING (DYNAMIC TEST STAND)

Figure V-1. Root Loci of Cantilever Wing Comp

300-099-004

FOLDOUT FRAME

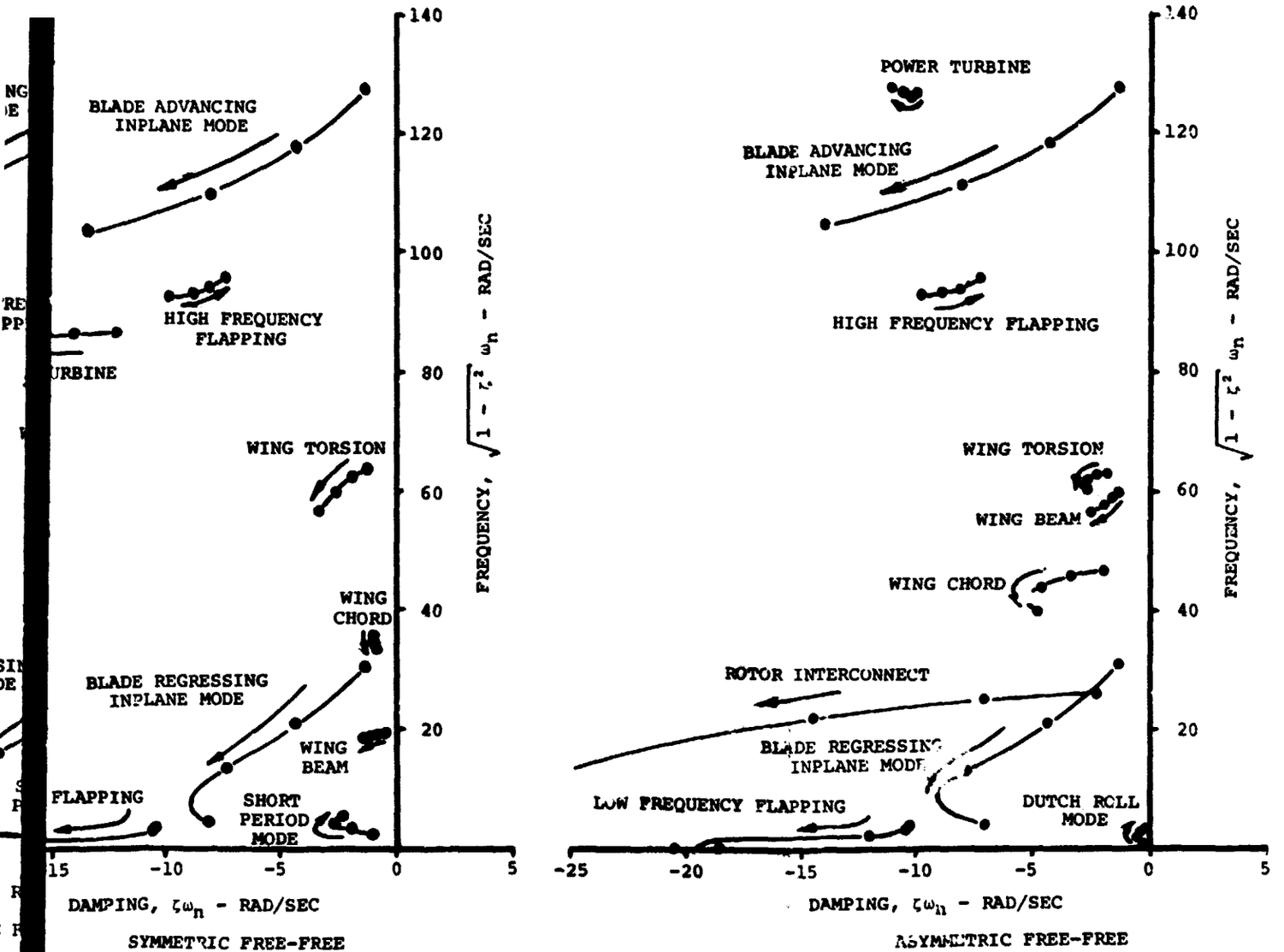

(b) COMPLETE AIRCRAFT

tilever Wing Compared to Complete Aircraft Root Loci.

FOLDOUT FRAME 2

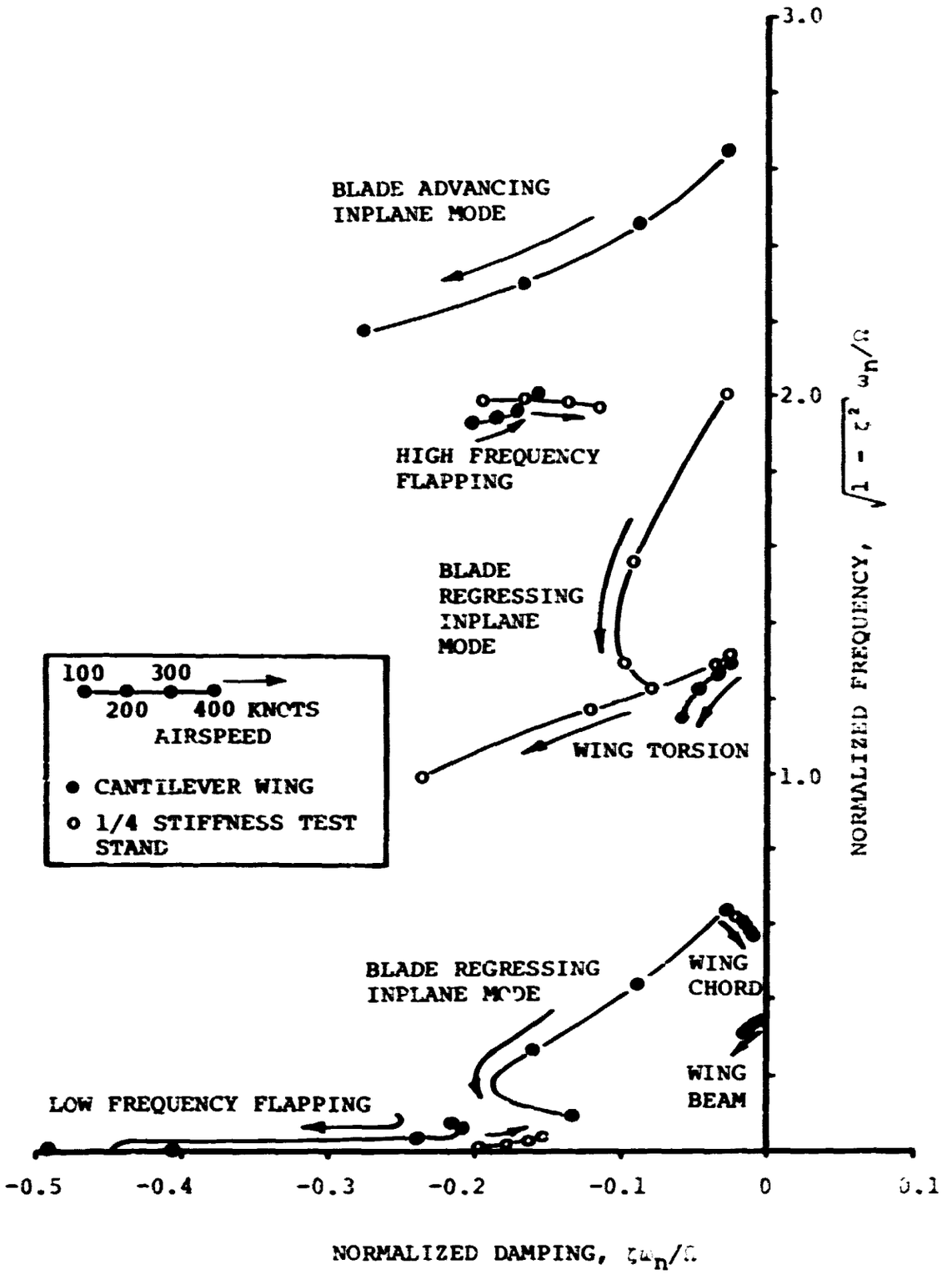

Figure V-2. Comparison of Root Loci for Semispan Cantilever Wing and One-Fourth-Stiffness Test Stand.

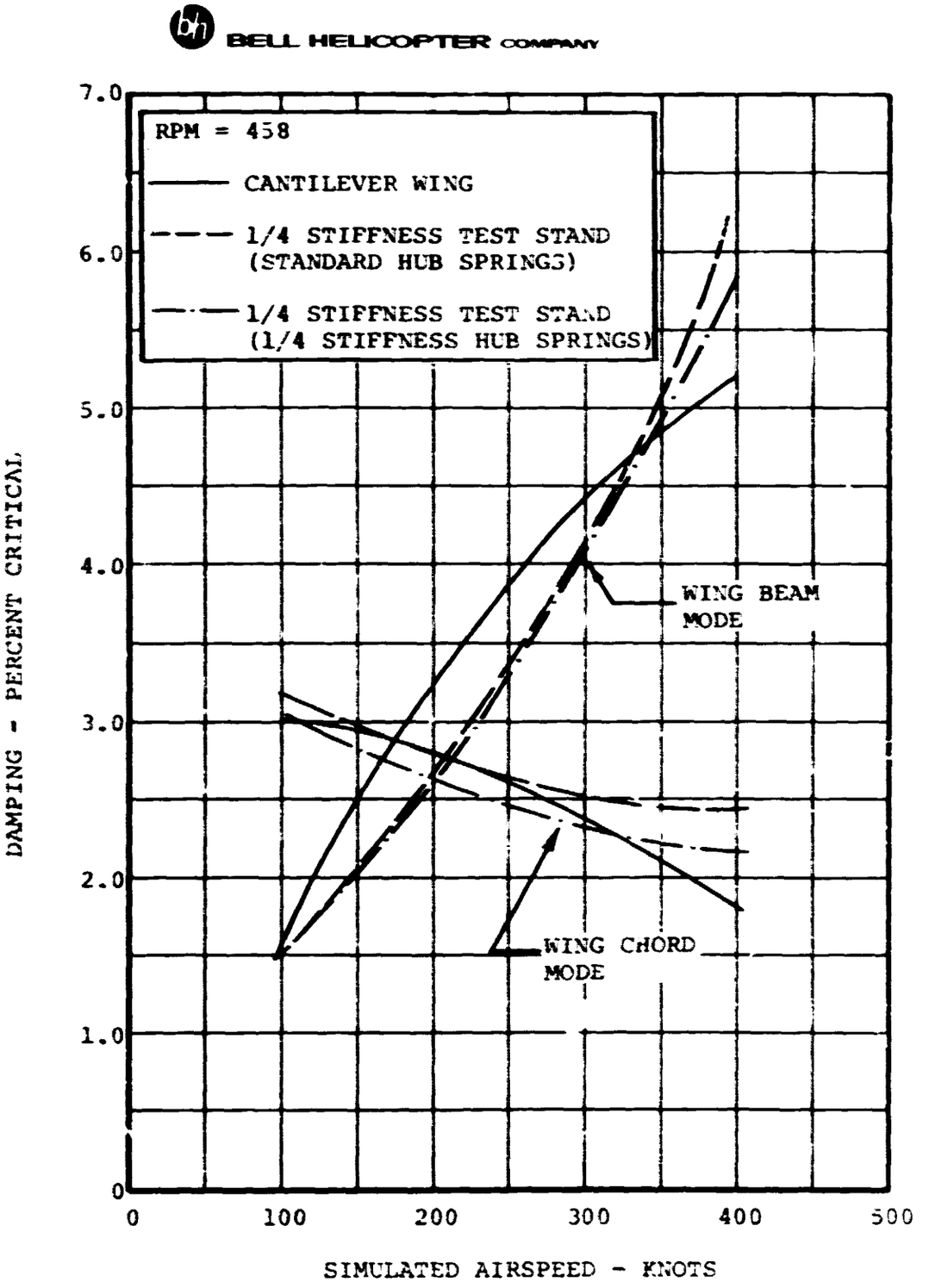

Figure V-3. Wing Beam and Chord Damping Versus Simulated Airspeed.

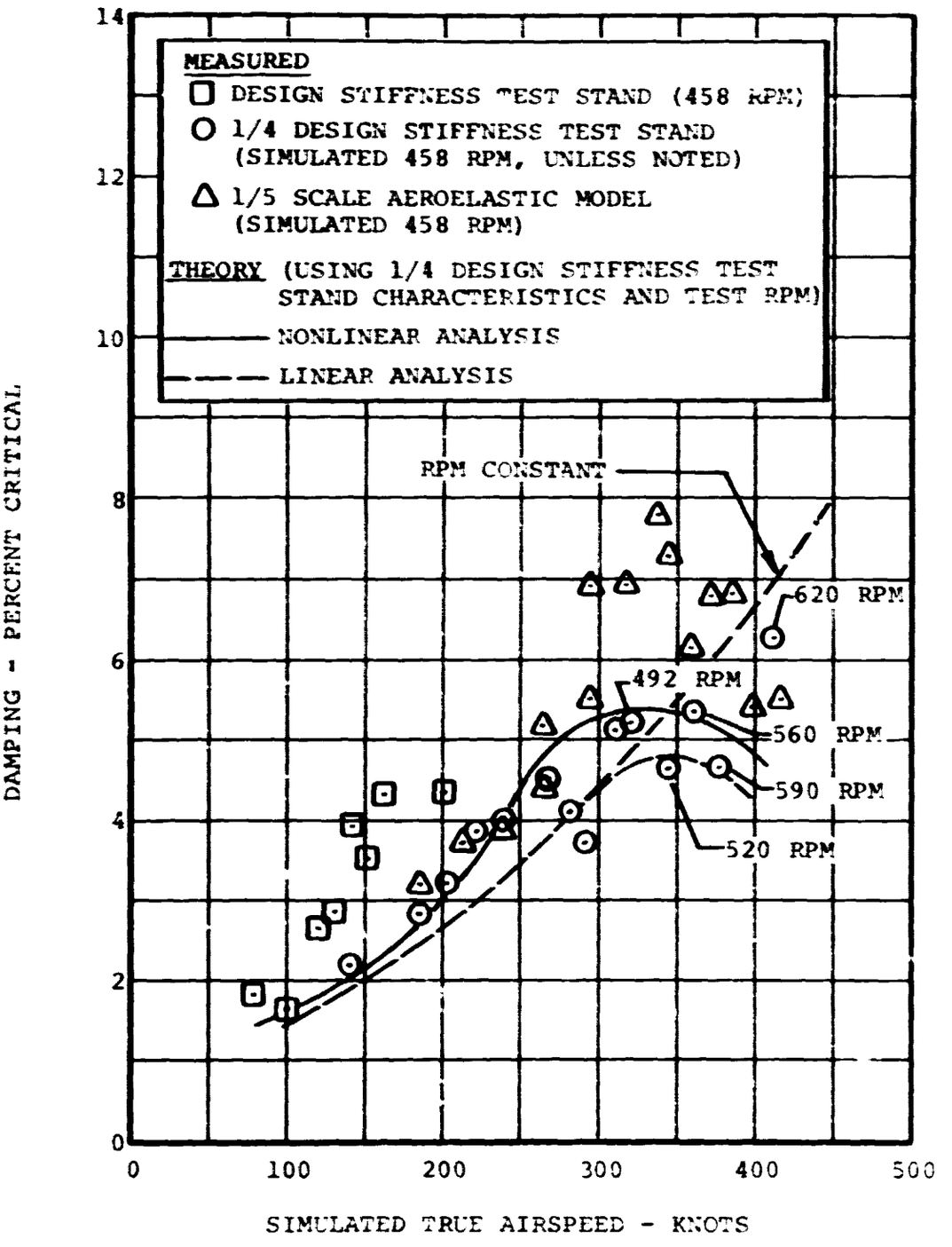

Figure V-4. Wing Beam Bending Mode Stability versus Airspeed.

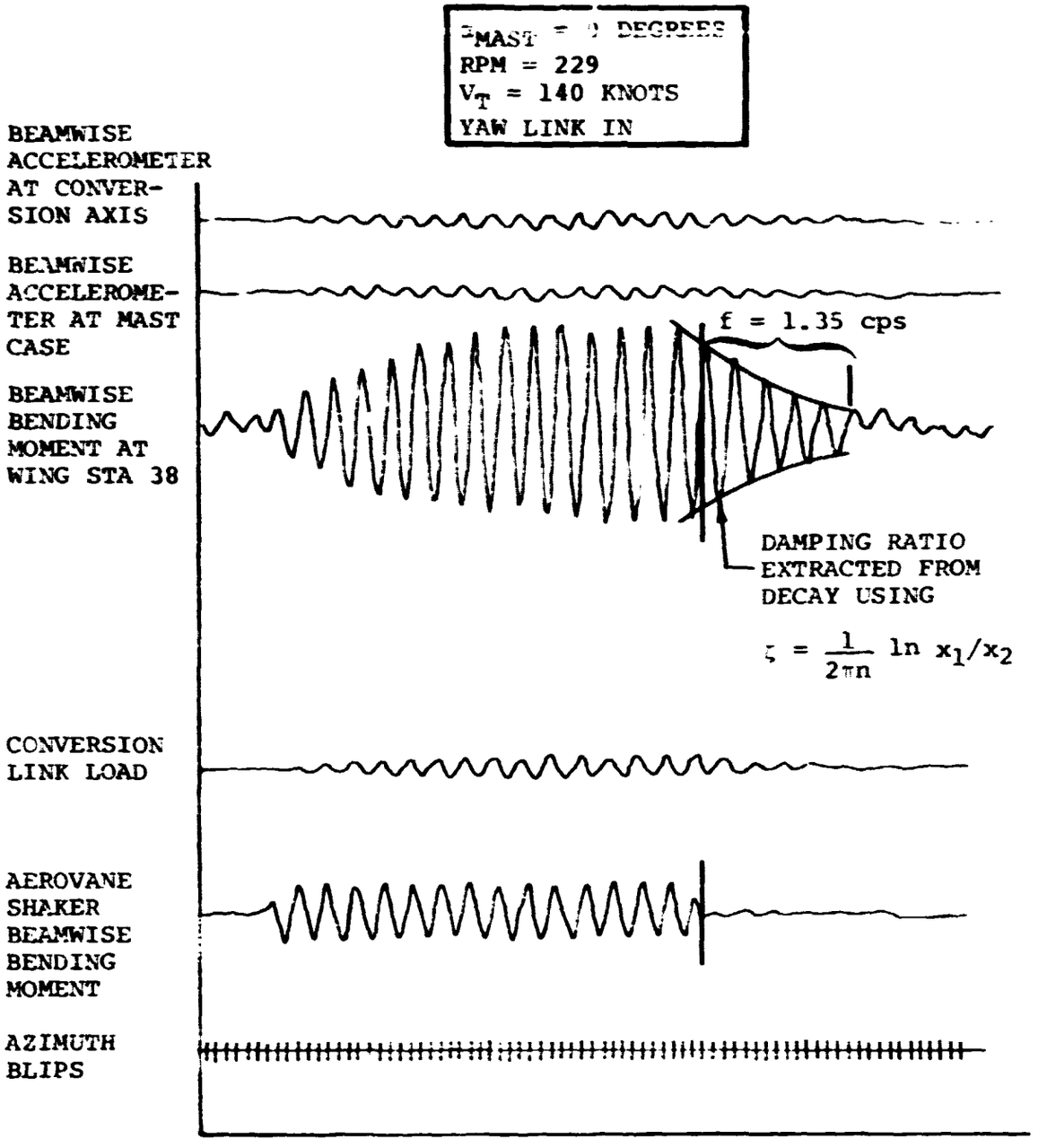

Figure V-5. Traces of Decay of Wing Beam Vibrations for One-Fourth-Stiffness Test Stand.

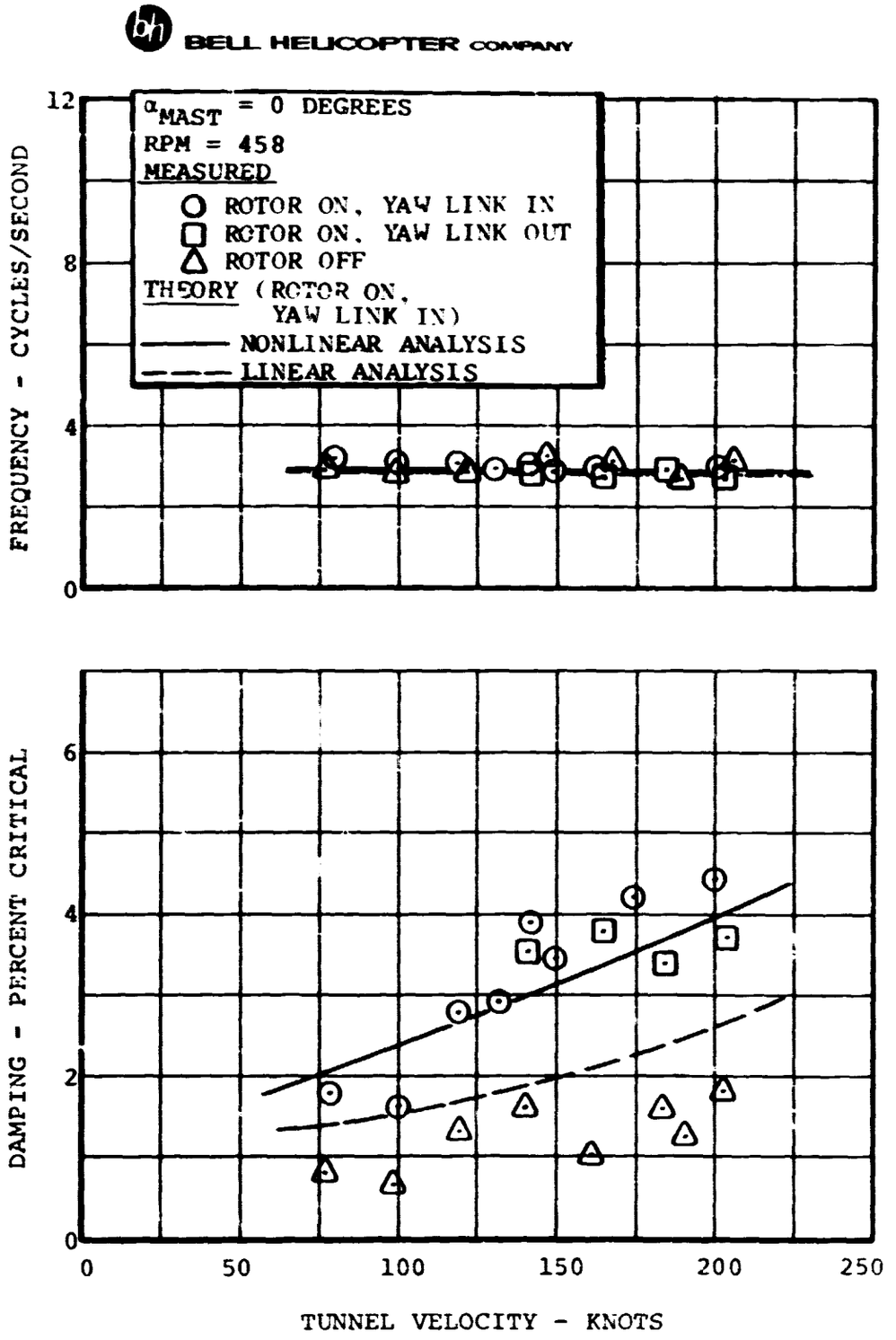

Figure V-6. Wing Beam Frequency and Damping Variation with Tunnel Velocity for Standard Stiffness Test Stand.

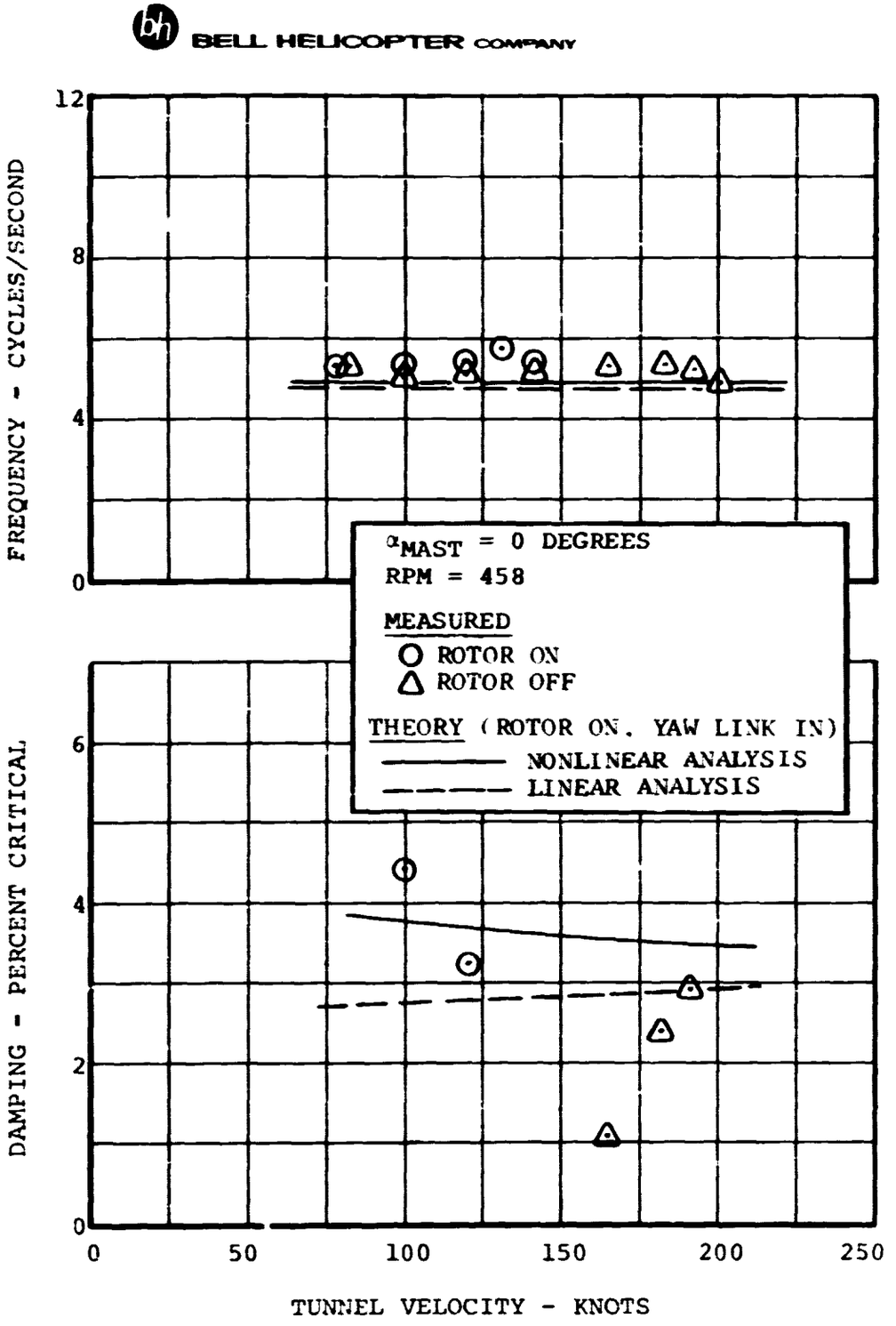

Figure V-7. Wing Chord Frequency and Damping Variation with Tunnel Velocity for Standard Stiffness Test Stand.

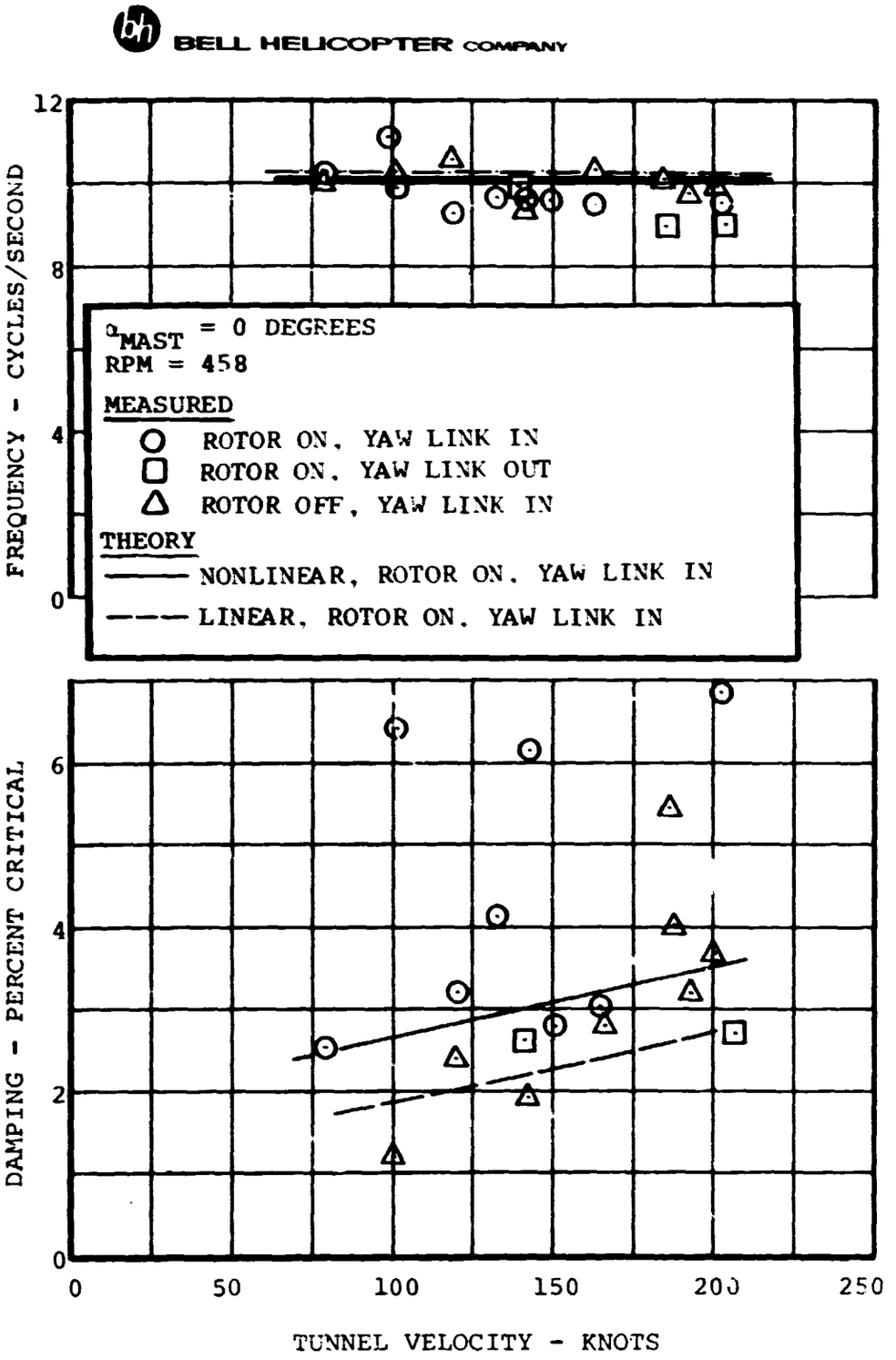

Figure V-8. Wing Torsion Frequency and Damping Variation with Tunnel Velocity for Standard Stiffness Test Stand.

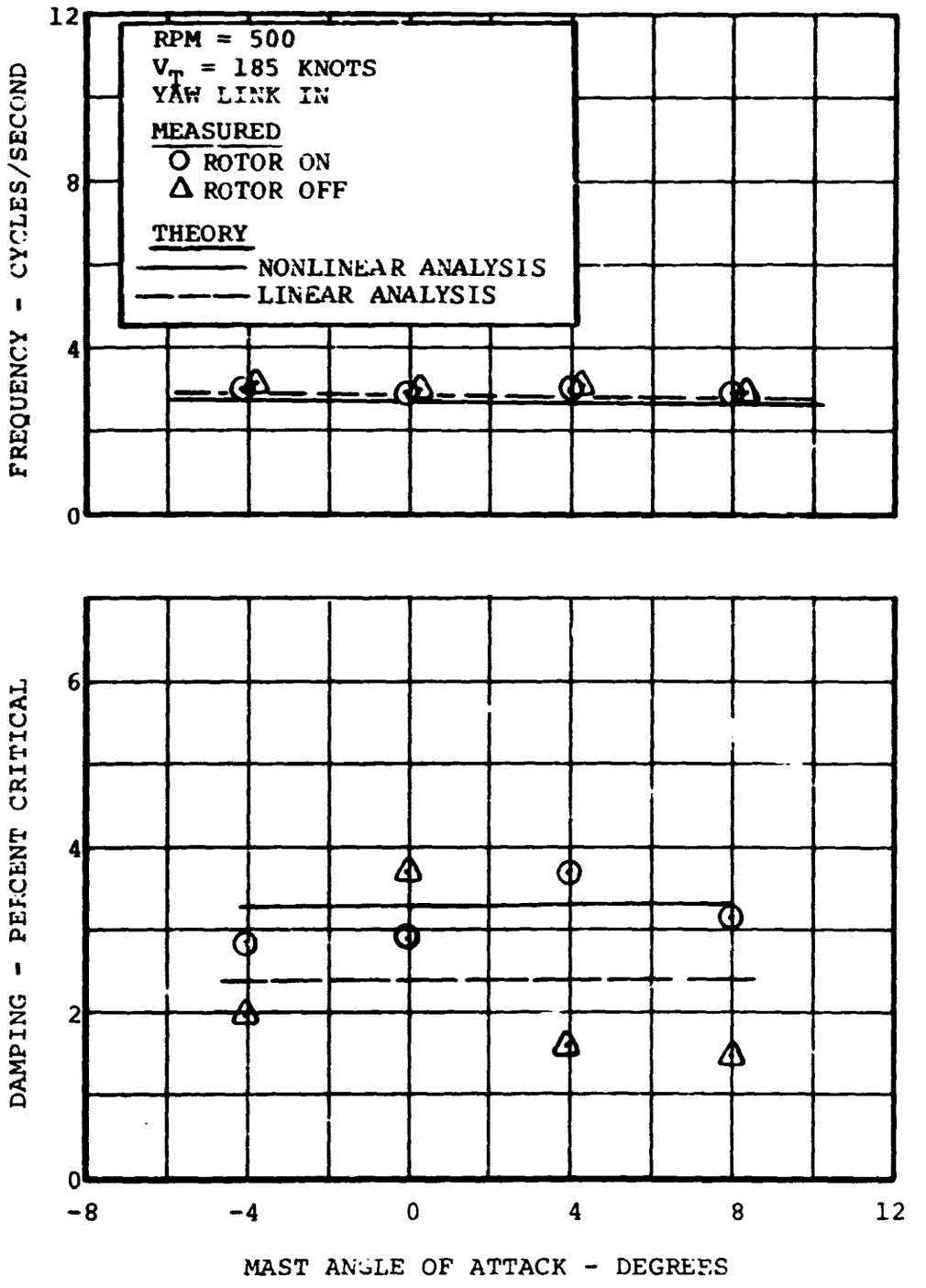

Figure V-9. Wing Beam Frequency and Damping Variation with Angle-of-Attack for Standard Stiffness Test Stand.

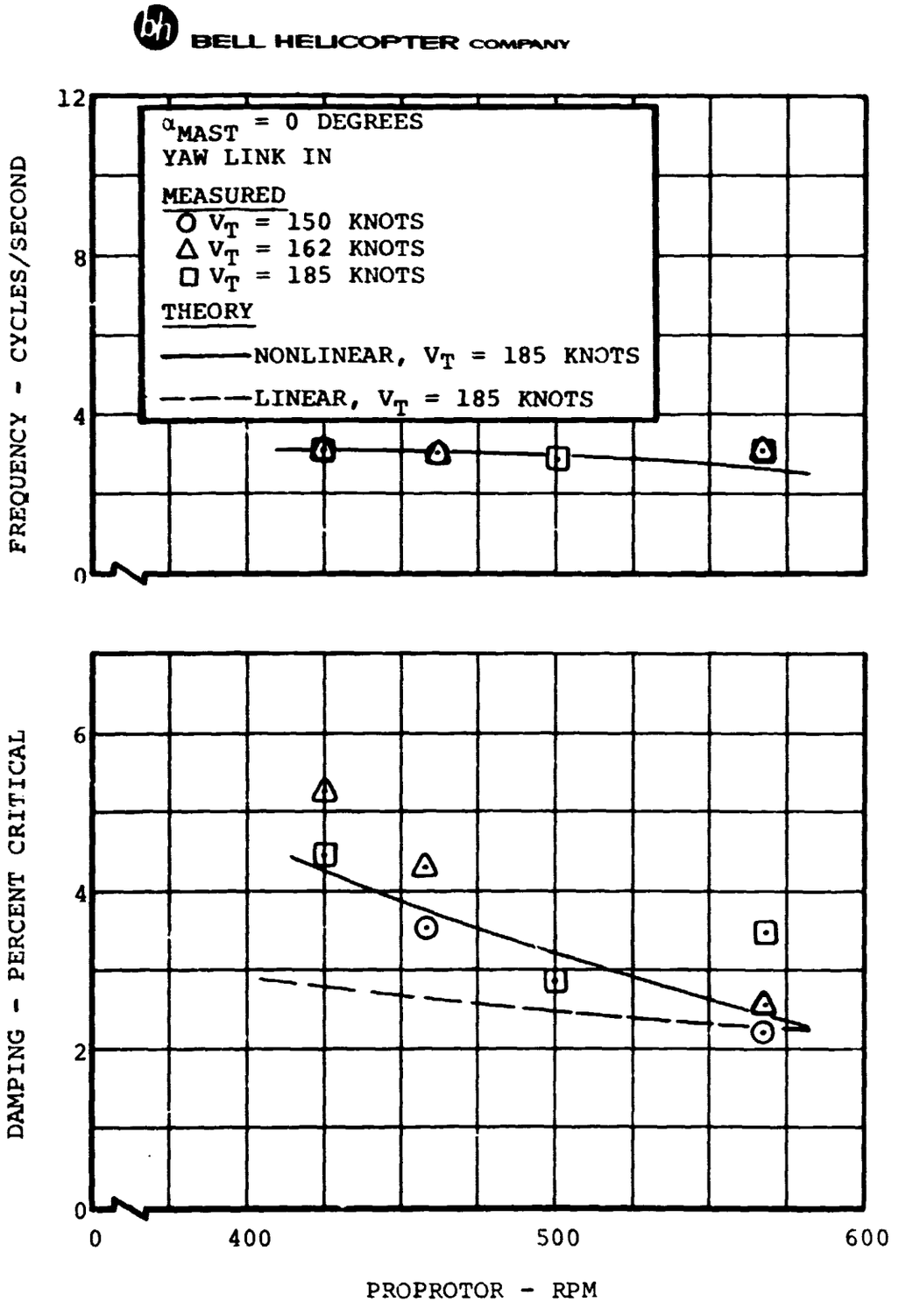

Figure V-10. Wing Beam Frequency and Damping Variation with Proprotor RPM for Standard Stiffness Test Stand.

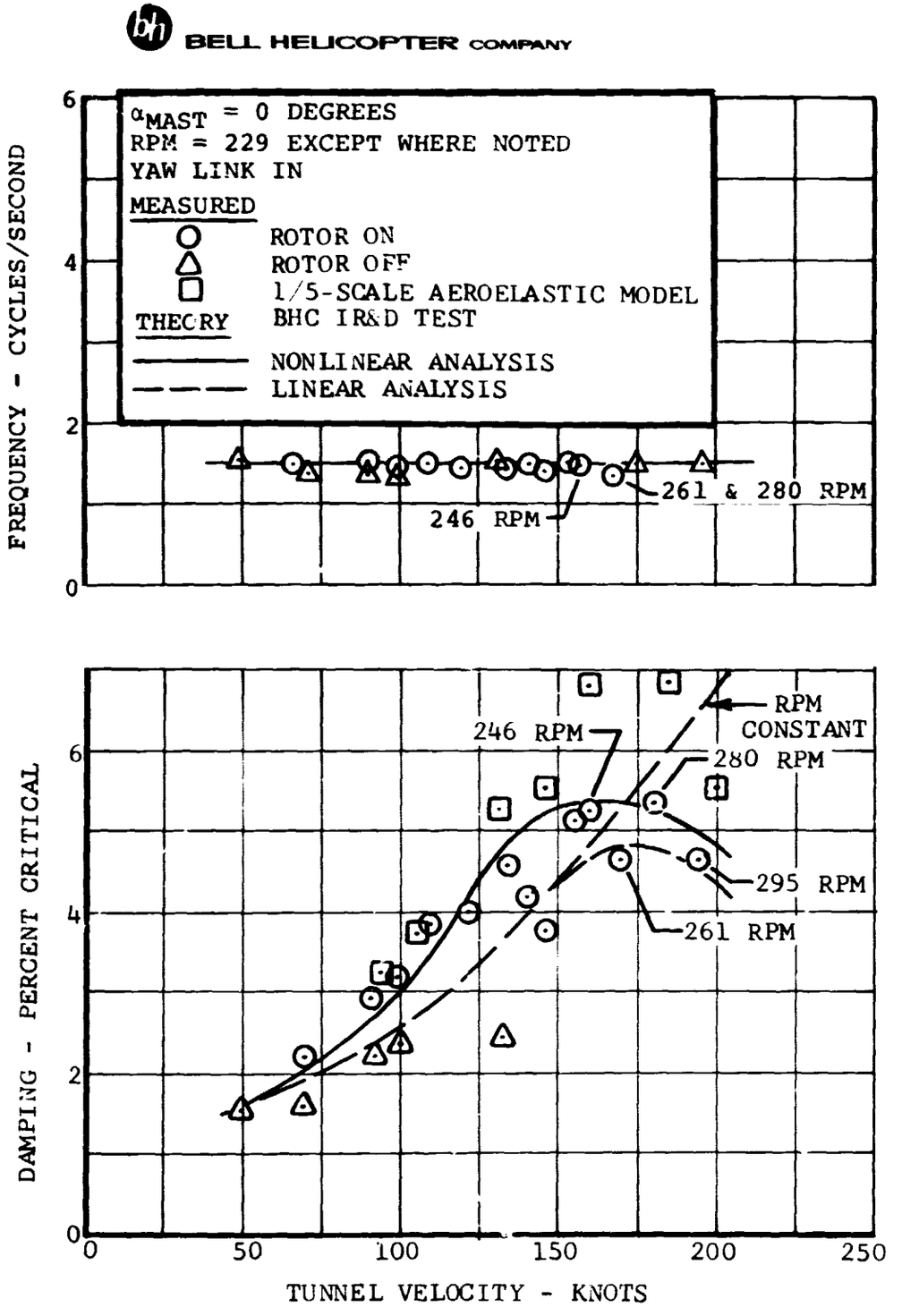

Figure V-11. Wing Beam Frequency and Damping Variation with Tunnel Velocity for One-Fourth-Stiffness Test Stand.

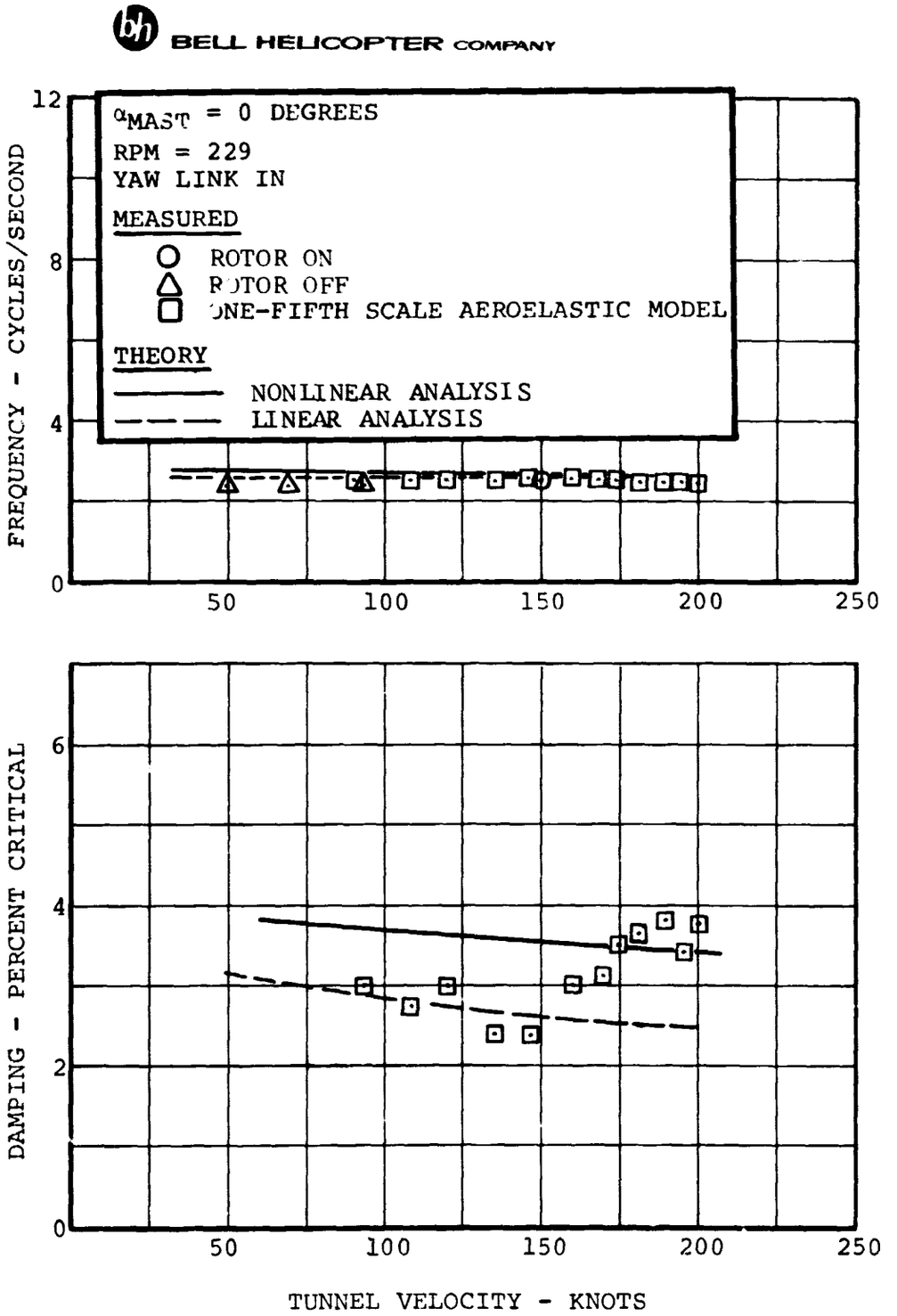

Figure V-12. Wing Chord Frequency and Damping Variation with Tunnel Velocity for One-Fourth-Stiffness Test Stand.

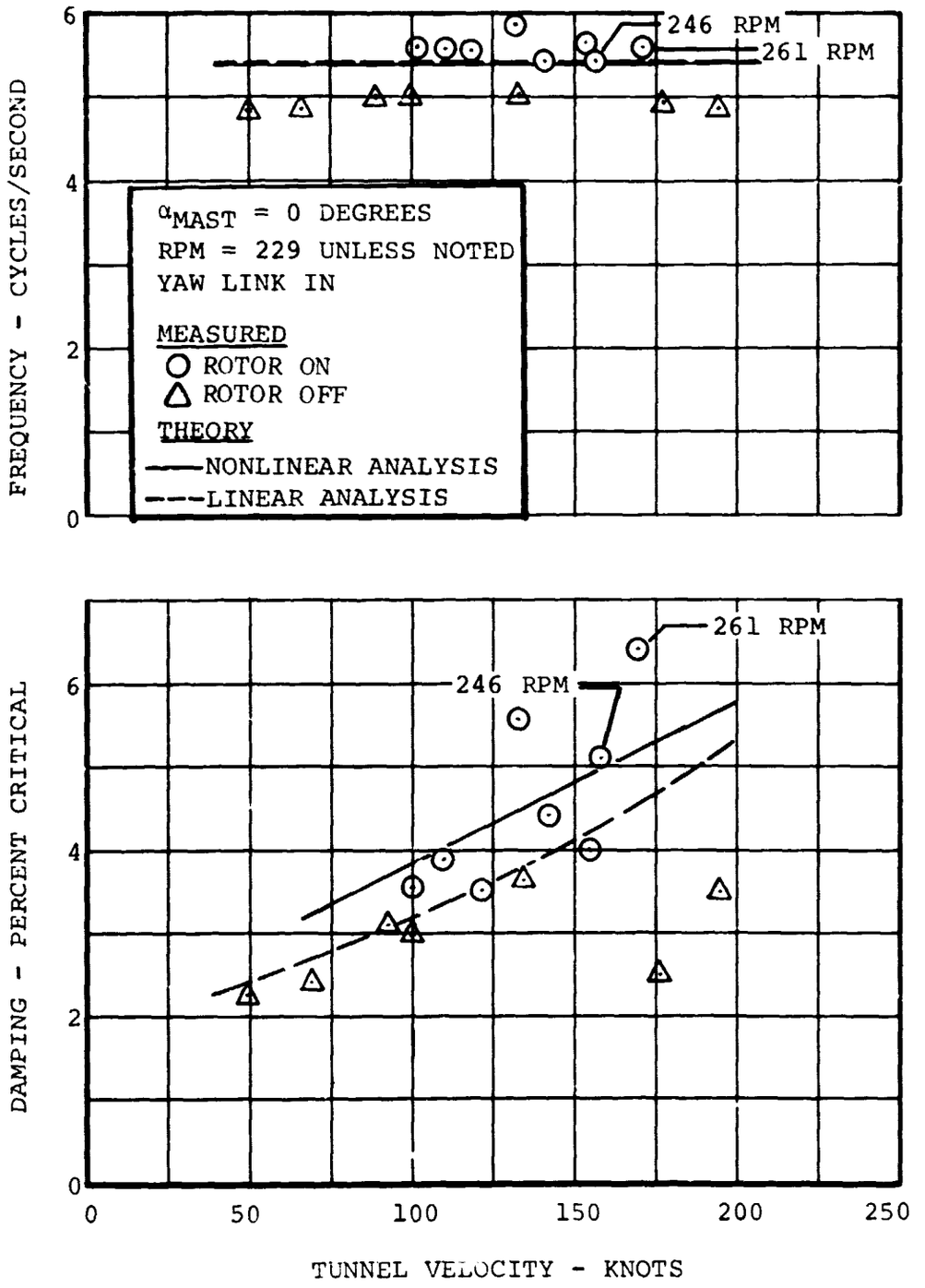

Figure V-13. Wing Torsion Frequency and Damping Variation with Tunnel Velocity for One-Fourth-Stiffness Test Stand.

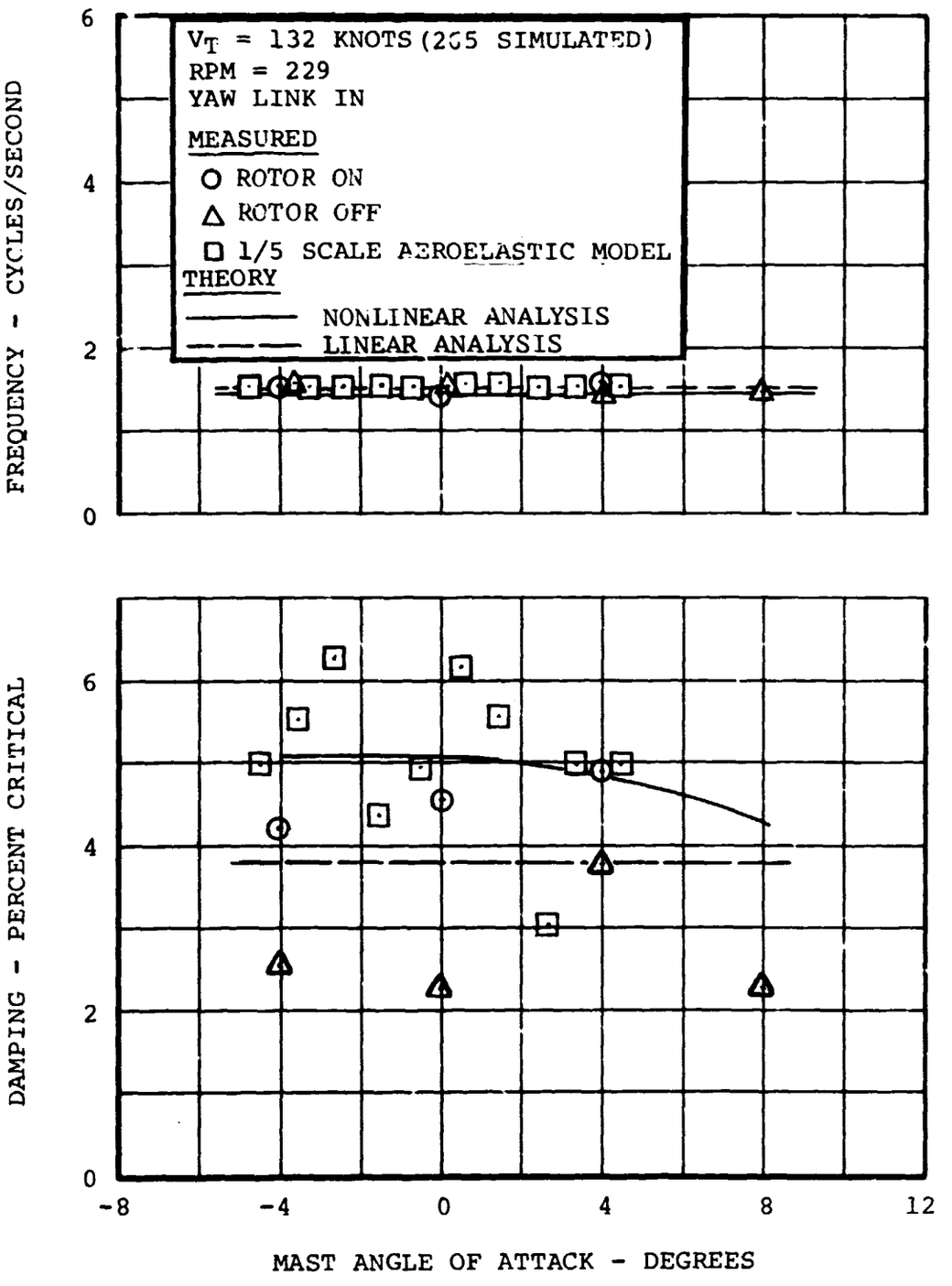

Figure V-14. Wing Beam Frequency and Damping Variation with Angle-of-Attack for One-Fourth-Stiffness Test Stand.

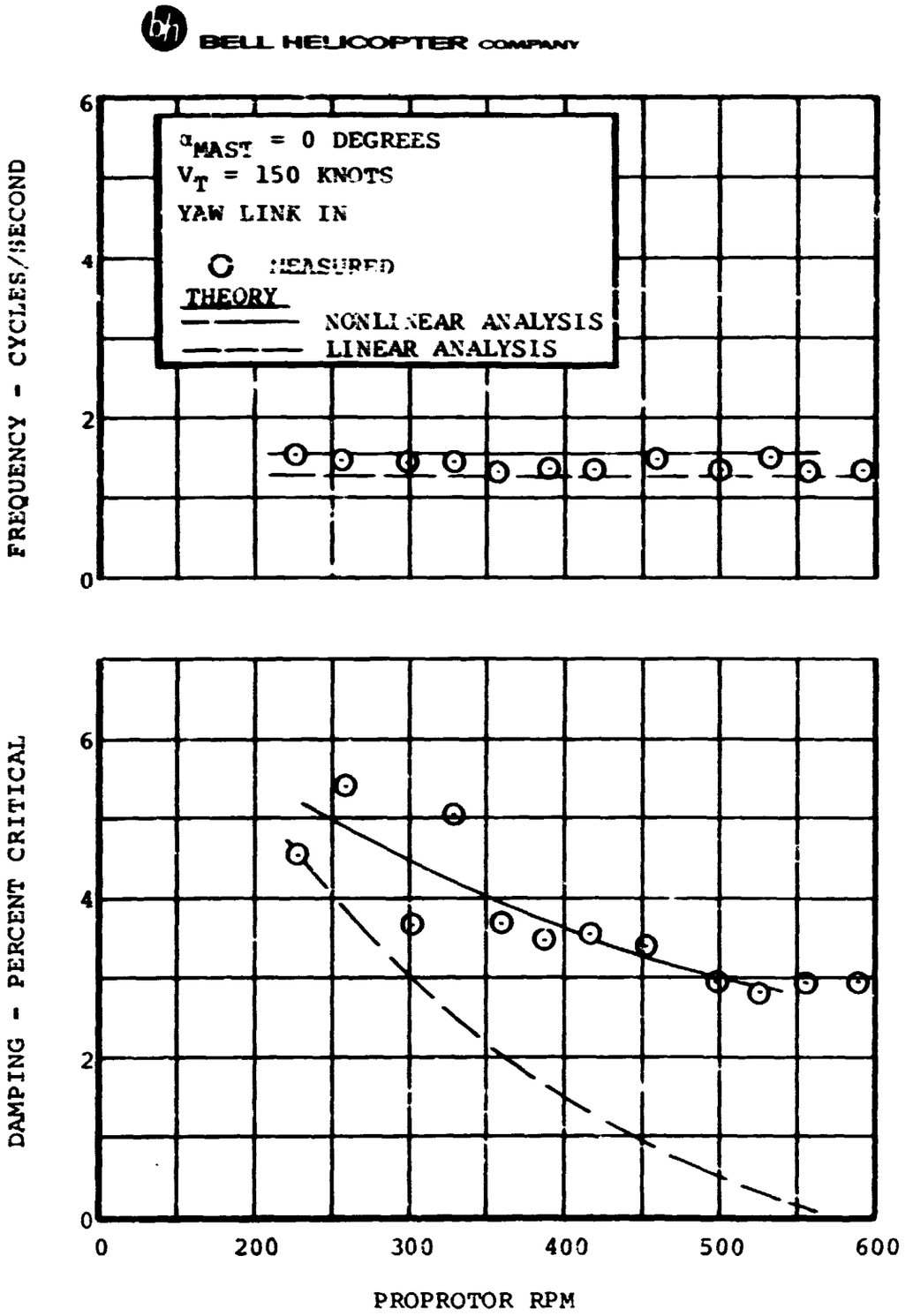

Figure V-15. Wing Beam Frequency and Damping Variation with Proprotor RPM for One-Fourth-Stiffness Test Stand, 150 Knots.

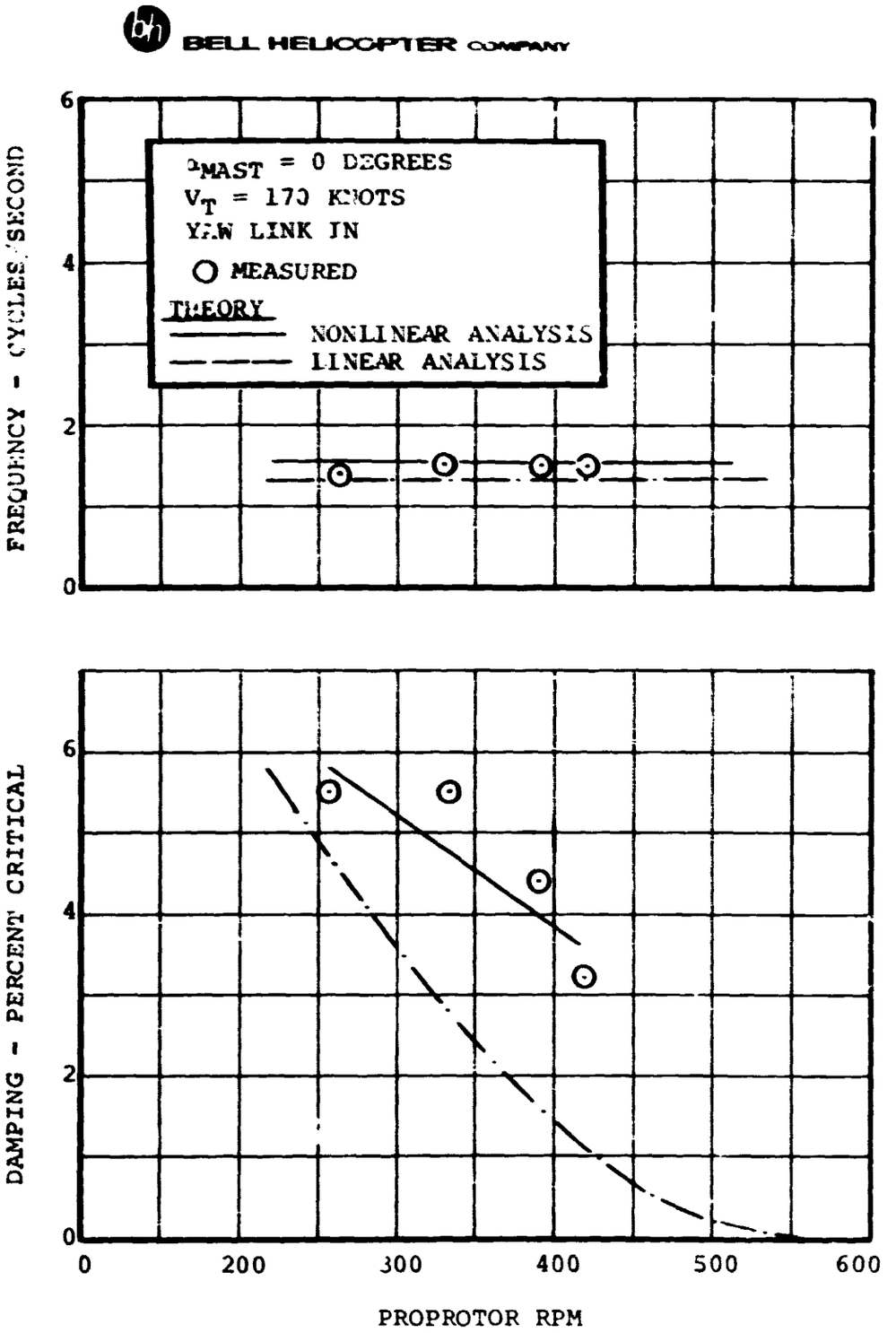

Figure V-16. Wing Beam Frequency and Damping Variation with Proprotor RPM for One-Fourth-Stiffness Test Stand, 170 Knots.

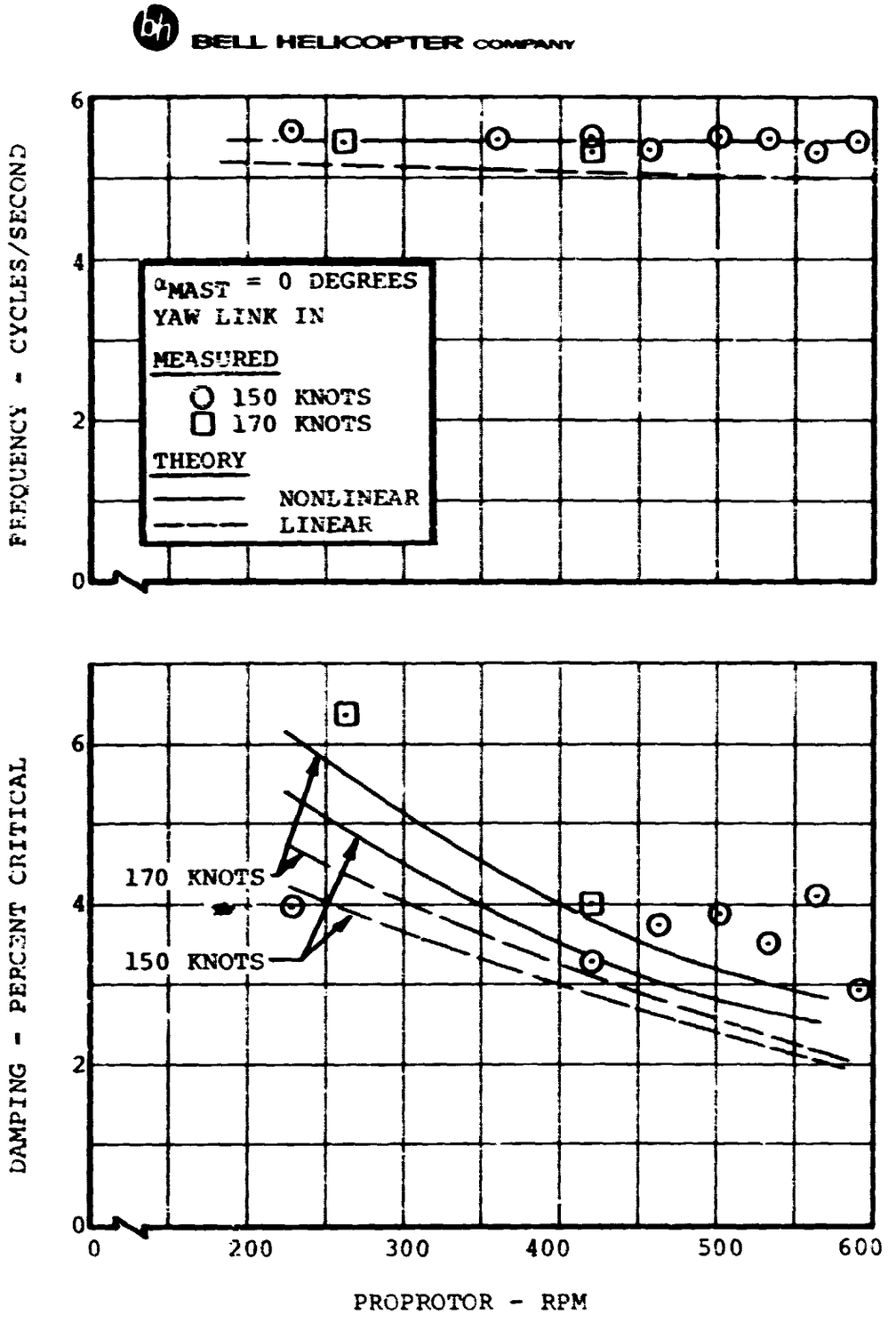

Figure V-17. Wing Torsion Frequency and Damping Variation with Proprotor RPM for One-Fourth-Stiffness Test Stand.

VI. BLADE FLAPPING

A. AIRPLANE MODE DERIVATIVES

Blade flapping in airplane mode, manifested as steady tilting of the proprotor disc, was measured for eight combinations of rpm and wind-tunnel speed during the dynamic stability test. One combination was repeated during the powered test to obtain an indication of the influence of wing-proprotor aerodynamic interference on blade flapping.

1. Measured Derivatives

Figure VI-1 shows an example of the measured blade flapping versus mast angle of attack. The measured longitudinal flapping (a_1), is nearly linear in nature; a straight line approximation was made to arrive at the derivative, $\partial a_1/\partial \alpha_{TPP}$. The lateral flapping ($b_1$), is nearly linear from $\alpha_{TPP} = 0$ to $\alpha_{TPP} = +6$, but has a shift between $\alpha_{TPP} = 0$ and $\alpha_{TPP} = -2$. This shift appears in other flapping versus mast angle of attack data and is believed to be caused by an instrumentation irregularity. The measured lateral flapping derivative, $\partial b_1/\partial \alpha_{TPP}$ was estimated using the slope between $\alpha_{TPP} = 0$ and $\alpha_{TPP} = +6$.

The flapping derivatives for the other rpm-wind speed combinations are tabulated in Table VI-I. Comparison of the 185-knot, 500-rpm data from the dynamic stability test with those from the powered test indicates that wing-proprotor aerodynamic interference has no influence on the longitudinal flapping response but nearly doubles the lateral flapping response. However, since the lateral flapping is relatively small, the overall influence on the flapping response to angle of attack appears to be negligible.

2. Correlation of Theory with Measured Flapping

Two analytical methods are compared with the measured flapping derivatives shown in Figure VI-1 and Table VI-I. The linear theory is based on the linear, small perturbation, proprotor dynamic stability analysis; the nonlinear theory is based on the linear open-form proprotor aeroelastic analysis. The bases, assumptions, and limitations of these analyses, discussed earlier in Section V, also apply to the flapping derivative theory.

Both theories accurately predict the measured longitudinal derivatives. The nonlinear theory is in better agreement with the lateral derivatives than is the linear theory. This is due to the secondary factors such as precone, blade flexibility, and wing-proprotor aerodynamic interference included in the nonlinear theory.

In general, the correlation between theory and measured flapping is excellent. Figure VI-2 summarizes the correlation with regard to the total flapping derivative $\partial\beta/\partial\alpha_{TPP}$.

TABLE VI-I. MEASURED AND CALCULATED FLAPPING DERIVATIVES IN AIRPLANE MODE

Velocity	RPM	$\partial\beta/\partial\alpha$			$\partial a_1/\partial\alpha$			$\partial b_1/\partial\alpha$		
		Measured	Calculated		Measured	Calculated		Measured	Calculated	
			Linear	Nonlinear		Linear	Nonlinear		Linear	Nonlinear
100	425	.182	.167	.167	.187	.163	.147	.096	.038	.097
140	425	.320	.316	.354	.328	.305	.295	.171	.084	.171
140	458	.300	.290	.266	.357	.263	.234	.171	.074	144
185*	500	.415	.380	.415	.398	.369	.362	.219	.125	.218
100	422	.179	.169	.180	.181	.165	.150	.078	.038	.100
92.5	250	.475	.475	.480	.440	.476	.465	.120	.060	.131
132.5	229	.970	.988	.960	.960	.961	.925	.300	.071	.256
185**	500	.408	.380	-	.390	.369	-	.125	.125	-

*Dynamic test

** Powered test

B. FLAPPING CONTROLLER INVESTIGATION

The automatic flapping controller was tested only on the one-fourth-design-stiffness stand. As noted earlier in Section V, the one-fourth-design-stiffness hub restraint was not used during the one-fourth-design-stiffness stand test. Since the flapping controller was configured to be used with the one-fourth-design-stiffness hub restraint, its performance was somewhat reduced. Furthermore, the swashplate phasing was not optimum for the monocyclic controller. However, the test data are adequate to verify correlation between theory and measured controller characteristics and to demonstrate the feasibility of a flapping controller.

1. Test Results

To evaluate controller stability and performance, the following procedure was employed:

- The controller was turned off except for the hydraulic actuator.
- The controller gains were selected.
- A step was put into the actuator, simulating to some extent a step vertical gust, transiently exciting both the wing and the proprotor.
- The controller was activated, resulting in a reduction of flapping.
- The step was removed. This initiated a transient response which could be compared to the response with the controller inactive, obtained in Step 3 above.
- A triangular pulse was input to the actuator to measure the transient response.
- When desired, the frequency response was measured by inputing a sinusoidal signal to the actuator.

Two types of feedback were tested: (1) integral feedback, where the rate of cyclic input from the controller was proportional to the flapping, and (2) lagged position feedback. Lateral b_1 feedback was also investigated but because of the limited b_1 feedback data, the results were not conclusive.

Figure VI-3 shows the normalized flapping and wing beam bending response to a step input for various values of integral gain at a simulated 185 knots. Note that for all gains the a_1 flapping is completely eliminated, but the magnitude of the transient reduction and the time to wash out the flapping are functions of the gain. Also evident is the apparent reduction in damping

of the blade flapping mode as the gain is increased. Extrapolation of the damping with gain relationships indicates neutral stability at a gain of approximately 11 to 12 degrees per second per degree.

Also evident in Figure VI-3 is an increase in the wing beamwise motion with increasing gain. In the simple controller tested (which could be duplicated using a hydromechanical system in an operational aircraft), there were no compensation networks to mitigate inputs at the test stand natural frequencies. At the wing beam frequency the input was phased so as to increase flapping and hence the wing response. A notch filter could be employed in an operational controller to eliminate the increased response or networks added which would even reduce the unaugmented response.

Data similar to those shown in Figure VI-3 were also taken at a simulated 265 knots. The system became unstable at a gain of approximately five.

Figure VI-4 summarizes the system stability boundaries, the reduction in transient flapping, and the increase in wing beam response as a function of gain. The recommended gain level shown in Figure VI-4(a) is based on the generally accepted gain margin of 6-8. Note that the gain will have to be varied with airspeed or the value at the limit dive speed employed.

Noteworthy is the evidence that for a relatively low-gain integral controller, a large reduction in transient flapping can be achieved. For example, for a gain of unity, the transient flapping is reduced by approximately 30 percent. This gain controller has a negligible effect on stability and causes only a small increase in wing-beam bending response.

The measured system response to lagged position gain is shown in Figure VI-5. Lagged position gain was somewhat more effective than integral gain in reducing transient flapping, but produced more wing response. A reduction in stability with gain was also evident.

Combinations of integral gain and lagged position gain were tested to determine an optimum controller configuration. Figure VI-6 shows the measured flapping response at simulated airspeeds of 185 knots and 265 knots for two combinations of gains. In this case a significant reduction in flapping is evident, but at the expense of a reduction in system damping.

The response of the optimum configuration to step and triangular shaped pulses is shown in Figures VI-7 and -8, respectively. A significant reduction in transient flapping is achieved with negligible reduction in system damping. The increase in wing beam response is small with this configuration.

2. Correlation of Theory with Measured Stability and Performance

The BHC flapping controller theory is based on the linear, small perturbation dynamic stability analysis described in Section V. The method involves generating transfer functions for longitudinal and lateral flapping as a function of the swashplate input, and coupling them with equations representing the controller. The system stability and frequency response is then calculated using the coupled equations.

Correlation between theory and measured characteristics is good. This is best indicated by comparison between the measured and predicted longitudinal flapping frequency response, shown in Figure VI-9. Note that the general shape of the amplitude and phase compares very well with the predicted response. However, the low-frequency response is higher than predicted. (The predicted wing resonant frequency is higher than tested because the root flexibility introduced by the wind-tunnel mount was not known when the predictions were made.)

A comparison of the predicted and measured stability boundaries with integral gain is shown in Figure VI-4. The relatively small difference is probably due to differences between the test stand configuration analyzed and the one tested: namely the beamwise frequency and the hub restraint.

The measured stability boundary for position gain is somewhat higher than the predicted value. At a simulated 185 knots, the neutral stability gain with an 0.18-second lag is 3.0 compared to a predicted 2.2. This error is not readily explained by the data and was possibly due to an error in the system calibration, e.g., the lag may have been slightly longer than 0.18 and or the gain may have been slightly lower than it was thought to be.

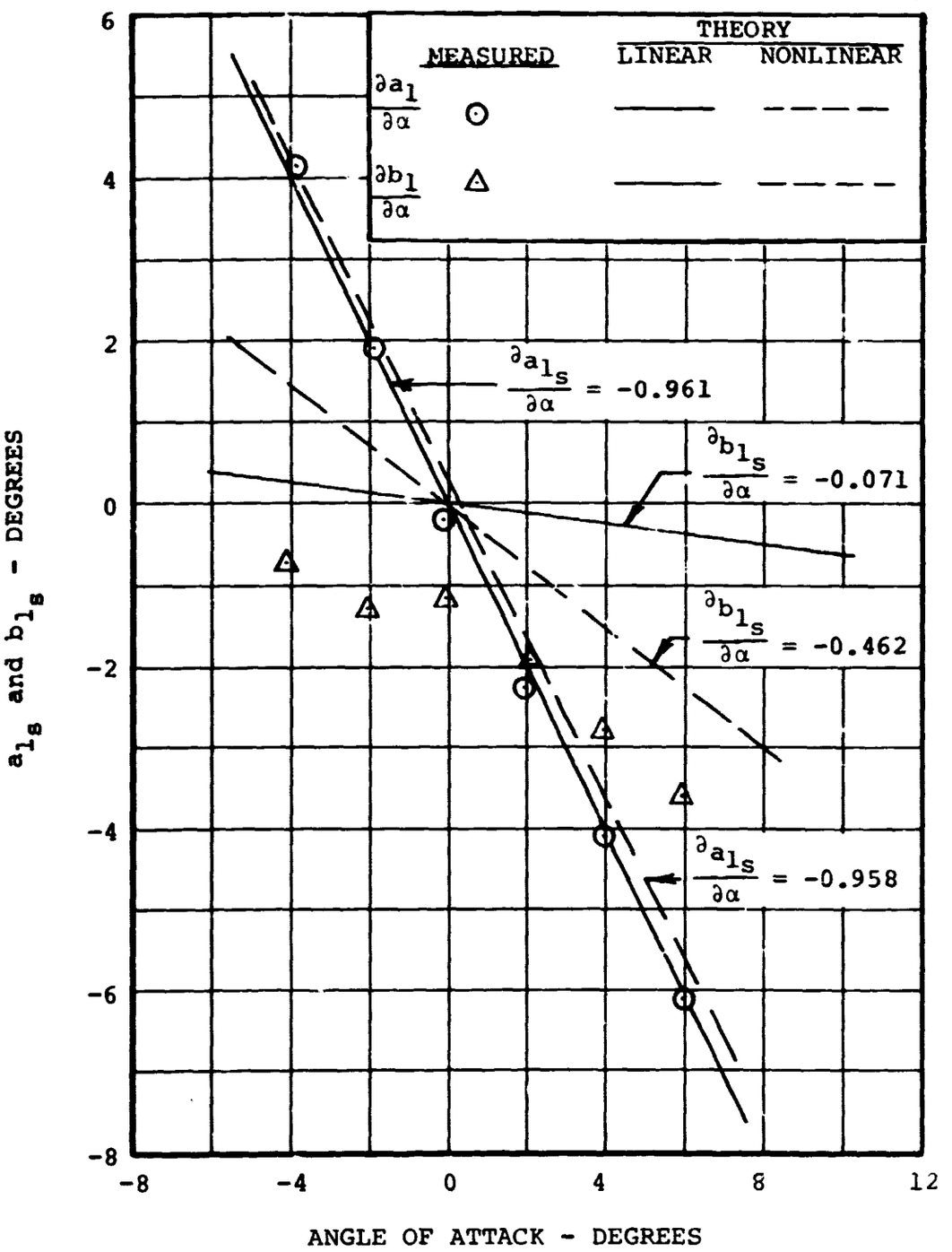

Figure VI-1. Proprotor Longitudinal and Lateral Flapping versus Angle of Attack, Simulated 265 Knots, 458 rpm.

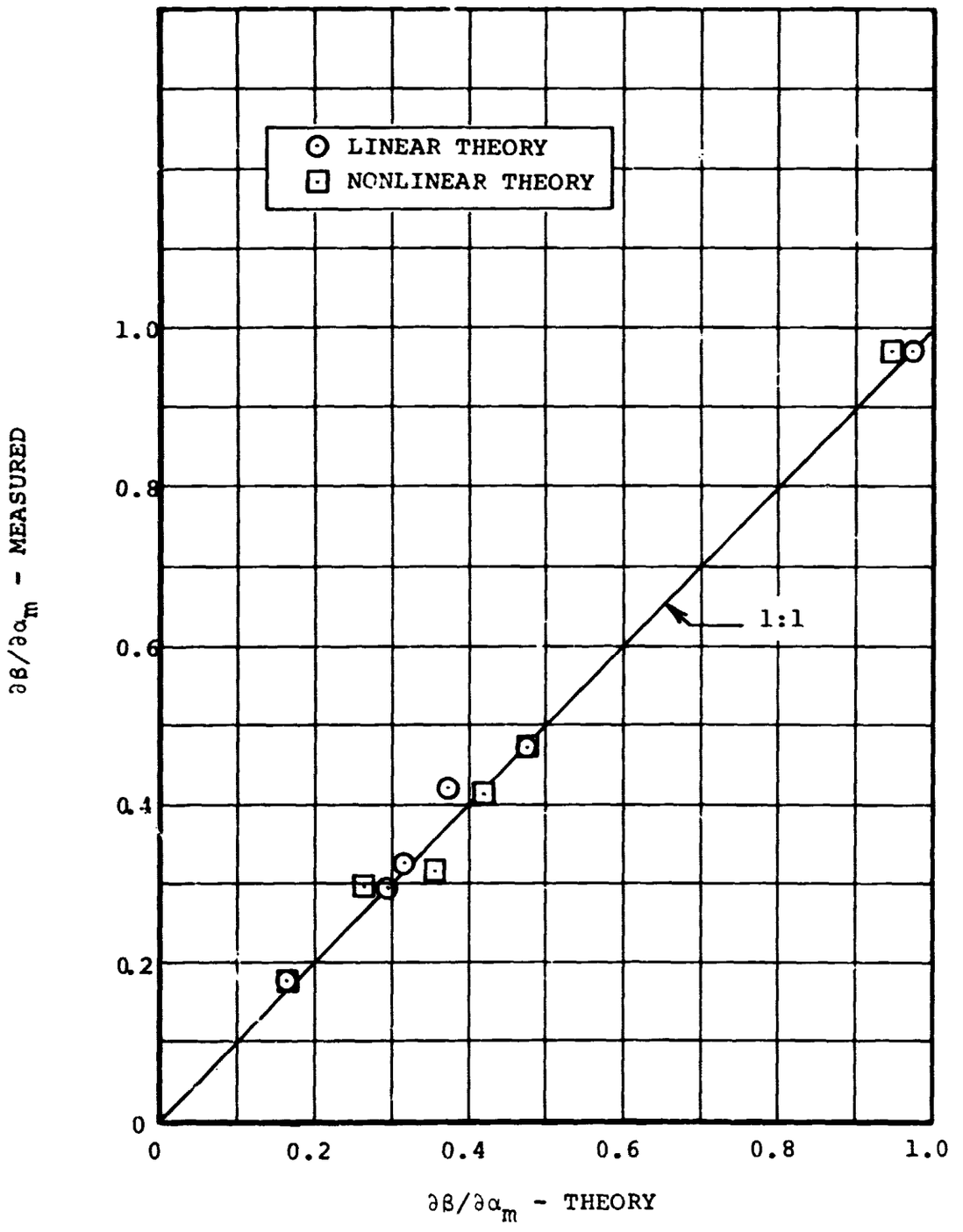

Figure VI-2. Correlation of Flapping Theory with Measured Total Flapping Derivative.

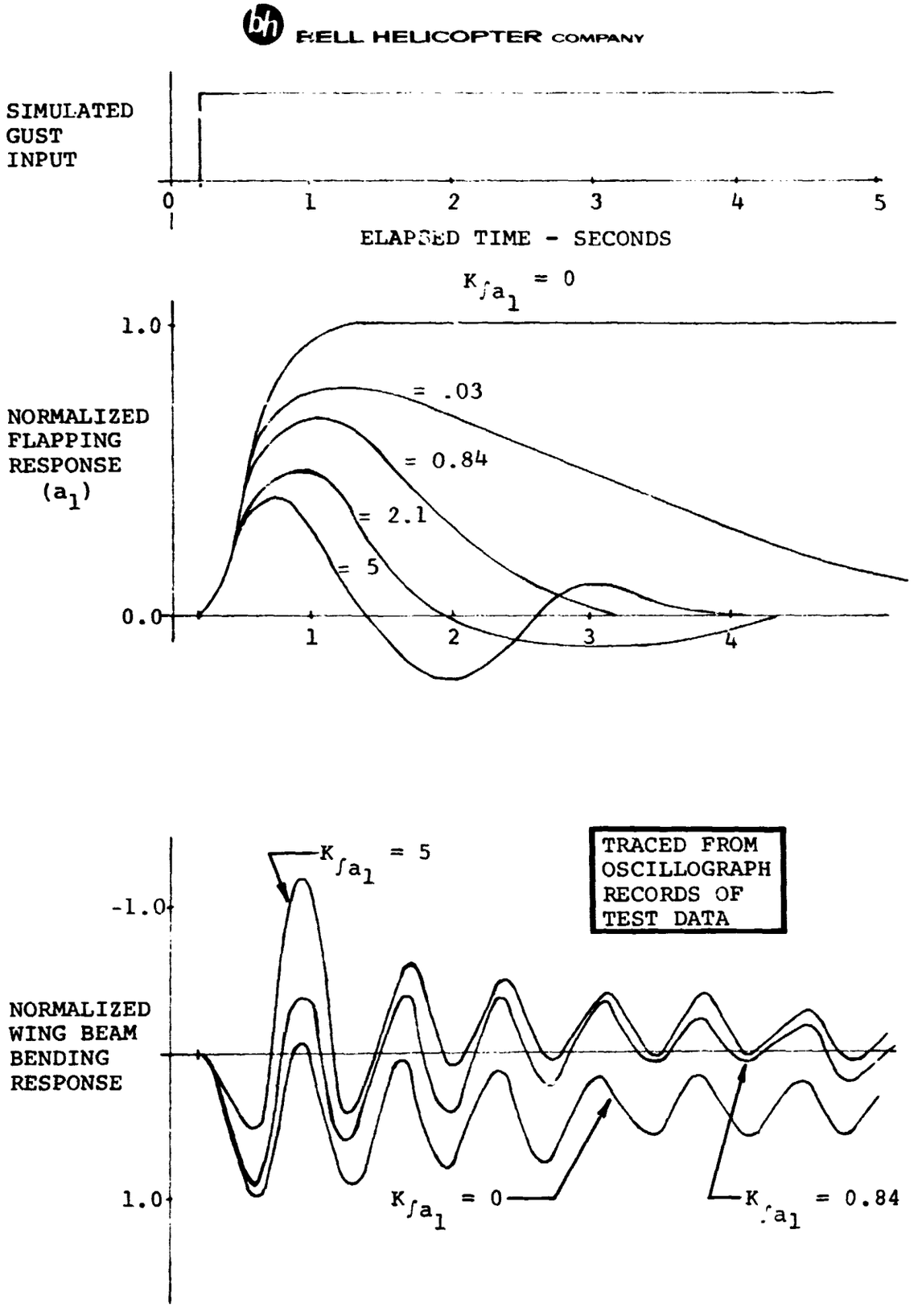

Figure VI-3. Measured Response to Step Input for Various Values of Integral Gain at a Simulated 185 Knots.

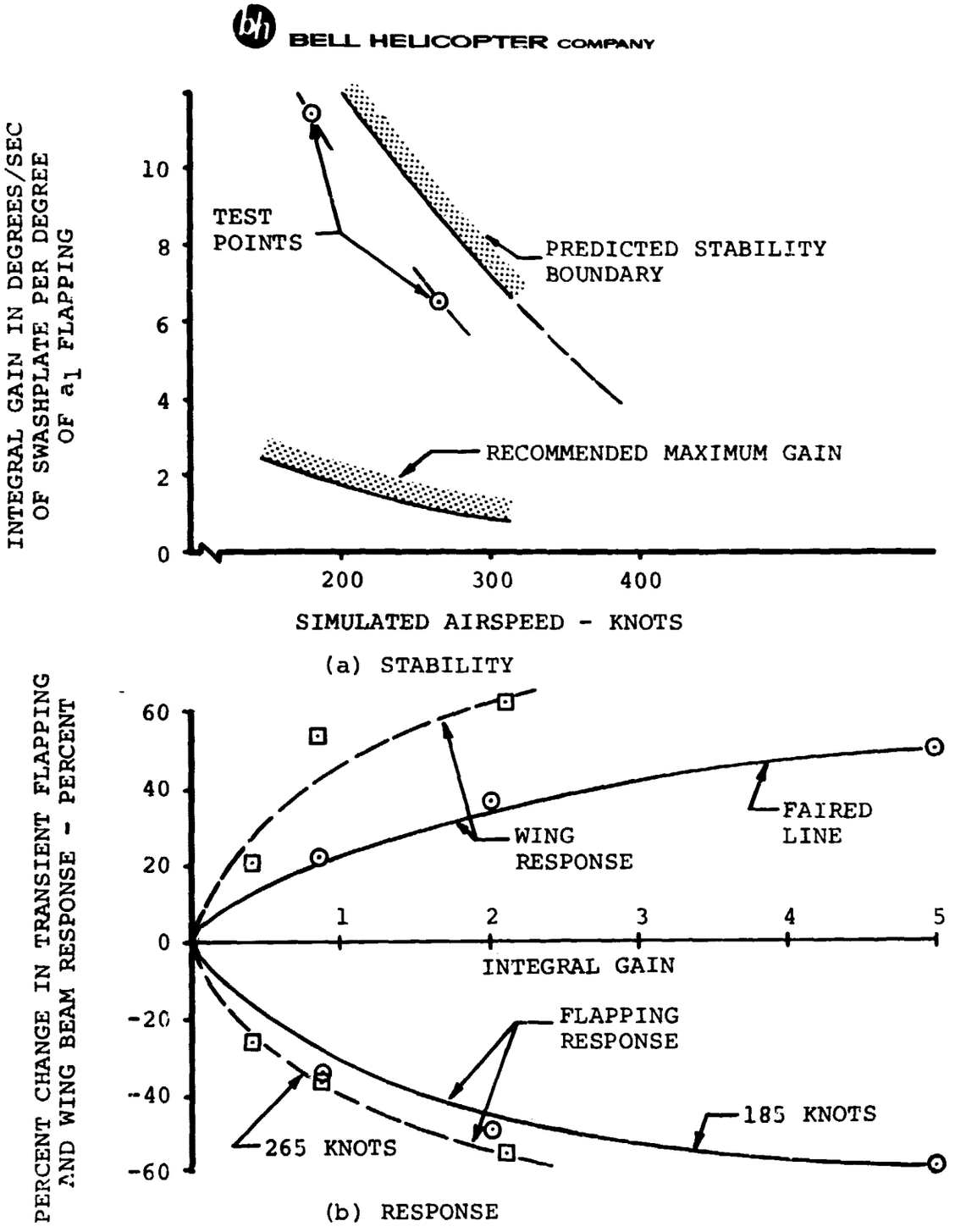

Figure VI-4. Summary of Stability and Response Characteristics with Integral Gain Feedback.

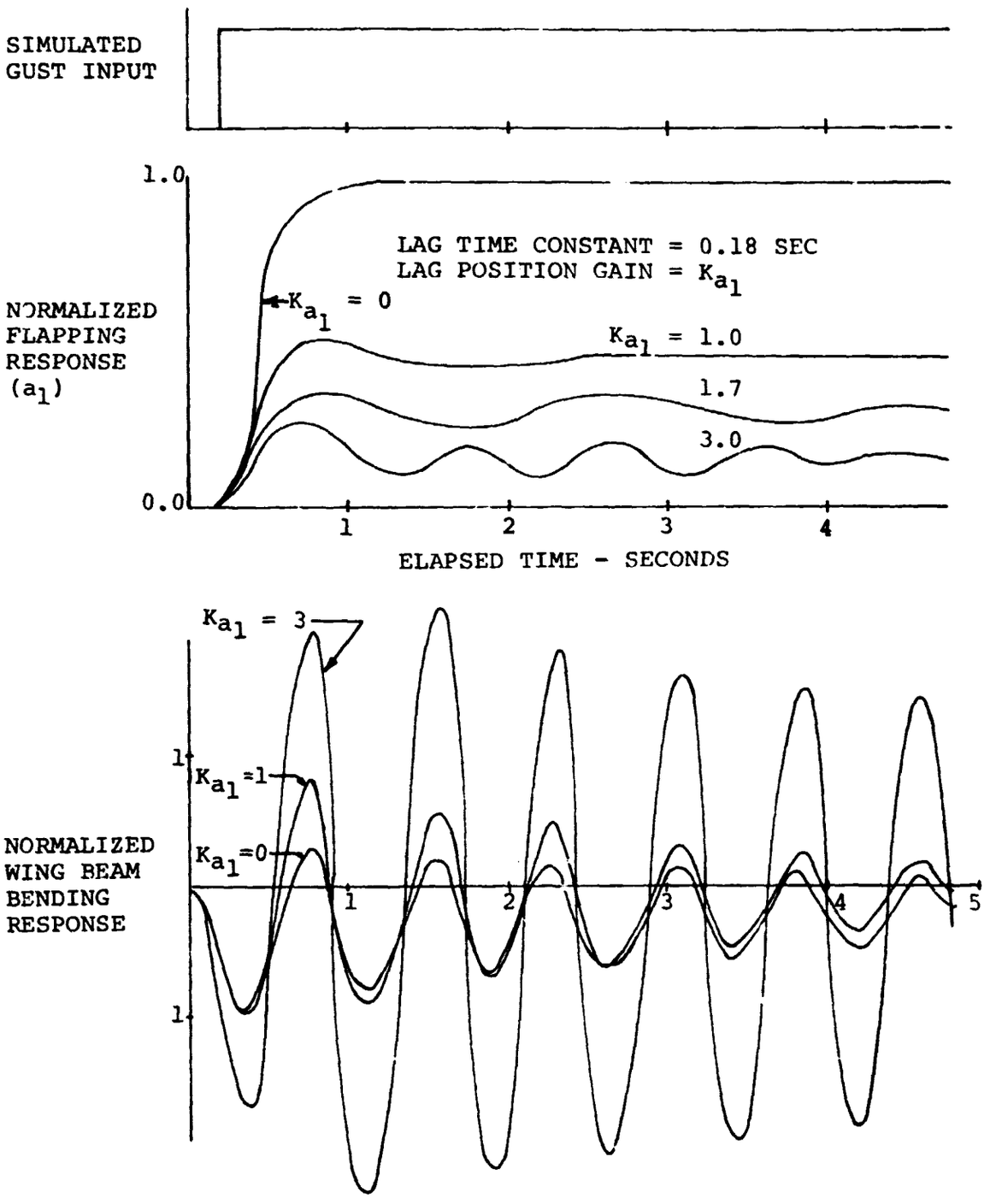

Figure VI-5. Gust Response for Various Values of Lagged Position Gain at 92 Knots.

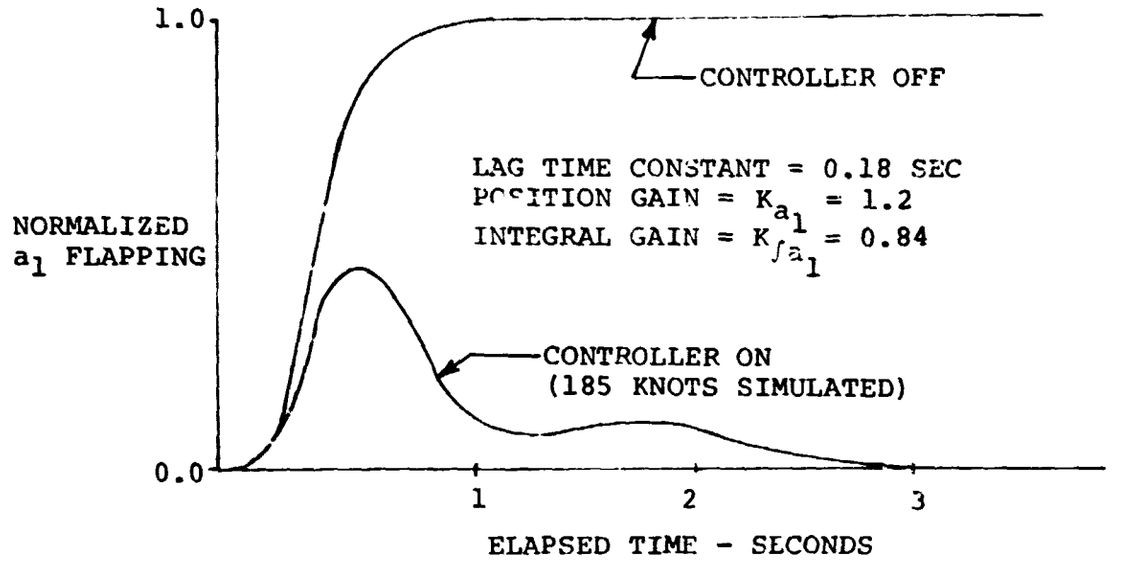

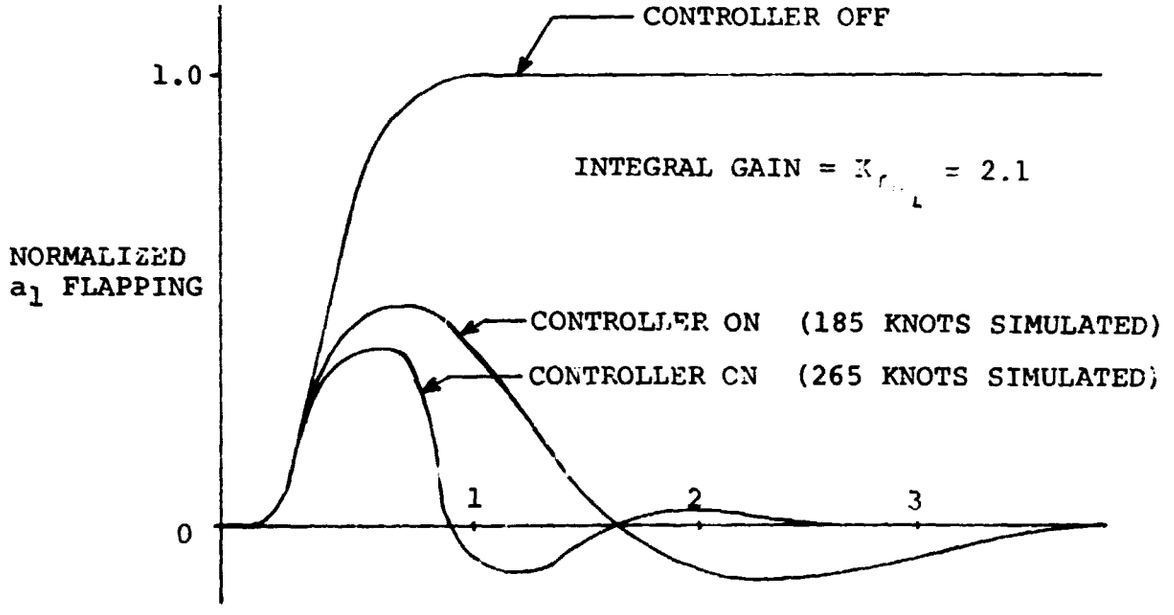

Figure VI-6. Measured Flapping Response at Simulated 185 Knots and 265 Knots, for Combined Integral and Lagged Position Gains (Step Input).

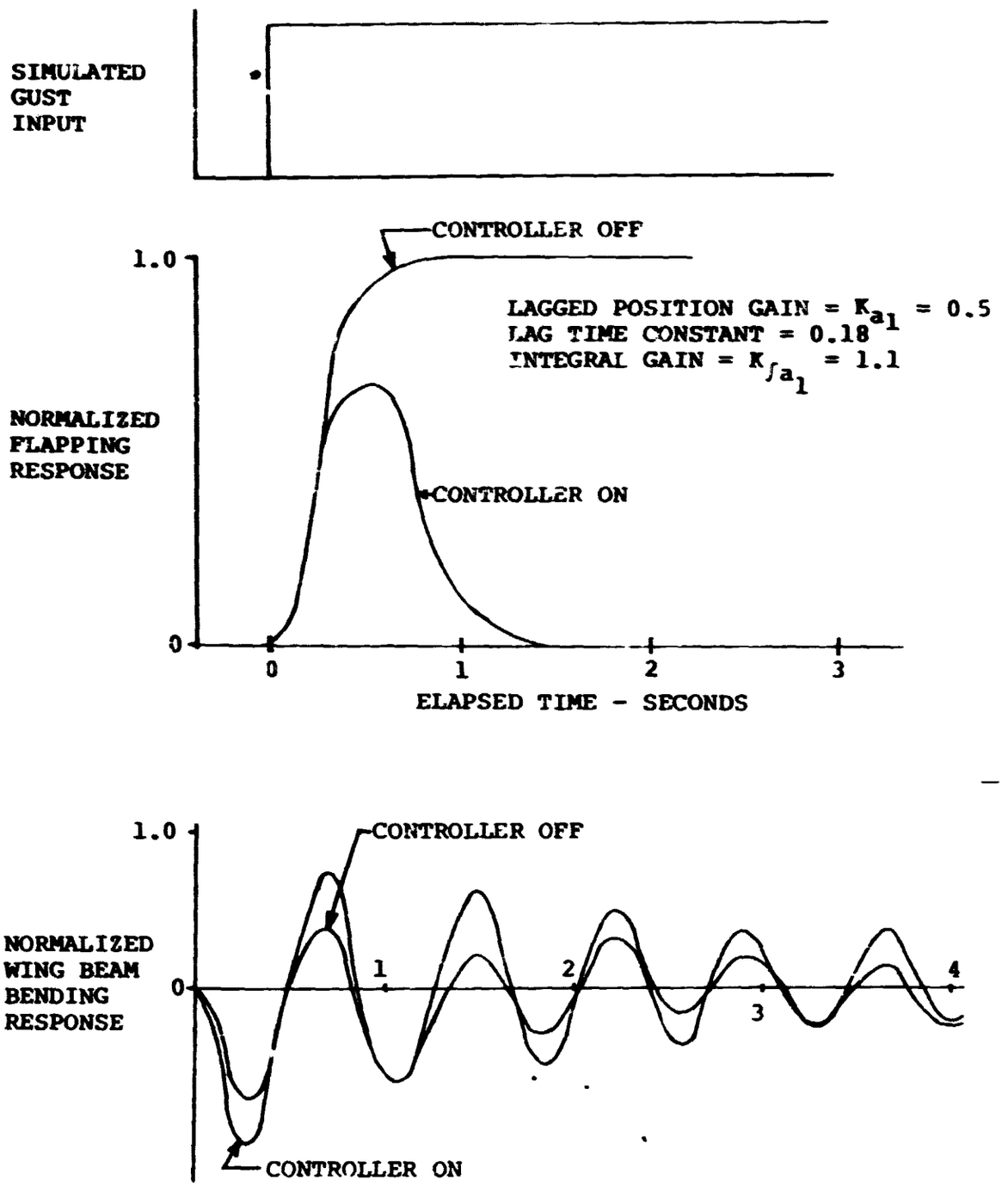

Figure VI-7. Response to Step Gust for Combined Integral and Lagged Position Gains (240 Knots, Simulated).

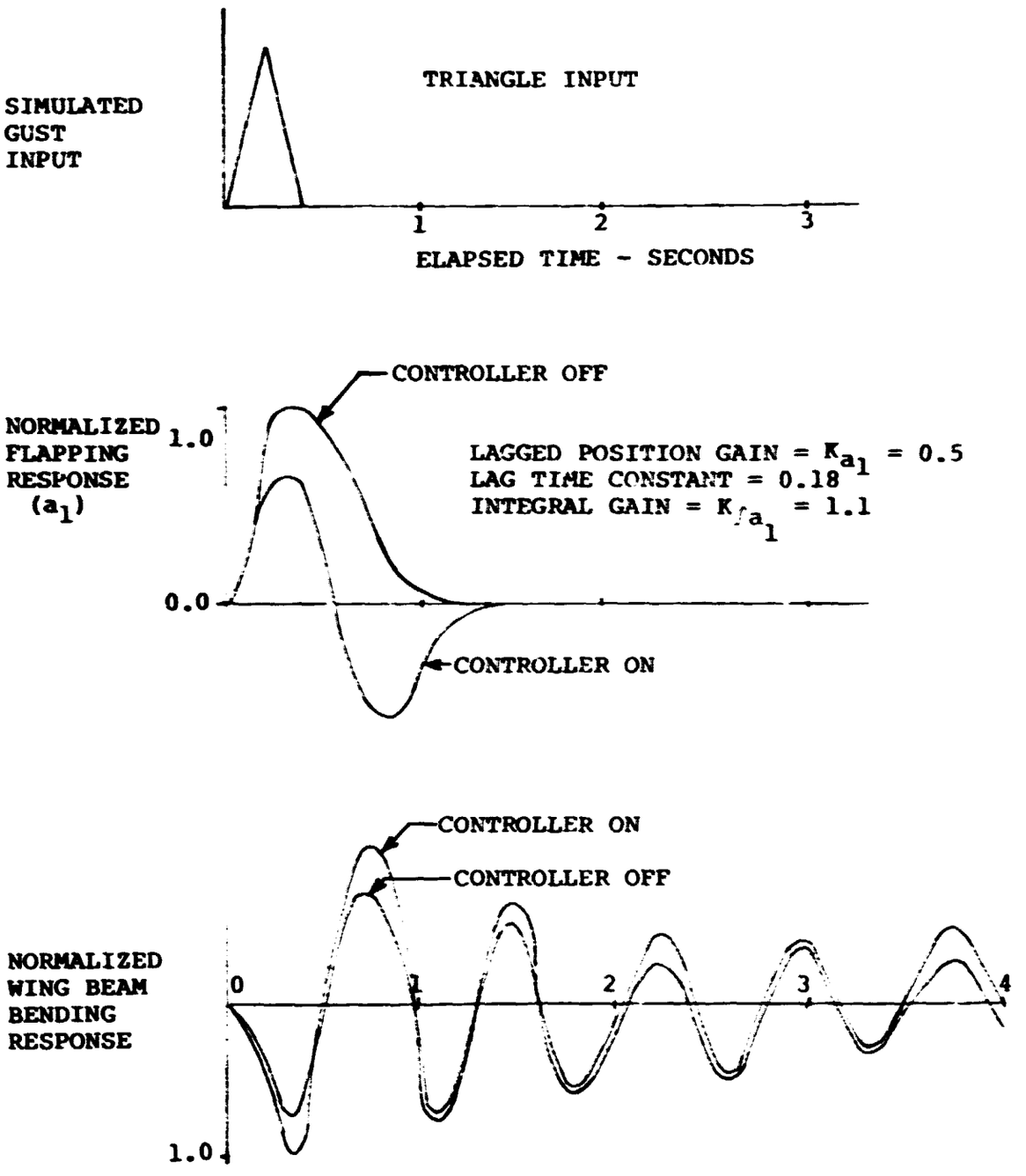

Figure VI-8. Response to Triangular Pulse Gust for Combined Integral and Lagged Position Gains (240 Knots, Simulated).

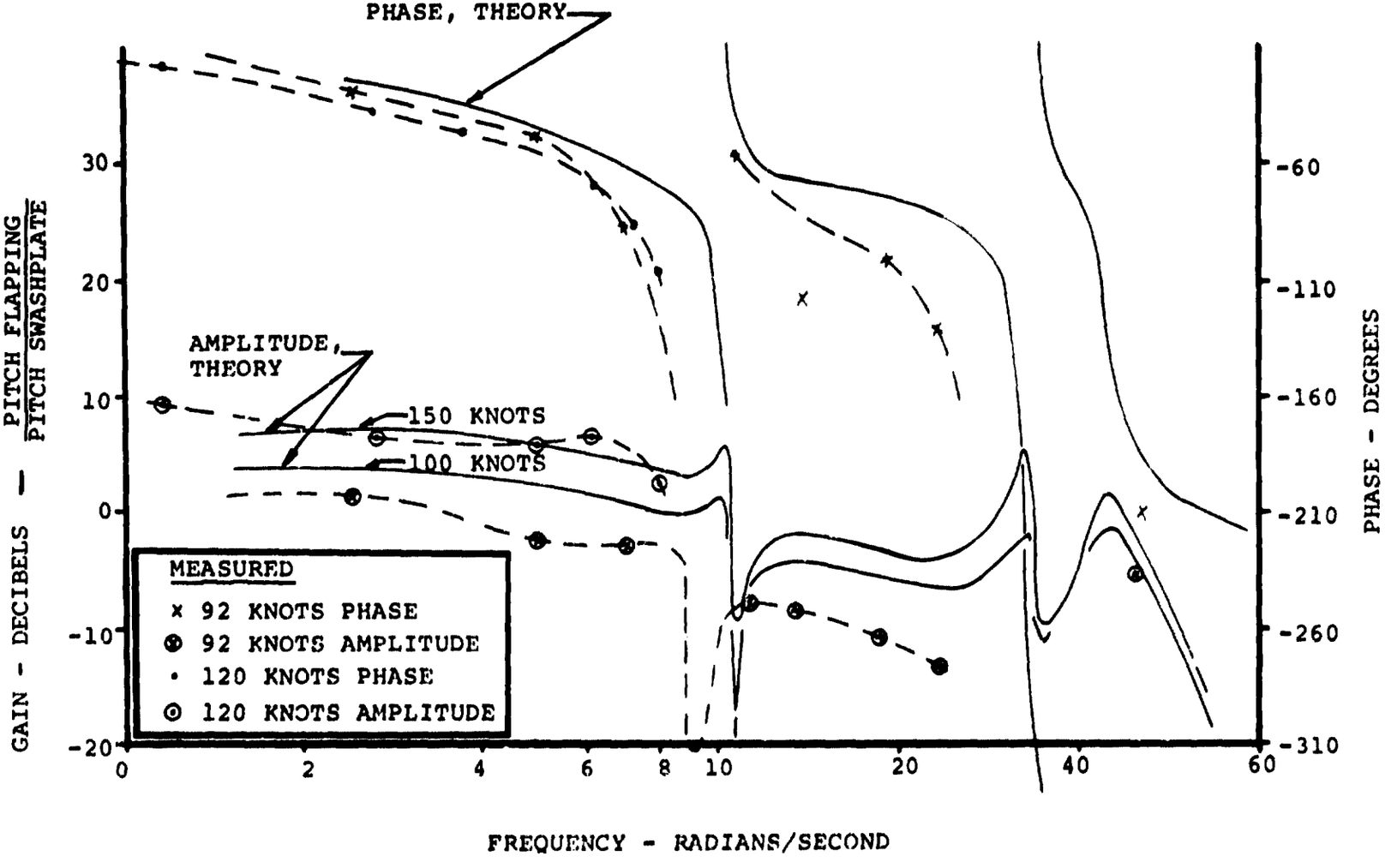

Figure VI-9. Correlation Between Theory and Measured Longitudinal Flapping Frequency Response.

VII. BLADE AND CONTROL SYSTEM LOADS

A. GENERAL

Blade and control loads were recorded throughout the performance tests, and during the airplane mode portions of the dynamic tests. Several additional runs were made for the primary purpose of obtaining loads data.

During the powered tests, the majority of the data were obtained with the proprotor longitudinal flapping (a_1) trimmed to zero by the application of cyclic pitch to simplify the test procedure. Extrapolating the data to simulate conversion at a constant fuselage angle-of-attack results in a wide, insensitive conversion corridor. Figure VII-1 shows that conversion corridor based on the measured loads.

Prior to the test, calculations of predicted blade loads erroneously incorporated a swashplate arrangement such that for cyclic inputs the maximum blade angle variation occurred at an azimuth of 90 degrees. The actual arrangement of the nonocyclic swashplate was such that the maximum blade angle variation occurred at an azimuth of 75 degrees. The loads measured during the test were in reasonable agreement with the predicted loads for helicopter and airplane modes, but were higher than the predicted loads for conversion mode. When the prediction calculations were conducted to reflect the actual swashplate arrangement, predicted loads for the conversion mode correlated with the measured loads.

B. MEASURED BLADE AND CONTROL LOADS

Figure VII-2 shows the waveforms of the blade and control loads for a range of mast angles corresponding to helicopter, conversion, and airplane modes. Several characteristics are evident: (1) One-per-rev loads are dominant, a normal characteristic of the semirigid rotor, and peak at an azimuth of 270 degrees because of the drag load of the retreating blade in helicopter mode and the gravity-induced load as the pylon is converted. (2) Higher harmonic loads are low, confirming that the Model 300 proprotor is free of resonance problems. (3) The pitch-link trace is free of stall-flutter characteristics, confirming freedom from stall-flutter problems. The blade loads smooth out progressively as the pylon is converted from helicopter to airplane mode, reflecting the reduction in skewed flow. In airplane mode, the only oscillatory force is from gravity at one per rev. Consequently, the airplane mode oscillatory loads are extremely low.

1. Loads in Helicopter Mode, α_{MAST} = +75 Degrees

Figure VII-3 shows a typical distribution of spanwise oscillatory bending moments for a relatively high thrust, high windspeed condition. For comparison, the calculated endurance limit is also shown. When the ratio of the measured load to the oscillatory load is considered, the station 52.5 beamwise bending moment and the spindle chordwise bending moment are the most critical. (This is also true for conversion and airplane mode.) Consequently, the loads data presented in this report pertain to the station 52.5 beamwise and the spindle chordwise loads (and the pitch link load, which indicates blade torsional loads and control system loads).

The variation in oscillatory loads versus thrust for three wind speeds is shown in Figures VII-4 through VII-6 for station 52.5 beamwise bending moment, the spindle chordwise bending moment, and the pitch link loads. Figure VII-7 shows the variation in blade and control loads with airspeed for a constant thrust.

2. Conversion Mode, α_{MAST} = +60 Degrees, +30 Degrees, and +15 Degrees

The design tip speed in conversion mode is 700 fps, but most of the test data for conversion mode were taken at 740 fps since a test stand frequency was in resonance with two per rev at the rpm corresponding to 700 fps (see Sections III and VIII). Test stand oscillatory load considerations dictated limited use of the rpm corresponding to a tip speed of 700 fps. Comparison of the small amount of blade load data taken at 700 fps with those taken at 740 fps reveals a negligible difference in magnitude and trend.

Figures VII-8 through VII-10 show the measured blade and yoke bending moments and pitch link loads versus thrust for several conversion angles. The most noticeable trend with conversion angle is the steady reduction in sensitivity to thrust as the shaft angle of attack is reduced.

3. Airplane Mode, α_{MAST} = 0 Degrees

The airplane mode data were taken with zero cyclic pitch, in contrast to helicopter and conversion mode where longitudinal cyclic was used to zero the longitudinal flapping.

The variation in blade and control oscillatory loads with airspeed and thrust was small, as shown in Figure VII-11. This was expected, because the oscillating excitation in the axial flow condition is primarily due to gravity.

The variation with mast angle of attack is shown in Figure VII-12 for 500 rpm and a wind speed of 185 knots. This same variation at the identical test conditions was determined during the dynamic

test with the proprotor mounted at the wing tip. A comparison of the data was made to determine the influence of wing-proprotor aerodynamic interference on blade loads. That influence was found to be small.

The steady pitch link loads are higher in airplane mode than they are in helicopter and conversion modes because the collective pitch is higher. Figure VII-13 shows the variation in pitch-link steady loads with airspeed in airplane mode. The influence of thrust on the steady load is small. Representative pitch link steady loads for helicopter and conversion mode are also shown for comparison.

C. CORRELATION OF THEORY WITH MEASURED OSCILLATORY LOADS

Theoretical blade loads were calculated by means of a hybrid computer version of the BHC Proprotor Aeroelastic Analysis, Program DYN5, described in Section V. The hybrid version has been developed specifically for the purpose of computing blade loads for wind tunnel test conditions. While there were some differences between the loads predicted before the test and the measured loads, these have been traced to the swashplate phasing error discussed in Subsection VII.A.

With the input errors corrected, the correlation is excellent. (The theory appears to be slightly conservative.) The predicted oscillatory loads are plotted in Figures VII-3 through VII-13 with the measured data shown for comparison.

No attempt has been made to predict the oscillatory pitch link loads, hence correlative data are not shown. The design oscillatory loads were established by means of an empirical method which BHC uses for semirigid rotors. The steady pitching moment of the blade has been calculated for airplane mode and is compared with the measured steady load in Figure VII-13. The correlation is excellent.

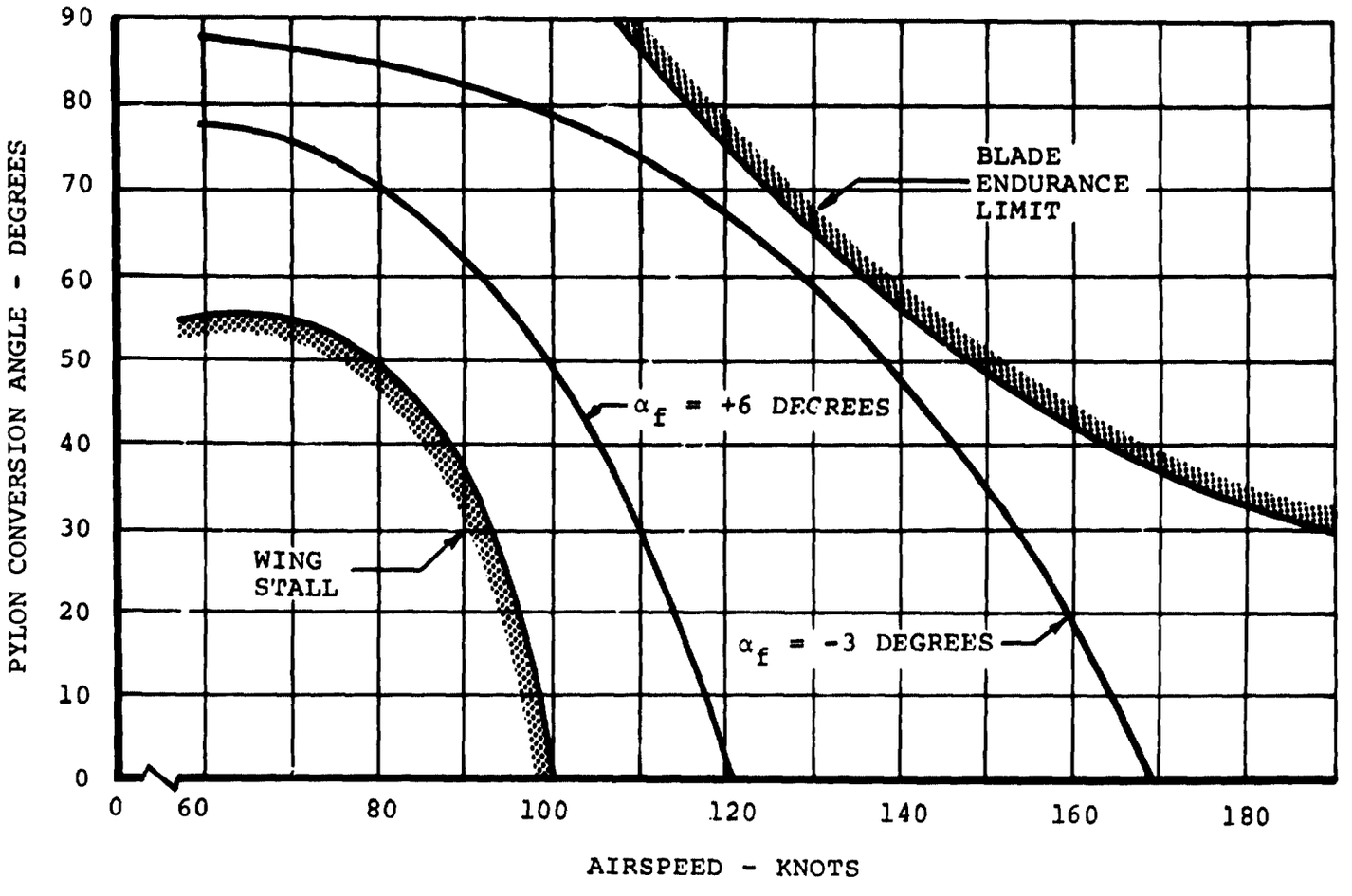

Figure VII-1. Conversion Corridor Based on Measured Blade Loads.

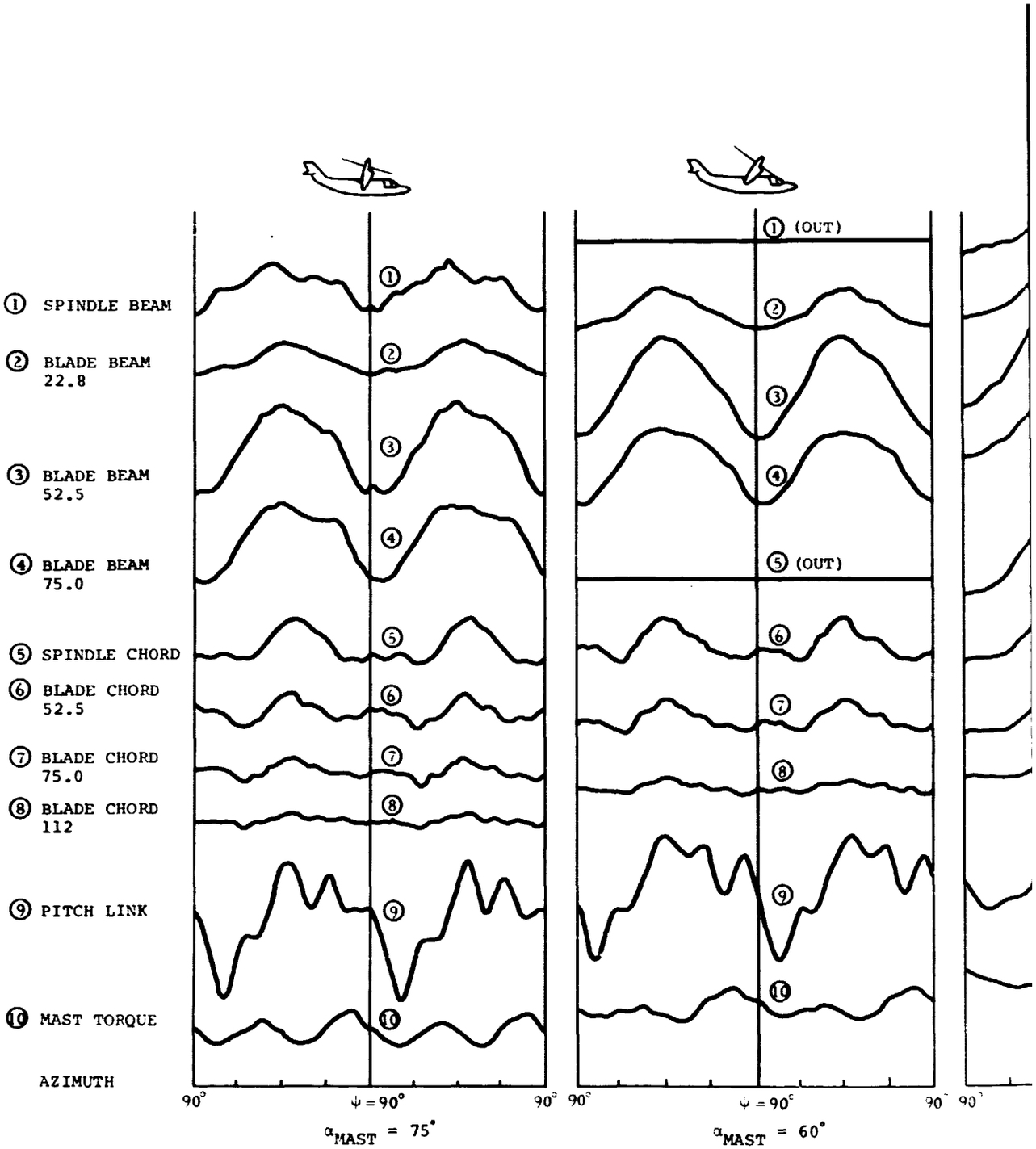

Figure VII-2. Blade and Control Loads Wa

FOLDOUT FRAME

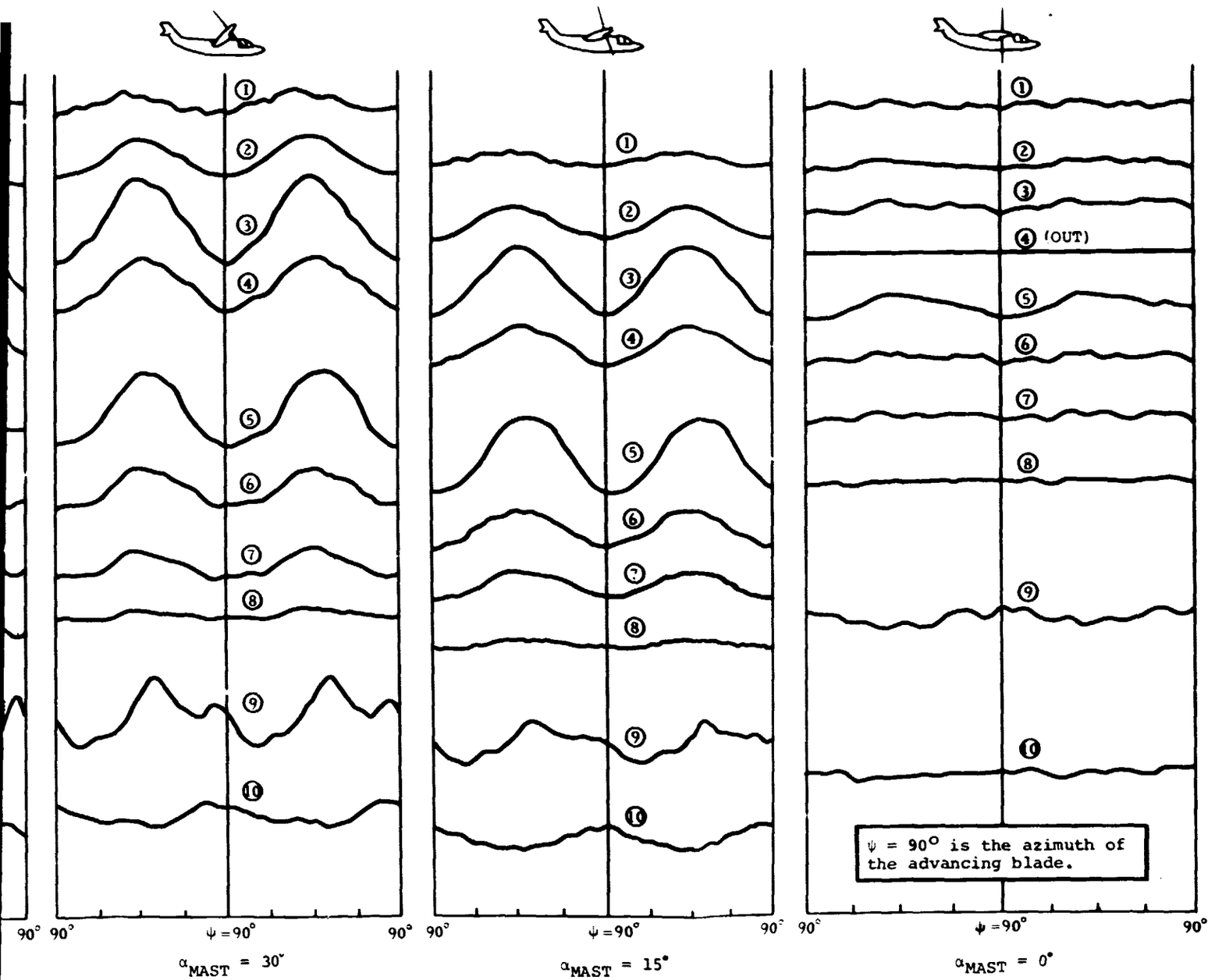

rol Loads Waveforms in Helicopter, Conversion, and Airplane Modes.

FOLDOUT FRAME

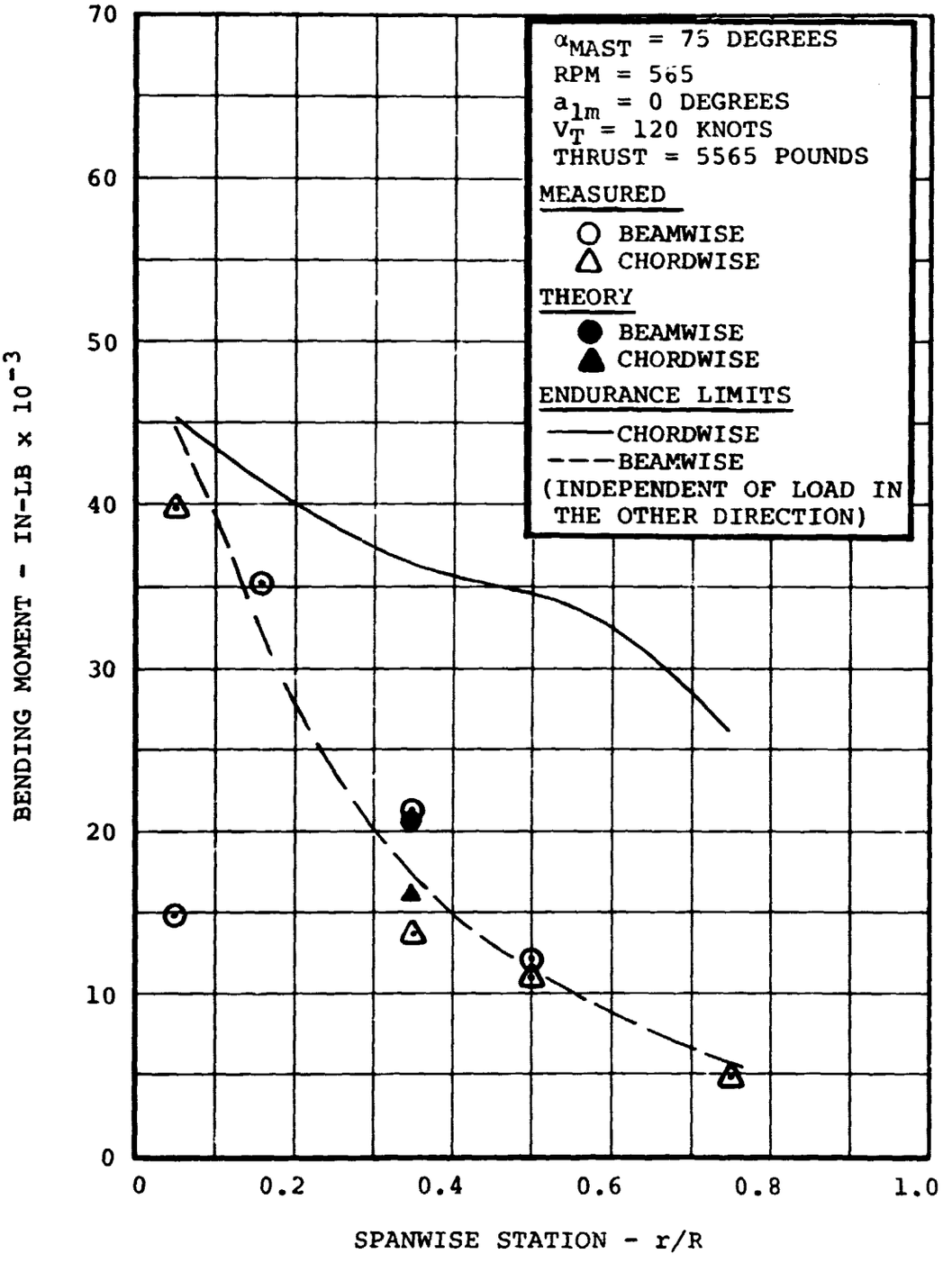

Figure VII-3. Spanwise Oscillatory Bending Moment Distribution in Helicopter Mode.

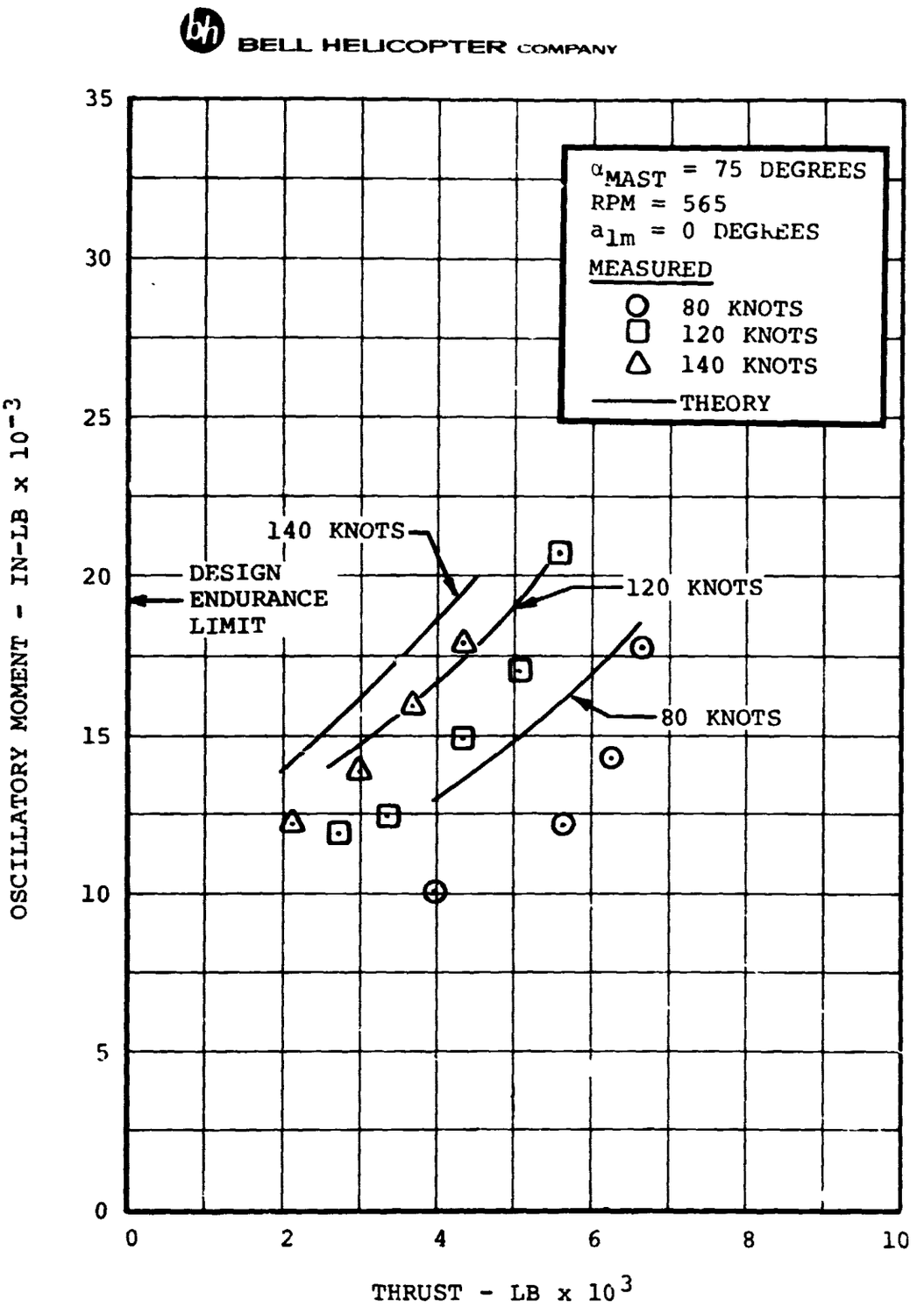

Figure VII-4. Blade Station 52.5 Beam Oscillatory Bending Moment versus Thrust in Helicopter Mode.

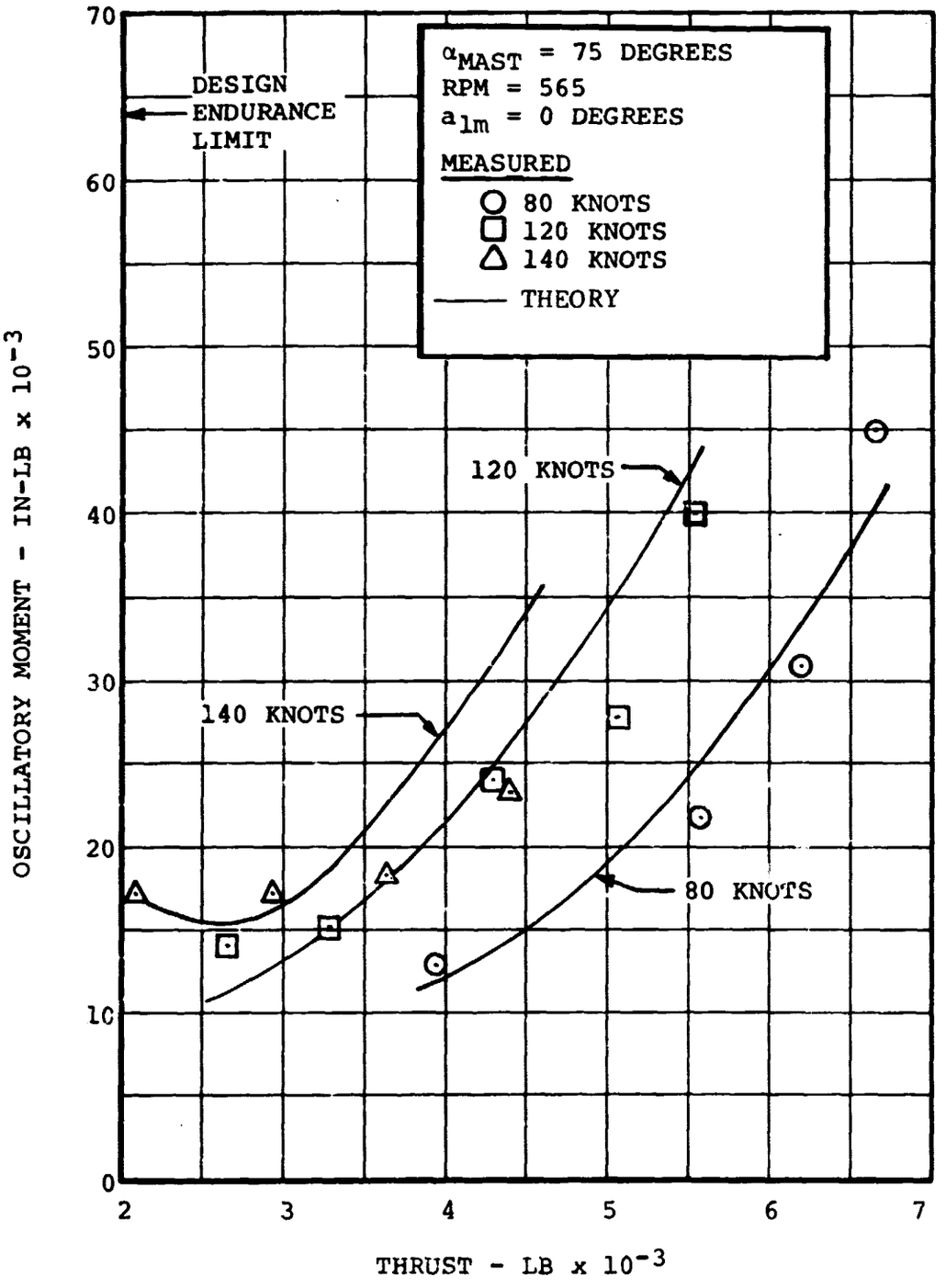

Figure VII-5. Spindle Chord Oscillatory Bending Moment Versus Thrust in Helicopter Mode.

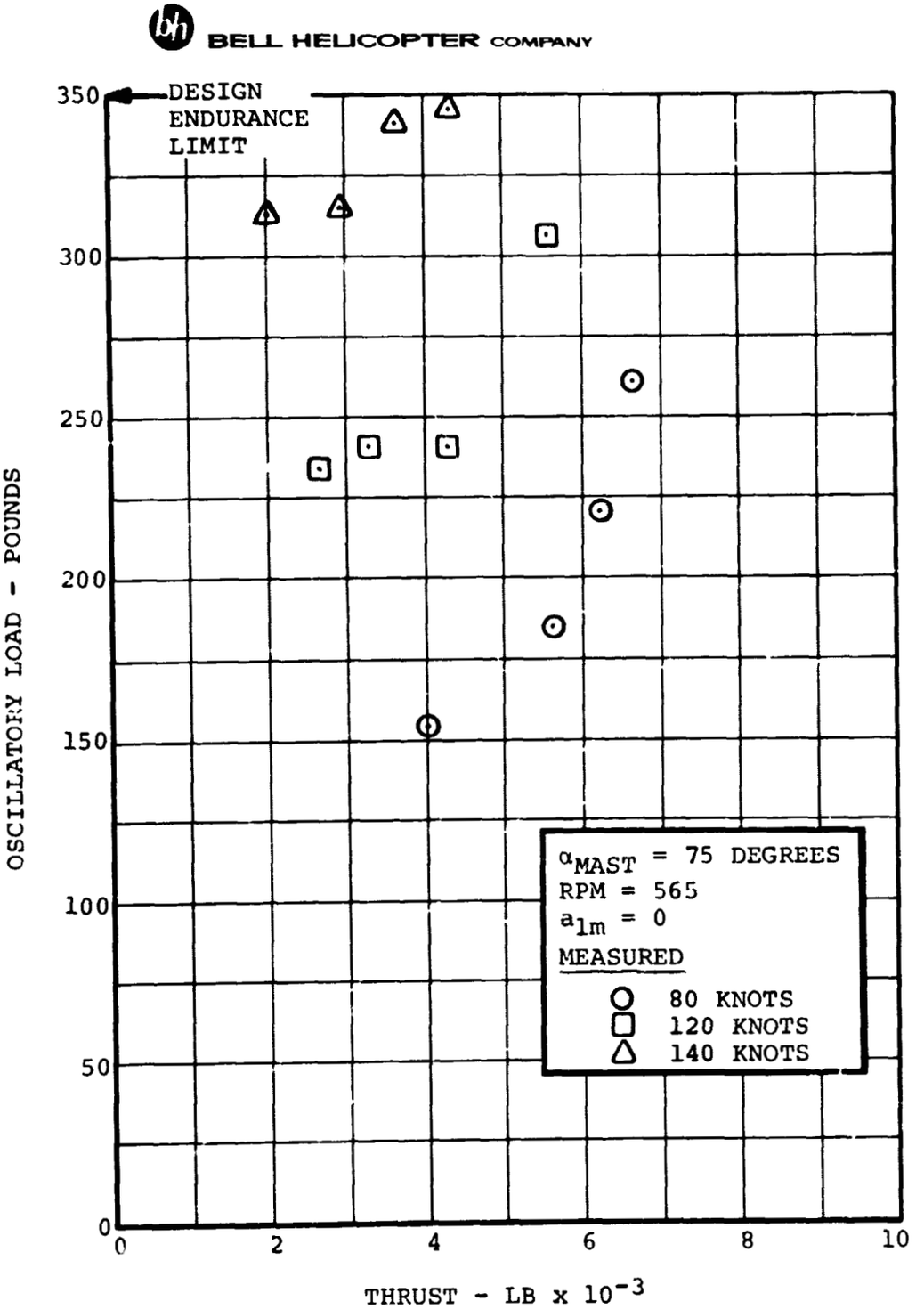

Figure VII-6. Blade Pitch-Link Oscillatory Load Versus Thrust in Helicopter Mode.

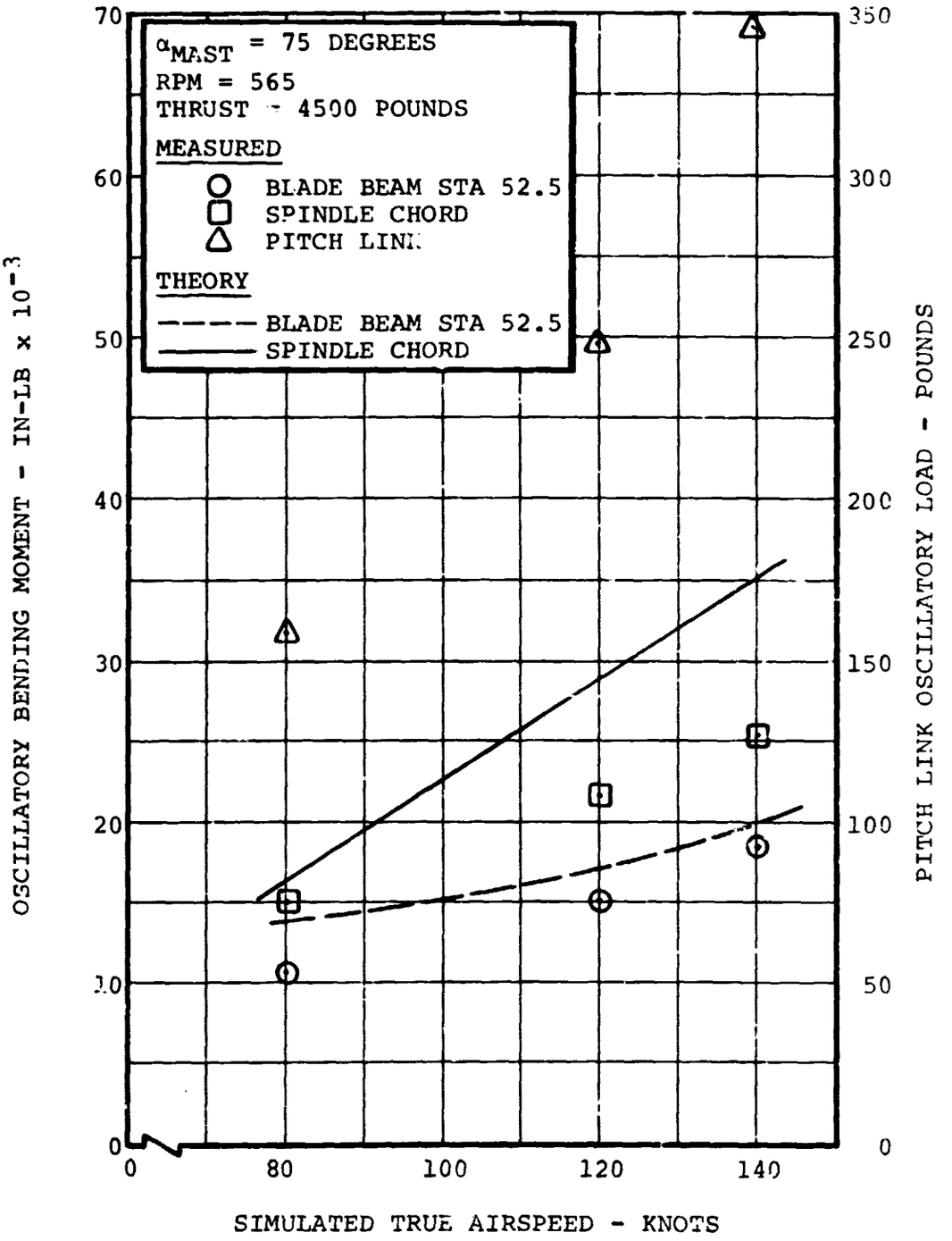

Figure VII-7. Oscillatory Loads Versus Airspeed, Helicopter Mode.

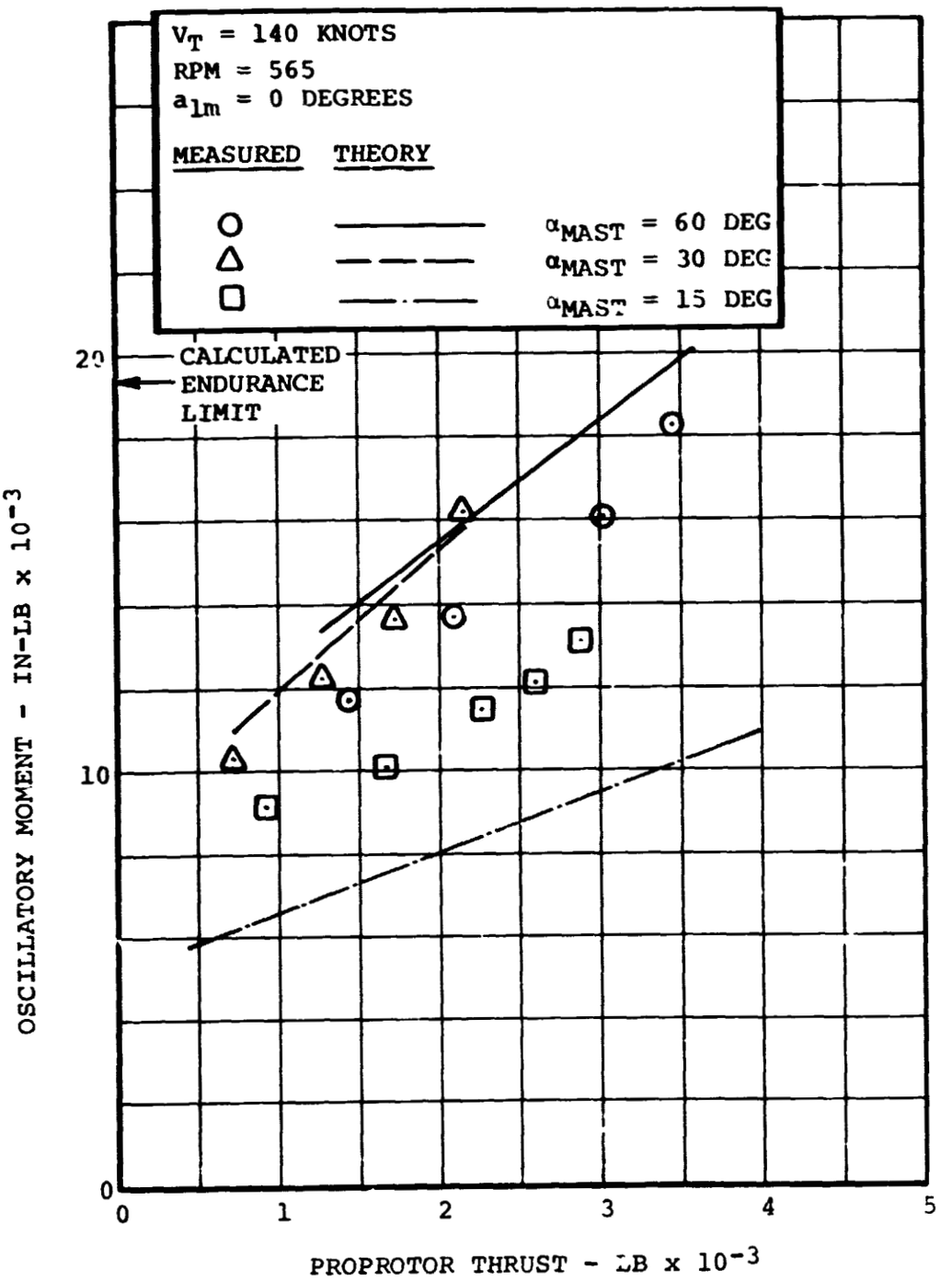

Figure VII-8. Blade Station 52.5 Oscillatory Beamwise Bending Moment Versus Thrust in Conversion Mode.

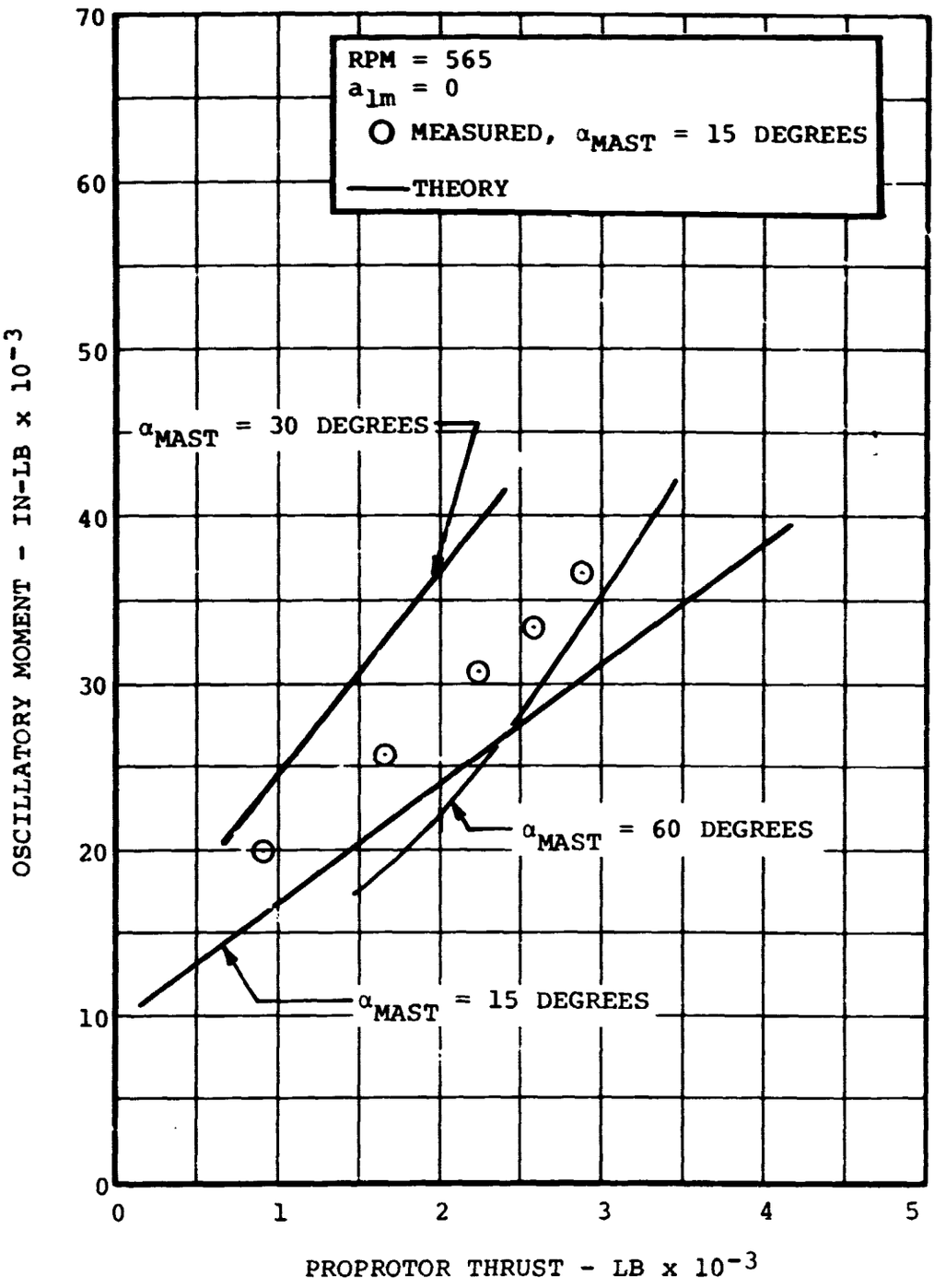

Figure VII-9. Yoke Spindle Chord Oscillatory Bending Moment - Conversion Mode.

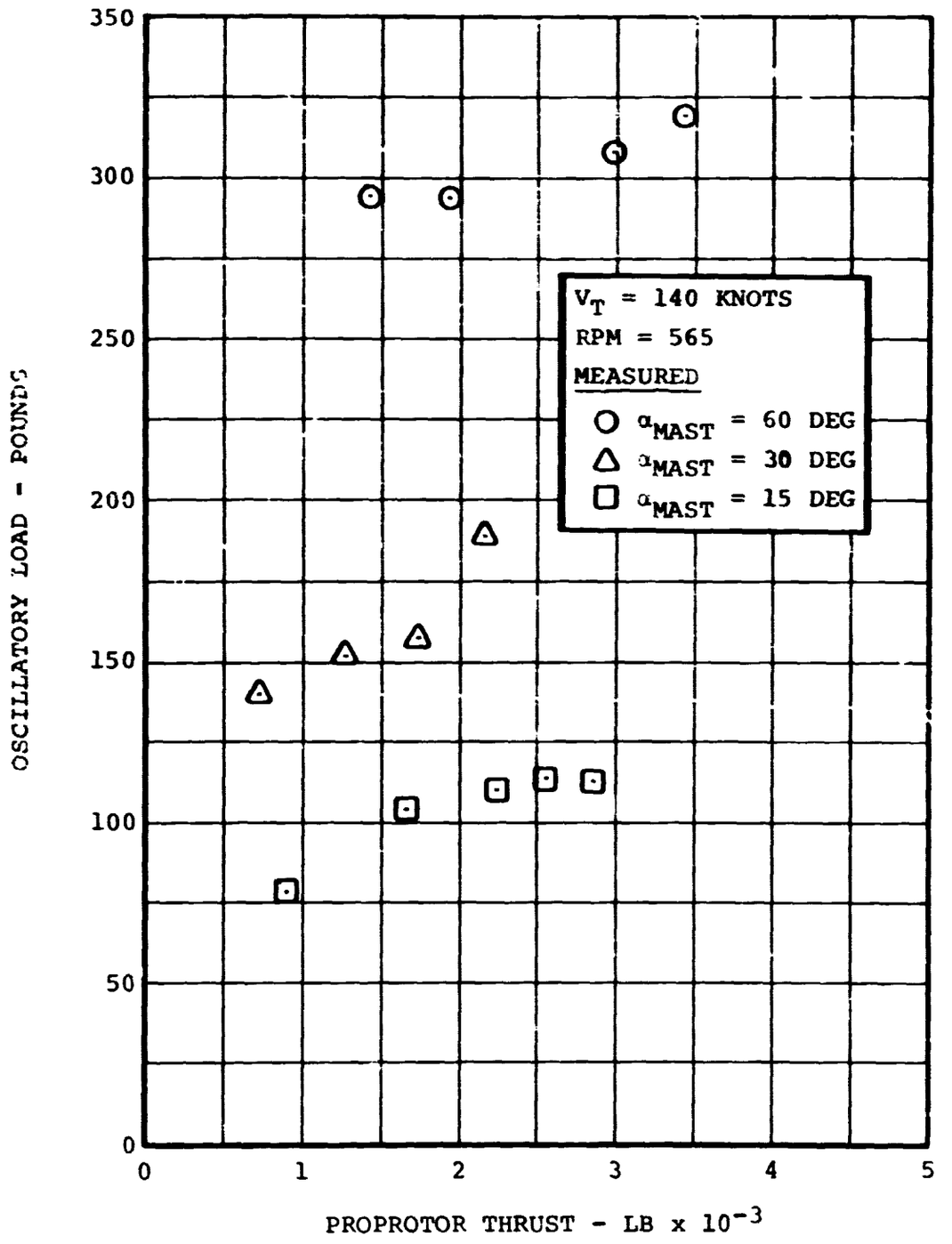

Figure VII-10. Pitch-Link Oscillatory Load Versus Thrust in Conversion Mode.

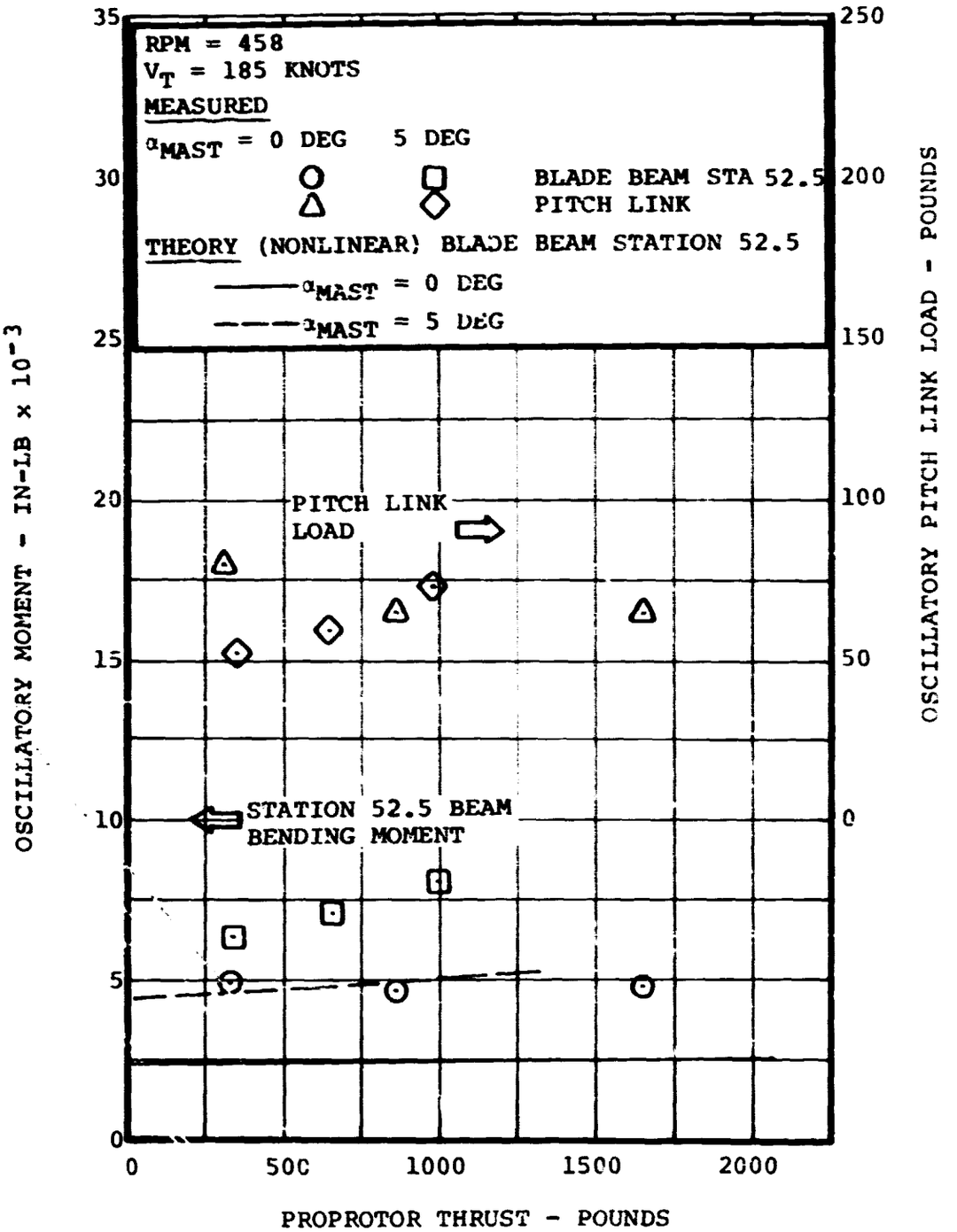

Figure VII-11. Blade Station 52.5 Beam Bending Moment and Pitch Link Loads versus Proprotor Thrust in Airplane Mode.

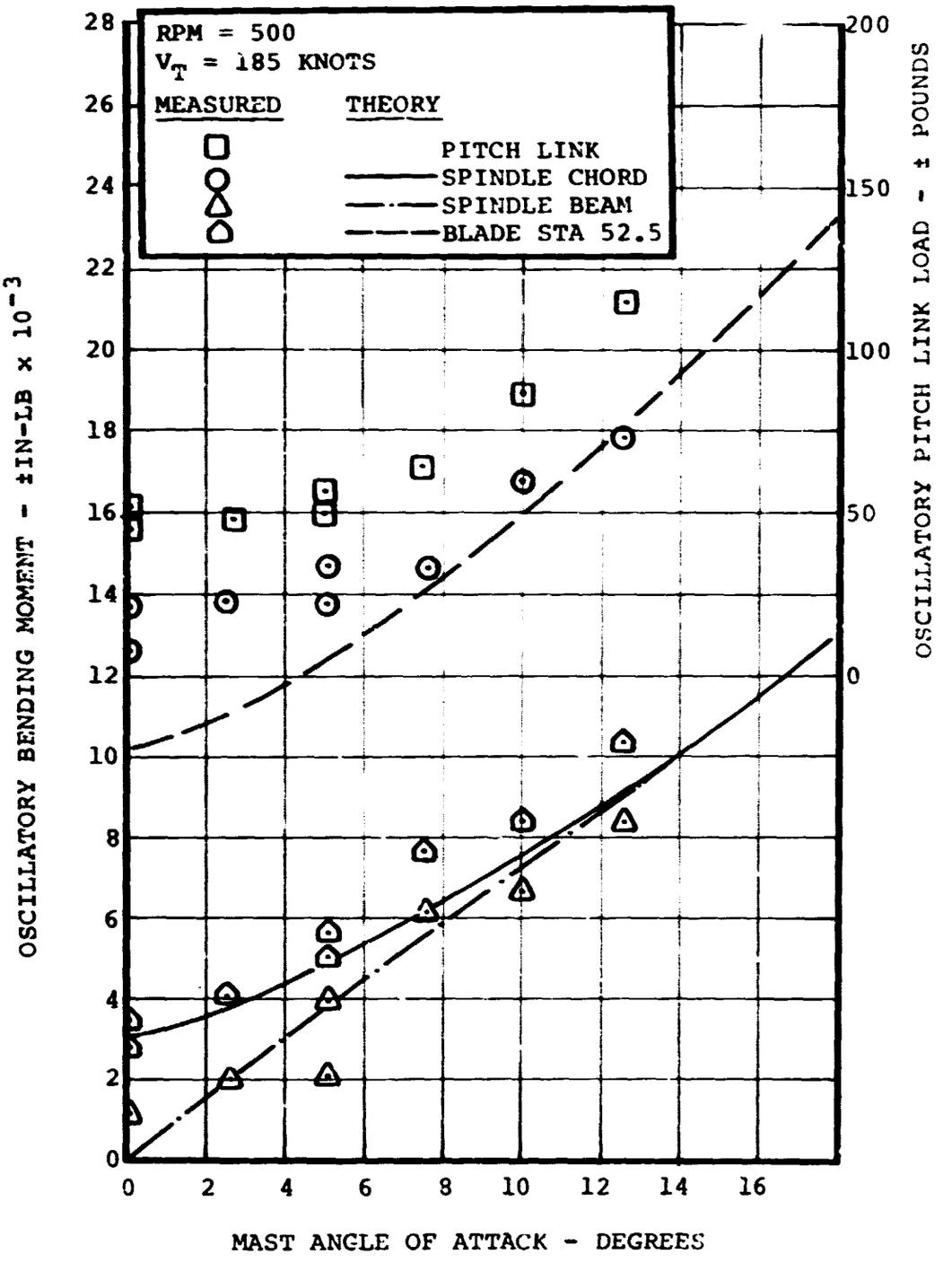

Figure VII-12. Blade and Pitch Link Loads Versus Angle of Attack in Airplane Mode.

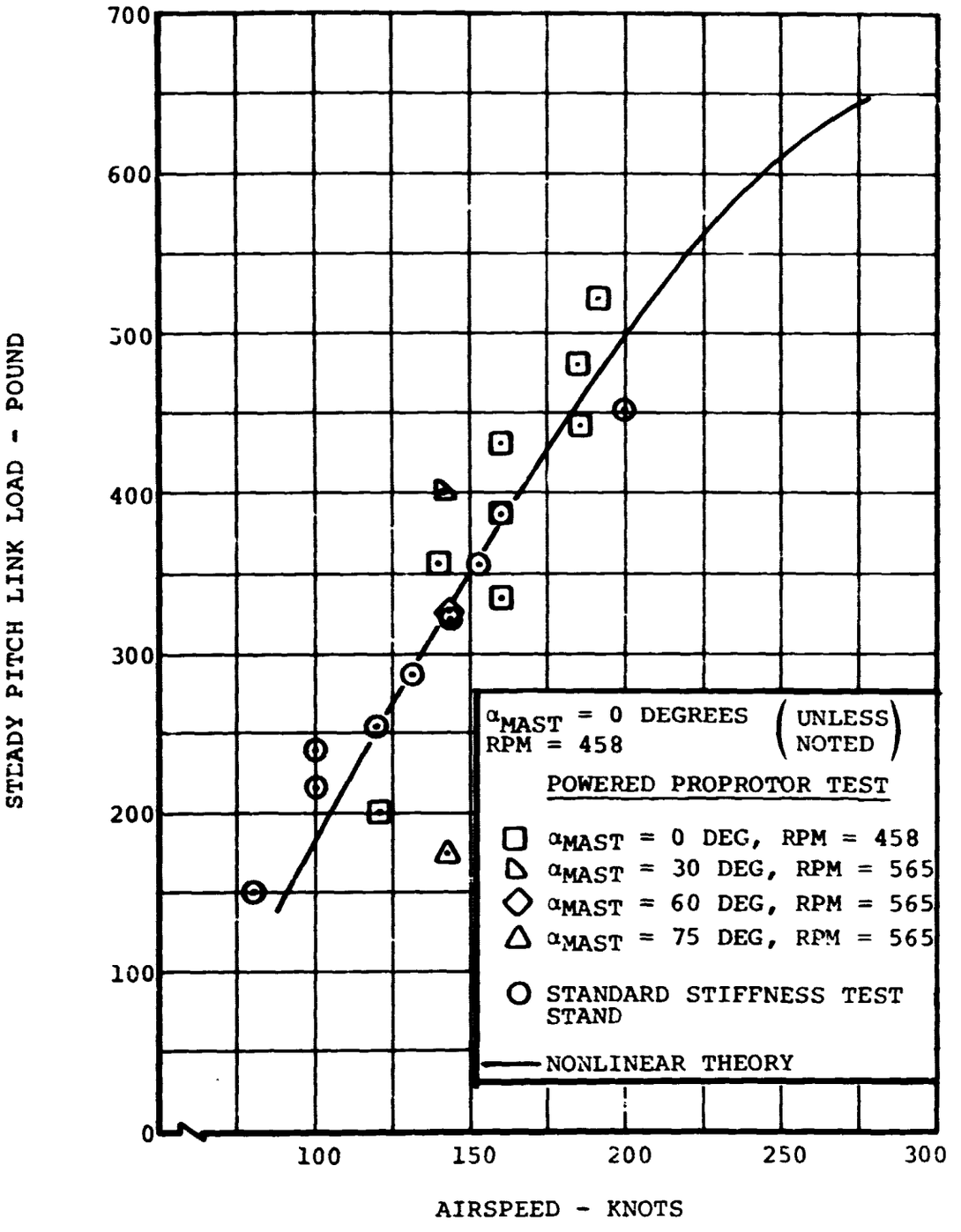

Figure VII-13. Pitch Link Steady Load Versus Airspeed in Airplane Mode.

VIII. NOISE AND VIBRATION

A. NOISE

During powered testing a microphone 68 feet upstream of the model and 5 feet above the floor on the centerline of the tunnel monitored the noise level. (This location is the same as that for a past program which measured the noise of conventional rotors. See References 29 and 30.) The output of the microphone was recorded for mast tilt angles from zero to 75 degrees, for several tip speeds, and at various thrust and power settings.

Figure VIII-1 shows the comparison between proprotor and conventional rotor noise. For tunnel velocities above about 80 knots, the noise of the proprotor in takeoff mode is lower than that of a square-tipped conventional rotor. Also, the rate of increase in proprotor noise, as tunnel velocity increases, is somewhat less than for conventional rotors. The proprotor's noise in cruise mode, at tilt angles between zero and 30 degrees, is at least 7 decibels lower than that for the takeoff mode. (Predictions show a reduction on the order of 15 decibels.)

The proprotor sounds more like a propeller than a rotor, lacking the loud blade slap which is characteristic of conventional rotors at high speeds. In cruise mode, the proprotor is reasonably quiet--quiet enough, in fact, that the sound of the wind tunnel masks it almost completely.

The noise measurements shown in Figure VIII-1 can be extrapolated to give estimated noise levels for the Model 300. Figure VIII-2 shows the results of such an extrapolation, and shows the noise characteristics of a variety of other air and surface vehicles for purposes of comparison. As the figure shows, the noise of the Model 300 during takeoff will be about the same as that of a medium helicopter, whereas its noise in cruise flight will be about the same as that of a light helicopter. The observer on a busy street corner would be unable to hear the Model 300 passing over in cruise flight at an altitude of 1000 feet.

B. VIBRATION

Vibration levels were measured at two stations on the dynamic test stand pylon: the intersection of the centerlines of the conversion spindle and mast (Pylon Station 0), and at Pylon Station 36. At Station 0 the vibration was measured along the shaft axis, in the wing beam sense, and in the pylon yaw sense. At Station 36, the vibration was measured in the wing beam and pylon yaw senses.

The dominant vibration was at the blade passage frequency (three per rev) and was due to aerodynamic interference between the wing and the proprotor. Its amplitude increased with both airspeed

and mast angle of attack. The amplitude was extremely sensitive to rpm in the case of the design-stiffness test stand since the lateral bending natural frequency of the mast was in resonance with three-per-rev excitations at 470 rpm.

As noted in Section III, the dynamic test stands do not respond exactly as the Model 300 wing-pylon system would in the normal operating rpm, three-per-rev frequency range because their structural details (such as the transmission and pylon case, engine installation, and the mast) are not dynamically similar. Detailed scaling of these features was not necessary to duplicate dynamic stability characteristics. Natural frequencies of both test stands were close to resonance with three per rev, producing relatively high three-per-rev vibrations. Even so, the test operation was not significantly restricted.

Five accelerometers were installed on the powered test stand, primarily for the purpose of monitoring test stand oscillatory loads. The torquemeter bolt ring was estimated to be the critical member of the test stand, and therefore acceleration limits were established which would preclude exceeding its endurance limit. During the conversion and helicopter mode tests, operation of the proprotor at 535 rpm (ΩR = 700 ft/sec) was avoided because the two-per-rev vibration levels exceeded the established limit. (These resulted from a test stand mode being in resonance at 535 rpm, with the two-per-rev torque generated by the gimbal when the rotor flapped.) Vibration at other proprotor speeds was not a problem.

1. Vibration Characteristics of the Test Stands During Normal Proprotor Operation

Figure VIII-3 shows how the three-per-rev vibration of the design-stiffness dynamic test stand varied with rpm. The installation of the pylon yaw link simulated fully converted airplane mode flight (pylon on the downstop). The large amplitude in the 450-470 rpm range is due to resonance of the mast lateral bending mode with three per rev. Figure VIII-4 shows the variation in amplitude with airspeed at constant 458 rpm. There are no data in the 170-190-knot range because of the mast lateral bending mode resonance at 458 rpm in this speed range.

Without the yaw link the amplitude of the three per rev was much lower (as shown in Figure VIII-5). In this case the introduction of the pylon yaw mode (14.1 cps, or 1.85 per rev) forces the mast lateral bending mode to over 50 cps (greater than eight per rev at 458 rpm). For that condition there are no modes near three per rev (see Section III).

Figure VIII-6 shows how the vertical (beamwise) three-per-rev vibration at Pylon Station 36 varied with simulated airspeed or both the one-fourth and design stiffness test stands. Note that the one-fourth-design-stiffness test stand data are not

at constant rpm because of the collective pitch limitations discussed in Section V. At 300 knots the vibration level (1.2g) is less than 50 percent of the Model 300 design limit (+2.5g).

Figure VIII-7 shows the influence of angle of attack on the vertical vibration at Pylon Station 36. The increase in amplitude with angle of attack is due to the increasing wing upwash.

Vibration data from the powered test are summarized in Figure VIII-8. It illustrates the trend in vibration level during a conversion at constant airspeed and rpm. Since the response of the powered test stand in the three-per-rev frequency range is essentially invariant with conversion angle (see Section III), the reduction in vibration level as the pylon is converted is due to reduced excitation.

2. Vibration During Stop-Start Operation

Exploratory tests to simulate the stop-start phase of the folding proprotor concept were made on both the standard and one-quarter-stiffness dynamic test stands. Of primary interest were the vibration levels that would be encountered as a starting or stopping operation passed through the various resonant frequencies of the blades, wings, and pylons. The 25-foot proprotor of these tests was not designed to be folded in flight, therefore did not have a flapping lockout or a high-rate collective pitch arrangement, features which would improve its feathering characteristics. Nevertheless, the proprotor feathered without difficulty at airspeeds up to 265 knots (simulated) and angles of attack up to 6 degrees.

The stop-start tests on the design-stiffness test stand were conducted at an airspeed of 136 knots. The collective pitch range restricted the rpm sweeps from the low pitch limit (600 rpm) to the high pitch limit (250 rpm). Several resonances of the blade and wing were transited during these sweeps without any significant increase in loads or vibration. The time to change from 600 to 250 rpm was 2.75 seconds; and to return to 600 rpm, 2.48 seconds.

On the one-fourth-design-stiffness stand, stop-start tests were at simulated speeds of 185 and 265 knots. Full stops to zero rpm were made in both cases. At 185 knots the angle of attack was varied from 0 degrees to +6 degrees. The time to stop or start was approximately 6 seconds (equivalent to 3 seconds in real time). The optimum real time required for the stop-start operation has been shown by model tests to be 2 to 3 seconds.

Figure VIII-9 shows a time history of proprotor and test stand response during stopping at 185 knots and zero angle of attack. As the blade passage frequency transits each of the stand natural modes, a buildup appears. Model tests and theory (see References 22 and 28) have established that the aerodynamic interference

between wing and rotor causes hub shears at the blade passage frequency and generates a small amount of excitation at twice the blade passage frequency. The shorter the time required for stopping, the smaller the amplitude of the buildup--down to the time for minimum buildup, given as $\Delta t = 2.75\sqrt{D}/38.5$ seconds (Reference 26) or about 2.2 seconds in the case of a 25-foot-diameter proprotor.

As Figure VIII-10 shows, the amplitude of the response increases with angle of attack. The angle of attack illustrated (4 degrees) corresponds to a 1.5g maneuver. The amplitude also increases with airspeed as shown in Figure VIII-11.

The limited number of data points keeps the results of the stop-start tests essentially qualitative, but the tests did show that feathering the blades and stopping the rotor is feasible. Loads and accelerations were well within allowable limits and there was no evidence of instability. A modified version of the 25-foot proprotor which incorporates a flapping lockout and blade folding will be tested in the fall of 1971.

3. Correlation of Theory with Measured Vibration

Under contract to the U.S. Air Force Flight Dynamics Laboratory, BHC has developed a highly refined theory which predicts the aerodynamic interference between wing and proprotor (Reference 28). Good correlation with measured vibration data from dynamically scaled models has been established and is shown in that report.

A study of the correlation of BHC vibration theory with the vibration measured during the dynamic stability test has not been made. A large amount of digital computer time would be required for such a study and because accuracy of the theory has already been investigated, the expense was considered unwarranted. Furthermore, the data indicate the vibration problem is essentially one of avoiding resonance with three per rev.

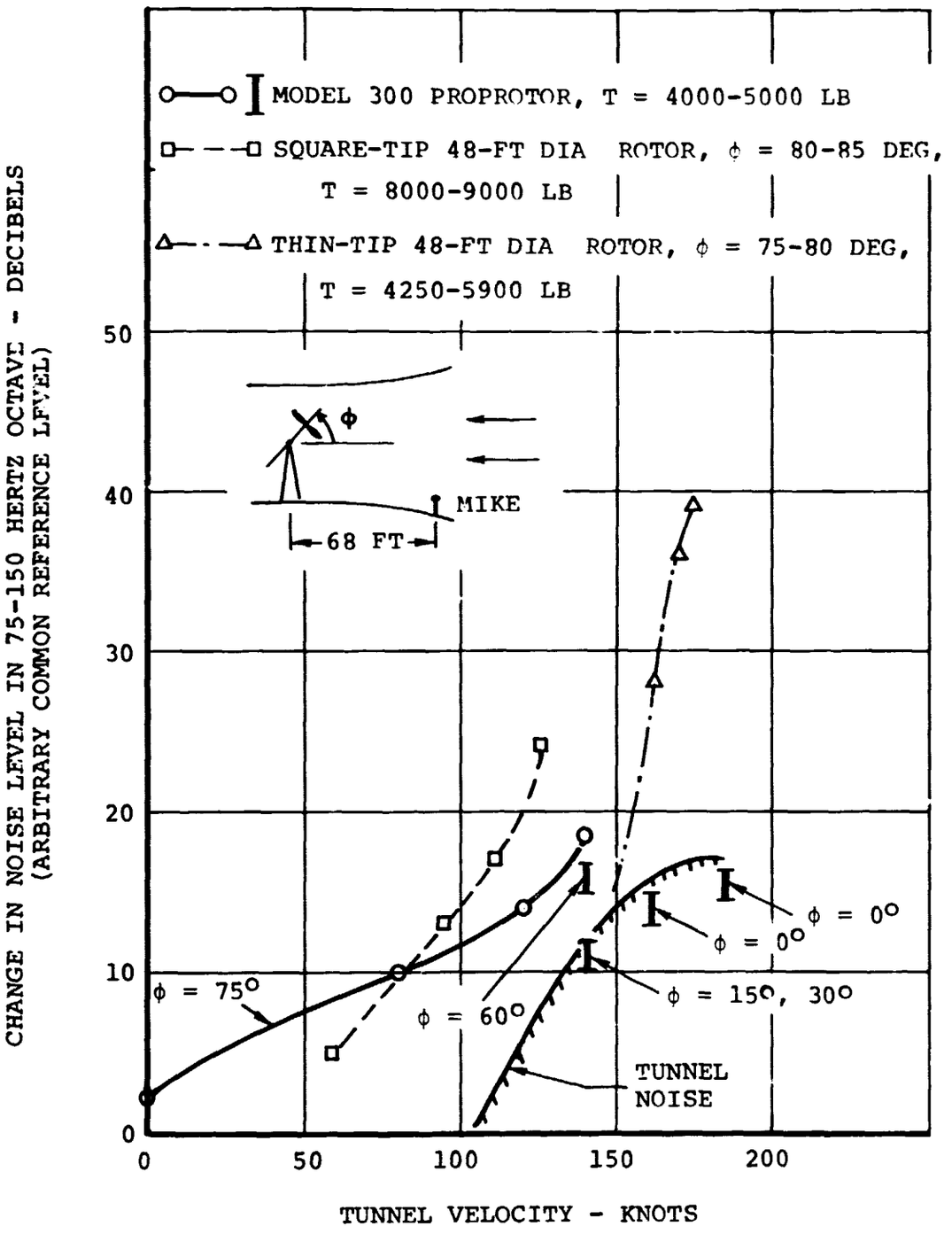

Figure VIII-1. Comparison of Model 300 Proprotor and Conventional Rotor Noise Levels Measured in Ames 40- by 80-Foot Wind Tunnel.

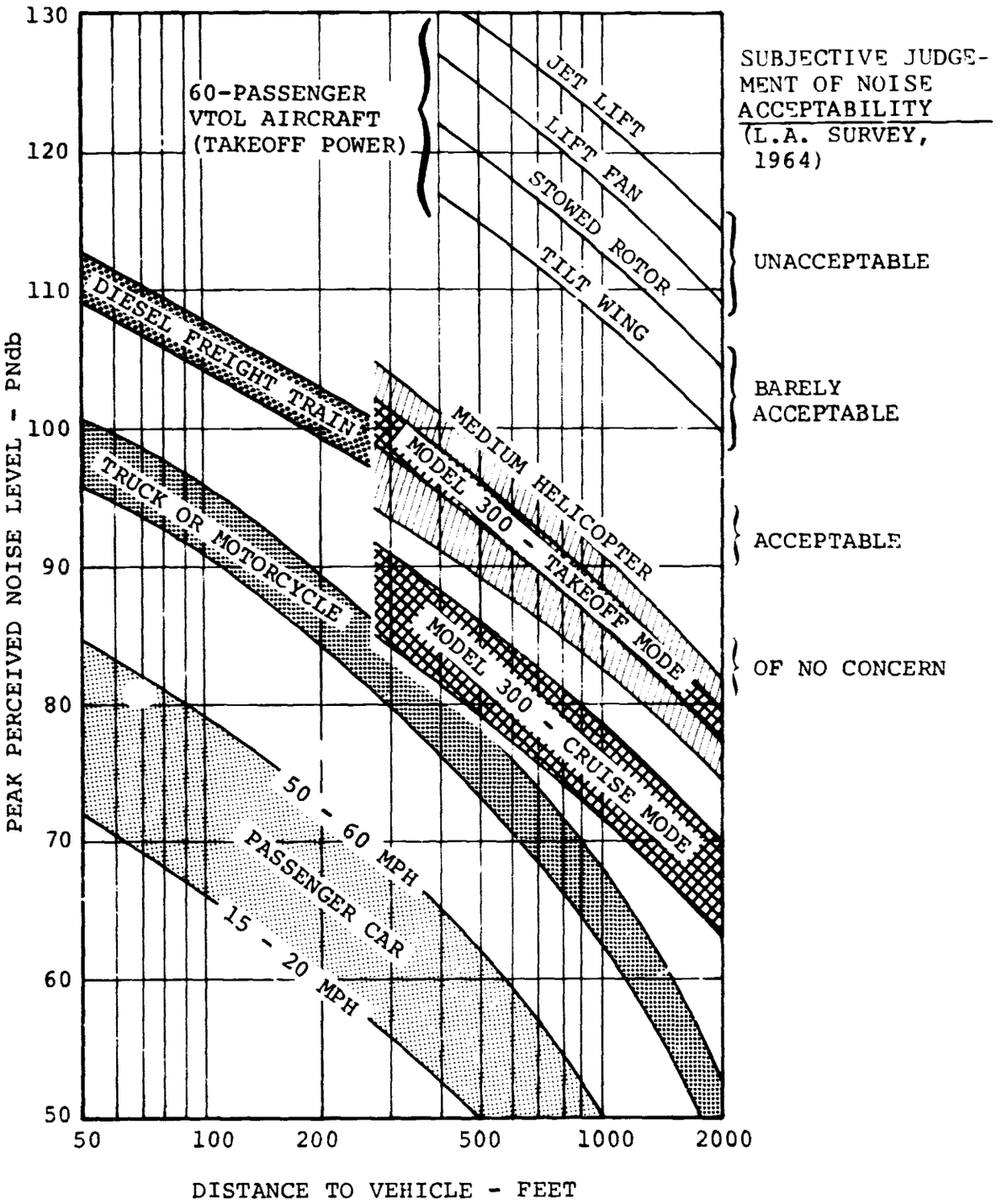

Figure VIII-2. Estimated External Noise Levels.

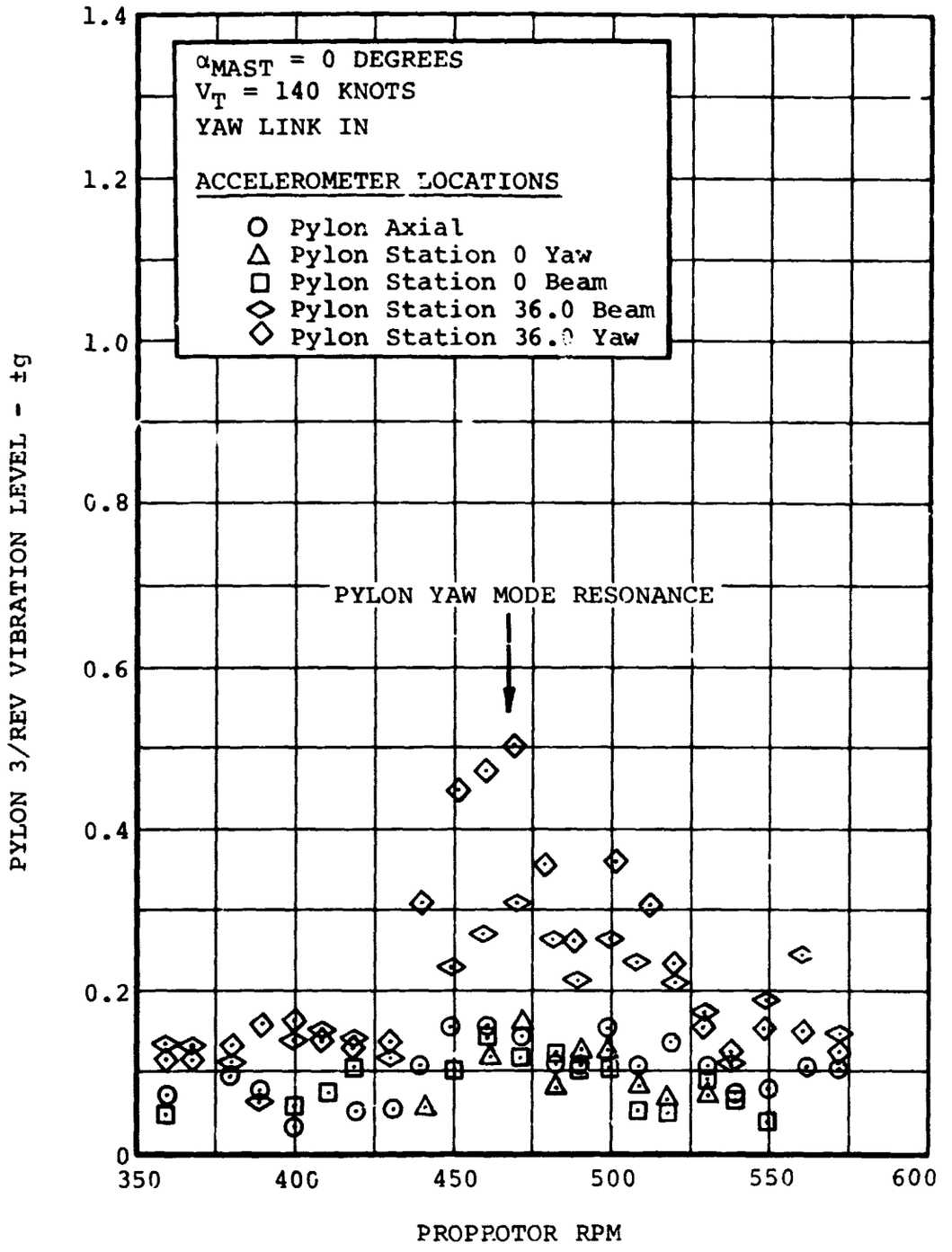

Figure VIII-3. Pylon Three-Per-Rev Vibration Level Versus Proprotor RPM for Standard Stiffness Test Stand (Airplane Mode).

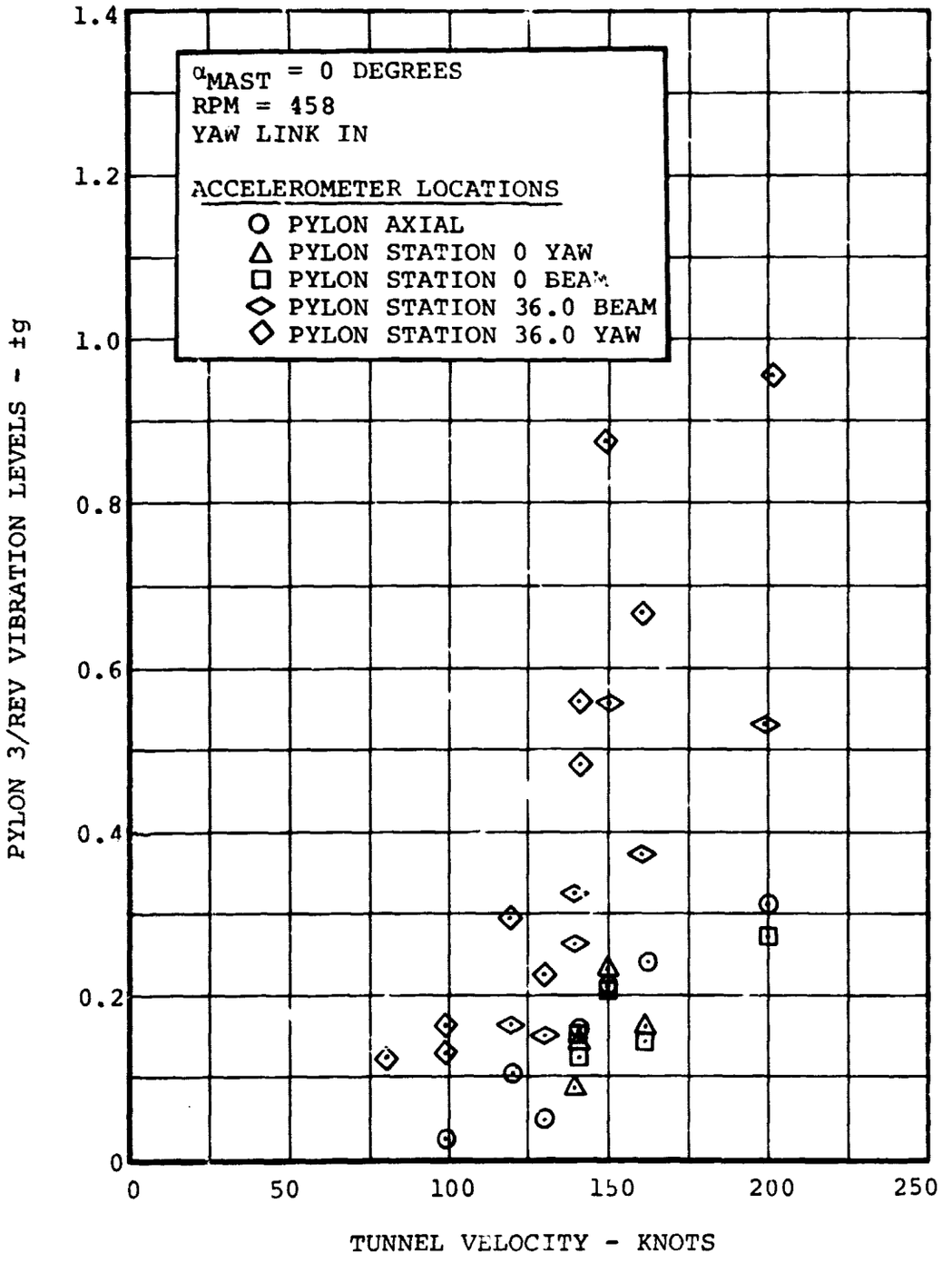

Figure VIII-4. Pylon Three-Per-Rev Vibration Level Versus Tunnel Velocity for Standard Stiffness Test Stand (Airplane Mode).

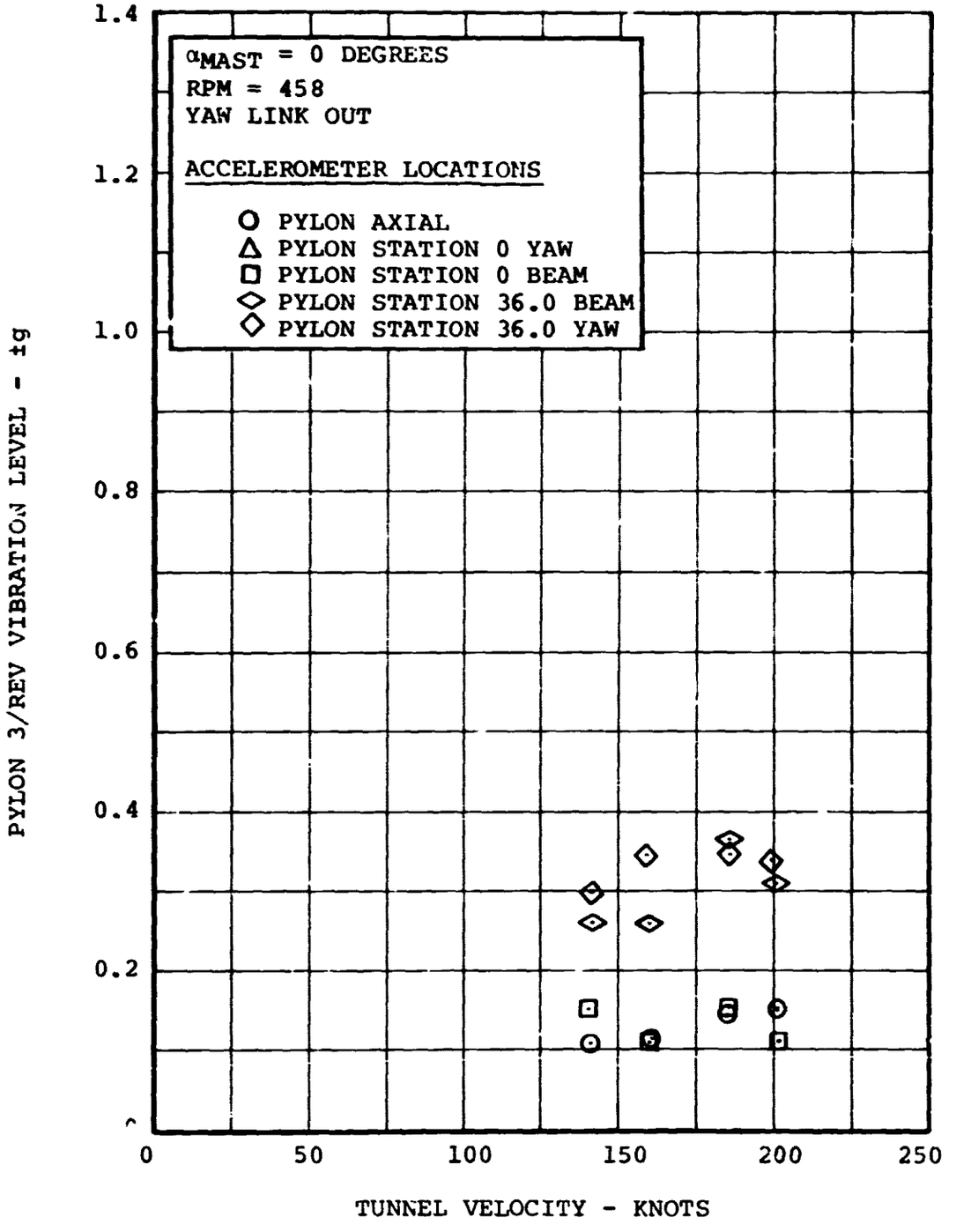

Figure VIII-5. Pylon Three-Per-Rev Vibration Level Versus Tunnel Velocity for Standard Stiffness Test Stand (Airplane Mode - Yaw Link Out).

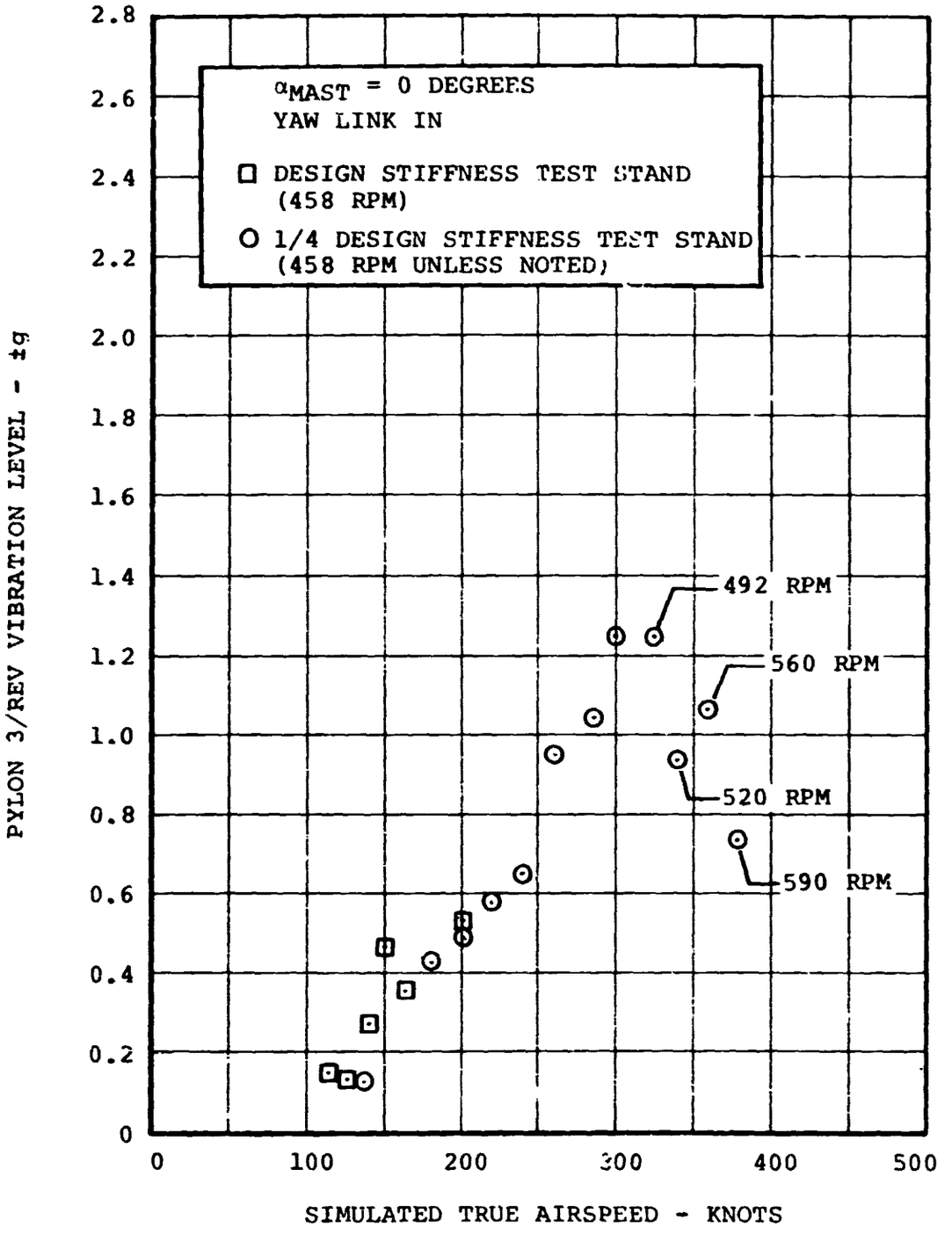

Figure VIII-6. Three-Per-Rev Beamwise Vibration at Pylon Station 36 Versus Simulated Airspeed (Airplane Mode).

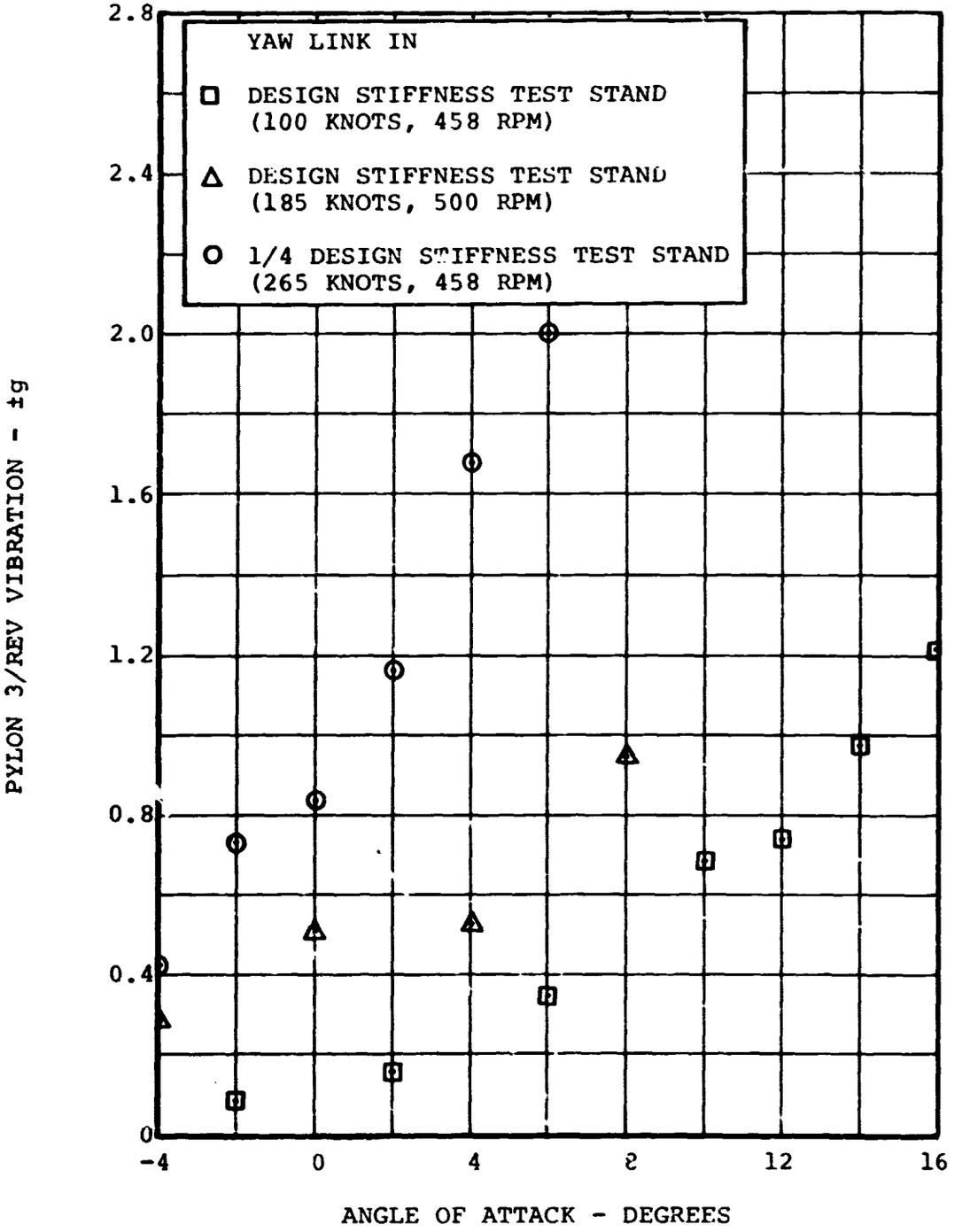

Figure VIII-7. Three-Per-Rev Beamwise Vibration at Pylon Station 36 Versus Angle of Attack (Airplane Mode).

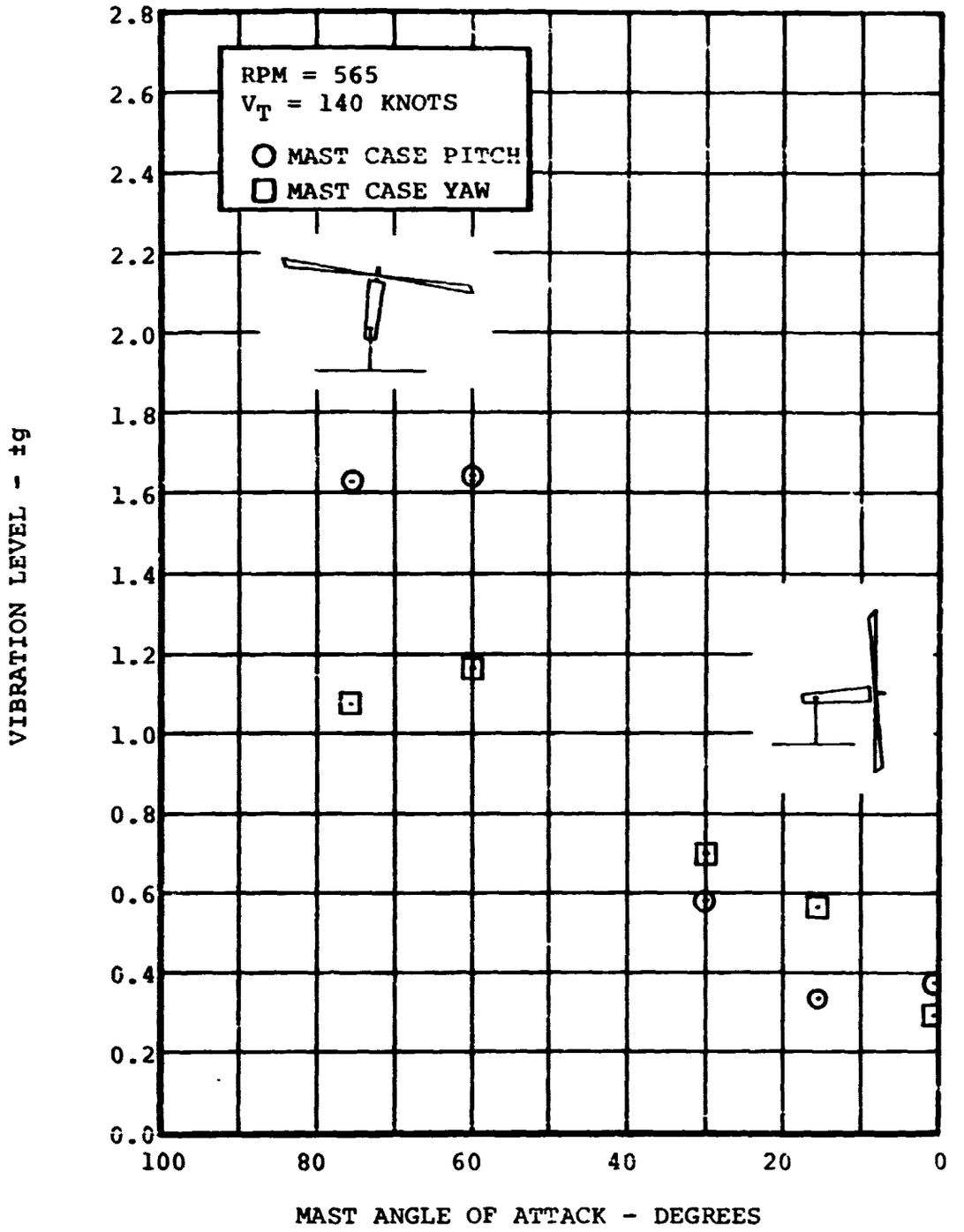

Figure VIII-8. Mast Case Three-Per-Rev Vibration Levels Versus Mast Angle of Attack, Helicopter and Conversion Modes.

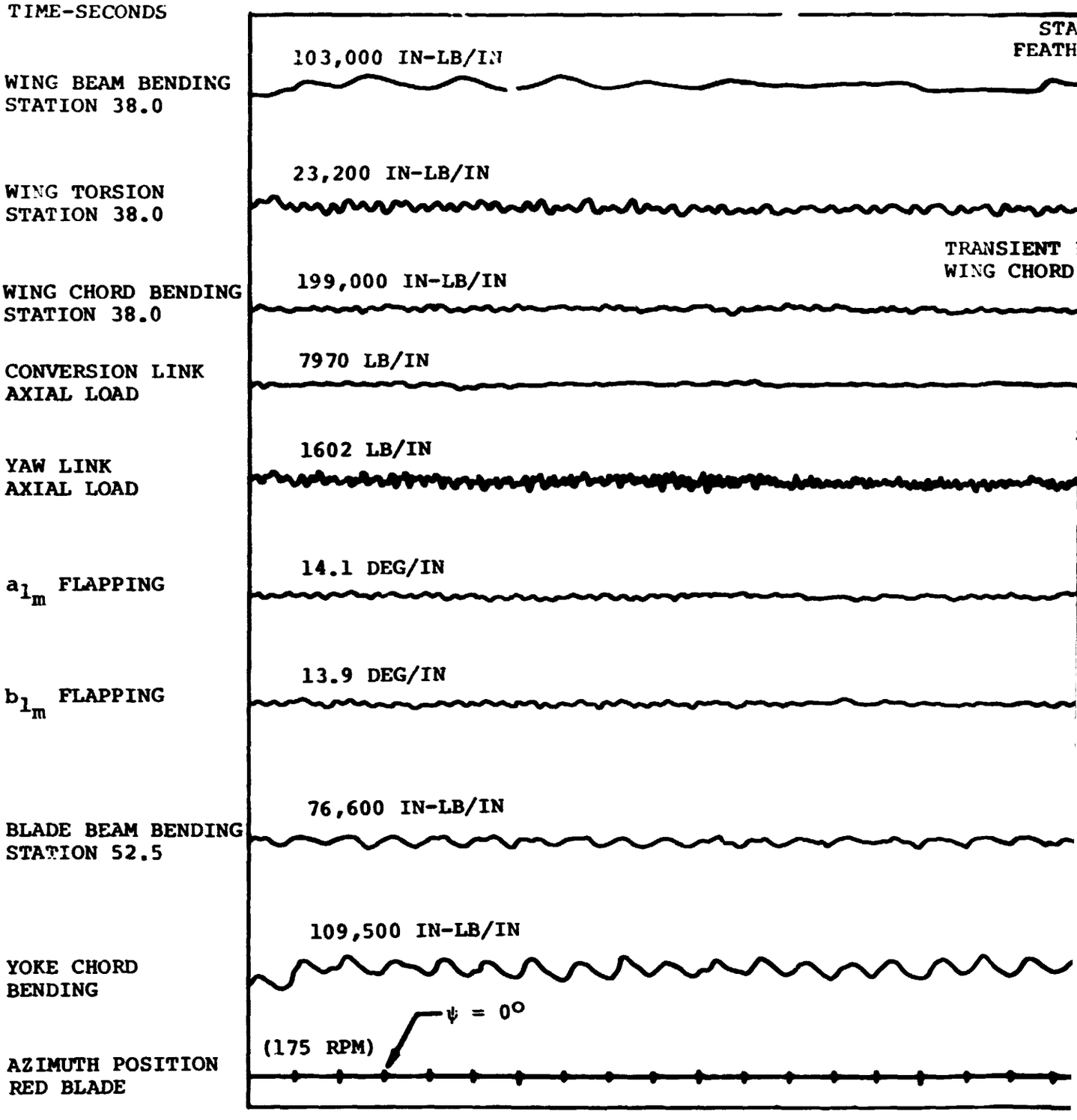

Figure VIII-9. Time History of Feather-Stop
Test Stand, Zero Degrees Ang
Tunnel Speed = 92.5 Knots.

300-099-004

FOLDOUT FRAME

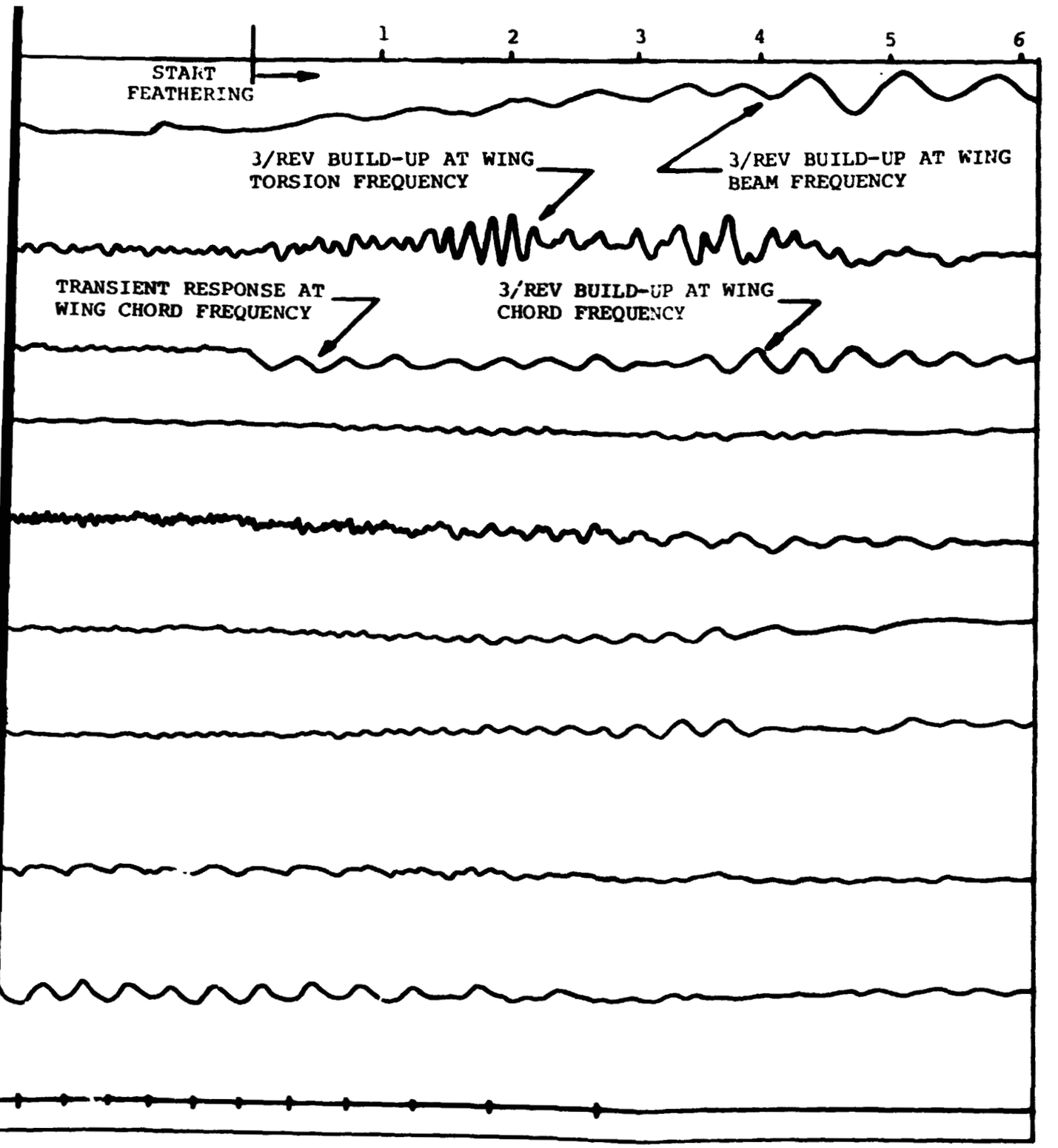

Feather-Stop for Quarter Stiffness
o Degrees Angle-of-Attack,
92.5 Knots.

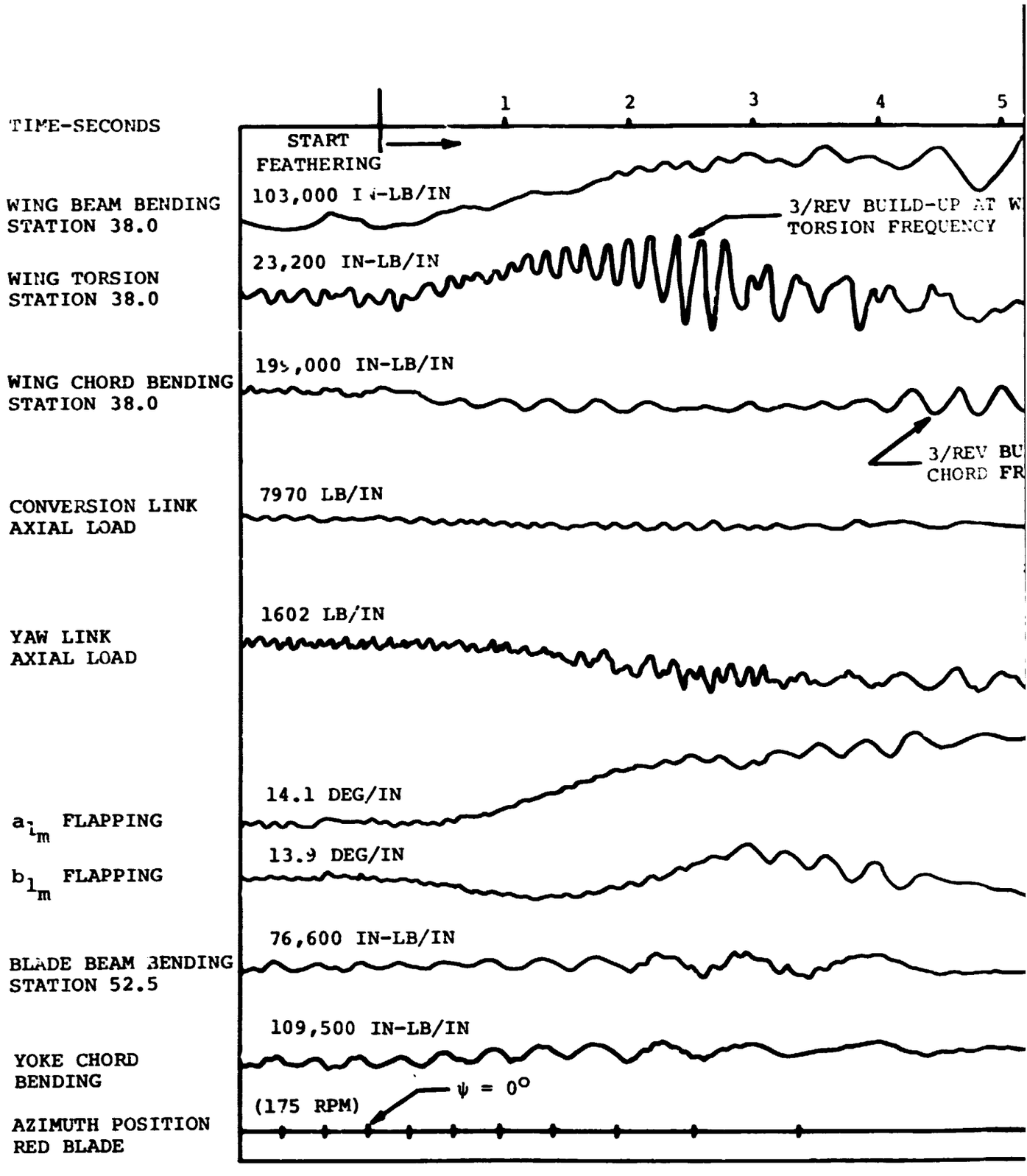

Figure VIII-10. Time History of Feather-
Test Stand, Four Degrees
Tunnel Speed = 92.5 Knot

300-099-004

FOLDOUT FRAME

/

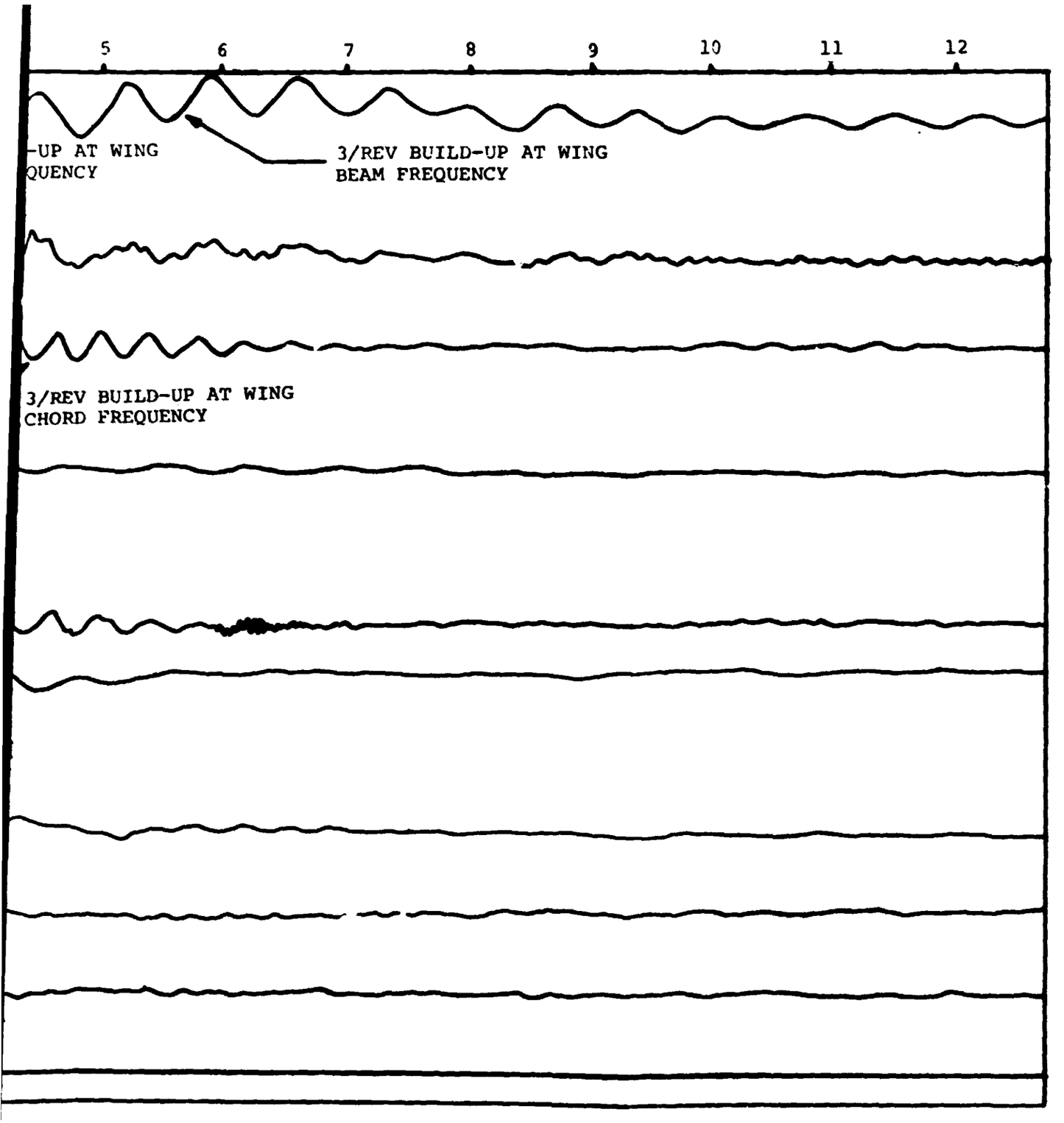

f Feather-Stop for Quarter Stiffness
ur Degrees Angle-of-Attack,
92.5 Knots.

FOLDOUT FRAME

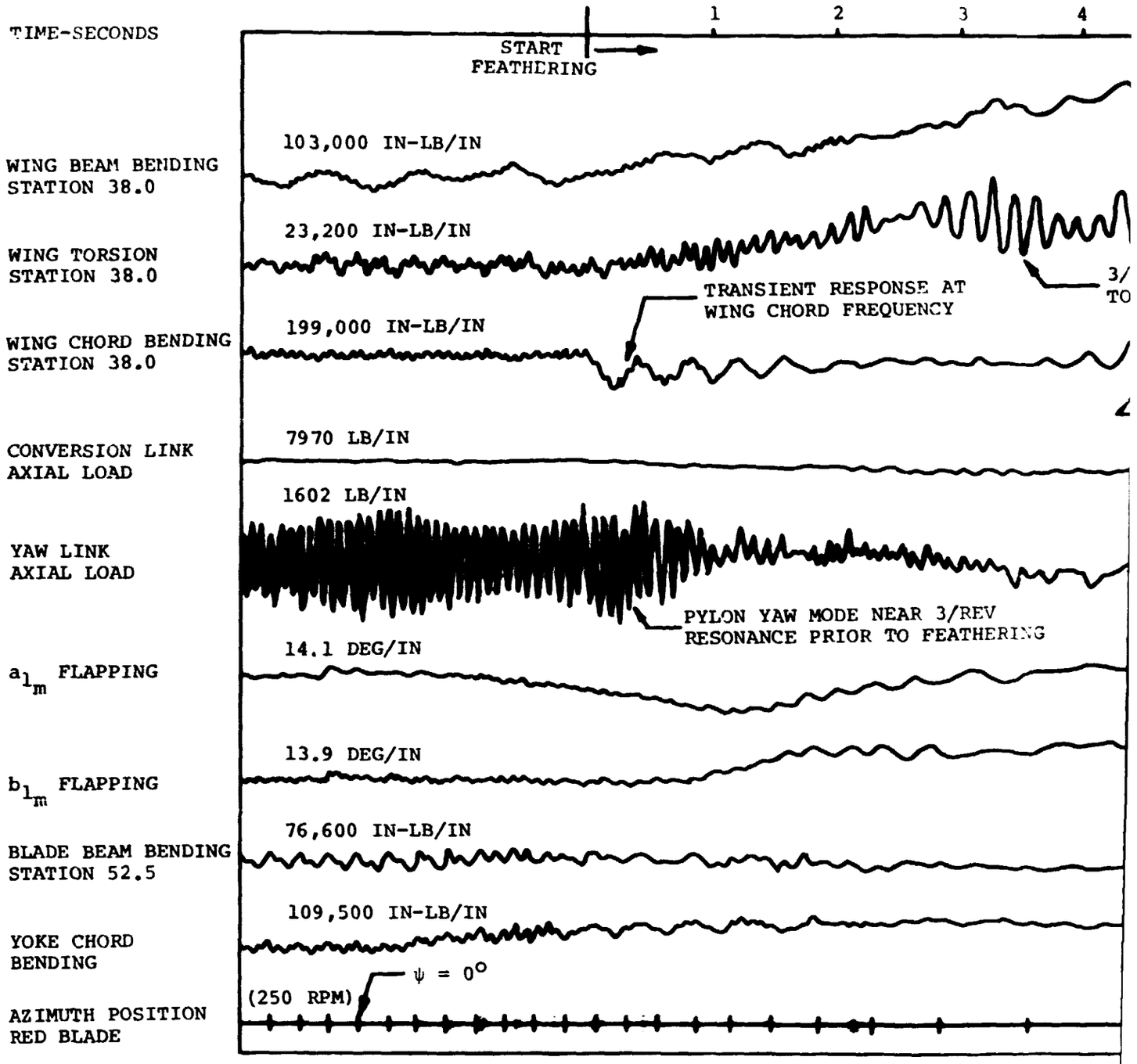

Figure VIII-11. Time History of Feather-St
Test Stand, Zero Degrees A
Tunnel Speed = 132 Knots.

FOLDOUT FRAME

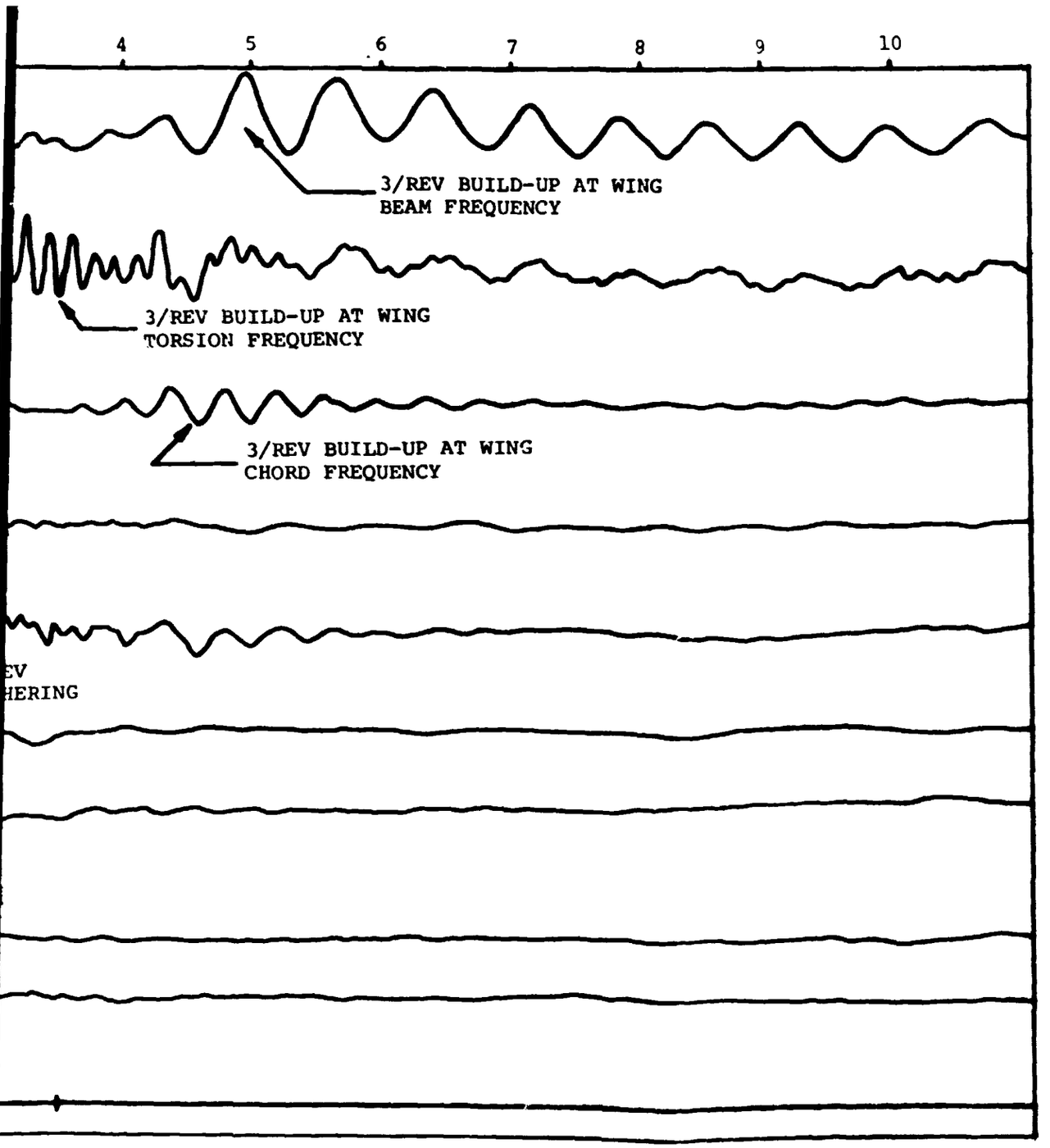

f Feather-Stop for Quarter Stiffness
ro Degrees Angle-of-Attack,
132 Knots.

FOLDOUT FRAME

IX. CONCLUSIONS

A. GENERAL

1. Full-scale wind-tunnel tests have verified the proprotor technology developed during the Army Composite Aircraft Program.

2. Theory and model tests form a reliable basis for the design of full-scale proprotors.

3. The advanced design 25-foot-diameter proprotor will provide good performance in helicopter flight, will attain high propulsive efficiency in airplane flight, and will have positive dynamic stability and acceptable blade loads.

4. These tunnel tests, by establishing that the predicted levels of performance, stability, and load margins are attainable, provide a firm base for the next logical step in the development of proprotor technology--a research aircraft flight program.

B. PERFORMANCE

1. Proprotors can provide lift efficiently in hover (at a typical operating condition, thrust was measured at 8.5 pounds per horsepower and the figure of merit was 0.78).

2. Measured static thrust exceeded the maximum predicted thrust by 15 percent (maximum thrust was not defined in the test due to test stand power limitations at the test rpm).

3. In the blade element momentum analysis, the use of the classical helicopter tip loss factor $B = 1 - \sqrt{2C_T}/b$, leads to under prediction of the maximum attainable static thrust. In addition to a decreased tip loss, maximum lift coefficients higher than measured during the two-dimensional airfoil tests must be used in the calculations to match the highest thrust measured.

4. The proprotor provides a broad range of lift and propulsive force for conversion.

5. For a given level of lift and propulsive force, power can be predicted accurately. Proprotor tip path plane orientation predictions for the given force combinations are good except for mast angles greater than about 60 degrees at which point the predictions begin to be less accurate and over predict the required angle by 2 to 3 degrees.

6. Propulsive efficiencies were measured in excess of 90 percent and were generally slightly higher than predicted by theory.

7. The test results confirmed that typical cruise efficiency of approximately 75 percent are possible with a proprotor as predicted in the Task I Design Study.

C. DYNAMIC STABILITY

1. All proprotor/pylon/wing modes exhibited good stability through a simulated speed of 408 knots.

2. The critical mode, the fundamental wing bending mode, exhibited increased damping with airspeed (at constant proprotor rpm).

3. There was close agreement between the 200-knot simulated speed and the 200-knot actual speed.

4. The full-scale test results were in excellent agreement with theory and one-fifth-scale aeroelastic model tests.

D. BLADE FLAPPING

1. Blade flapping produced no restrictions on the operation of the proprotor.

2. A simulated 3.0g maneuver at 265 knots produced less than 7 degrees of flapping as compared with the 12-degree design allowable.

3. Measured flapping derivatives agree with theory.

4. Evaluation of an electronic flapping controller showed steady flapping reduction of 100 percent with reductions of transient flapping of 40 to 40 percent.

5. The flapping controller increased the wing's response to simulated gusts

6. Increasing the response rate of the flapping controller to reduce transient flapping reduced the dynamic stability of the proprotor/pylon/wing system.

7. The effect of the flapping controller on flapping and dynamic stability agreed with theory.

E. BLADE AND CONTROL SYSTEM LOADS

1. Measured blade and control system loads were acceptable in all flight modes.

2. Oscillatory loads were less than the calculated fatigue endurance limit in helicopter and conversion modes even though little time is spent in those modes and complete conversion can be made in 11 seconds. Oscillatory loads were very low in airplane mode.

3. Oscillatory blade loads were in good agreement with predictions in helicopter mode but were in poor agreement with original predictions at intermediate conversion angles.

4. The original predictions were found to have errors in the input data (relating to swashplate phasing and hub spring moments). When these errors were corrected, the theory predicted oscillatory loads slightly higher than those measured.

5. The test results and theory show that the flapping restraint produced by the hub spring increases the oscillatory blade loads. Only a moderate level of flapping restraint, such as that incorporated in the system tested, appear practical.

F. NOISE AND VIBRATION

1. Measured proprotor noise in helicopter mode was comparable to noise measured from isolated helicopter main rotors in the tunnel. It can therefore be concluded that the noise from a proprotor aircraft will be lower than that from a helicopter operating at equal tip speed and gross weight, because of the absence of a tail rotor or the overlap effects of a tandem rotor helicopter.

2. In airplane flight, noise levels will be extremely low. Proprotor noise levels in propeller operation were too low to be distinguished from background tunnel noise.

3. During the powered test the test stand three-per-rev vibration level decreased rapidly as the stand was converted from helicopter to airplane mast angle of attack, reflecting the reduction in oscillatory airloading.

4. In airplane mode the blade passage frequency vibration is dominant. Aerodynamic interference between the wing and proprotor is the source of vibration in airplane mode.

5. Crew station and cabin vibration levels in airplane mode will be very low, provided that wing and pylon natural frequencies are not in resonance with the blade passage frequency.

6. Start-stops simulating this operation for a stop-fold proprotor were performed without difficulty at simulated speeds up to 265 knots.

X. REFERENCES

1. "Advancement of Proprotor Technology Task I - Design Study Summary," NASA Contractor Report CR 114363, September 1969.

2. Scherrer, Richard, et al., "NASA-Lockheed Short-Haul Transport Study," NASA Report SP-116, April 1966.

3. Armstrong, LTC Marshall B., "Tactical Uses and Future Concepts for Tilting-Proprotor Low-Disc-Loading VTOL Aircraft in Marine Corps Operation," presented at AHS/U. S. Army Symposium on Operational Characteristics and Tactical Uses of Vertical Lift Aircraft, November 1967.

4. "Model 266 Composite Aircraft Program: Explor[illegible] ·finition Final Report," Bell Helicopter Compan[illegible] 266-099-217, July 1967.

5. Hafner, R., "The Domain of the Convertible Rotor," AGARD V/STOL Aircraft, September 1964.

6. Lichten, R. L., et al., "A Survey of Low-Disc-Loading VTOL Aircraft Designs," AIAA Paper 67-756, November 1965.

7. Lichten, Robert L., "An Analysis of Low-Disc-Loading VTOL Aircraft Types," presented at AGARD, Paris, January 1966.

8. Fischer, J. Nile, et al., "VTOL versus Alternative Intra-Theater Air Transport Systems - A Cost Effectiveness Comparison," presented at AIAA Military Aircraft Systems Meeting, October 1966.

9. Stepniewski, W. Z. and Prager, P. C., "VTOL - New Frontier of Flight," Verti-Flite, April 1967.

10. Brown, E. L. and Fischer, J. N., "Comparative Projections of Helicopters, Compound Helicopters and Tilting-Proprotor Low-Disc-Loading VTOL Aircraft for Civil Applications," AIAA Paper 67-939, presented at the 4th Annual Meeting, October 1967.

11. Deckert, W. H. and Ferry, R. G., "Limited Flight Evaluation of the XV-3 Aircraft," TR-60-4, Air Force Flight Test Center, May 1960.

12. "Pilot Evaluation of the Bell Model XV-3 Vertical Takeoff and Landing Aircraft," Report ATO-TR-62-1, U. S. Army Transportation Material Command, February 1962.

13. Reeder, John P., "Handling Qualities Experiences with Several VTOL Research Aircraft," NASA TN-D-735, March 1961.

14. Hall, W. Earl, "Proprotor Stability at High Advance Ratios," Journal of the American Helicopter Society, June 1966.

15. "Rotor/Pylon Stability at High Advance Ratios," Bell Helicopter Company Report 599-063-903.

16. Brown, E. L., et al., "Results of Tilting-Rotor Dynamic Stability Model Tests, November 1965-March 1966," Bell Helicopter Company Report 599-063-904, April 28, 1966.

17. "D266 Composite Research Aircraft Design Concept," Bell Helicopter Company Report D266-099-101, May 1966.

18. "D266 Composite Research Aircraft Results of Analytical Studies," Bell Helicopter Company Report D266-099-110, May 1966.

19. "Model 266 Composite Aircraft Program: Design Concepts," Bell Helicopter Company Report 266-099-201.

20. "Model 266 Composite Aircraft Program: Dynamic Model Tests and Analytical Studies of High-Risk Areas," Bell Helicopter Company Report 266-099-212.

21. Wernicke, K. G., "Tilt-Proprotor Composite Aircraft, Design State of the Art," presented at the 24th Annual National Forum of the American Helicopter Society, May 1968.

22. Gaffey, T. M., et al., "Analysis and Model Tests of the Proprotor Dynamics of a Tilt-Proprotor VTOL Aircraft," presented at the Air Force V/STOL Technology and Planning Conference, September 1969.

23. "Advancement of Proprotor Technology," NASA Contract NAS2-5386, May 7, 1969.

24. Wernicke, K. G., and Edenborough, H. K., "Full-Scale Proprotor Development," presented at the 27th Annual National V/STOL Forum of the American Helicopter Society, May 1971.

25. "NASTRAN Users Manual," National Aeronautics and Space Administration Report NASA SP-222, Washington, D. C., October 1969.

26. Livingston, C. L., "Rotor Aerodynamic Characteristics Program F35(J)," Bell Helicopter Company Report 599-004-900, 24 June 1967.

27. Neal, G. T., "Proprotor Dynamic Stability Analysis - Program DYN-4," Bell Helicopter Company Report 599-099-011, to be published.

28. Yen, Jing G., et al., "A Study of Folding Proprotor VTOL Dynamics," AFFDL-TR-71-7, February 1971.

29. Cox, C. R., "Rotor Noise Measurements in Wind Tunnels," Proceedings Third Cal/AVLABS Symposium, Buffalo, New York, Aerodynamics of Rotary Wing and V/STOL Aircraft, Vol. 1, June 1969.

30. Cox, C. R., "Full-Scale Helicopter Rotor Noise Measurements in Ames 40- by 80-Foot Wind Tunnel," Bell Helicopter Company Report 576-099-052, July 1967.

APPENDIX

Nomenclature

Powered Test Data Listings

Drawings

NOMENCLATURE

Symbol	Computer Output	Description
AF		Rotor activity factor = 218 (based on a constant blade chord of 14 inches).
a_{1_S}	FLAP	Fore and aft flapping angle with respect to the shaft (deg) (see Figure A-1).
B_{1_S}	CYCLIC	Fore and aft cyclic angle with respect to the shaft (deg) (see Figure A-1).
C	C	Speed of sound (fps).
C_L	CL	Lift coefficient = $L/(16\rho n^2R^4)$.
C_{L_H}	CLH	Helicopter lift coefficient = $L/(\rho\pi\Omega^2R^4)$.
C_P	CPB	Airplane power coefficient based on the mast torque power data = $550\ (H_P)/(32\rho n^3R^5)$. This value used in the text and figures.
C_{P_F}	CPF	Propulsive force coefficient = $PF/16\rho n^2R^4$.
C_{P_H}	CPBH	Helicopter power coefficient based on the mast torque power data = $550\ (H_P)/[\rho\pi R^2(\Omega R)^3]$.
	CPHSOL	Helicopter power coefficient/rotor solidity ratio = C_{P_H}/σ.
C_{P_1}	CP1	Airplane power coefficient based on the wind-tunnel balance power data = $550\ (Hp_1)/(32\rho n^3R^5)$.
$C_{P_{1_H}}$	CP1H	Helicopter power coefficient based on the wind-tunnel balance power data = $550\ (Hp_1)/[\rho\pi R^2(\Omega R)^3]$.
C_{P_2}	CP2	Airplane power coefficient based on the test-stand cell power data = $550\ (Hp_2)/(32\rho n^3R^5)$.
$C_{P_{2_H}}$	CP2H	Helicopter power coefficient based on the test-stand load cell power data = $550\ (Hp_2)/[\rho\pi R^2(\Omega R)3]$.
C_T	CT	Airplane thrust coefficient = $T/16\rho n^2R^4$.

Symbol	Computer Output	Description
	CTHSOL	Helicopter thrust coefficient/rotor solidity ratio = C_{T_H}/σ.
D	D	Drag (lb).
	DSIG	Drag referred to sea level standard conditions = D/σ' (lb).
f	F	Flat plate drag area = FF/q (ft^2).
	FM	Figure of merit = $0.707\ C_{T_H}{}^{3/2}/C_{P_H}$ = $0.798\ C_T{}^{3/2}/C_P$.
H	H	Rotor "H" force, perpendicular to the shaft axis (lb).
	HSIG	Rotor "H" force referred to sea level standard conditions = H/σ' (lb).
H_P	HPB	Horsepower based on the mast torque. This value used in the text and figures.
	HPBSIG	Horsepower based on the mast torque referred to sea level standard conditions = H_P/σ'.
H_{P_1}	HP1	Horsepower based on the wind-tunnel balance data.
	HP1SIG	Horsepower based on the wind-tunnel balance data referred to sea level standard conditions = H_{P_1}/σ'.
H_{P_2}	HP2	Horsepower based on the test stand load cell data.
	HP2SIG	Horsepower based on the test stand load cell data referred to sea level standard conditions = H_{P_2}/σ'.
J	J	Airplane advance ratio = V/2nR.
J'	JP	Airplane advance ratio corrected for shaft angle of attack = (V/2nR) cos (α_{MAST}).
J"	JPP	Airplane advance ratio corrected for tip path plane angle = (V/2nR) cos (α_{TPP}).

Symbol	Computer Output	Description
L	L	Lift (lb).
	LSIG	Lift referred to sea-level standard conditions = L/σ' (lb).
M_{AT}	MAT	Advancing tip Mach number $= (1/C)\sqrt{V^2 + (\Omega R)^2 + 2V\Omega R \cos(\alpha_{TPP})}$
n	RPS	Rotor rps.
PF	PF	Propulsive force = -D (lb).
	PFSIG	Propulsive force referred to sea level standard conditions = PF/σ' (lb).
	PT	Data point number.
q	Q	Dynamic pressure (psf).
Q_B	QB	Mast torque (ft-lb).
R		Rotor radius (ft).
RF	RF	Resultant force = $\sqrt{L^2 + (PF)^2}$ (lb).
	RFSIG	Resultant force referred to sea level standard conditions = RF/σ' (lb).
	RPM	Rotor rpm.
	RUN	Run number.
T	T	Thrust along the shaft axis (lb).
	TSIG	Thrust along the shaft axis referred to sea level standard conditions = T/σ' (lb).
V		Velocity (fps).
V_T	V(KTS)	Tunnel speed (knots).
α_{MAST}	ALN	Mast angle of attack (deg).
α_{TPP}	ALTPP	Tip path plane angle of attack $= \alpha_{MAST} = a_{1S} - 90$ (deg).
β		Proprotor blade flapping angle, measured between the blade-span axis and the mast axis. Positive for blade flapping up.

Symbol	Computer Output	Description
ΔP		Change in spinner base pressure relative to free stream static pressure.
η	ETA B	Propulsive efficiency based on the mast torque power data = (TV) cos $(\alpha_{MAST})/(550\ H_P)$. This value used in the text and figures.
η_1	ETA1	Propulsive efficiency based on the wind-tunnel balance power data = (TV) cos $(\alpha_{MAST})/(550\ H_{P_1})$.
η_2	ETA2	Propulsive efficiency based on the test stand load cell power data = (TV) cos $(\alpha_{MAST})/(550\ H_{P_2})$.
θ_R	THERF	Resultant force angle = arctan (L/PF) (deg).
θ_{TIP}	COLLECT	Tip collective angle (deg).
μ	MU	Helicopter advance ratio corrected for tip path plane angle = $(V/\Omega R)$ cos (α_{TPP}).
μ'	MUP	Helicopter advance ratio = $V/\Omega R$.
ΩR	T.SPEED	Rotor tip speed = ΩR (fps).
ρ	RHO	Air density (slug/ft^3).
σ		Rotor solidity = 0.089 (based on a constant blade chord of 14 inches).
σ'	SIGMA-P	Air density ratio = ρ/ρ_o.
Ω		Rotor angular velocity (rad/sec).

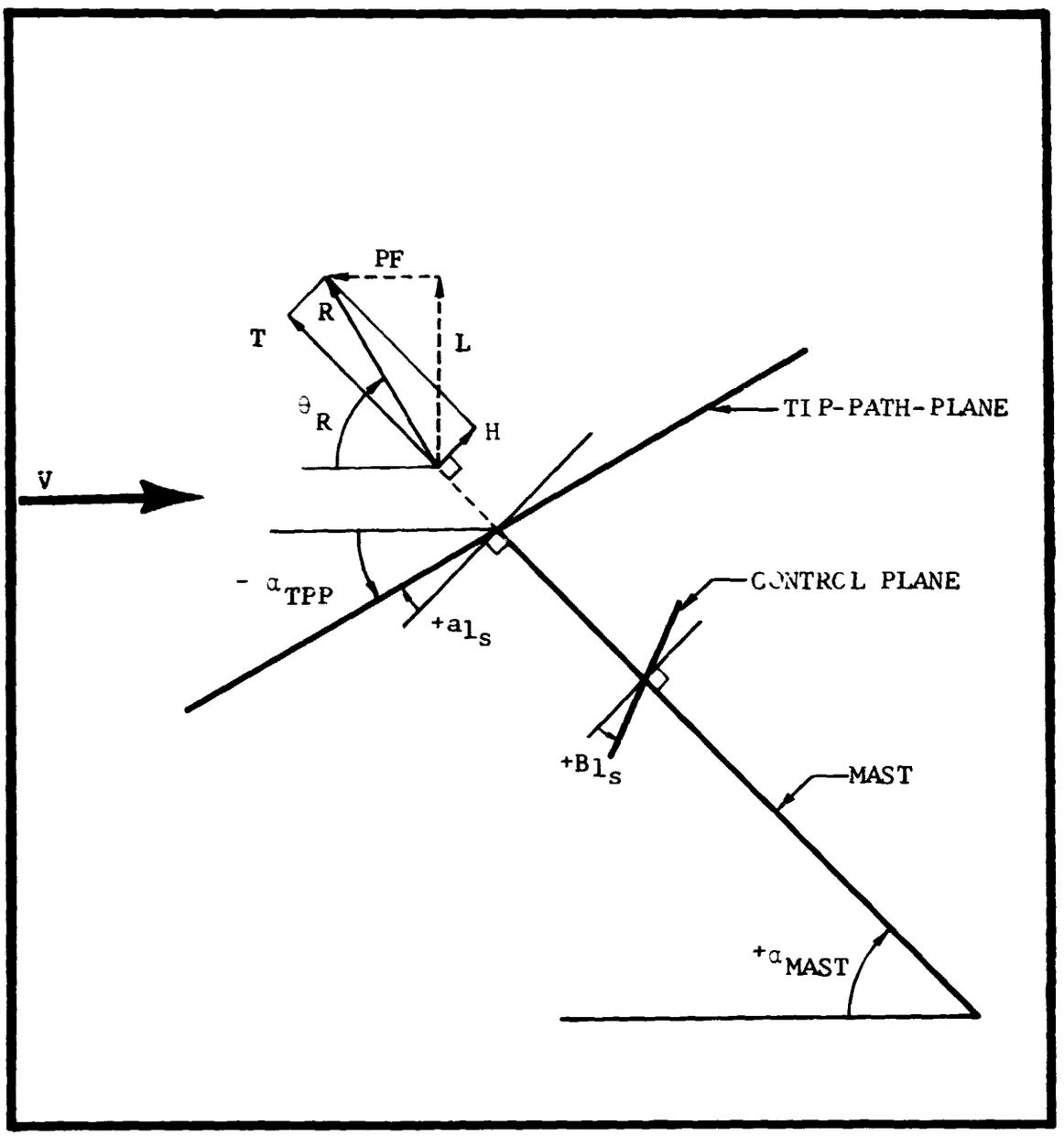

Figure A-1. Direction of Angles and Forces.

POWERED TEST DATA LISTINGS

The following listings were prepared using test data cards supplied by NASA. The format is shown at the beginning of each page for convenience. Refer to the nomenclature for definition of terms.

RUN P. / SIGMA-P / RHO	ALN / A.TPP / FLAP / CYCLIC / COLLECT.	V(KTS) / Q / C	T.SPEED / RPM / RPS / MAT	MU / MU-P / J / J-P / J-PP	L / LSIG / CLH / CL	PF / PFSIG / F / CPF	D / DSIG / FM	T / TSIG / CT / CTH / CTHSOL	RF / RFSIG / THERF / CPHSOL	H / HSIG / QB	HP1 / HP1SIG / CP1 / CP1H / ETA1	HP2 / HP2SIG / CP2 / CP2H / ETA2	HPB / HPBSIG / CPB / CPBH / ETAB
1 1	0.0	2.8	739.8	-0.000	-10.	733.	-733.	733.	733.	-10.	141.	148.	145.
0.9647	-90.1	0.0	565.2	0.006	-10.	760.	-760.	760.	760.	-10.	146.	153.	151.
0.002294	-0.1	1132.	9.420	0.020	-0.000016	9302.67		0.009219	-0.8		0.004136	0.004345	0.004267
	0.3		0.654	0.020	-0.000126	0.009218		0.001189			0.000170	0.000178	0.000175
	8.9			-0.000			0.1655	0.01336	0.00197	1350.	0.044	0.042	0.043
1 2	0.0	13.5	739.8	0.000	-10.	3685.	-3685.	3685.	3685.	-10.	448.	438.	455.
0.9647	-90.0	0.6	565.2	0.031	-10.	3820.	-3820.	3820.	3820.	-10.	465.	454.	471.
0.002294	0.0	1132.	9.420	0.100	-0.000016	6142.45		0.046346	-0.2		0.013161	0.012875	0.013356
	0.3		0.654	0.100	-0.000126	0.046343		0.005979			0.000540	0.000529	0.000549
	13.1			0.000			0.5958	0.06717	0.00616	4226.	0.342	0.349	.347
1 3	0.0	19.7	739.8	0.000	7.	4928.	-4928.	4928.	4928.	7.	685.	670.	669.
0.9643	-90.0	1.3	565.2	0.045	7.	5111.	-5111.	5111.	5111.	7.	711.	695.	694.
0.002293	0.0	1132.	9.420	0.140	0.000011	3904.31		0.062006	0.1		0.020141	0.019683	0.019670
	0.3		0.654	0.140	0.000088	0.062002		0.007999			0.000827	0.000808	0.000808
	15.0			0.000			0.6261	0.08987	0.00908	6221.	0.434	0.444	0.441
1 4	0.0	26.2	740.6	0.000	1075.	5928.	-5928.	5928.	6025.	1075.	938.	930.	942.
0.9638	-90.0	2.2	565.8	0.060	1115.	6150.	-6150.	6150.	6251.	1115.	973.	965.	977.
0.002292	0.0	1132.	9.430	0.190	0.001742	2635.83		0.074462	10.3		0.027488	0.027264	0.027604
	0.3		0.655	0.190	0.013503	0.074458		0.009606			0.001129	0.001120	0.001134
	16.0			0.000			0.5871	0.10793	0.01274	8745.	0.509	0.513	0.513
1 5	0.0	30.1	735.9	0.000	5.	6178.	-6178.	6178.	6178.	5.	1039.	1027.	1043.
0.9634	-90.0	2.9	562.2	0.069	5.	6413.	-6413.	6413.	6413.	5.	1079.	1066.	1083.
0.002291	0.0	1132.	9.370	0.220	0.000008	2095.67		0.078634	0.0		0.031053	0.030701	0.031163
	0.3		0.652	0.220	0.000064	0.078629		0.010144			0.001275	0.001261	0.001280
	16.8			0.000			0.5644	0.11397	0.01438	9743.	0.548	0.555	0.555
1 6	0.0	25.0	735.9	-0.000	-45.	6597.	-6597.	6597.	6597.	-45.	1067.	1053.	1055.
0.9638	-90.4	2.0	562.2	0.057	-47.	6845.	-6845.	6845.	6945.	-47.	1107.	1092.	1095.
0.002292	-0.4	1132.	9.370	0.180	-0.000074	3238.63		0.083930	-0.4		0.031872	0.031441	0.031524
	0.3		0.651	0.180	-0.000573	0.083925		0.010827			0.001309	0.001291	0.001295
	16.8			-0.001			0.6152	0.12165	0.01455	9860.	0.474	0.480	0.479

RUN PT	ALN	V(KTS)	T.SPEED	MU	L	PF	D	T	RF	H	MP1	MP2	MPB
SIGMA-P	ALTPP	Q	RPM	MU-P	LSIG	PFSIG	DSIG	TSIG	RFSIG	HSIG	MP1SIG	MP2SIG	MPBSIG
RHO	FLAP	C	RPS	J	CLM	F		CT	THERF		CP1	CP2	CPB
	CYCLIC		MAT	J-P	CL	CPF		CTH			CP1M	CP2M	CPBM
	COLLECT.			J-PP			FM	CTHSOL	CPHSOL	QB	ETA1	ETA2	ETAB
2 1	30.0	4.8	739.8	0.005	707.	1280.	-1280.	1462.	1462.	-28.	183.	171.	183.
0.9676	-60.0	0.1	565.2	0.011	731.	1323.	-1323.	1511.	1511.	-29.	190.	176.	189.
0.002301	0.0	1130.	9.420	0.035	0.001144	17083.49		0.018331	28.9		0.005370	0.004994	0.005363
	0.0		0.658	0.030	0.008865	0.016048		0.002365			0.000221	0.000205	0.000220
	10.4			0.017			0.3691	0.02657	0.00247	1702.	0.101	0.109	0.103
2 2	30.0	12.8	739.8	0.015	1693.	2970.	-2970.	3419.	3419.	-19.	395.	378.	398.
0.9697	-59.8	0.5	565.2	0.029	1746.	3063.	-3063.	3526.	3525.	-19.	407.	390.	410.
0.002306	0.2	1129.	9.420	0.092	0.002732	5526.14		0.042776	29.7		0.011535	0.011047	0.011627
	0.0		0.665	0.080	0.021182	0.037157		0.005518			0.000474	0.000454	0.000477
	12.8			0.046			0.6069	0.06200	0.00537	3698.	0.294	0.307	0.294
2 3	30.0	19.3	739.8	0.022	2491.	4249.	-4249.	4925.	4925.	33.	642.	625.	632.
0.9693	-59.7	1.2	565.2	0.044	2570.	4384.	-4384.	5081.	5081.	34.	663.	644.	652.
0.002305	0.3	1129.	9.420	0.139	0.004022	3469.05		0.061645	30.4		0.018774	0.018259	0.018461
	0.0		0.670	0.120	0.031179	0.053181		0.007952			0.000771	0.000750	0.000758
	14.6			0.070			0.6613	0.08935	0.00852	5869.	0.393	0.405	0.401
2 4	30.0	23.7	739.8	0.027	2888.	4933.	-4933.	5717.	5716.	35.	816.	801.	815.
0.9689	-59.6	1.8	565.2	0.054	2981.	5091.	-5091.	5901.	5900.	36.	842.	826.	841.
0.002304	0.4	1129.	9.420	0.173	0.004665	2668.31		0.071590	30.3		0.023861	0.023415	0.023825
	0.0		0.674	0.150	0.036164	0.061769		0.009235			0.000980	0.000962	0.000978
	15.6			0.088			0.6413	0.10376	0.01099	7571.	0.442	0.450	0.451

RUN	PT	ALN	V(KTS)	T.SPEED	MU	L	PF	D	T	RF	H	HP1	HP2	HPB
SIGMA-P		ALTPP	Q	RPM	MU-P	LSIG	PFSIG	DSIG	TSIG	RFSIG	HSIG	HP1SIG	HP2SIG	HPBSIG
RHO		FLAP	C	RPS	J	CLM	F		CT	THERF		CP1	CP2	CPB
		CYCLIC		MAT	J-P	CL	CPF		CTH			CP1M	CP2M	CPBM
		COLLECT.			J-PP			FM	CTHSOL	CPHSOL	QB	ETA1	ETA2	ETAB
3	1	0.0	121.0	599.3	0.004	12.	181.	-181.	181.	181.	12.	85.	124.	150.
0.9428		-89.3	46.8	457.8	0.341	13.	192.	-192.	192.	192.	13.	90.	131.	159.
0.002242		0.7	1129.	7.630	1.070	0.000030	3.87		0.003550	3.8		0.004800	0.006988	0.008483
		0.1		0.563	1.070	0.000235	0.003550		0.000456			0.000197	0.000287	0.000348
		17.7			0.012			0.0199	0.00515	0.00391	1721.	0.793	0.545	0.448
3	2	0.0	120.6	599.3	0.002	13.	748.	-748.	748.	748.	13.	284.	321.	331.
0.9411		-89.6	46.4	457.8	0.340	14.	795.	-795.	795.	795.	14.	302.	341.	352.
0.002238		0.4	1130.	7.630	1.070	0.000033	16.13		0.014698	1.0		0.016110	0.018172	0.018749
		0.0		0.561	1.070	0.000255	0.014697		0.001896			0.000662	0.000746	0.000770
		18.8			0.007			0.0758	0.02130	0.00865	3797.	0.973	0.863	0.839
3	3	0.0	121.1	598.5	0.002	19.	1062.	-1062.	1062.	1062.	19.	405.	440.	449.
0.9390		-89.7	46.6	457.2	0.341	20.	1131.	-1131.	1131.	1131.	20.	432.	469.	479.
0.002233		0.3	1131.	7.620	1.070	0.000048	22.78		0.020970	1.0		0.023102	0.025099	0.025614
		0.1		0.560	1.070	0.000375	0.020968		0.002705			0.000949	0.001031	0.001052
		19.5			0.005			0.0946	0.03039	0.01182	5162.	0.974	0.896	0.876
3	4	0.0	121.3	595.3	0.002	22.	1824.	-1824.	1824.	1824.	22.	700.	734.	755.
0.9386		-89.7	46.8	454.8	0.344	23.	1943.	-1943.	1943.	1943.	23.	746.	782.	805.
0.002232		0.3	1131.	7.580	1.080	0.000057	39.01		0.036413	0.7		0.040576	0.042525	0.043751
		0.0		0.558	1.080	0.000439	0.036411		0.004697			0.001666	0.001746	0.001797
		21.5			0.005			0.1267	0.05278	0.02019	8721.	0.969	0.925	0.899
3	5	0.0	121.5	600.8	0.002	15.	2182.	-2182.	2182.	2182.	15.	841.	876.	897.
0.9369		-89.7	46.9	459.0	0.341	16.	2329.	-2329.	2329.	2329.	16.	898.	935.	957.
0.002228		0.3	1132.	7.650	1.070	0.000038	46.54		0.042843	0.4		0.047505	0.049462	0.050645
		0.0		0.562	1.070	0.000295	0.042841		0.005527			0.001951	0.002031	0.002080
		22.0			0.005			0.1397	0.06210	0.02337	10264.	0.967	0.929	0.905

RUN PT	ALN	V(KTS)	T.SPEED	MU	L	PF	D	T	RF	H	HP1	HP2	HPB
SIGMA-P	ALTPP	Q	RPM	MU-P	LSIG	PFSIG	DSIG	TSIG	RFSIG	HSIG	HP1SIG	HP2SIG	HPBSIG
RHO	FLAP	C	RPS	J	CLH	F		CT	THERF		CP1	CP2	CPB
	CYCLIC		MAT	J-P	CL	CPF		CTH			CP1H	CP2H	CPBH
	COLLECT.			J-PP			FM	CTHSOL	CPHSOL	QB	ETA1	ETA2	ETAB
4 1	0.0	160.1	596.9	0.005	19.	-256.	256.	-256.	257.	19.	-85.	0.	-5.
0.9214	-89.3	80.0	456.0	0.453	21.	-278.	278.	-278.	279.	21.	-93.	0.	-6.
0.002191	0.7	1132.	7.600	1.420	0.000050	-3.20		-.005179	-4.2		-0.005004	0.000013	-0.000300
	-2.1		0.581	1.420	0.000384	-0.005179		-.000668			-0.000205	0.000001	-0.000012
	26.5			0.016			-.9911	-.00751	-.00014	-59.	-7.370	-7.370	24.518
4 2	0.0	161.2	595.3	0.007	15.	441.	-441.	441.	441.	15.	230.	303.	298.
0.9151	-89.1	80.6	454.8	0.457	16.	482.	-482.	482.	482.	16.	251.	331.	326.
0.002176	0.9	1135.	7.580	1.440	0.000040	5.47		0.009030	1.9		0.013670	0.018010	0.017707
	-2.1		0.580	1.440	0.000307	0.009030		0.001165			0.000561	0.000740	0.000727
	27.5			0.023			0.0387	0.01309	0.00817	3441.	0.949	0.720	0.734
4 3	0.0	161.8	598.5	0.005	20.	1036.	-1036.	1036.	1036.	20.	526.	593.	584.
0.9108	-89.4	80.8	457.2	0.456	22.	1137.	-1137.	1137.	1138.	22.	578.	651.	641.
0.002166	0.6	1137.	7.620	1.430	0.000053	12.82		0.021089	1.1		0.030934	0.034841	0.034294
	-2.1		0.581	1.430	0.000407	0.021088		0.002720			0.001270	0.001431	0.001408
	29.0			0.015			0.0712	0.03057	0.01582	6704.	0.978	0.868	0.879
4 4	0.0	162.2	598.5	0.005	31.	1302.	-1302.	1302.	1302.	31.	653.	726.	723.
0.9071	-89.3	80.9	457.2	0.458	34.	1435.	-1435.	1435.	1436.	34.	720.	800.	797.
0.002157	0.7	1139.	7.620	1.440	0.000082	16.10		0.026614	1.4		0.038536	0.042828	0.042666
	-2.1		0.580	1.440	0.000634	0.026613		0.003433			0.001587	0.001759	0.001752
	29.4			0.017			0.0812	0.03858	0.01969	8306.	0.992	0.893	0.898
4 5	0.0	121.5	599.3	0.002	21.	1709.	-1709.	1709.	1709.	21.	645.	694.	662.
0.9104	-89.7	45.5	457.8	0.342	23.	1877.	-1877.	1877.	1877.	23.	708.	762.	727.
0.002165	0.3	1146.	7.630	1.070	0.000055	37.53		0.034714	0.7		0.037758	0.040631	0.038763
	-2.2		0.554	1.070	0.000427	0.034712		0.004478			0.001551	0.001669	0.001592
	22.5			0.005			0.1331	0.05031	0.01789	7594.	0.989	0.919	0.958

RUN PT SIGMA-P RHO	ALN ALTPP FLAP CYCLIC COLLECT.	V(KTS) Q C	T.SPEED RPM RPS MAT	MU MU-P J J-P J-PP	L LSIG CLH CL	PF PFSIG F CPF	D DSIG FM	T TSIG CT CTH THSOL	RF RFSIG THERF CPHSOL	H HSIG QB	HP1 HP1SIG CP1 CP1H ETA1	HP2 HP2SIG CP2 CP2H ETA2	HPB HPBSIG CPB CPBH ETAB
5 1	0.0	160.5	599.3	0.003	29.	79.	-79.	79.	84.	29.	78.	133.	129.
0.9260	-89.6	80.8	457.8	0.452	31.	85.	-85.	85.	91.	31.	84.	144.	140.
0.002202	0.4	1131.	7.630	1.420	0.000075	0.98		0.001574	20.2		0.004497	0.007655	0.007443
	0.0		0.583	1.420	0.000579	0.0 4578		0.000204			0.000185	0.000314	0.000306
	27.3			0.010			0.0067	0.00229	0.00343	1483.	0.499	0.293	0.301
5 2	0.0	160.4	599.3	0.004	36.	154.	-154.	154.	158.	36.	111.	165.	160.
0.9222	-89.5	80.4	457.8	0.452	39.	167.	-167.	167.	171.	39.	120.	179.	174.
0.002193	0.5	1133.	7.630	1.420	0.000093	1.92		0.003088	13.2		0.006388	0.009543	0.009267
	0.0		0.582	1.420	0.000722	0.003088		0.000398			0.000262	0.000392	0.000381
	27.5			0.013			0.0148	0.00448	0.00428	1839.	0.686	0.459	0.473
5 3	0.0	161.4	599.3	-0.043	23.	559.	-559.	559.	559.	23.	295.	356.	367.
0.9180	-89.4	81.0	457.8	0.455	25.	609.	-609.	609.	609.	25.	322.	388.	400.
0.002183	-5.4	1135.	7.630	1.430	0.000060	6.90		0.011261	2.4		0.017142	0.020672	0.021322
	0.0		0.559	1.430	0.000463	0.011260		0.001453			0.000704	0.000849	0.000876
	28.3			-0.136			0.0447	0.01632	0.00784	4212.	0.938	0.777	0.755
5 4	0.0	162.0	599.3	-0.000	43.	1269.	-1269.	1269.	1270.	43.	634.	701.	677.
0.9138	-90.1	81.3	457.8	0.456	47.	1389.	-1389.	1389.	1390.	47.	694.	768.	741.
0.002173	-0.1	1137.	7.630	1.430	0.000112	15.61		0.025681	1.9		0.036987	0.040923	0.039325
	0.0		0.579	1.430	0.000870	0.025680		0.003313			0.001519	0.001681	0.001623
	29.0			-0.001			0.0831	0.03722	0.01824	7772.	0.996	0.900	0.929
5 5	0.0	162.2	599.3	0.000	33.	1670.	-1670.	1670.	1670.	33.	857.	910.	884.
0.9117	-90.0	81.3	457.8	0.457	36.	1832.	-1832.	1832.	1832.	36.	939.	998.	970.
0.002168	0.0	1138.	7.630	1.440	0.000086	20.54		0.033875	1.1		0.050088	0.053190	0.051713
	0.0		0.579	1.440	0.000669	0.033873		0.004370			0.002057	0.002184	0.002124
	29.8			0.000			0.0962	0.04910	0.02386	10145.	0.971	0.914	0.943
5 6	0.0	162.1	599.3	0.000	-6.	1890.	-1890.	1890.	1890.	-6.	962.	1026.	1003.
0.9100	-90.0	81.1	457.8	0.457	-7.	2077.	-2077.	2077.	2077.	-7.	1058.	1128.	1103.
0.002164	0.0	1139.	7.630	1.430	-0.000016	23.32		0.038408	-0.2		0.056387	0.060114	0.058779
	0.0		0.578	1.430	-0.000122	0.038406		0.004955			0.002316	0.002469	0.002414
	30.5			0.000			0.1021	0.05567	0.02712	11510.	0.977	0.917	0.934

RUN PT	ALN	V(KTS)	T.SPEED	MU	L	PF	D	T	RF	H	HP1	HP2	HPR
SIGMA-P	ALTPP	Q	RPM	MU-P	LS10	PFS10	DS10	TS10	RFS10	HS10	HP1S10	HP2S10	HPRS10
RHO	FLAP	C	RPS	J	CLH	F		CT	THERF		CP1	CP2	CPR
	CYCLIC		MAT	J-P	CL	CPF		CTH			CP1H	CP2H	CPRH
	COLLECT			J-PP			FM	ST'MAL	CPHSPI	SR	ETA1	ETA2	ETAR
5 7	0.0	161.9	599.3	0.000	38.	-196.	196.	-196.	200.	38.	-62.	6.	5.
0.9041	-89.9	80.3	457.8	0.456	42.	-217.	217.	-217.	221.	42.	-68.	7.	6.
0.002150	0.1	1143.	7.630	1.430	0.000100	-2.44		-.004009	-11.0		-0.002434	0.000360	0.000303
	0.0		0.577	1.430	0.000777	-0.004009		-.000517			-0.000142	0.000015	0.000012
	24.9			0.002			0.6676	-.00581	0.00014	59.	-5.727	-5.727	-18.904

RUN PT	AI	V(KTS)	T.SPEED	MU	L	PF	D	T	RF	M	MP1	MP2	MPB
SIGMA-P	AL	Q	RPM	MU-P	LSIG	PFSIG	DSIG	TSIG	RFSIG	MSIG	MP1SIG	MP2SIG	MPBSIG
RHO	FL	C	RPS	J	CLH	F		CT	THERF		CP1	CP2	CPB
	CYCL		MAT	J-P	CL	CPF		CTH			CP1H	CP2H	CPBH
	COLLECT			J-PP			FM	CTHSOL	CPHSOL	QB	ETA1	ETA2	ETAB
6 1	0.0	188.8	599.3	0.000	31.	186.	-186.	186.	189.	31.	177.	229.	284.
0.8785	-90.0	106.1	457.8	0.532	35.	212.	-212.	212.	215.	35.	202.	261.	324.
0.002089	0.0	150.	7.630	1.670	0.000084	1.75	0.003916		9.5		0.010764	0.013859	0.017262
	0.0		0.590	1.670	0.000033	0.003915	0.000505				0.000442	0.000570	0.000709
	31.7			0.000			0.0113	0.00568	0.00797	3263.	0.607	0.471	0.379

RUN PT SIGMA-P RHO	ALN ALTPP FLAP CYCLIC COLLECT.	V(KTS) Q C	T.SPEED RPM RPS MAT	MU MU-P J J-P J-PP	L LSIG CLH CL	PF PFSIG F CPF	D DSIG FM	T TSIG CT CTH CTHSOL	RF RFSIG THERF CPHSOL	M MSIG QB	HP1 HP1SIG CP1 CP1H ETA1	HP2 HP2SIG CP2 CP2H ETA2	HPB HPBSIG CPB CPBH ETAB
7 1	30.0	15.0	599.3	0.021	1061.	1835.	-1835.	2120.	2120.	1.	203.	199.	212.
0.9462	-59.6	0.7	457.8	0.042	1121.	1939.	-1939.	2241.	2240.	2.	214.	210.	224.
0.002250	0.4	1139.	7.630	0.139	0.002475	2532.22		0.041435	30.0		0.011428	0.011218	0.011950
	2.5		0.538	0.120	0.020737	0.035863		0.005345			0.000469	0.000461	0.000491
	1.2			0.070			0.5630	0.06006	0.00551	2433.	0.418	0.425	0.416
7 2	30.0	16.5	599.3	0.023	1263.	2149.	-2149.	2492.	2493.	19.	244.	240.	243.
0.9462	-59.7	0.9	457.8	0.047	1335.	2271.	-2271.	2634.	2634.	20.	258.	254.	257.
0.002250	0.3	1139.	7.630	0.150	0.004184	2457.53		0.048706	30.4		0.013736	0.013530	0.013693
	0.0		0.539	0.130	0.024685	0.042000		0.006283			0.000564	0.000556	0.000562
	2.3			0.076			0.6261	0.07060	0.00632	2788.	0.449	0.456	0.462
7 3	30.0	19.3	602.4	0.027	1513.	2596.	-2596.	3005.	3005.	12.	325.	315.	338.
0.9462	-59.6	1.2	460.2	0.054	1599.	2744.	-2744.	3176.	3176.	13.	344.	333.	357.
0.002250	0.4	1139.	7.670	0.173	0.003775	2163.32		0.058122	30.2		0.018039	0.017480	0.018742
	0.0		0.544	0.150	0.029264	0.050208		0.007498			0.000741	0.000718	0.000770
	4.0			0.088			0.5963	0.08424	0.00865	3856.	0.475	0.490	0.465
7 4	30.0	22.5	596.9	0.032	1879.	3200.	-3200.	3710.	3711.	27.	442.	434.	458.
0.9479	-59.4	1.6	456.0	0.064	1982.	3376.	-3376.	3914.	3915.	29.	466.	458.	484.
0.002254	0.6	1138.	7.600	0.196	0.004766	1964.27		0.072956	30.4		0.025133	0.024702	0.026092
	0.0		0.542	0.170	0.036950	0.062923		0.009411			0.001032	0.001014	0.001072
	6.8			0.100			0.6024	0.10574	0.01204	5280.	0.503	0.512	0.475
7 5	30.0	24.6	596.9	0.036	2402.	3992.	-3992.	4658.	4659.	84.	626.	614.	623.
0.9479	-59.1	1.9	456.0	0.069	2534.	4212.	-4212.	4914.	4915.	89.	661.	648.	658.
0.002254	0.9	1138.	7.600	0.219	0.006093	2058.68		0.091598	31.0		0.035633	0.034947	0.035476
	0.0		0.544	0.190	0.047234	0.078496		0.011816			0.001463	0.001435	0.001457
	9.4			0.113			0.6233	0.13276	0.01637	7179.	0.486	0.495	0.491
7 6	30.0	25.7	596.9	0.037	2603.	4336.	-4336.	5056.	5057.	86.	719.	703.	706.
0.9479	-59.0	2.1	456.0	0.073	2746.	4575.	-4575.	5334.	5336.	91.	759.	741.	745.
0.002254	1.0	1138.	7.600	0.231	0.006603	2051.11		0.099424	31.0		0.040920	0.039983	0.040166
	0.0		0.545	0.200	0.051187	0.085261		0.012826			0.001681	0.001642	0.001650
	10.8			0.119			0.6226	0.14411	0.01853	8128.	0.480	0.491	0.495

RUN	PT	ALN	V(KTS)	T.SPEED	MU	L	PF	D	T	PF	W	HP1	HP2	HPR
SIGMA-P		ALTPP	Q	RPM	MU-P	LSIG	PFSIG	DSIG	TSIG	PFSIG	WSIG	HP1SIG	HP2SIG	HPRSIG
RHO		FLAP		RPS	J	CLH	F		CT	THEPF		CP1	CP2	CPR
		CYCLIC		MAT	J-P	CL	CPF		CTH			CP1H	CP2H	CPRH
		COLLECT.			J-PP			FM	CT/SIGL	CPWSIG	PP	FTA1	FTA2	FTAR
7	7	30.0	26.9	596.9	0.039	2852.	4717.	-4717.	5511.	5512.	112.	827.	810.	829.
0.9500		-58.9	2.3	456.0	0.076	3002.	4965.	-4965.	5801.	5803.	117.	870.	853.	873.
0.002259		1.1	1137.	7.600	0.242	0.007219	2029.71		0.108132	31.2		0.046947	0.046020	0.047098
		0.0		0.547	0.210	0.055959	0.092547		0.013949			0.001928	0.001890	0.001934
		12.0			0.125			0.6022	0.15673	0.02173	9552.	0.476	0.486	0.482
7	8	30.0	28.5	596.9	0.042	2968.	4877.	-4877.	5707.	5709.	132.	895.	883.	901.
0.9495		-58.6	2.6	456.0	0.081	3126.	5136.	-5136.	6010.	6013.	139.	943.	930.	949.
0.002258		1.4	1137.	7.600	0.254	0.007516	1870.21		0.112027	31.3		0.050867	0.050179	0.051218
		0.0		0.548	0.220	0.058261	0.095729		0.014451			0.002089	0.002061	0.002103
		13.1			0.132			0.5839	0.16237	0.02363	1[illegible].	0.482	0.489	0.481

RUN	PT	ALN	V(KTS)	T.SPEED	MU	L	PF	D	T	PF	H	HP1	HP2	HPR
SIGMA-P		ALTPP	Q	RPM	MU-P	L/Q	PFSTR		TSTR	PCSTR		HP1STR	HP2STR	HPRSTR
RHO		FLAP	P	PRS	J	CLM	F		CT	THFRF		CP1	CP2	CPR
		CYCLIC		MAT	J-P	CL	CPF		CTM			CP1M	CP2M	CPRM
		COLLECT.			J-PP			FM	CTMSTL	CONTROL	DP	PTR1	PTR2	PTRR
8	7	30.0	31.0	738.3	0.036	3[illegible]1.	5855.	-5855.	6801.	6801.	70.	1128.	1115.	1128.
0.9617		-59.5	3.1	564.0	0.071	3599.	6088.	-6088.	7072.	7072.	73.	1173.	1159.	1173.
0.002287		0.5	1131.	9.400	0.219	0.005656	1869.06		0.086162	30.6		0.033440	0.033045	0.033432
		0.0		0.678	0.190	0.043848	0.074173		0.011115			0.001373	0.001357	0.001373
		8.8			0.112			0.6034	0.12489	0.01543	10501.	0.497	0.503	0.490

RUN PT SIGMA-P RHO	ALN ALTPP FLAP CYCLIC COLLECT.	V(KTS) Q G	T.SPEED RPM RPS MAT	MU MU-P J J-P J-PP	L LSIG CLM CL	PF PFSIG F CPF	USIG FM	T TSIG CT CTH CTHSOL	RF RFSIG THERF CPHSOL	H HSIG QB	HP1 HP1SIG CP1 CP1H ETA1	HP2 HP2SIG CP2 CP2H ETA2	HPB HPBSIG CPB CPBH ETAB
8 1	30.0	17.5	739.8	0.020	1117.	1926.	-1926.	2227.	2226.	4.	261.	260.	262.
0.9588	-59.9	1.0	565.2	0.040	1165.	2009.	-2009.	2323.	2322.	5.	273.	271.	273.
0.002280	0.1	1133.	9.420	0.127	0.001823	1925.67		0.028181	30.1		0.007722	0.007676	0.007737
	0.0		0.666	0.110	0.014135	0.024370		0.003635			0.000317	0.000315	0.000318
	-3.5			0.064			0.4877	0.04085	0.00357	2433.	0.397	0.400	0.401
8 2	30.0	18.5	738.3	0.021	1529.	2648.	-2648.	3058.	3058.	0.	359.	357.	363.
0.9588	-59.9	1.1	564.0	0.042	1595.	2762.	-2762.	3189.	3189.	0.	374.	373.	379.
0.002280	0.1	1133.	9.400	0.139	0.002507	2375.52		0.038861	30.0		0.010662	0.010622	0.010800
	0.0		0.666	0.120	0.019430	0.033649		0.005013			0.000438	0.000436	0.000444
	0.5			0.069			0.5058	0.05633	0.00498	3382.	0.420	0.421	0.432
8 3	30.0	21.3	739.8	0.024	1853.	3201.	-3201.	3699.	3699.	4.	465.	455.	466.
0.9584	-59.8	1.5	565.2	0.049	1933.	3340.	-3340.	3860.	3859.	5.	485.	475.	486.
0.002279	0.2	1133.	9.420	0.150	0.003026	2171.16		0.044828	30.1		0.013738	0.013458	0.013778
	0.0		0.669	0.130	0.023458	0.040521		0.006041			0.000564	0.000553	0.000566
	2.2			0.075			0.5866	0.06787	0.00636	4331.	0.451	0.460	0.442
8 4	30.0	24.6	739.8	0.028	2413.	4110.	-4110.	4766.	4766.	35.	665.	648.	658.
0.9584	-59.7	2.0	565.2	0.056	2518.	4289.	-4289.	4973.	4973.	36.	694.	676.	686.
0.002279	0.3	1133.	9.420	0.173	0.003941	2097.30		0.060336	30.4		0.019661	0.019147	0.019441
	0.0		0.672	0.150	0.030548	0.052028		0.007783			0.000807	0.000786	0.000799
	4.3			0.087			0.6080	0.08745	0.00897	6111.	0.468	0.480	0.466
8 5	30.0	27.0	738.3	0.031	2674.	4545.	-4545.	5274.	5273.	43.	771.	751.	758.
0.9579	-59.7	2.4	564.0	0.062	2791.	4745.	-4745.	5506.	5505.	45.	805.	784.	791.
0.002278	0.3	1133.	9.400	0.196	0.004387	1914.82		0.067081	30.5		0.022951	0.022355	0.022566
	0.0		0.673	0.170	0.034011	0.057805		0.008653			0.000943	0.000918	0.000927
	5.5			0.099			0.6141	0.09723	0.01041	7060.	0.492	0.505	0.505
8 6	30.0	26.9	738.3	0.031	2955.	5042.	-5042.	5844.	5844.	38.	872.	866.	886.
0.9579	-59.7	2.3	564.0	0.061	3085.	5263.	-5263.	6101.	6101.	40.	911.	904.	925.
0.002278	0.3	1133.	9.400	0.196	0.004848	2151.46		0.074331	30.4		0.025966	0.025775	0.026360
	0.0		0.673	0.170	0.037585	0.064126		0.009589			0.001066	0.001059	0.001083
	6.5			0.099			0.6132	0.10774	0.01216	8247.	0.478	0.482	0.479

RUN PT SIGMA-P RHO	ALN ALTPP FLAP CYCLIC COLLECT.	V(KTS) Q C	T.SPEED RPM KPS MAT	MU MU-P J J-P J-PP	L LSIG CLH CL	PF PFSIG F CPF	D DSIG FM	T TSIG CT CTH CTHSOL	RF RFSIG THERF CPHSOL	H HSIG QB	HP1 HP1SIG CP1 CP1H ETA1	HP2 HP2SIG CP2 CP2H ETA2	HPB HPBSIG CPB CPBH ETAB
9 1	30.0	96.4	700.6	0.116	700.	785.	-785.	1030.	1052.	214.	270.	308.	299.
0.9651	-60.0	30.4	535.2	0.232	725.	813.	-813.	1067.	1090.	221.	279.	319.	310.
0.002295	0.0	1120.	8.920	0.727	0.001266	25.82		0.014441	41.7		0.039326	0.010645	0.010341
	2.4		0.709	0.630	0.009814	0.011005		0.001863			0.000383	0.000437	0.000425
	10.8			0.364			0.1339	0.02093	0.00477	2935.	0.979	0.857	0.880
9 2	30.0	98.3	700.6	0.118	1170.	1623.	-1623.	1991.	2001.	202.	536.	575.	568.
0.9622	-60.2	31.5	535.2	0.237	1216.	1687.	-1687.	2069.	2079.	210.	557.	598.	591.
0.002288	-0.2	1121.	8.920	0.733	0.002123	51.58		0.028000	35.8		0.018594	0.019948	0.019706
	2.4		0.710	0.640	0.016454	0.022823		0.003612			0.000764	0.000819	0.000809
	12.2			0.367			0.1896	0.04058	0.00909	5576.	0.969	0.904	0.909
9 3	30.0	99.8	700.6	0.120	1644.	2499.	-2499.	2986.	2991.	174.	838.	883.	909.
0.9601	-60.0	32.4	535.2	0.240	1712.	2603.	-2603.	3110.	3116.	182.	873.	920.	947.
0.002283	0.0	1122.	8.920	0.751	0.002989	77.1		0.042084	33.3		0.029142	0.030702	0.031596
	2.8		0.711	0.650	0.023170	0.035219		0.005429			0.001197	0.001261	0.001298
	14.2			0.375			0.2179	0.06100	0.01458	8921.	0.944	0.896	0.866
9 4	30.0	99.4	700.6	0.119	2121.	3385.	-3385.	3992.	3995.	144.	1168.	1215.	1154.
0.9601	-60.2	32.1	535.2	0.239	2209.	3526.	-3526.	4158.	4161.	151.	1217.	1266.	1202.
0.002283	-0.2	1122.	8.920	0.751	0.003856	105.43		0.056263	32.1		0.040607	0.042241	0.040121
	3.5		0.710	0.650	0.029893	0.047705		0.007258			0.001668	0.001735	0.001648
	16.0			0.373			0.2653	0.08155	0.01851	11328.	0.902	0.867	0.912

RUN PT SIGMA-P RHO	ALN ALTPP FLAP CYCLIC COLLECT.	V(KTS) Q C	T.SPEED RPM RPS MAT	MU MU-P J J-P J-PP	L LSIG CLH CL	PF PFSIG F CPF	D DSIG FM	T TSIG CT CTH CTHSOL	RF RFSIG THERF CPHSOL	H HSIG OB	HP1 HP1SIG CP1 CP1H ETA1	HP2 HP2SIG CP2 CP2H ETA2	HPB HPBSIG CPB CPBH ETAB
10 1	30.0	141.1	700.6	0.170	1105.	1123.	-1123.	1525.	1575.	396.	534.	583.	598.
C.9386	-60.0	63.3	535.2	0.340	1177.	1196.	-1196.	1625.	1679.	421.	569.	621.	637.
0.002232	0.0	1126.	8.920	1.074	0.002055	17.73		0.021984	44.5		0.018991	0.020731	0.021262
	4.8		0.751	0.930	0.015930	0.016188		0.002836			0.000780	0.000851	0.000873
	18.8			0.537			0.1223	0.03186	0.00981	5869.	1.071	0.981	0.962
10 2	30.0	141.5	700.6	0.175	1552.	1904.	-1904.	2425.	2456.	392.	878.	950.	921.
0.9365	-59.1	63.5	535.2	0.341	1657.	2033.	-2033.	2589.	2623.	419.	937.	1014.	984.
0.002227	0.9	1127.	8.920	1.074	0.002893	24.98		0.035037	39.2		0.031269	0.033835	0.032819
	4.6		0.753	0.930	0.022424	0.027508		0.004520			0.001284	0.001390	0.001348
	19.8			0.551			0.1594	0.05078	0.01514	9039.	1.039	0.960	0.993
10 3	30.0	141.8	700.6	0.176	1787.	2308.	-2308.	2892.	2919.	394.	1095.	1156.	1166.
0.9344	-59.0	63.7	535.2	0.342	1912.	2470.	-2470.	3095.	3124.	421.	1172.	1237.	1248.
0.002222	1.0	1128.	8.920	1.074	0.003338	36.25		0.041878	37.8		0.039112	0.041278	0.041648
	4.5		0.753	0.930	0.025877	0.033420		0.005402			0.001606	0.001695	0.001710
	20.9			0.553			0.1641	0.06070	0.01922	11445.	0.995	0.943	0.935
10 4	30.0	141.6	700.6	0.176	1060.	964.	-964.	1365.	1433.	436.	475.	525.	544.
0.9327	-59.0	63.4	535.2	0.341	1136.	1034.	-1034.	1463.	1536.	467.	509.	563.	584.
0.002218	1.0	1129.	8.920	1.074	0.001984	15.21		0.019802	47.7		0.016980	0.018775	0.019471
	4.0		0.752	0.930	0.015377	0.013984		0.002554			0.000697	0.000771	0.000800
	18.7			0.554			0.1141	0.02870	0.00898	5341.	1.082	0.979	0.946
10 5	30.0	141.4	700.6	0.144	528.	225.	-225.	459.	574.	345.	165.	206.	269.
C.9306	-64.9	63.0	535.2	0.341	567.	242.	-242.	493.	617.	370.	177.	221.	289.
0.002213	-4.9	1130.	8.920	1.074	0.000990	3.57		0.006674	66.9		0.005923	0.007391	0.009650
	8.6		0.735	0.930	0.007677	0.003271		0.000861			0.000243	0.000304	0.000396
	18.9			0.455			0.0451	0.00967	0.00445	2641.	1.044	0.836	0.643
10 6	30.0	142.7	700.6	0.202	1777.	1614.	-1614.	2287.	2401.	732.	776.	842.	855.
0.9281	-54.0	64.0	535.2	0.344	1915.	1739.	-1739.	2464.	2587.	789.	837.	907.	922.
0.002207	6.0	1131.	8.920	1.085	0.003342	25.22		0.033343	47.8		0.027914	0.030258	0.030750
	-0.4		0.764	0.940	0.025907	0.023529		0.004301			0.001146	0.001243	0.001263
	18.9			0.638			0.1579	0.04833	0.01419	8393.	1.117	1.030	1.019

RUN PT SIGMA-P RHO	ALN ALTPP FLAP CYCLIC COLLECT.	V(KTS) Q C	T.SPEED RPM RPS MAT	MU MU-P J J-P J-PP	L LSIG CLH CL	PF PFSIG F CF	D DSIG FM	T TSIG CT CTH CTHSOL	RF RFSIG THERF CPHSOL	H HSIG QB	HP1 HP1SIG CP1 CP1H ETA1	HP2 HP2SIG CP2 CP2H ETA2	HPB HPBSIG CPB CPBH ETAB
11 1	30.0	141.8	739.8	0.160	1317.	1456.	-1456.	1919.	1963.	413.	685.	733.	773.
0.9420	-60.4	64.1	565.2	0.323	1398.	1546.	-1546.	2037.	2084.	438.	728.	778.	820.
0.002240	-0.4	1121.	9.420	1.016	0.002188	22.70		0.024717	42.1		0.020612	0.022055	0.023240
	4.6		0.787	0.880	0.016963	0.018752		0.003188			0.000846	0.000906	0.000954
	19.5			0.502			0.1334	0.03583	0.01072	7180.	1.055	0.986	0.936
11 2	30.0	141.9	739.8	0.160	1119.	1012.	-1012.	1436.	1509.	463.	494.	524.	572.
0.9399	-60.4	64.1	565.2	0.324	1191.	1077.	-1077.	1528.	1605.	493.	526.	557.	608.
0.002235	-0.4	1122.	9.420	1.016	0.001863	15.79		0.018537	47.9		0.014902	0.015783	0.017232
	4.2		0.787	0.880	0.014445	0.013063		0.002391			0.000612	0.000648	0.000708
	18.6			0.502			0.1168	0.02687	0.00795	5312.	1.095	1.034	0.947
11 3	30.	141.8	739.8	0.158	730.	337.	-337.	657.	804.	464.	223.	250.	289.
0.9382	-60.7	63.9	5 5.2	0.323	778.	359.	-359.	700.	857.	494.	238.	266.	308.
0.002231	-0.7	1123.	9.420	1.016	0.001218	5.27		0.008496	65.2		0.006744	0.007534	0.008726
	4.2		0.785	0.880	0.009440	0.004358		0.001096			0.000277	0.000309	0.000358
	18.0			0.498			0.0716	0.01231	0.00403	2685.	1.108	0.992	0.857
11 4	30.0	141.9	739.8	0.159	628.	129.	-129.	426.	641.	479.	115.	174.	168.
0.9361	-60.5	63.8	565.2	0.324	671.	138.	-138.	455.	685.	512.	123.	186.	179.
0.002226	-0.5	1125.	9.420	1.016	0.001050	2.02		0.005521	78.4		0.003494	0.005275	0.005081
	4.0		0.785	0.880	0.008140	0.001672		0.000712			0.000143	0.000217	0.000209
	17.9			0.500			0.0644	0.00800	0.00234	1560.	1.391	0.922	0.956
11 5	30.0	141.8	739.8	0.159	1153.	1134.	-1134.	1558.	1617.	432.	542.	598.	603.
0.9344	-60.6	63.6	565.2	0.324	1234.	1214.	-1214.	1667.	1731.	462.	580.	640.	645.
0.002222	-0.6	1126.	9.420	1.016	0.001931	17.82		0.020230	45.5		0.016444	0.018134	0.018273
	4.3		0.784	0.880	0.014971	0.014723		0.002610			0.000675	0.000745	0.000750
	19.1			0.500			0.1256	0.02932	0.00843	5600.	1.083	0.982	0.974
11 6	30.0	142.2	739.8	0.149	780.	583.	-583.	895.	974.	384.	295.	370.	402.
0.9323	-62.7	63.8	565.2	0.324	837.	625.	-625.	960.	1045.	412.	316.	396.	431.
0.002217	-2.7	1127.	9.420	1.016	0.001309	9.13		0.011647	53.2		0.008956	0.011230	0.012218
	6.1		0.778	0.880	0.010151	0.007586		0.001502			0.000368	0.000461	0.000502
	19.2			0.466			0.0321	0.01688	0.00564	3736.	1.147	0.915	0.839

RUN	PT	ALN	V(KTS)	T.SPEED	MU	L	PF	D	T	PF	W	HP1	HP2	HPR
~~SIGMA-P~~		~~ALTPP~~	Q	RPM	~~MU-P~~	~~LSIG~~	~~PFSIG~~	~~DSIG~~	~~TSIG~~	~~PFSIG~~	~~WSIG~~	~~HP1SIG~~	~~HP2SIG~~	~~HPRSIG~~
RHO		FLAP	C	RPS	J	CLH	F		CT	THERF		CP1	CP2	CPR
		CYCLIC		MAT	J-P	CL	CPF		CTH			CP1H	CP2H	CPRH
		~~COLLECT.~~			~~J-PP~~			~~FM~~	~~CTHSQL~~	~~CPHSQL~~	~~QR~~	~~CT01~~	~~CT02~~	~~CTQR~~
11	7	30.0	141.5	739.8	0.130	590.	342.	-342.	591.	682.	340.	198.	247.	264.
0.9323		-66.2	63.2	565.2	0.323	633.	367.	-367.	634.	731.	365.	212.	265.	283.
0.002217		-6.2	1127.	9.420	1.016	0.000990	5.41		0.007691	59.9		0.006003	0.007516	0.008019
		3.4		0.767	0.880	0.007678	0.004450		0.000992			0.000247	0.000309	0.000329
		19.2			0.410			0.0671	0.01115	0.00370	2452.	1.125	0.899	0.844

RUN	PT	ALN	V(KTS)	T.SPEED	MU		PF	D	T	RF	M	MP1	MP2	MP8
SIGMA-P		ALTPP	Q	RPM	MU-P	LS	PFSIG	DSIG	TSIG	RFSIG	MSIG	MP1SIG	MP2SIG	MP8SIG
RHO		FLAP	C	RPS	J	CLM	F		CT	THERF		CP1	CP2	CP8
		CYCLIC		MAT	J-P	CL	CPF		CTM			CP1M	CP2M	CP8M
		COLLECT.			J-PP			FM	CTMSOL	CPMSOL	QB	ETA1	ETA2	ETA8
12	1	60.0	99.1	739.8	0.196	2309.	995.	-995.	2497.	2514.	293.	452.	464.	496.
0.9706		-30.0	32.3	565.2	0.226	2379.	1025.	-1025.	2573.	2591.	302.	465.	478.	511.
0.002308		0.0	1121.	9.420	0.720	0.003723	30.81		0.031214	66.7		0.013182	0.013544	0.014488
		3.2		0.793	0.360	0.028864	0.012437		0.004027			0.000541	0.000556	0.000595
		4.8			0.623			0.3036	0.04524	0.00669	4612.	0.841	0.819	0.776
12	2	60.0	98.7	738.3	0.195	3575.	1733.	-1733.	3962.	3973.	287.	724.	747.	759.
0.9706		-30.0	32.0	564.0	0.226	3683.	1786.	-1786.	4082.	4093.	296.	746.	770.	782.
0.002308		0.0	1121.	9.400	0.700	0.005789	54.09		0.049738	64.1		0.021274	0.021954	0.022285
		4.2		0.791	0.350	0.044880	0.021754		0.006416			0.000874	0.000902	0.000915
		7.0			0.696			0.3970	0.07209	0.01028	7064.	0.829	0.803	0.781
12	3	60.0	99.6	738.3	0.197	4530.	2278.	-2278.	5062.	5071.	293.	965.	989.	1003.
0.9685		-30.0	32.6	564.0	0.228	4678.	2352.	-2352.	5227.	5236.	302.	997.	1022.	1036.
0.002303		0.0	1122.	9.400	0.720	0.007352	69.97		0.063685	63.3		0.028422	0.029126	0.029529
		5.0		0.791	0.360	0.056992	0.028658		0.008215			0.001167	0.001196	0.001213
		9.0			0.623			0.4341	0.09231	0.01363	9340.	0.801	0.782	0.776
12	4	60.0	99.5	738.3	0.197	4967.	2533.	-2533.	5568.	5576.	290.	1066.	1103.	1110.
0.9643		-30.1	32.3	564.0	0.228	5151.	2627.	-2627.	5774.	5782.	301.	1105.	1144.	1151.
0.002293		-0.1	1125.	9.400	0.720	0.008096	78.32		0.070357	63.0		0.031513	0.032617	0.032811
		5.4		0.789	0.360	0.062763	0.032005		0.009076			0.001294	0.001340	0.001347
		10.0			0.623			0.4537	0.10198	0.01514	10333.	0.798	0.771	0.772
12	5	60.0	99.5	739.8	0.196	5041.	2570.	-2570.	5651.	5658.	295.	1085.	1124.	1150.
0.9643		-30.1	32.3	565.2	0.227	5228.	2665.	-2665.	5860.	5868.	306.	1125.	1165.	1192.
0.002293		-0.1	1125.	9.420	0.720	0.008182	79.50		0.071103	63.0		0.031871	0.033019	0.033779
		5.4		0.791	0.360	0.063427	0.032335		0.009172			0.001309	0.001356	0.001387
		10.2			0.623			0.4477	0.10306	0.01559	10683.	0.795	0.768	0.758
12	6	60.0	99.4	739.8	0.197	-662.	-731.	731.	-939.	986.	302.	-27.	-9.	-6.
0.9643		-29.8	32.3	565.2	0.227	-687.	-758.	758.	-974.	1023.	313.	-28.	-9.	-6.
0.002293		0.2	1125.	9.420	0.720	-0.001074	-22.66		-.011815	42.2		-0.000805	-0.000255	-0.000183
		1.0		0.791	0.360	-0.008329	-0.009197		-.001524			-0.000033	-0.000010	-0.000008
		-0.4			0.625			******	-.01712	-.00008	-58.	-4.212	-4.212	23.193

RUN PT	ALN	V(KTS)	T.SPEED	MU	L	PF	D	T	RF	H	HP1	HP2	HPB
SIGMA-P	ALTPP	Q	RPM	MU-P	LSIG	PFSIG	DSIG	TSIG	RFSIG	HSIG	HP1SIG	HP2SIG	HPBSIG
RHO	FLAP	C	RPS	J	CLH	F		CT	THERF		CP1	CP2	CPB
	CYCLIC		MAT	J-P	CL	CPF		CTH			CP1H	CP2H	CPBH
	COLLECT.			J-PP			FM	CTHSOL	CPHSOL	QB	ETA1	ETA2	ETAB
13 1	60.0	140.7	739.8	0.278	1532.	261.	-261.	1457.	1554.	540.	340.	332.	314.
0.9441	-29.3	63.3	565.2	0.321	1623.	276.	-276.	1543.	1646.	572.	361.	351.	333.
0.002245	0.1	1126.	9.420	1.000	0.002540	4.12		0.018724	80.3		0.010217	0.009957	0.009427
	4.4		0.847	0.500	0.019688	0.003354		0.002415			0.000420	0.000409	0.000387
	8.0			0.866			0.2168	0.02714	0.00435	2919.	0.924	0.948	0.993
13 2	60.0	140.8	739.8	0.278	2134.	628.	-628.	2162.	2224.	523.	517.	494.	471.
0.9424	-30.0	63.3	565.2	0.321	2264.	666.	-666.	2294.	2360.	555.	549.	525.	500.
0.002241	0.0	1127.	9.420	1.000	0.003544	9.92		0.027834	73.6		0.015547	0.014862	0.014164
	5.3		0.846	0.500	0.027474	0.008085		0.003591			0.000638	0.000610	0.000582
	9.2			0.866			0.2615	0.04034	0.00654	4378.	0.903	0.945	0.983
13 3	60.0	140.6	739.8	0.278	2855.	1066.	-1066.	3006.	3048.	505.	705.	701.	679.
0.9386	-30.0	62.9	565.2	0.321	3042.	1136.	-1136.	3203.	3247.	538.	751.	747.	723.
0.002232	0.0	1129.	9.420	1.000	0.004761	16.96		0.038856	69.5		0.021288	0.021156	0.020481
	6.0		0.844	0.500	0.036904	0.013778		0.005012			0.000874	0.000869	0.000841
	10.6			0.866			0.2983	0.05632	0.00945	6305.	0.919	0.925	0.949
13 4	60.0	141.1	739.8	0.279	3257.	1303.	-1303.	3472.	3508.	500.	826.	822.	785.
0.9344	-30.0	63.1	565.2	0.322	3486.	1394.	-1394.	3716.	3754.	535.	884.	880.	840.
0.002222	0.0	1131.	9.420	1.020	0.005455	20.67		0.045082	68.2		0.025048	0.024935	0.023810
	6.3		0.843	0.510	0.042290	0.016918		0.005815			0.001029	0.001024	0.000978
	11.2			0.883			0.3207	0.06534	0.01099	7297.	0.910	0.914	0.966

RUN PT SIGMA-P RMU	ALN ALTPP FLAP CYCLIC COLLECT.	V(KTS) Q C	T.SPEED RPM RPS MAT	MU MU-P J J-P J-PP	L LSIG CLM CL	PF PFSIG F CPF	D DSIG FM	T TSIG CT CTH CTHSOL	RF RFSIG THERF CPHSOL	H HSIG QB	HP1 HP1SIG CP1 CP1H ETA1	HP2 HP2SIG CP2 CP2H ETA2	HPB HPBSIG CPB CPBH ETAB
14 1	75.0	0.0	599.3	0.0	2678.	625.	-625.	2749.	2750.	90.	236.	229.	227.
C.9903	-14.7	0.0	457.8	0.0	2704.	631.	-631.	2776.	2777.	91.	238.	232.	229.
0.002355	0.3	1120.	7.630	0.039	0.006451	625.00		0.051333	76.9		0.012708	0.012344	0.012210
	-0.3		0.535	0.010	0.050008	0.011670		0.006622			0.000522	0.000507	0.000501
	2.0			0.037			0.7598	0.07440	0.00563	2602.	0.0	0.0	0.042
14 2	75.0	5.5	599.3	0.015	3656.	821.	-821.	3744.	3747.	154.	368.	355.	348.
0.9899	-14.5	0.1	457.8	0.015	3693.	829.	-829.	3782.	3785.	155.	372.	358.	351.
0.002354	0.4	1120.	7.630	0.039	0.004811	8205.50		0.069943	77.3		0.019817	0.019095	0.018731
	-0.8		0.543	0.010	0.068299	0.015337		0.009023			0.000814	0.000784	0.000769
	4.3			0.037			0.7877	0.10138	0.00864	3990.	0.044	0.046	0.037
14 3	75.0	4.9	599.3	0.013	4372.	977.	-977.	4476.	4480.	188.	480.	472.	473.
0.9899	-14.1	0.1	457.8	0.013	4417.	987.	-987.	4522.	4526.	190.	485.	477.	478.
0.002354	0.9	1120.	7.630	0.039	0.010536	12225.43		0.083618	77.4		0.025834	0.025422	0.025487
	1.0		0.542	0.010	0.081675	0.018251		0.010787			0.001061	0.001044	0.001047
	6.8			0.037			0.7567	0.12120	0.01176	5429.	0.036	0.037	0.033
14 4	75.0	5.5	599.3	0.015	5007.	1161.	-1161.	5137.	5140.	175.	602.	590.	611.
0.9899	-14.7	0.1	457.8	0.015	5058.	1173.	-1173.	5189.	5192.	177.	608.	596.	617.
0.002354	0.3	1120.	7.630	0.039	0.012066	11603.64		0.095967	77.0		0.032410	0.031787	0.032886
	0.0		0.543	0.010	0.093538	0.021688		0.012380			0.001331	0.001305	0.001351
	8.8			0.037			0.7211	0.13910	0.01517	7005.	0.037	0.038	0.029
14 5	75.0	6.0	599.3	0.016	5648.	1305.	-1305.	5793.	5797.	202.	721.	710.	687.
0.9899	-15.0	0.1	457.8	0.017	5706.	1318.	-1318.	5852.	5856.	204.	728.	718.	694.
0.002354	0.0	1120.	7.630	0.039	0.013611	10869.05		0.108222	77.0		0.038819	0.038253	0.036998
	0.3		0.544	0.010	0.105513	0.024378		0.013960			0.001594	0.001571	0.001519
	10.5			0.037			0.7675	0.15686	0.01707	7881.	0.038	0.039	0.029
14 6	75.0	5.8	599.3	0.016	5956.	1336.	-1336.	6099.	6104.	252.	828.	830.	809.
0.9899	-14.4	0.1	457.8	0.016	6017.	1350.	-1350.	6161.	6166.	254.	837.	838.	817.
0.002354	0.5	1120.	7.630	0.039	0.014353	11867.32		0.113938	77.4		0.044606	0.044675	0.043575
	0.3		0.543	0.010	0.111267	0.024957		0.014698			0.001832	0.001835	0.001790
	12.1			0.037			0.7040	0.16514	0.02011	9282.	0.034	0.034	0.026

RUN	PT	ALN	V(KTS)	T.SPEED	MU	L	PF	D	T	RF	H	HP1	HP2	HPB
SIGMA-P		ALTPP	Q	RPM	MU-P	LSIG	PFSIG	DSIG	TSIG	RFSIG	HSIG	HP1SIG	HP2SIG	HPBSIG
RHO		FLAP	C	RPS	J	CLH	F		CT	THERF		CP1	CP2	CPB
		CYCLIC		MAT	J-P	CL	CPF		CTH			CP1H	CP2H	CPBH
		COLLECT.			J-PP			FM	CTHSOL	CPHSOL	QB	ETA1	ETA2	ETAB
15	1	75.0	17.0	739.8	0.039	3123.	702.	-702.	3198.	3201.	131.	335.	309.	320.
0.9895		-14.3	1.0	565.2	0.039	3156.	709.	-709.	3232.	3235.	132.	339.	312.	324.
0.002353		0.7	1120.	9.420	0.116	0.004940	720.38		0.039212	77.3		0.009596	0.008837	0.009173
		-0.8		0.685	0.030	0.038293	0.008607		0.005059			0.000394	0.000363	0.000377
		0.0			0.112			0.6752	0.05684	0.00423	2977.	0.129	0.140	0.128
15	2	75.0	17.0	739.8	0.038	4198.	971.	-971.	4306.	4309.	149.	479.	450.	471.
0.9895		-14.5	1.0	565.2	0.039	4243.	981.	-981.	4352.	4355.	151.	484.	455.	476.
0.002353		0.5	1120.	9.420	0.116	0.006640	996.43		0.052798	77.0		0.013725	0.012888	0.013490
		-0.4		0.685	0.030	0.051474	0.011905		0.006811			0.000564	0.000529	0.000554
		2.5			0.112			0.7173	0.07653	0.00622	4378.	0.122	0.130	0.117
15	3	75.0	17.0	739.8	0.038	5619.	1277.	-1277.	5768.	5772.	224.	708.	673.	679.
0.9895		-14.3	1.0	565.2	0.039	5689.	1291.	-1291.	5829.	5833.	226.	716.	680.	686.
0.002353		0.7	1120.	9.420	0.116	0.008903	1310.44		0.070724	77.2		0.020277	0.019257	0.019428
		-0.4		0.685	0.030	0.069020	0.015657		0.009123			0.000833	0.000791	0.000798
		4.9			0.112			0.7722	0.10251	0.00896	6305.	0.110	0.116	0.109
15	4	75.0	17.0	739.8	0.038	6880.	1626.	-1626.	7066.	7070.	211.	939.	923.	942.
0.9895		-14.6	1.0	565.2	0.039	6953.	1643.	-1643.	7141.	7145.	213.	948.	933.	952.
0.002353		0.4	1120.	9.420	0.116	0.010882	1668.58		0.086640	76.7		0.026852	0.026421	0.026983
		0.0		0.685	0.030	0.084359	0.019936		0.011176			0.001103	0.001085	0.001108
		7.0			0.112			0.7538	0.12558	0.01245	8757.	0.102	0.104	0.096
15	5	75.0	17.0	739.8	0.038	7235.	1637.	-1637.	7412.	7418.	292.	1037.	1011.	1037.
0.9895		-14.2	1.0	565.2	0.039	7312.	1654.	-1654.	7491.	7497.	295.	1048.	1022.	1048.
0.002353		0.8	1120.	9.420	0.116	0.011764	1679.87		0.090882	77.3		0.029696	0.028947	0.029679
		-0.3		0.685	0.030	0.088252	0.020071		0.011724			0.001220	0.001139	0.001219
		8.1			0.112			0.7363	0.13173	0.01369	9632.	0.097	0.099	0.092
15	6	75.0	17.0	739.8	0.038	7885.	1858.	-1858.	8097.	8101.	247.	1178.	1154.	1175.
0.9895		-14.4	1.0	565.2	0.039	7969.	1878.	-1878.	8183.	8187.	250.	1191.	1166.	1187.
0.002353		0.6	1120.	9.420	0.116	0.012472	1906.66		0.099281	76.7		0.033731	0.033047	0.033638
		0.2		0.685	0.030	0.096682	0.022780		0.012807			0.001385	0.001357	0.001381
		9.0			0.112			0.7418	0.14390	0.01552	10917.	0.093	0.095	0.089

RUN	PT	ALN	V(KTS)	T.SPEED	MU	L	PF	D	T	RF	H	HP1	HP2	HP8
SIGMA	-P	ALTPP	Q	RPM	MU-P	LSIG	PFSIG	DSIG	TSIG	RFSIG	HSIG	HP1SIG	HP2SIG	HP8SIG
RHO		FLAP	C	RPS	J	CLH	F		CT	THERF		CP1	CP2	CP8
		CYCLIC		MAT	J-P	CL	CPF		CTH			CP1H	CP2H	CP8H
		COLLECT.			J-PP			FM	CTHSOL	CPHSOL	QB	ETA1	ETA2	ETA8
16	1	75.0	79.9	739.8	0.176	3900.	693.	-693.	3946.	3961.	340.	412.	401.	415.
0.9807		-14.5	21.2	565.2	0.182	3977.	707.	-707.	4024.	4039.	347.	420.	409.	423.
0.002332		0.5	1120.	9.420	0.579	0.006224	32.71		0.048819	79.9		0.011894	0.011575	0.011979
		-2.2		0.778	0.150	0.048250	0.008573		0.006298			0.000488	0.000475	0.000492
		1.8			0.561			0.7182	0.07076	0.00553	3853.	0.608	0.625	0.611
16	2	75.0	80.1	739.8	0.177	5464.	1072.	-1072.	5556.	5568.	379.	615.	612.	628.
0.9786		-14.7	21.3	565.2	0.183	5584.	1095.	-1095.	5678.	5690.	388.	629.	625.	642.
0.002327		0.3	1121.	9.420	0.579	0.008739	50.34		0.068886	78.9		0.017817	0.017713	0.018190
		-3.5		0.777	0.150	0.067745	0.013290		0.008886			0.000732	0.000727	0.000747
		4.5			0.560			0.7928	0.09984	0.00839	5838.	0.575	0.578	0.568
16	3	75.0	80.2	739.8	0.177	6092.	1208.	-1208.	6197.	6211.	410.	718.	723.	735.
0.9786		-14.5	21.3	565.2	0.183	6276.	1234.	-1234.	6333.	6347.	419.	733.	739.	751.
0.002327		0.5	1121.	9.420	0.579	0.009743	56.62		0.076833	78.8		0.020780	0.020938	0.021280
		-4.1		0.777	0.150	0.075531	0.014976		0.009911			0.000853	0.000860	0.000874
		5.8			0.561			0.7983	0.11136	0.00982	6830.	0.550	0.546	0.542
16	4	75.0	80.2	739.8	0.177	6519.	1359.	-1359.	6649.	6659.	375.	862.	873.	873.
0.9786		-14.7	21.3	565.2	0.183	6662.	1389.	-1389.	6795.	6805.	383.	881.	892.	892.
0.002327		0.3	1121.	9.420	0.579	0.010426	63.78		0.082437	78.2		0.024950	0.025272	0.025284
		-5.1		0.777	0.150	0.080826	0.016849		0.010634			0.001025	0.001038	0.001038
		7.2			0.560			0.7467	0.11949	0.01167	8115.	0.491	0.485	0.489

BELL HELICOPTER COMPANY

RUN	PT	ALN	V(KTS)	T.SPEED	MU	L	PF	D	T	RF	H	HP1	HP2	HP8
SIGMA	-P	ALTPP	Q	RPM	MU-P	LSIG	PFSIG	DSIG	TSIG	RFSIG	HSIG	HP1SIG	HP2SIG	HP8SIG
RHO		FLAP	C	RPS	J	CLM	F		CT	THERF		CP1	CP2	CP8
		CYCLIC		MAT	J-P	CL	CPF		CTH			CP1M	CP2M	CP8M
		COLLECT.			J-PP			FM	CTHSOL	CPHSOL	QB	ETA1	ETA2	ETA8
17	1	75.0	120.5	739.8	0.266	2674.	277.	-277.	2655.	2688.	425.	357.	341.	371.
0.9622		-14.5	47.3	565.2	0.275	2779.	288.	-288.	2759.	2794.	441.	371.	354.	385.
0.002288		0.5	1123.	9.420	0.850	0.004350	5.85		0.033479	84.1		0.010498	0.010030	0.010913
		0.0		0.833	0.220	0.033719	0.003493		0.004319			0.000431	0.000412	0.000448
		1.5			0.823			0.4477	0.04853	0.00504	3444.	0.713	0.746	0.675
17	2	75.0	120.5	739.8	0.266	3287.	446.	-446.	3290.	3317.	420.	429.	420.	433.
0.9601		-14.8	47.3	565.2	0.275	3424.	465.	-465.	3427.	3455.	438.	447.	438.	452.
0.002283		0.2	1125.	9.420	0.850	0.005359	9.44		0.041577	82.3		0.012651	0.012399	0.012792
		0.0		0.834	0.220	0.041539	0.005636		0.005363			0.000520	0.000509	0.000525
		3.0			0.822			0.5286	0.06026	0.00590	4028.	0.735	0.750	0.715
17	3	75.0	120.3	739.8	0.265	4246.	662.	-662.	4272.	4297.	460.	551.	542.	565.
0.9579		-14.7	47.0	565.2	0.274	4432.	691.	-691.	4460.	4486.	480.	575.	565.	590.
0.002278		0.3	1126.	9.420	0.850	0.006937	14.10		0.054106	81.1		0.016282	0.016020	0.016722
		4.8		0.833	0.220	0.053776	0.008384		0.006980			0.000669	0.000658	0.000687
		4.7			0.822			0.6003	0.07842	0.00772	5254.	0.742	0.754	0.712
17	4	75.0	120.3	739.8	0.265	4978.	861.	-861.	5031.	5052.	457.	666.	667.	685.
0.9579		-14.9	47.0	565.2	0.274	5197.	899.	-899.	5252.	5274.	477.	695.	696.	715.
0.002278		0.1	1126.	9.420	0.850	0.008133	18.33		0.063718	80.2		0.019694	0.019720	0.020252
		5.9		0.833	0.220	0.063047	0.010904		0.008220			0.000809	0.000810	0.000832
		6.0			0.821			0.6335	0.09236	0.00934	6363.	0.722	0.721	0.692
17	5	75.0	120.7	739.8	0.266	5477.	984.	-984.	5545.	5565.	468.	787.	795.	810.
0.9558		-14.7	47.2	565.2	0.275	5730.	1029.	-1029.	5801.	5822.	489.	823.	831.	848.
0.002273		0.3	1127.	9.420	0.850	0.008968	20.85		0.070383	79.8		0.023325	0.023557	0.024022
		6.8		0.833	0.220	0.069520	0.012489		0.009079			0.000958	0.000967	0.000987
		7.5			0.822			0.6200	0.10201	0.01108	7531.	0.676	0.669	0.645

RUN PT SIGMA-P RHO	ALN ALTPP FLAP CYCLIC COLLECT.	V(KTS) Q C	T.SPEED RPM RPS MAT	MU MU-P J J-P J-PP	L LSIG CLM CL	PF PFSIG F CPF	D DSIG FM	T TSIG CT CTM CTMSOL	RF RFSIG THERF CPMSOL	M MSIG QB	MP1 MP1SIG CP1 CP1M ETA1	MP2 MP2SIG CP2 CP2M ETA2	MPB MPBSIG CPB CPBM ETAB
18 1	75.0	140.2	739.8	0.310	2114.	57.	-57.	2056.	2115.	492.	321.	310.	320.
0.9428	-14.4	62.8	565.2	0.320	2242.	60.	-60.	2181.	2243.	522.	341.	329.	340.
0.002242	0.5	1130.	9.420	1.004	0.003509	0.91		0.026458	88.5		0.009658	0.009323	0.009627
	3.0		0.859	0.260	0.027204	0.000733		0.003413			0.000397	0.000383	0.000395
	1.2			0.972			0.3566	0.03835	0.00444	2977.	0.713	0.738	0.715
18 2	75.0	139.9	739.8	0.309	2960.	276.	-276.	2931.	2973.	500.	427.	414.	421.
0.9407	-14.7	62.4	565.2	0.319	3147.	293.	-293.	3116.	3160.	531.	454.	440.	447.
0.002237	0.3	1131.	9.420	1.004	0.004925	4.42		0.037802	84.7		0.012865	0.012480	0.012676
	4.2		0.858	0.260	0.038176	0.003559		0.004876			0.000528	0.000513	0.000521
	3.2			0.971			0.4625	0.05479	0.00585	3911.	0.763	0.786	0.775
18 3	75.0	140.4	739.8	0.310	3689.	437.	-437.	3676.	3715.	533.	535.	519.	515.
0.9407	-14.5	62.8	565.2	0.320	3972.	465.	-465.	3908.	3949.	567.	569.	551.	548.
0.002237	0.5	1131.	9.420	1.004	0.006138	6.96		0.047410	83.3		0.016116	0.015616	0.015515
	5.1		0.859	0.260	0.047578	0.005636		0.006116			0.000662	0.000641	0.000637
	4.6			0.972			0.5307	0.06872	0.00716	4787.	0.766	0.790	0.795
18 4	75.0	140.5	739.8	0.312	4356.	600.	-600.	4363.	4397.	548.	631.	625.	622.
0.9386	-13.1	62.8	565.2	0.321	4641.	639.	-639.	4648.	4685.	584.	673.	666.	663.
0.002232	1.9	1132.	9.420	1.004	0.007263	9.56		0.056397	82.2		0.019060	0.018860	0.018772
	6.0		0.859	0.260	0.056306	0.007755		0.007275			0.000783	0.000775	0.000771
	6.0			0.978			0.5691	0.08174	0.00866	5779.	0.771	0.779	0.781

RUN	PT	ALN	V(KTS)	T.SPEED	MU	L	PF	D	T	RF	M	MP1	MP2	MPB
SIGMA-P		ALTPP	Q	RPM	MU-P	LSIG	PFSIG	DSIG	TSIG	RFSIG	MSIG	MP1SIG	MP2SIG	MPBSIG
RHO		FLAP	C	RPS	J	CLM	F		CT	THERF		CP1	CP2	CPB
		CYCLIC		MAT	J-P	CL	CPF		CTM			CP1M	CP2M	CPBM
		COLLECT.			J-PP			FM	CTMSOL	CPMSOL	QB	ETA1	ETA2	ETAB
19	1	0.0	184.8	599.3	0.005	20.	272.	-272.	272.	273.	20.	304.	237.	271.
0.9205		-89.5	106.5	457.8	0.521	22.	295.	-295.	295.	296.	22.	331.	257.	295.
0.002189		0.5	1127.	7.630	1.630	0.000052	2.55		0.005464	4.2		0.017632	0.013716	0.015706
		0.1		0.602	1.630	0.000402	0.005464		0.000705			0.000724	0.000563	0.000645
		30.0			0.014			0.0205	0.00792	0.00725	3111.	0.507	0.651	0.567
19	2	0.0	141.0	595.3	-0.001	8.	1008.	-1008.	1008.	1008.	8.	498.	499.	476.
0.9209		-90.1	62.0	457.8	0.397	9.	1095.	-1095.	1095.	1095.	9.	541.	542.	517.
0.002190		-0.1	1137.	7.630	1.250	0.000021	16.25		0.020241	0.5		0.028838	0.028880	0.027542
		0.1		0.567	1.250	0.000161	0.020240		0.002611			0.001184	0.001186	0.001131
		24.2			-0.002			0.0834	0.02934	0.01271	5458.	0.875	0.874	0.919
19	3	0.0	141.0	641.7	-0.001	13.	2144.	-2144.	2144.	2144.	13.	1033.	1009.	997.
0.9188		-90.2	61.9	490.2	0.371	14.	2333.	-2333.	2333.	2333.	14.	1124.	1098.	1085.
0.002185		-0.2	1138.	8.170	1.170	0.000029	34.63		0.037635	0.3		0.048800	0.047693	0.047121
		0.1		0.601	1.170	0.000228	0.037633		0.004855			0.002004	0.001959	0.001935
		24.2			-0.003			0.1236	0.05455	0.02174	10682.	0.899	0.920	0.934
19	4	0.0	141.0	618.1	-0.001	13.	1422.	-1422.	1422.	1422.	13.	678.	688.	681.
0.9188		-90.1	61.9	472.2	0.385	14.	1548.	-1548.	1548.	1548.	14.	738.	749.	741.
0.002185		-0.1	1138.	7.870	1.210	0.000032	22.96		0.026901	0.5		0.035853	0.036384	0.035992
		0.1		0.582	1.210	0.000246	0.026899		0.003470			0.001472	0.001494	0.001478
		24.2			-0.002			0.0978	0.03899	0.01661	7571.	0.908	0.895	0.904
19	5	0.0	141.2	579.6	0.000	20.	367.	-367.	367.	368.	20.	222.	230.	242.
0.9188		-90.0	62.1	442.8	0.411	22.	399.	-399.	399.	400.	22.	241.	250.	264.
0.002185		0.0	1138.	7.380	1.290	0.000053	5.91		0.007895	3.1		0.014215	0.014725	0.015548
		0.1		0.551	1.290	0.000430	0.007895		0.001018			0.000584	0.000605	0.000639
		24.2			0.000			0.0360	0.01144	0.00717	2876.	0.718	0.693	0.655
19	6	0.0	140.9	560.0	0.000	20.	-143.	143.	-143.	144.	20.	15.	4.	14.
0.9188		-89.9	61.8	427.8	0.425	22.	-156.	156.	-156.	157.	22.	16.	5.	16.
0.002185		0.1	1138.	7.130	1.330	0.000059	-2.31		-.003296	-8.0		0.001042	0.000311	0.001019
		0.1		0.535	1.330	0.000461	-0.003296		-.000425			0.000043	0.000013	0.000042
		24.2			0.002			0.1481	-.00478	0.00047	176.	-4.222	-4.395	-4.300

RUN PT SIGMA-P RHO	ALN ALTPP FLAP CYCLIC COLLECT.	V(KTS) Q C	T.SPEED RPM RPS MAT	MU MU-P J J-P J-PP	L LSIG CLH CL	PF PFSIG F CP	D DSIG FM	T TSIG CT CTH CTHSOL	RF RFSIG THERF CPHSOL	H HSIG QB	HP1 HP1SIG CP1 CP1H ETA1	HP2 HP2SIG CP2 CP2H ETA2	HPB HPBSIG CPB CPBH ETAB
20 1	0.0	162.0	599.3	0.004	22.	684.	-684.	684.	684.	22.	403.	402.	404.
0.9045	-89.6	80.4	457.8	0.456	24.	756.	-756.	756.	757.	24.	445.	445.	447.
0.002151	0.4	1141.	7.630	1.430	0.000058	8.50		0.013984	1.8		0.023726	0.023720	0.023823
	0.1		0.579	1.430	0.000450	0.013983		0.001804			0.000974	0.000974	0.000978
	27.0			0.011			0.0554	0.02027	0.01099	4637.	0.845	0.845	0.839
20 2	0.0	161.8	599.3	0.003	-3.	929.	-929.	929.	929.	-3.	522.	518.	542.
0.9024	-89.6	80.0	457.8	0.456	-3.	1029.	-1029.	1029.	1029.	-3.	578.	574.	601.
0.002146	0.4	1143.	7.630	1.430	-0.000008	11.61		0.019037	-0.2		0.030824	0.030623	0.032036
	0.1		0.578	1.430	-0.000061	0.019036		0.002456			0.001266	0.001258	0.001316
	27.5			0.010			0.0654	0.02759	0.01478	6221.	0.884	0.890	0.850
20 3	0.0	161.4	599.3	0.002	17.	1693.	-1693.	1693.	1693.	17.	916.	886.	885.
0.9008	-89.7	79.5	457.8	0.455	19.	1880.	-1880.	1880.	1880.	19.	1017.	984.	983.
0.002142	0.3	1144.	7.630	1.430	0.000045	21.29		0.034758	0.6		0.054216	0.052456	0.052387
	0.1		0.577	1.430	0.000349	0.034756		0.004484			0.002227	0.002154	0.002151
	28.5			0.007			0.0987	0.05038	0.02417	10154.	0.916	0.946	0.949
20 4	0.0	161.6	594.5	0.003	17.	1888.	-1888.	1888.	1888.	17.	995.	986.	1035.
0.9008	-89.7	79.7	454.2	0.459	19.	2096.	-2096.	2096.	2096.	19.	1105.	1095.	1150.
0.002142	0.3	1144.	7.570	1.440	0.000046	23.70		0.039378	0.5		0.060317	0.059761	0.062754
	0.1		0.573	1.440	0.000355	0.039376		0.005080			0.002477	0.002454	0.002577
	29.0			0.008			0.0993	0.05708	0.02896	11973.	0.941	0.949	0.904
20 5	0.0	161.6	500.3	0.004	17.	365.	-365.	365.	365.	17.	232.	232.	239.
0.8987	-89.6	79.5	382.2	0.545	19.	406.	-406.	406.	407.	19.	258.	258.	266.
0.002137	0.4	1145.	6.370	1.710	0.000065	4.59		0.010776	2.7		0.023619	0.023648	0.024388
	0.1		0.499	1.710	0.000502	0.010776		0.001390			0.000970	0.000971	0.001002
	31.5			0.013			0.0366	0.01562	0.01125	3287.	0.781	0.780	0.756
20 6	0.0	162.4	500.3	0.003	-3.	899.	-899.	899.	899.	-3.	483.	478.	500.
0.8966	-89.7	80.1	382.2	0.548	-3.	1003.	-1003.	1003.	1003.	-3.	539.	533.	557.
0.002132	0.3	1146.	6.370	1.720	-0.000011	11.23		0.026605	-0.2		0.049355	0.048805	0.051069
	0.1		0.499	1.720	-0.000089	0.026603		0.003432			0.002027	0.002004	0.002097
	32.3			0.010			0.0678	0.03856	0.02357	6867.	0.928	0.938	0.896

RUN	DT	ALN	VKTS	T.SPEED	MU	L	DF	D	T	PF	H	HP1	HP2	HPP
SIGMA-P		ALTPP	Q	RPM	MU-P	+SIG	PFSIG	DSIG	TSIG	PFSIG	HSIG	HP1SIG	HP2SIG	HPPSIG
RHO		FLAP	C	RPS	J	CLH	F		CT	THEPF		CP1	CP2	CPP
		CYCLIC							CTH			CP1H	CP2H	CPPH
		COLLECT		MAT	J-P	CL	CPF	FM	CTHSQU	CPHSQU	QR	FTA1	FTA2	FTAP
20	7	0.0	162.8	500.3	0.004	15.	1179.	-1179.	1179.	1179.	15.	622.	615.	645.
0.8961		-89.6	80.4	382.2	0.549	17.	1316.	-1316.	1316.	1316.	17.	694.	686.	720.
0.002131		0.4	1146.	6.370	1.730	0.000057	14.66		0.034907	0.7		0.063619	0.062853	0.065936
		0.0		0.500	1.730	0.000444	0.034905		0.004503			0.002613	0.002581	0.002708
		32.8			0.012			0.0789	0.05060	0.03043	8862.	0.946	0.958	0.916
20	8	0.0	162.7	500.3	0.004	22.	1404.	-1404.	1404.	1404.	22.	741.	729	765.
0.8961		-89.6	80.4	382.2	0.549	25.	1567.	-1567.	1567.	1567.	25.	827.	813.	853.
0.002131		0.4	1146.	6.370	1.730	0.000084	17.46		0.041569	0.9		0.075733	0.074514	0.078168
		0.1		0.500	1.730	0.000651	0.041567		0.005362			0.003110	0.003060	0.003210
		33.4			0.012			0.0865	0.06025	0.03607	10506.	0.947	0.962	0.920
20	9	0.0	161.7	402.9	0.006	2.	314.	-314.	314.	314.	2.	198.	188.	199.
0.8949		-89.5	79.3	307.8	0.678	2.	351.	-351.	351.	351.	2.	222.	210.	223.
0.002128		0.5	1147.	5.130	2.130	0.000012	3.96		0.014355	0.4		0.038855	0.036877	0.039105
		0.1		0.426	2.130	0.000091	0.014354		0.001852			0.001596	0.001514	0.001606
		36.7			0.019			0.0351	0.02081	0.01804	3404.	0.786	0.828	0.782
20	10	0.0	161.8	400.	0.005	17.	316.	-316.	316.	316.	17.	189.	192.	192.
0.8928		-89.6	79.2	306.0	0.682	19.	354.	-354.	354.	354.	19.	212.	215.	215.
0.002123		0.4	1148.	5.100	2.140	0.000102	3.99		0.014651	3.1		0.037808	0.038436	0.038297
		0.1		0.424	2.140	0.000788	0.014650		0.001890			0.001553	0.001578	0.001573
		36.8			0.015			0.0369	0.02124	0.01767	3287.	0.830	0.816	0.819

RUN PT	ALN	V(KTS)	T.SPEED	MU	L	PF	D	T	RF	H	HP1	HP2	HPB
SIGMA-P	ALTPP	Q	RPM	MU-P	LSIG	PFSIG	DSIG	TSIG	RFSIG	HSIG	HP1SIG	HP2SIG	HPBSIG
RHO	FLAP	C	RPS	J	CLH	F		CT	THERF		CP1	CP2	CPB
	CYCLIC		MAT	J-P	CL	CPF		CTH			CP1H	CP2H	CPBH
	COLLECT.			J-PP			FM	CTHSOL	CPHSOL	QB	ETA1	ETA2	ETAB
21 1	0.0	105.4	400.6	0.002	-12.	1527.	-1527.	1527.	1527.	-12.	535.	526.	525.
0.9706	-89.8	36.5	306.0	0.444	-12.	1573.	-1573.	1573.	1573.	-12.	551.	542.	541.
0.002308	0.2	1121.	5.100	1.390	-0.000066	41.84		0.065122	-0.5		0.098442	0.096683	0.096604
	0.0		0.391	1.390	-0.000512	0.065118		0.008401			0.004043	0.003971	0.003967
	30.0			0.005			0.1372	0.09439	0.04458	9014.	0.923	0.939	0.937
21 2	0.0	105.5	599.3	0.000	-14.	1560.	-1560.	1560.	1560.	-14.	558.	552.	556.
0.9706	-90.0	36.6	457.8	0.297	-14.	1607.	-1607.	1607.	1607.	-14.	574.	569.	572.
0.002308	0.0	1121.	7.630	0.930	-0.000034	42.65		0.029724	-0.5		0.030626	0.030334	0.030515
	0.0		0.558	0.930	-0.000267	0.029722		0.003834			0.001258	0.001246	0.001253
	19.2			0.000			0.1340	0.04308	0.01408	6373.	0.906	0.915	0.906
21 3	0.0	107.0	659.7	-0.000	-14.	2958.	-2958.	2958.	2958.	-14.	1073.	1060.	1047.
0.9701	-90.1	37.6	504.0	0.274	-14.	3049.	-3049.	3049.	3049.	-14.	1106.	1092.	1079.
0.002307	-0.1	1121.	8.400	0.860	-0.000028	78.58		0.046522	-0.3		0.044179	0.043647	0.043116
	0.0		0.610	0.860	-0.000220	0.046519		0.006001			0.001814	0.001792	0.001771
	19.2			-0.002			0.1856	0.06743	0.01990	10909.	0.906	0.917	0.928
21 4	0.0	99.2	490.9	0.001	0.	-64.	64.	-64.	64.	0.	19.	15.	20.
0.9685	-89.9	32.3	375.0	0.341	0.	-66.	66.	-66.	66.	0.	20.	15.	21.
0.002303	0.1	1123.	6.250	1.070	0.0	-1.98		-.001821	0.0		0.001930	0.001480	0.002053
	0.0		0.462	1.070	0.0	-0.001821		-.000235			0.000079	0.000061	0.000084
	19.2			0.002			0.0302	-.00264	0.00095	287.	-1.019	-1.328	-0.949
21 5	0.0	160.5	400.6	0.001	-4.	372.	-372.	372.	372.	-4.	216.	226.	224.
0.9411	-89.9	82.2	306.0	0.677	-4.	395.	-395.	395.	395.	-4.	230.	240.	238.
0.002238	0.1	1126.	5.100	2.130	-0.000023	4.53		0.016361	-0.6		0.040991	0.042915	0.042518
	0.0		0.430	2.130	-0.000176	0.016360		0.002111			0.001683	0.001762	0.001746
	37.5			0.004			0.0393	0.02371	0.01962	3847.	0.848	0.810	0.820
21 6	0.0	161.2	406.8	0.001	-3.	750.	-750.	750.	750.	-3.	399.	409.	414.
0.9369	-89.9	82.5	310.8	0.669	-3.	800.	-800.	800.	800.	-3.	426.	436.	442.
0.002228	0.0	1128.	5.180	2.100	-0.000017	9.09		0.032118	-0.2		0.072591	0.074302	0.075321
	0.0		0.434	2.100	-0.000128	0.032116		0.004143			0.002981	0.003051	0.003093
	37.9			0.002			0.0610	0.04655	0.03476	6999.	0.930	0.909	0.895

RUN PT	ALN	V(KTS)	T.SPEED	MU	L	PF	D	T	RF	M	MP1	MP2	MPB
SIGMA-P	ALTPP	Q	RPM	MU-P	LSIG	PFSIG	DSIG	TSIG	RFSIG	MSIG	MP1SIG	MP2SIG	MPBSIG
RHO	FLAP	C	RPS	J	CLH	F		CT	THERF		CP1	CP2	CPB
	CYCLIC		MAT	J-P	CL	CPF		CTH			CP1H	CP2H	CPBH
	COLLECT.			J-PP			FM	CTHSOL	CPHSOL	QB	ETA1	ETA2	ETAB
22 1	0.0	159.7	697.4	0.002	2.	658.	-658.	658.	658.	2.	412.	431.	390.
0.9466	-89.7	81.8	532.8	0.386	2.	695.	-695.	695.	695.	2.	435.	455.	412.
0.002251	0.3	1125.	8.880	1.210	0.000004	8.05		0.009491	0.2		0.014721	0.015395	0.013944
	0.0		0.666	1.210	0.000029	0.009490		0.001224			0.000605	0.000632	0.000573
	23.8			0.006			0.0529	0.01376	0.00643	3847.	0.782	0.748	0.824
22 2	0.0	160.4	700.6	0.001	-3.	1009.	-1009.	1009.	1009.	-3.	579.	600.	591.
0.9424	-89.8	82.1	535.2	0.386	-3.	1071.	-1071.	1071.	1071.	-3.	614.	637.	627.
0.002241	0.2	1127.	8.920	1.210	-0.000006	12.29		0.014487	-0.2		0.020489	0.021240	0.020924
	0.0		0.667	1.210	-0.000043	0.014486		0.001869			0.000841	0.000872	0.000859
	24.0			0.004			0.0665	0.02100	0.00965	5799.	0.858	0.828	0.838
22 3	0.0	160.1	700.6	0.000	-12.	1504.	-1504.	1504.	1504.	-12.	817.	831.	802.
0.9369	-89.9	81.4	535.2	0.386	-13.	1605.	-1605.	1605.	1605.	-13.	872.	887.	856.
0.002228	0.0	1130.	8.920	1.210	-0.000022	18.48		0.021720	-0.5		0.029109	0.029587	0.028547
	0.0		0.665	1.210	-0.000173	0.021719		0.002802			0.001195	0.001215	0.001172
	24.5			0.001			0.0894	0.03148	0.01317	7866.	0.905	0.890	0.921
22 4	0.0	160.7	705.3	0.000	-16.	2055.	-2055.	2055.	2055.	-16.	1109.	1115.	1090.
0.9327	-90.0	81.6	538.8	0.385	-17.	2203.	-2203.	2203.	2203.	-17.	1189.	1195.	1168.
0.002216	0.0	1132.	8.980	1.210	-0.000030	25.19		0.029415	-0.4		0.038873	0.039080	0.038207
	0.0		0.668	1.210	-0.000229	0.029413		0.003794			0.001596	0.001605	0.001569
	25.0			0.000			0.1053	0.04263	0.01763	10622.	0.914	0.909	0.932

RUN PT	ALN	V(KTS)	T.SPEED	MU	L	PF	D	T	RF	H	HP1	HP2	HPB
SIGMA-P	ALTPP	Q	RPM	MU-P	LSIG	PFSIG	DSIG	TSIG	RFSIG	HSIG	HP1SIG	HP2SIG	HPBSIG
RHO	FLAP	C	RPS	J	CLH	F		CT	THERF		CP1	CP2	CPB
	CYCLIC		MAT	J-P	CL	CPF		CTH			CP1H	CP2H	CPBH
	COLLECT.			J-PP			FM	CTHSOL	CPHSOL	QB	ETA1	ETA2	ETAB
23 2	0.0	159.5	739.8	0.004	-10.	706.	-706.	706.	706.	-10.	441.	462.	494.
0.9361	-89.4	80.7	565.2	0.364	-11.	754.	-754.	754.	754.	-11.	471.	493.	528.
0.002226	0.6	1131.	9.420	1.140-0.000017		8.75		0.009150	-0.8		0.013336	0.013975	0.014960
	0.1		0.699	1.140-0.000130		0.009150		0.001180			0.000548	0.000574	0.000614
	22.5			0.012			0.0467	0.01326	0.00690	4593.	0.784	0.748	0.697
23 3	0.0	159.7	739.8	0.002	-6.	1713.	-1713.	1713.	1713.	-6.	921.	952.	933.
0.9361	-89.7	80.9	565.2	0.364	-6.	1830.	-1830.	1830.	1830.	-6.	984.	1017.	997.
0.002226	0.3	1131.	9.420	1.150-0.000010		21.17		0.022202	-0.2		0.027875	0.028814	0.028239
	0.1		0.698	1.150-0.000078		0.022201		0.002864			0.001145	0.001183	0.001160
	23.3			0.007			0.0934	0.03218	0.01303	8670.	0.912	0.882	0.904
23 4	0.0	160.3	738.3	0.002	-1.	2062.	-2062.	2062.	2062.	-1.	1100.	1129.	1128.
0.9298	-89.6	80.9	564.0	0.366	-1.	2218.	-2218.	2218.	2218.	-1.	1183.	1214.	1214.
0.002211	0.4	1134.	9.400	1.150-0.000002		25.48		0.027022	-0.0		0.033743	0.034615	0.034601
	0.1		0.695	1.150-0.000013		0.027020		0.003486			0.001386	0.001422	0.001421
	23.8			0.008			0.1024	0.03917	0.01597	10507.	0.922	0.898	0.898
23 5	0.0	160.1	740.6	0.002	-4.	2516.	-2516.	2516.	2516.	-4.	1322.	209.	1367.
0.9260	-89.7	80.4	565.8	0.365	-4.	2717.	-2717.	2717.	2717.	-4.	1428.	226.	1476.
0.002202	0.3	1136.	9.430	1.150-0.000007		31.31		0.032895	-0.1		0.040322	0.006369	0.041691
	0.0		0.695	1.150-0.000052		0.032894		0.004243			0.001656	0.000262	0.001712
	24.2			0.007			0.1141	0.04768	0.01924	12689.	0.935	5.917	0.907
23 6	0.0	160.4	400.6	0.007	-11.	-207.	207.	-207.	207.	-11.	-58.	-5.	-30.
0.9201	-89.4	80.2	306.0	0.676	-12.	-225.	225.	-225.	225.	-12.	-63.	-6.	-33.
0.002188	0.5	1139.	5.109	2.120-0.000064		-2.58		-.009312	3.0		-0.011211	-0.001021	-0.005845
	0.1		0.426	2.120-0.000495		-0.009312		-.001201			-0.000460	-0.000042	-0.000240
	18.3			0.021			-.1226	-.01350	-.00270	-517.	-19.813	-19.813	3.378
23 7	0.0	159.7	420.2	0.004	-11.	405.	-405.	405.	405.	-11.	224.	239.	246.
0.9184	-89.6	79.4	321.0	0.642	-12.	441.	-441.	441.	441.	-12.	244.	261.	267.
0.002184	0.4	1140.	5.350	2.020-0.000058		5.10		0.016587	-1.6		0.037726	0.040322	0.041363
	0.1		0.439	2.020-0.000451		0.016586		0.002140			0.001549	0.001656	0.001699
	18.7			0.014			0.0412	0.02404	0.01909	4019.	0.886	0.829	0.810

RUN PT SIGMA-P PHO	ALN ALTPP FLAP CYCLIC COLLECT.	V(KTS) O F	T.SPEED RPM RPS MAT	MU MU-P J J-P J-PP	L LSIG CLH CL	PF PFSIG F CDF	D DSIG FM	T TSIG CT CTH CTHSQI	PF PFSIG THEOF CPHSQI	Q QSIG QR	HP1 HP1SIG CP1 CP1H ETA1	HP2 HP2SIG CP2 CP2H ETA2	HPR HPRSIG CPR CPRH ETAP
23 8	0.0	160.4	451.6	0.004	-3.	1176.	-1176.	1176.	1176.	-3.	645.	661.	660.
0.9180	-89.6	80.0	345.0	0.600	-3.	1281.	-1281.	1281.	1281.	-3.	702.	720.	719.
0.002183	0.4	1140.	5.750	1.880-0.000014		14.69		0.041714	-0.1		0.087460	0.089743	0.089566
	0.1		0.463	1.880-0.000106		0.041712		0.005361			0.003592	0.003686	0.003678
	18.2			0.013			0.0759	0.06046	0.04133	10048.	0.898	0.876	0.876
23 9	0.0	187.4	599.3	0.005	10.	262.	-262.	262.	262.	10.	230.	266.	245.
0.8961	-89.5	100.6	457.8	0.528	11.	292.	-292.	292.	293.	11.	256.	296.	274.
0.002131	0.5	1146.	7.630	1.660	0.000027	2.46		0.005407	2.2		0.013669	0.015795	0.014588
	0.0		0.594	1.660	0.000206	0.005406		0.000697			0.000561	0.000649	0.000599
	24.6			0.014			0.0217	0.00784	0.00673	2813.	0.655	0.567	0.615
23 10	0.0	185.9	599.3	0.003	-10.	862.	-862.	862.	862.	-10.	553.	590.	631.
0.8949	-89.7	104.8	457.8	0.524	-11.	963.	-963.	963.	963.	-11.	617.	659.	705.
0.002128	0.3	1147.	7.630	1.640-0.000027		8.22		0.017814	-0.7		0.032919	0.035138	0.037567
	0.1		0.591	1.640-0.000207		0.017813		0.002298			0.001352	0.001443	0.001543
	31.2			0.010			0.0505	0.02582	0.01733	7234.	0.890	0.834	0.778
23 11	0.0	187.0	599.3	0.001	-8.	1649.	-1649.	1649.	1649.	-8.	997.	1034.	1031.
0.8886	-89.9	105.2	457.8	0.527	-9.	1856.	-1856.	1856.	1856.	-9.	1122.	1164.	1160.
0.002113	0.1	1150.	7.630	1.650-0.000021		15.67		0.034319	-0.3		0.059845	0.062053	0.061861
	0.1		0.590	1.650-0.000166		0.034317		0.004427			0.002458	0.002548	0.002540
	22.8			0.003			0.0820	0.04974	0.02854	11828.	0.949	0.915	0.915
23 12	0.0	184.5	497.2	0.004	-4.	215.	-215.	215.	215.	-4.	173.	199.	224.
0.8856	-89.6	102.1	379.8	0.626	-5.	243.	-243.	243.	243.	-5.	195.	225.	253.
0.002106	0.4	1152.	6.330	1.970-0.000016		2.11		0.006523	-1.1		0.018236	0.020976	0.023635
	0.1		0.511	1.970-0.000121		0.006522		0.000841			0.000749	0.000861	0.000971
	34.3			0.013			0.0178	0.00945	0.01091	3100.	0.705	0.613	0.544
23 13	0.0	185.1	498.7	0.003	-9.	818.	-818.	818.	818.	-9.	487.	529.	533.
0.8835	-89.7	102.5	381.0	0.626	-10.	926.	-926.	926.	926.	-10.	551.	598.	603.
0.002101	0.3	1153.	6.350	1.970-0.000035		7.98		0.024720	-0.6		0.050995	0.055353	0.055810
	0.0		0.511	1.970-0.000272		0.024718		0.003189			0.002094	0.002273	0.002292
	35.6			0.010			0.0555	0.03583	0.02575	7349.	0.954	0.879	0.873

RUN PT SIGMA-P RHO	ALN ALTPP FLAP CYCLIC COLLECT.	VIKTSI Q C	T.SPEED RPM RPS MAT	MU MU-P J J-P J-PP	L LSIG CLH CL	PF PFSIG F CPF	D DSIG FM	T TSIG CT CTH CTHSOL	RF RFSIG THERF CPHSOL	H HSIG QB	HP1 HP1SIG CP1 CP1H ETA1	HP2 HP2SIG CP2 CP2H ETA2	HPB HPBSIG CPB CPBH ETAB
23 14	0.0	185.7	500.3	0.002	-5.	1284.	-1284.	1284.	1284.	-5.	761.	795.	806.
0.8814	-89.8	103.0	382.2	0.627	-6.	1457.	-1457.	1457.	1457.	-6.	864.	902.	915.
0.002096	0.2	1154.	6.370	1.970-0.000019		12.47		0.038651	-0.2		0.079148	0.082662	0.083823
	0.1		0.512	1.970-0.000151		0.038649		0.004986			0.003250	0.003395	0.003442
	36.5			0.006			0.0723	0.05602	0.03868	11081.	0.961	0.921	0.908
23 15	0.0	194.9	696.6	0.003	-1.	214.	-214.	214.	214.	-1.	233.	255.	291.
0.8755	-89.7	101.4	532.2	0.448	-1.	244.	-244.	244.	244.	-1.	266.	291.	332.
0.002082	0.3	1157.	8.870	1.410-0.000002		2.11		0.003345	-0.3		0.009020	0.009879	0.011272
	0.0		0.661	1.410-0.000016		0.003344		0.000431			0.000370	0.000406	0.000463
	26.3			0.008			0.0137	0.00485	0.00520	2870.	0.521	0.476	0.418
23 16	0.0	185.6	699.0	0.010	-8.	687.	-687.	687.	687.	-8.	479.	507.	520.
0.8734	-88.7	101.9	536.0	0.448	-9.	787.	-787.	787.	787.	-9.	548.	581.	595.
0.002077	1.3	1158.	8.900	1.410-0.000016		6.74		0.010691	-0.7		0.018408	0.019514	0.019983
	0.0		0.667	1.410-0.000124		0.010690		0.001379			0.000756	0.000801	0.000821
	26.8			0.032			0.0441	0.01550	0.00922	5110.	0.817	0.771	0.754
23 17	0.0	186.3	700.6	0.002	-13.	1525.	-1525.	1525.	1525.	-13.	940.	987.	989.
0.8730	-89.8	102.6	535.2	0.449	-15.	1747.	-1747.	1747.	1747.	-15.	1077.	1130.	1133.
0.002076	0.2	1158.	8.920	1.410-0.000026		14.86		0.023636	-0.5		0.035928	0.037711	0.037793
	0.0		0.664	1.410-0.000201		0.023635		0.003049			0.001475	0.001549	0.001552
	27.5			0.006			0.0767	0.03426	0.01744	9703.	0.927	0.883	0.882
23 18	0.0	185.0	739.8	0.002	0.	227.	-227.	227.	227.	0.	261.	272.	278.
0.8717	-89.7	101.1	565.2	0.422	0.	260.	-260.	260.	260.	0.	300.	312.	319.
0.002073	0.3	1159.	9.420	1.330 0.0		2.25		0.003159	0.0		0.008487	0.008826	0.009037
	0.0		0.694	1.330 0.0		0.003159		0.000408			0.000349	0.000362	0.000371
	24.8			0.008			0.0157	0.00458	0.00417	2584.	0.493	0.474	0.465
23 19	0.0	186.0	739.8	0.000	-9.	1276.	-1276.	1276.	1276.	-9.	811.	846.	-847.
0.8692	-90.0	101.9	565.2	0.424	-10.	1468.	-1468.	1468.	1468.	-10.	933.	973.	-974.
0.002067	0.0	1160.	9.420	1.330-0.000016		12.53		0.017810	-0.4		0.026437	0.027577	-0.027591
	0.0		0.693	1.330-0.000126		0.017809		0.002298			0.001086	0.001133	-0.001133
	25.9			0.000			-.0687	0.02581	-.01273	-7866.	0.898	0.861	-0.859

RUN	PT	ALN	V(KTS)	T.SPEED	MU	L	PF	D	T	RF	H	HP1	HP2	HPB
SIGMA-P		ALTPP	Q	RPM	MU-P	LSIG	PFSIG	DSIG	TSIG	RFSIG	HSIG	HP1SIG	HP2SIG	HPBSIG
RHO		FLAP	C	RPS	J	CLH	F		CT	THERF		CP1	CP2	CPB
		CYCLIC		MAT	J-P	CL	CPF		CTH			CP1H	CP2H	CPBH
		COLLECT.			J-PP			FM	CTHSQL	CPHSQL	QB	ETA1	ETA2	ETAB
24	1	5.0	176.5	599.3	0.064	214.	285.	-285.	302.	356.	188.	245.	263.	280.
0.9167		-82.6	96.8	457.8	0.497	233.	311.	-311.	329.	389.	205.	267.	287.	306.
0.002180		2.3	1138.	7.630	1.566	0.000557	2.94		0.006092	36.9		0.014256	0.015279	0.016298
		0.0		0.617	1.560	0.004317	0.005749		0.000786			0.000585	0.000627	0.000669
		28.7			0.200			0.0233	0.00883	0.00752	3215.	0.666	0.621	0.583
24	2	5.0	177.0	599.3	0.063	239.	623.	-623.	641.	667.	184.	419.	436.	425.
0.9125		-82.7	96.9	457.8	0.499	262.	683.	-683.	702.	731.	201.	459.	477.	466.
0.002170		2.3	1140.	7.630	1.566	0.000625	6.43		0.012990	21.0		0.024466	0.025451	0.024852
		0.0		0.616	1.560	0.004843	0.012625		0.001676			0.001005	0.001045	0.001021
		29.4			0.199			0.0475	0.01883	0.01147	4880.	0.828	0.796	0.815
24	3	5.0	176.8	599.3	0.064	270.	979.	-979.	998.	1016.	184.	609.	647.	616.
0.9071		-82.6	96.1	457.8	0.498	298.	1079.	-1079.	1100.	1120.	202.	671.	713.	679.
0.002157		2.3	1144.	7.630	1.566	0.000710	10.19		0.020347	15.4		0.035779	0.038012	0.036181
		0.0		0.615	1.560	0.005505	0.019958		0.002625			0.001469	0.001561	0.001486
		29.7			0.200			0.0640	0.02949	0.01670	7062.	0.887	0.835	0.877

RUN	PT	ALN	V(KTS)	T.SPEED	MU	L	PF	D	T	RF	M	HP1	HP2	HPB
SIGMA-P		ALTPP	Q	RPM	MU-P	LSIG	PFSIG	DSIG	TSIG	RFSIG	MSIG	HP1SIG	HP2SIG	HPBSIG
RHO		FLAP	C	RPS	J	CLH	F		CT	THERF		CP1	CP2	CPB
		CYCLIC		MAT	J-P	CL	CPF		CTH			CP1H	CP2H	CPBH
		COLLFCT			J-PP			FM	CTHSOL	CPHSOL	QB	ETA1	ETA2	ETAB
25	1	0.0	184.5	654.2	0.003	-90.	-134.	134.	-134.	161.	-90.	49.	68.	77.
0.9020		-89.6	104.0	499.8	0.476	-100.	-149.	149.	-149.	179.	-100.	54.	75.	85.
0.002145		0.4	1145.	8.330	1.500	-0.000200	-1.29		-.002305	33.9		0.002206	0.003076	0.003475
		0.0		0.635	1.500	-0.001548	-0.002305		-.000297			0.000091	0.000126	0.000143
		27.5			0.010			0.0254	-.00334	0.00160	804.	-1.559	-1.118	-0.995
25	5	10.0	185.8	654.2	0.112	113.	-11.	11.	9.	114.	113.	187.	206.	115.
0.8957		-76.4	104.7	499.8	0.479	126.	-12.	12.	10.	127.	126.	209.	230.	128.
0.002130		3.6	1148.	8.330	1.503	0.000253	-0.11		0.000156	-84.4		0.008576	0.009412	0.005250
		0.0		0.687	1.480	0.001957	-0.000191		0.000020			0.000352	0.000387	0.000216
		27.0			0.353			0.0003	0.00023	0.00242	1206.	0.026	0.023	0.044
25	6	10.0	186.0	654.2	0.120	256.	19.	-19.	63.	257.	249.	141.	200.	208.
0.8953		-75.5	104.9	499.8	0.480	286.	21.	-21.	70.	287.	278.	158.	224.	232.
0.002129		4.5	1148.	8.330	1.503	0.000572	0.18		0.001092	85.8		0.006465	0.009165	0.009503
		0.0		0.691	1.480	0.004437	0.000329		0.000141			0.000266	0.000376	0.000390
		27.0			0.376			0.0030	0.00158	0.00438	2182.	0.251	0.177	0.170
25	7	10.0	185.8	654.2	0.098	58.	-194.	194.	-181.	202.	91.	64.	42.	71.
0.8957		-78.2	104.8	499.8	0.479	65.	-217.	217.	-202.	226.	101.	71.	47.	79.
0.002130		1.8	1148.	8.330	1.503	0.000130	-1.85		-.003135	-16.6		0.002927	0.001936	0.003247
		0.0		0.681	1.480	0.001005	-0.003360		-.000404			0.000120	0.000080	0.000133
		27.3			0.308			0.0431	-.00454	0.00150	746.	-1.586	-2.397	-1.429
25	8	10.0	185.4	654.2	0.064	-356.	-331.	331.	-388.	486.	-293.	29.	9.	33.
0.8957		-79.8	104.3	499.8	0.478	-397.	-370.	370.	-433.	543.	-327.	33.	10.	37.
0.002130		0.2	1148.	8.330	1.503	-0.000795	-3.17		-.006721	47.1		0.001335	0.000404	0.001502
		0.0		0.674	1.480	-0.006167	-0.005733		-.000867			0.000055	0.000017	0.000062
		27.3			0.265			0.2926	-.00974	0.00069	345.	-7.442	-9.921	-6.623

RUN PT SIGMA-P RHO	ALN ALTPP FLAP CYCLIC COLLECT.	V(KTS) Q C	T.SPEED RPM RPS MAT	MU MU-P J J-P J-PP	L LSIG CLM CL	PF PFSIG F CPF	D DSIG FM	T TSIG CT CTM CTMSOL	RF RFSIG THERF CPMSOL	H HSIG 98	HP1 HP1SIG CP1 CP1M ETA1	HP2 HP2SIG CP2 CP2M ETA2	HPB HPBSIG CPB CPBM ETAB
26 1	30.0	139.5	739.8	0.159	756.	395.	-395.	720.	853.	457.	292.	283.	290.
0.9500	-59.9	62.7	565.2	0.318	796.	416.	-416.	758.	898.	481.	307.	298.	306.
0.002259	0.0	1131.	9.420	1.005	0.001246	6.30		0.009196	62.4		0.008700	0.008448	0.008662
	3.7		0.780	0.870	0.009655	0.005045		0.001186			0.000357	0.000347	0.000356
	15.7			0.503			0.0812	0.01333	0.00400	2699.	0.916	0.943	0.924
26 2	30.0	140.2	739.8	0.157	1024.	900.	-900.	1291.	1363.	437.	499.	549.	482.
0.9479	-60.7	63.1	565.2	0.320	1080.	950.	-950.	1362.	1438.	461.	526.	527.	508.
0.002254	-0.7	1132.	9.420	1.005	0.001691	14.26		0.016525	48.7		0.014906	0.014928	0.014404
	3.9		0.778	0.870	0.013107	0.011519		0.002132			0.000612	0.000613	0.000592
	16.3			0.492			0.1176	0.02395	0.00665	4478.	0.965	0.963	0.998
26 3	30.0	140.2	739.8	0.161	1245.	1277.	-1277.	1729.	1783.	440.	659.	661.	649.
0.9479	-59.9	63.1	565.2	0.320	1313.	1347.	-1347.	1824.	1882.	464.	695.	703.	685.
0.002254	0.1	1132.	9.420	1.005	0.002056	20.22		0.022131	44.3		0.019699	0.019925	0.019393
	4.0		0.780	0.870	0.015936	0.016345		0.002855			0.000809	0.000818	0.000796
	16.9			0.504			0.1354	0.03208	0.00895	6029.	0.978	0.967	0.993
26 4	30.0	140.2	739.8	0.160	1209.	1815.	-1815.	2176.	2181.	140.	928.	923.	896.
0.9458	-60.0	63.0	565.2	0.320	1278.	1919.	-1919.	2301.	2306.	148.	981.	976.	947.
0.002249	-0.0	1133.	9.420	1.005	0.002001	28.80		0.027915	33.7		0.027793	0.027638	0.026838
	4.5		0.779	0.870	0.015510	0.023282		0.003601			0.001141	0.001135	0.001102
	18.0			0.502			0.1386	0.04046	0.01238	8325.	0.874	0.879	0.905

RUN PT SIGMA-P RHO	ALN ALTPP FLAP CYCLIC COLLECT.	V(KTS) Q C	T.SPEED RPM RPS MAT	MU MU-P J J-P J-PP	L LSIG CLH CL	PF PFSIG F CPF	D DSIG FM	T TSIG CT CTH CTHSOI	RF RFSIG THERF CPHSOL	H HSIG QB	HP1 HP1SIG CP1 CP1H ETA1	HP2 HP2SIG CP2 CP2H ETA2	HPB HPBSIG CPB CPBH ETAB
28 1	15.0	139.3	736.7	0.081	463.	822.	-822.	914.	943.	234.	424.	443.	437.
0.9718	-75.3	63.9	562.8	0.319	476.	846.	-846.	940.	971.	241.	437.	458.	450.
0.002311	-0.3	1118.	9.380	1.004	0.000752	12.87		0.011508	29.4		0.012531	0.013148	0.012900
	2.6		0.741	0.970	0.005830	0.010349		0.001485			0.000515	0.000540	0.000530
	19.3			0.255			0.0763	0.01668	0.00595	4077.	0.889	0.848	0.865
28 2	15.0	140.1	738.3	0.081	635.	1560.	-1560.	1671.	1684.	210.	736.	762.	752.
0.9655	-75.3	64.2	564.0	0.320	658.	1616.	-1616.	1731.	1744.	217.	762.	790.	779.
0.002296	-0.3	1121.	9.400	1.004	0.001034	24.28		0.021087	22.2		0.021734	0.022517	0.022215
	2.6		0.741	0.970	0.008013	0.019685		0.002720			0.000893	0.000925	0.000912
	20.1			0.254			0.1099	0.03056	0.01025	7005.	0.943	0.911	0.921
28 3	15.0	139.8	738.3	0.082	771.	2123.	-2123.	2250.	2259.	195.	975.	1013.	999.
0.9617	-75.2	63.7	564.0	0.320	802.	2207.	-2207.	2340.	2349.	203.	1014.	1054.	1039.
0.002287	-0.2	1123.	9.400	1.004	0.001260	33.32		0.028505	20.0		0.028919	0.030042	0.029612
	2.6		0.739	0.970	0.009768	0.026895		0.003677			0.001188	0.001234	0.001216
	20.8			0.256			0.1296	0.04132	0.01366	9301.	0.956	0.920	0.934
28 4	15.0	139.9	738.3	0.082	833.	2437.	-2437.	2570.	2575.	174.	1123.	1164.	1159.
0.9617	-75.2	63.8	564.0	0.320	866.	2534.	-2534.	2672.	2678.	181.	1168.	1210.	1205.
0.002287	-0.2	1123.	9.400	1.004	0.001361	38.21		0.032559	18.9		0.033302	0.034500	0.034365
	2.6		0.739	0.970	0.010553	0.030873		0.004200			0.001368	0.001417	0.001411
	33.4			0.257			0.1364	0.04719	0.01586	10794.	0.949	0.916	0.919
28 5	15.0	139.5	738.3	0.082	939.	2739.	-2739.	2889.	2895.	198.	1244.	1286.	1289.
0.9596	-75.2	63.3	564.0	0.319	979.	2854.	-2854.	3011.	3017.	206.	1297.	1340.	1343.
0.002282	-0.2	1125.	9.400	1.004	0.001538	43.28		0.036681	18.9		0.036975	0.038196	0.038288
	2.6		0.738	0.970	0.011922	0.034774		0.004732			0.001518	0.001569	0.001572
	21.6			0.257			0.1464	0.05317	0.01767	12000.	0.960	0.929	0.929
28 6	15.0	139.8	738.3	0.082	327.	199.	-199.	276.	383.	264.	161.	192.	203.
0.9558	-75.0	63.3	564.0	0.320	342.	208.	-208.	289.	400.	277.	170.	201.	213.
0.002273	-0.0	1127.	9.400	1.004	0.000538	3.14		0.003518	58.7		0.004850	0.005718	0.006070
	2.7		0.738	0.970	0.004168	0.002537		0.000454			0.000199	0.000235	0.000249
	18.7			0.259			0.0274	0.00510	0.00280	1895.	0.705	0.597	0.562

RUN PT SIGMA-P RHO	ALN ALTPP SLAP CYCLIC COLLECT.	V(KTS) Q C	T.SPEED PPM RPS MAT	MU MU-P J CTH J-P	I TSIN CT CTH	PT PSFIG F CPF	D DSIG TM	T TSIN CT CTHSQ	PT PSFIG THSQF CPHSQ	H MSIG SR	HP1 HP1SIG CP1 CP1M ETA1	HP2 HP2SIG CP2 CP2M ETA2	HP HPSIG CPP CPPM ETAP
28 7	15.0	139.1	739.8	0.069	240.	124.	-124.	182.	270.	200.	135.	163.	167.
0.9558	-77.4	62.6	565.2	0.317	251.	130.	-130.	190.	283.	209.	141.	171.	175.
0.002273	-2.4	1127.	9.420	0.994	0.000393	1.98		0.002310	62.7		0.003994	0.004846	0.004944
	4.1		0.731	0.960	0.003046	0.001574		0.000298			0.000164	0.000199	0.000203
	18.7			0.217			0.0179	0.00335	0.00228	1550.	0.559	0.460	0.449
28 8	15.0	139.2	739.8	0.058	150.	-2.	2.	37.	150.	145.	109.	111.	124.
0.9542	-79.5	62.7	565.2	0.318	157.	-2.	2.	39.	157.	152.	115.	116.	129.
0.002269	-4.5	1128.	9.420	0.994	0.000246	-0.03		0.000470	-89.2		0.003247	0.003285	0.003668
	5.8		0.724	0.960	0.001907	-0.000025		0.000061			0.000133	0.000135	0.000151
	18.7			0.101			0.0022	0.00068	0.00169	1148.	0.141	0.139	0.123
28 9	15.0	139.1	739.8	0.052	153.	-34.	34.	7.	157.	157.	77.	96.	117.
0.9542	-80.5	62.5	565.2	0.317	160.	-36.	36.	7.	164.	164.	81.	100.	123.
0.002269	-5.5	1128.	9.420	0.994	0.000251	-0.54		0.000089	-77.5		0.002285	0.002840	0.003486
	6.7		0.720	0.960	0.001945	-0.000432		0.000011			0.000094	0.000117	0.000143
	18.7			0.164			0.0002	0.00013	0.00161	1091.	0.037	0.030	0.025
28 10	15.0	139.8	739.8	0.095	447.	435.	-435.	536.	624.	319.	252.	283.	371.
0.9516	-72.7	63.0	565.2	0.319	470.	457.	-457.	563.	655.	335.	265.	298.	390.
0.002263	2.3	1129.	9.420	1.004	0.000735	6.90		0.006834	45.8		0.007516	0.008437	0.011037
	0.4		0.745	0.970	0.005699	0.005546		0.000882			0.000309	0.000347	0.000453
	35.6			0.299			0.0408	0.00990	0.00509	3445.	0.880	0.783	0.601
28 11	15.0	139.9	735.9	0.106	570.	626.	-626.	752.	847.	389.	338.	366.	381.
0.9495	-70.8	63.0	562.2	0.321	600.	659.	-659.	792.	892.	409.	356.	386.	401.
0.002258	4.2	1130.	9.370	1.004	0.000950	9.94		0.009711	42.3		0.010257	0.011108	0.011553
	-1.6		0.747	0.970	0.007361	0.008084		0.001253			0.000421	0.000456	0.000474
	35.6			0.331			0.0661	0.01408	0.00533	3560.	0.922	0.851	0.815
28 12	15.0	139.6	735.9	0.111	725.	867.	-867.	1025.	1130.	476.	435.	472.	486.
0.9500	-69.6	62.7	562.2	0.320	763.	913.	-913.	1079.	1190.	501.	458.	497.	511.
0.002259	5.4	1130.	9.370	1.004	0.001207	13.83		0.013231	39.9		0.013164	0.014309	0.014714
	-2.6		0.750	0.970	0.009359	0.011191		0.001707			0.000541	0.000588	0.000604
	35.8			0.349			0.0825	0.01918	0.00679	4534.	0.975	0.898	0.872

BELL HELICOPTER COMPANY

DRAWINGS

Drawing Number	
300-960-002	Proprotor and Controls
300-010-001	Blade Assembly
300-010-100	Proprotor Assembly
300-018-013	Pylon and Controls Installation NASA Propeller Test Rig
300-018-014	Dynamic Test Stand Assembly and Installation

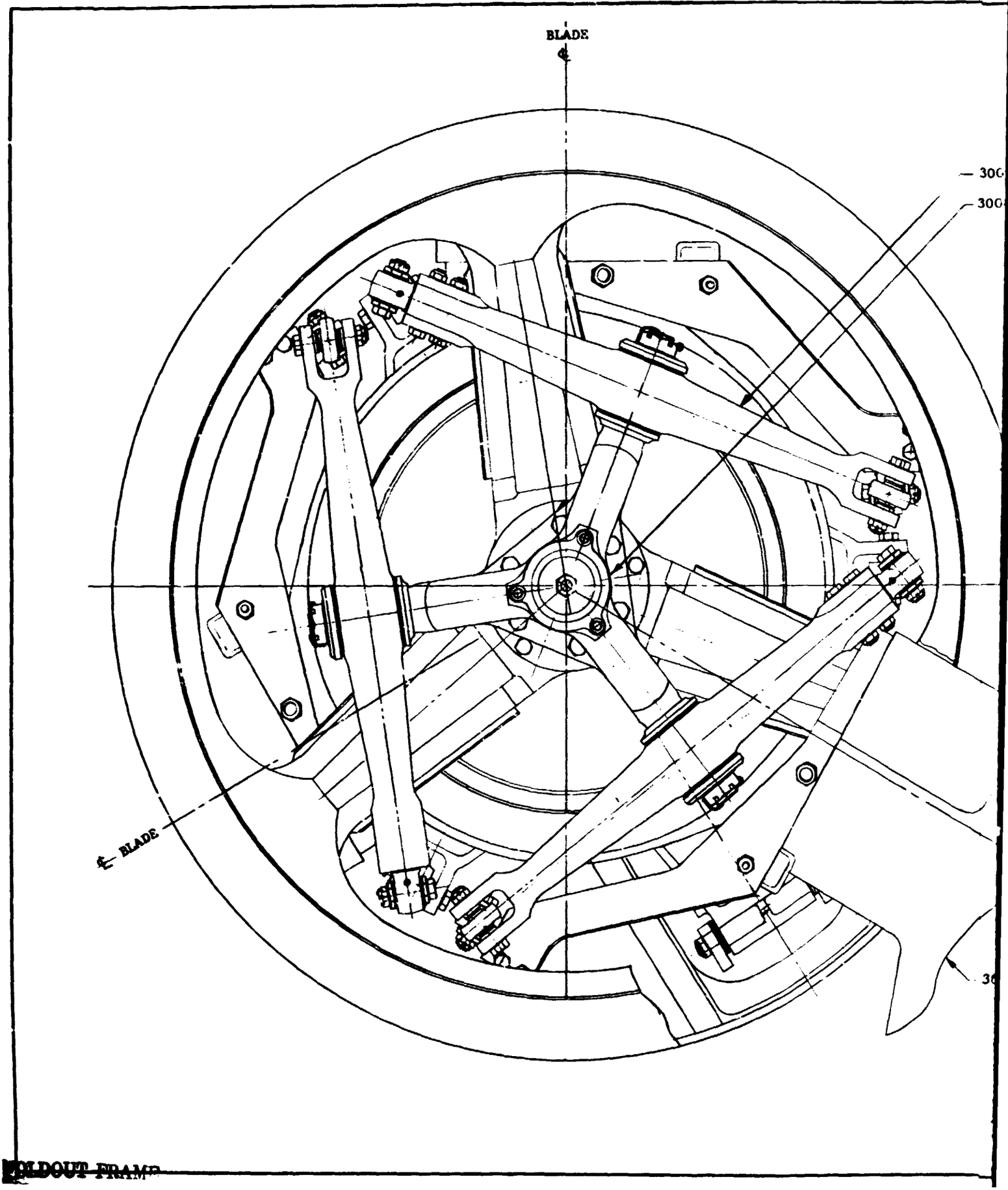

FOLDOUT FRAME

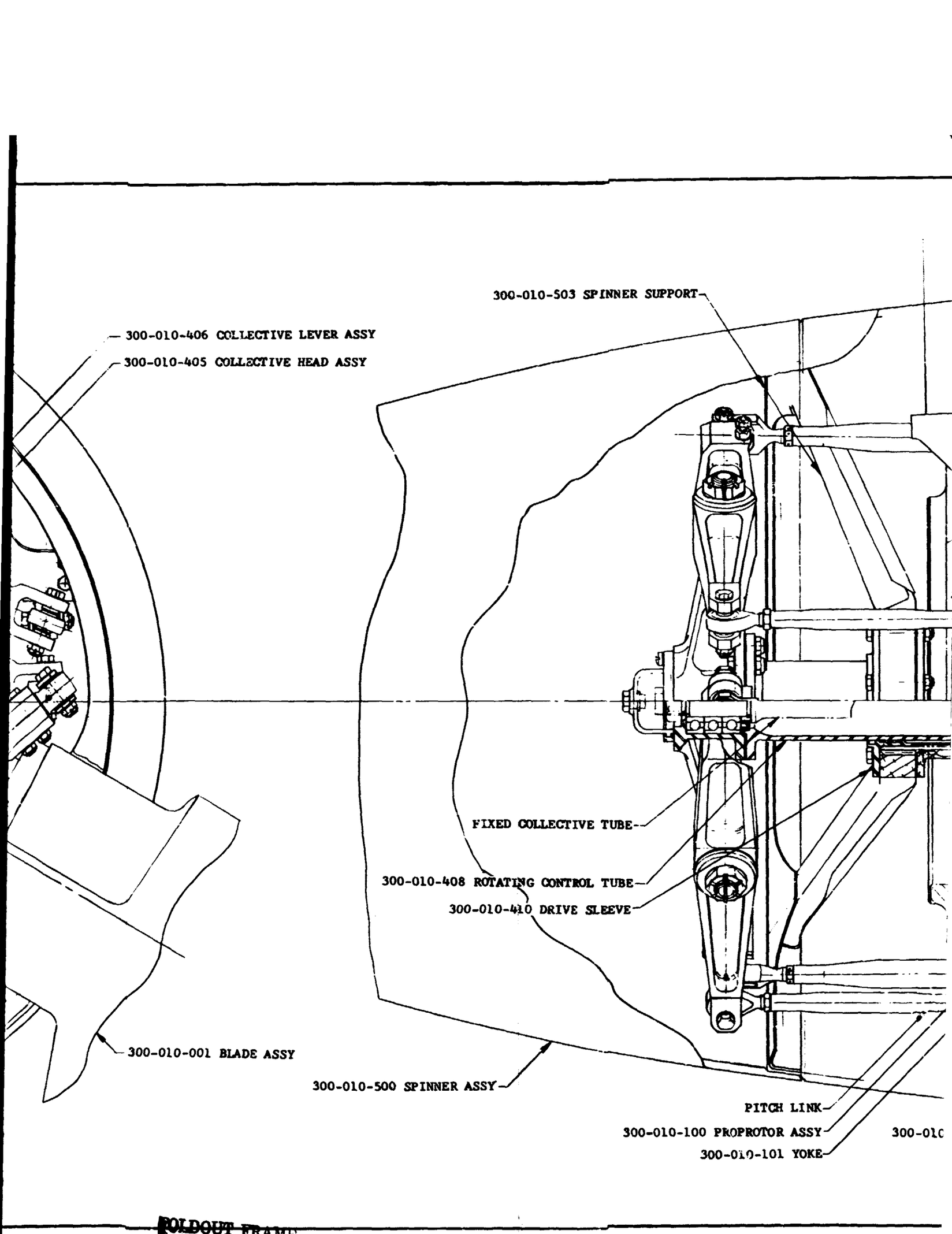

FOLDOUT FRAME 2

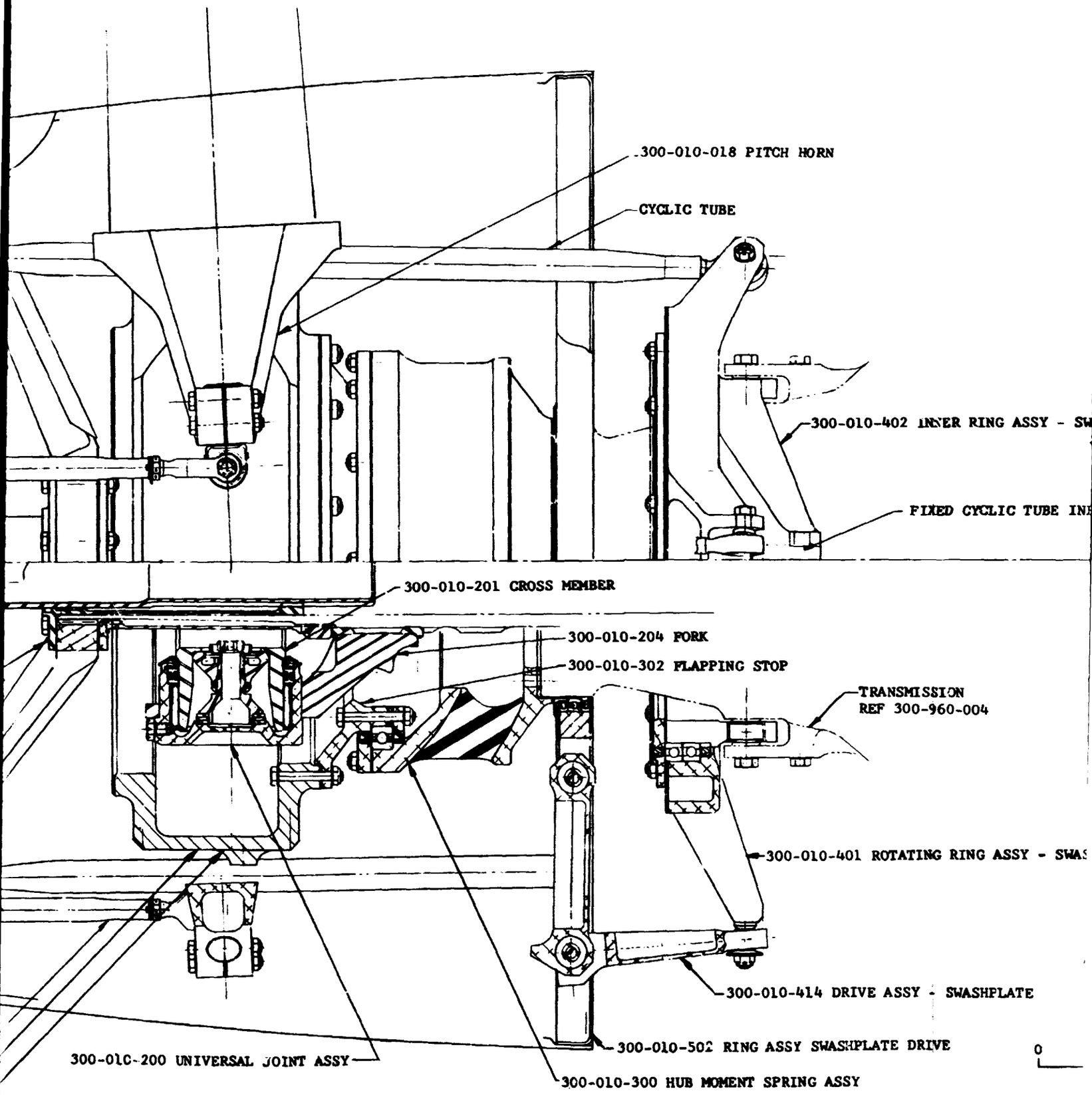

FOLDOUT FRA
3

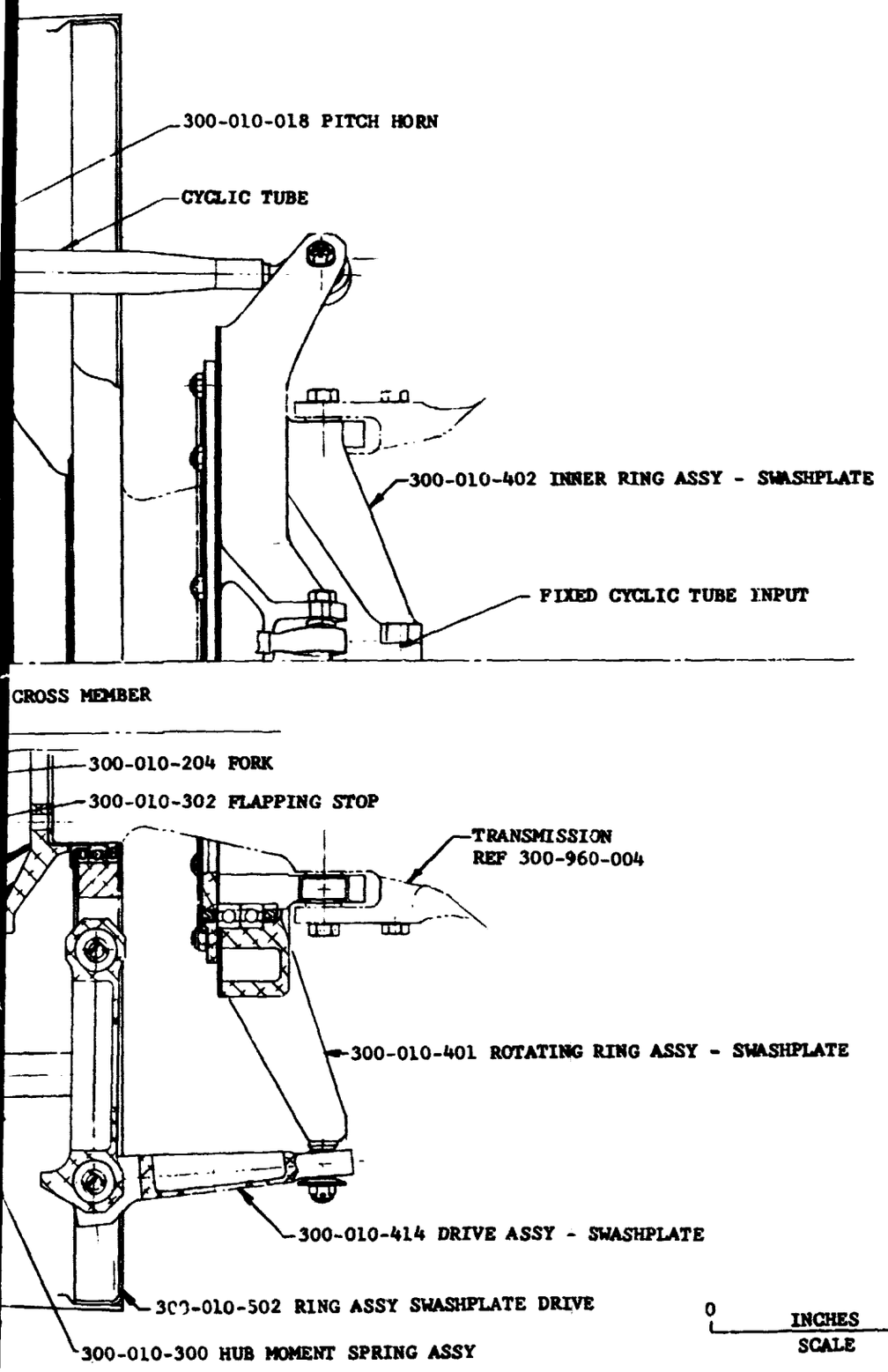

0 INCHES 5
SCALE

DESIGN LAYOUT

PROPROTOR AND CONTROLS

COVINGTON 8-69

300-960-002

FOLDOUT FRAME

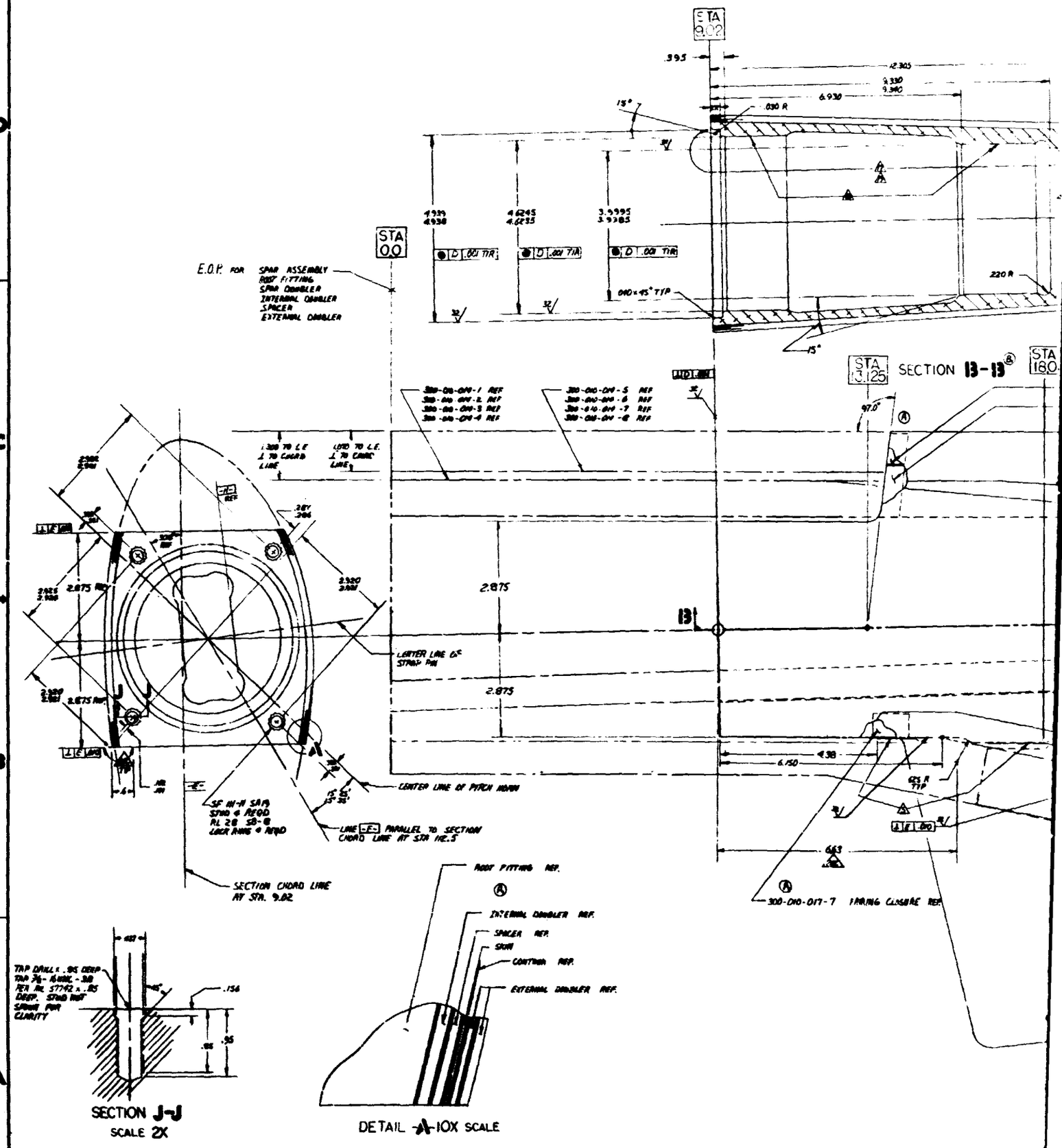

FOLDOUT FRAME

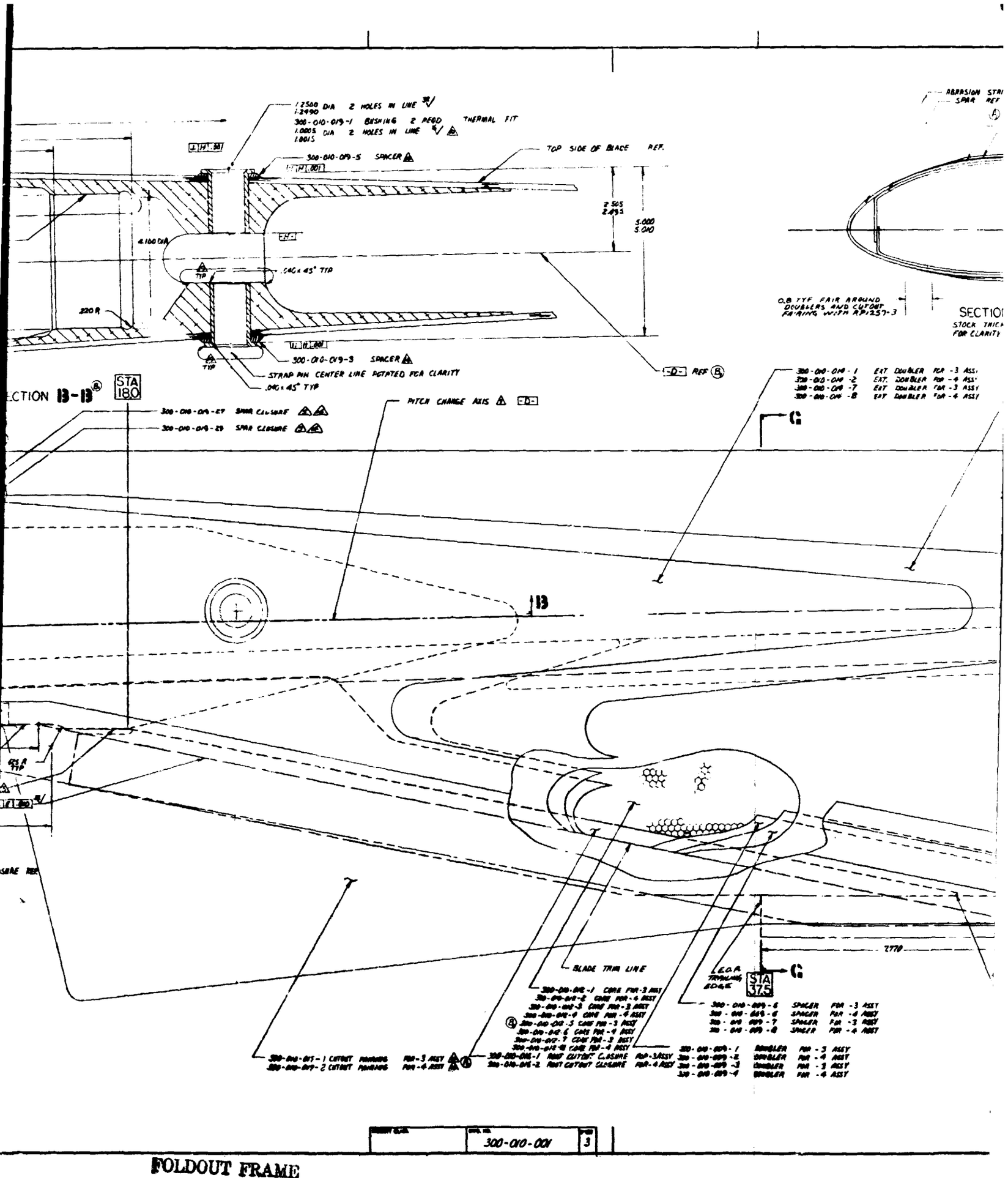

FOLDOUT FRAME
2

REF.

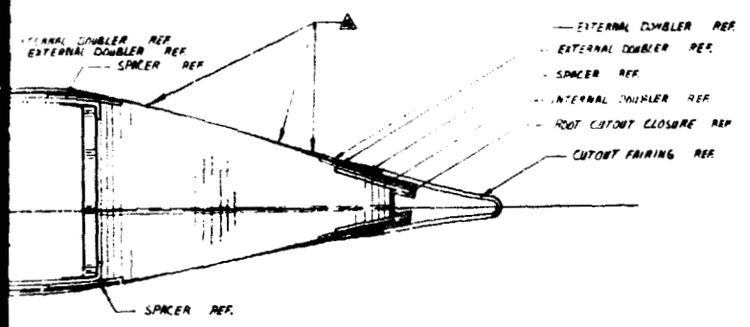

N G-G
MESS 2X SCALE

STA 112.5

300-010-004-3	EXT. DOUBLER	FOR -3 ASSY
300-010-004-4	EXT. DOUBLER	FOR -4 ASSY
300-010-004-5	EXT. DOUBLER	FOR -3 ASSY
300-010-004-6	EXT. DOUBLER	FOR -4 ASSY

300-010-009-9	SPACER	REF.
300-010-009-10	SPACER	REF.

300-010-001-1 SKIN (A)
300-010-001-3 SKIN

(4) BLADE, RANGED ASSY OF AS SHOWN RH
(5) BLADE, RANGED ASSY OF OPPOSITE

PLAN FORM VIEW SHOWN UNTWISTED

SECURITY CLASS.	DWG. NO. 300-010-000

FOLDOUT FRAME 3

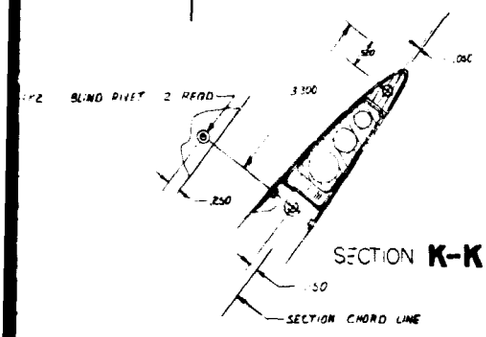

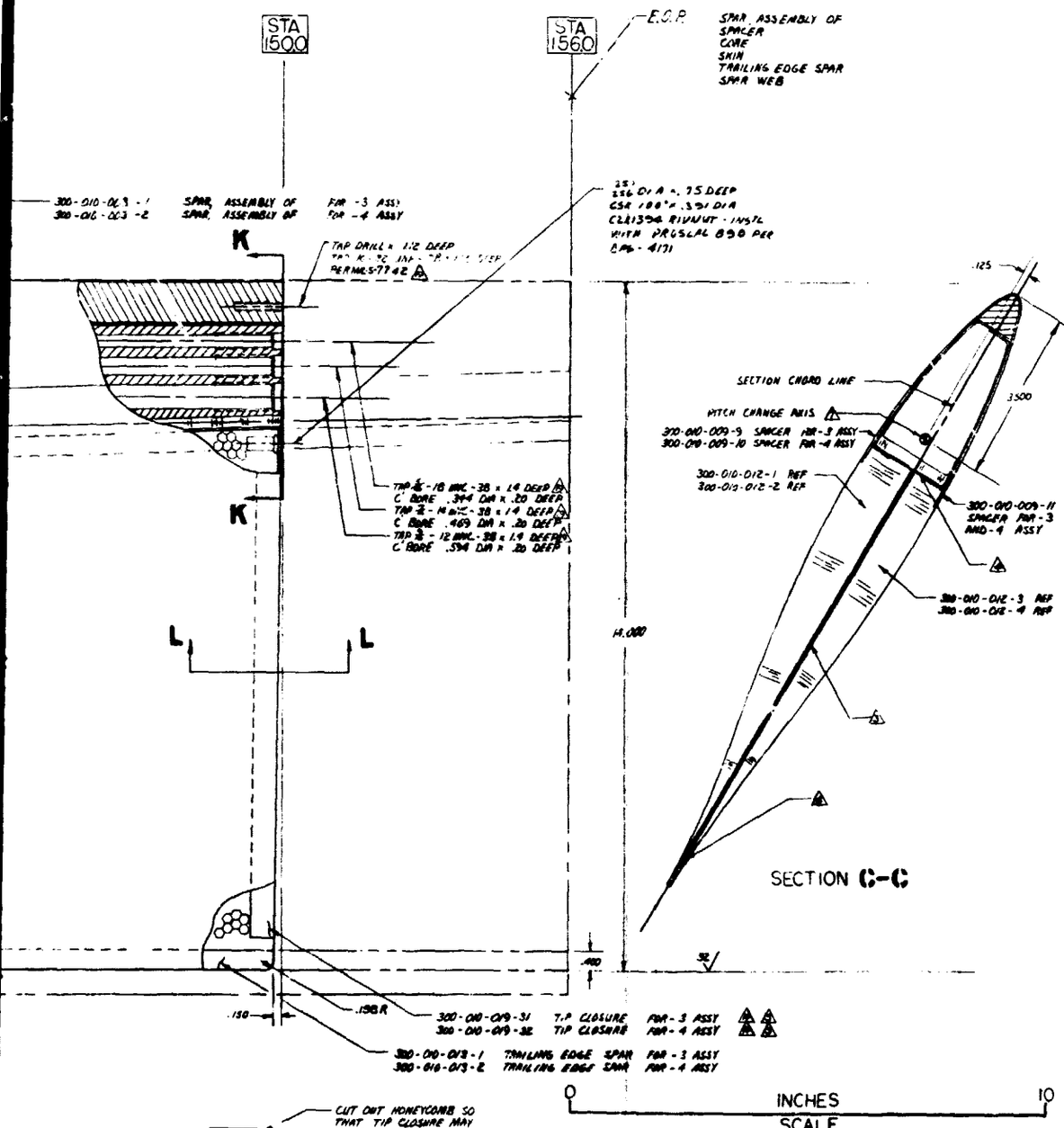

REVISIONS															
ZONE	LTR	DESCRIPTION	DATE	APPROVED	ZONE	LTR	DESCRIPTION	DATE	APPROVED	ZONE	LTR				
										A					
										C					

LAST SECTION
LETTER USED L

SEE SHEET 1 FOR BOM

ITEM NO.	PART OR IDENTIFYING NO.	NOMENCLATURE OR DESCRIPTION	STOCK SIZE

LIST OF MATERIAL OR PARTS

J.N. CARTER 10/16/68

-010-001 | SHEET 3

FOLDOUT FRAME

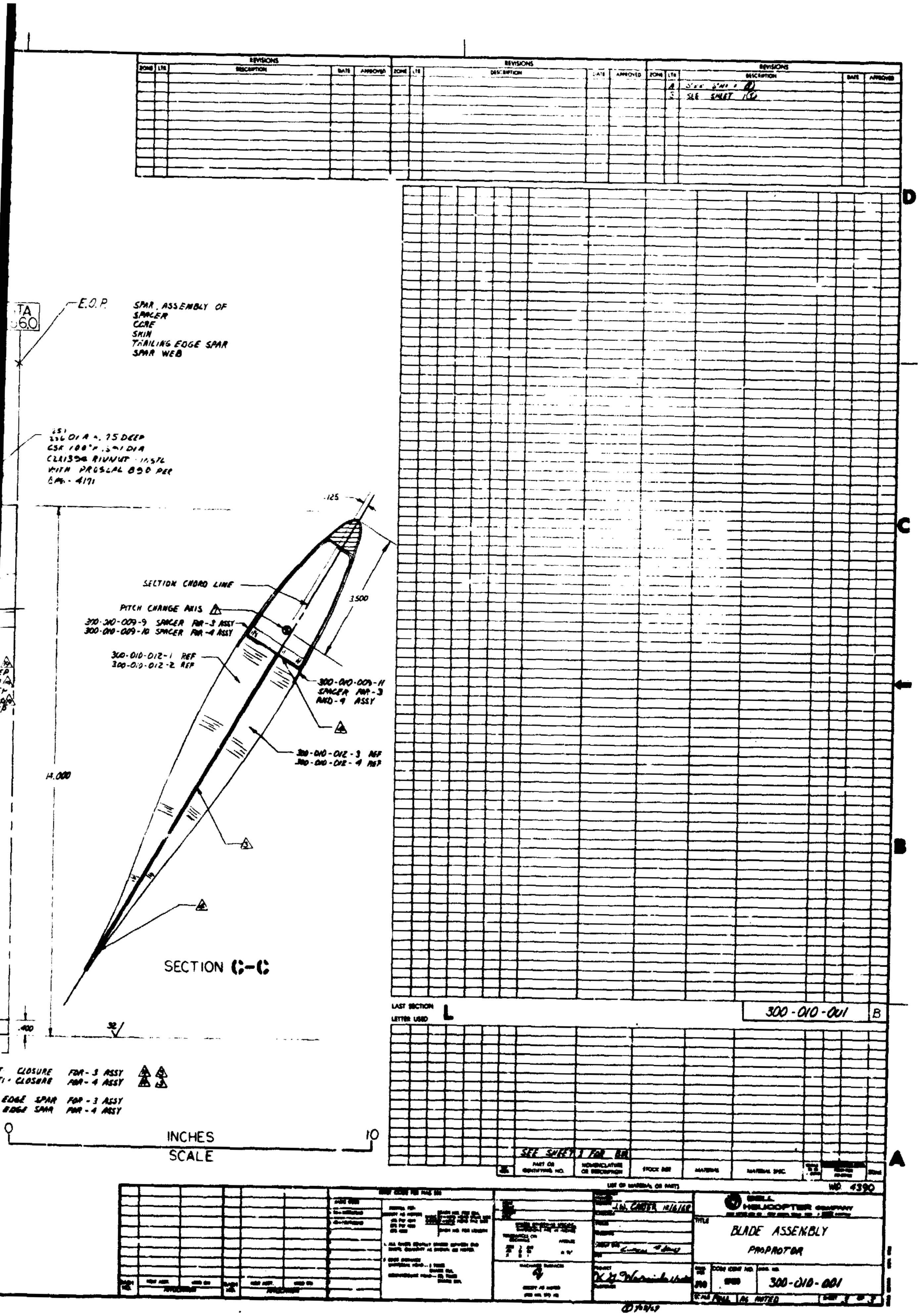

FOLDOUT FRAME 5

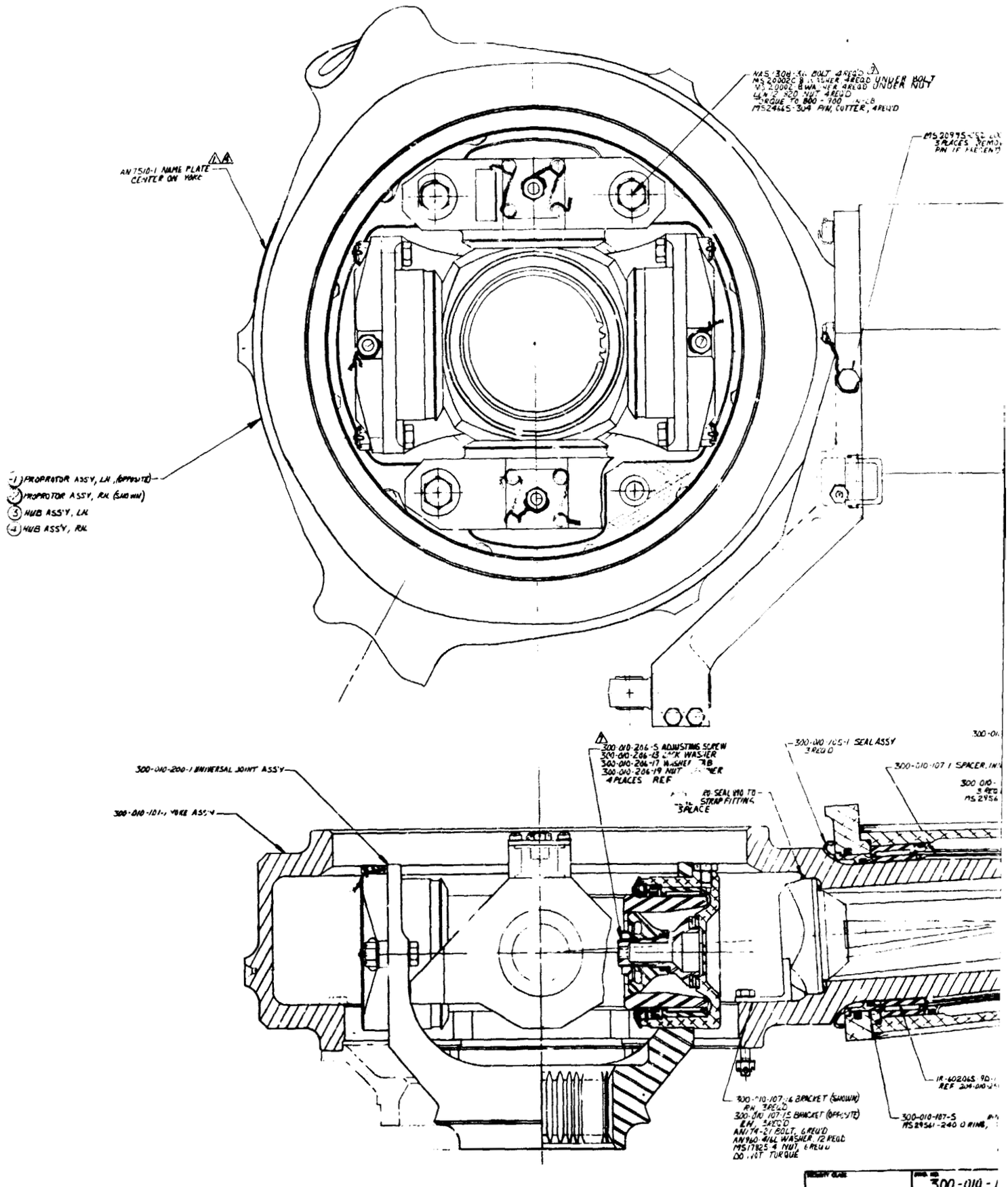

FOLDOUT FRAME

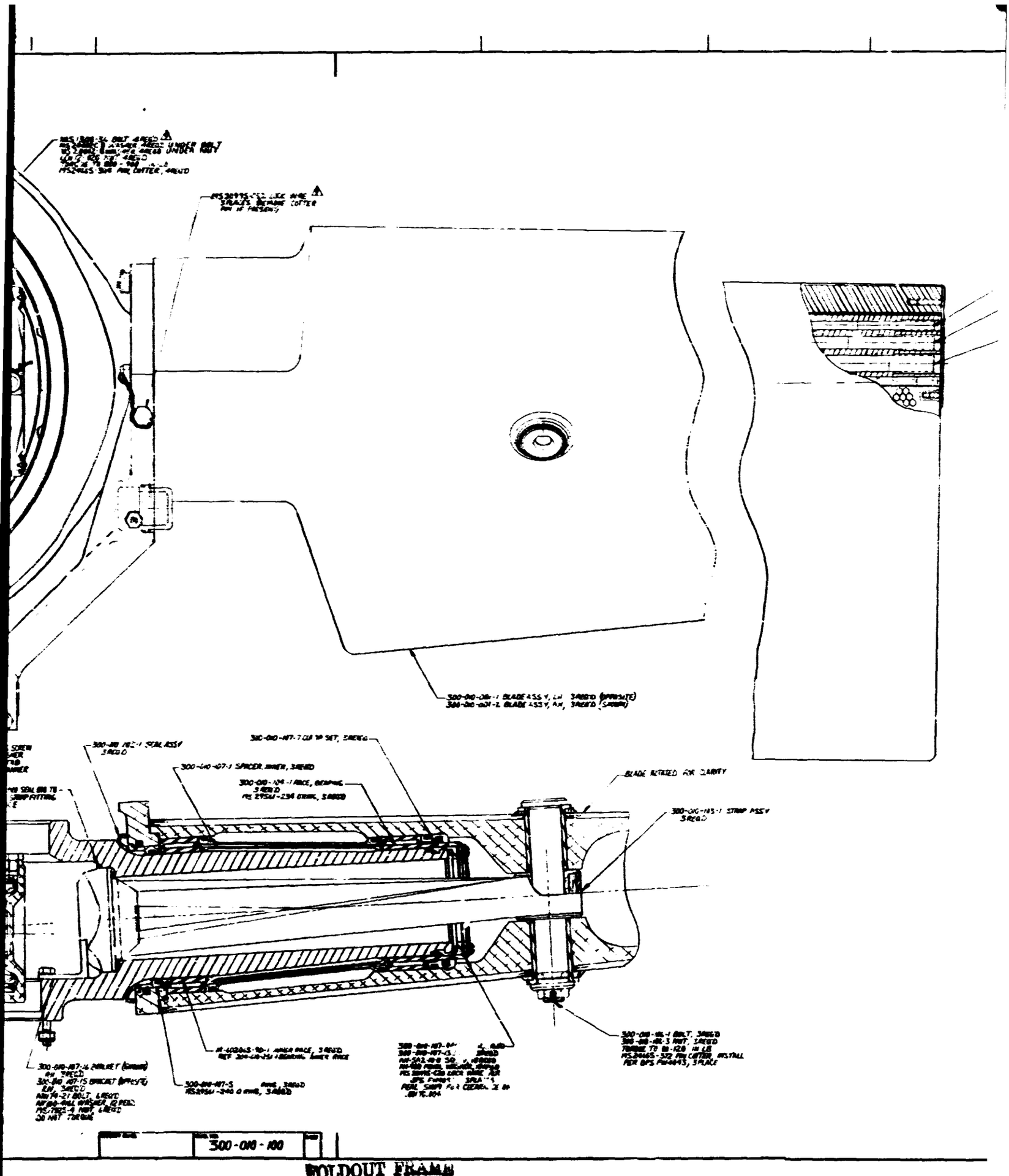

FOLDOUT FRAME

1

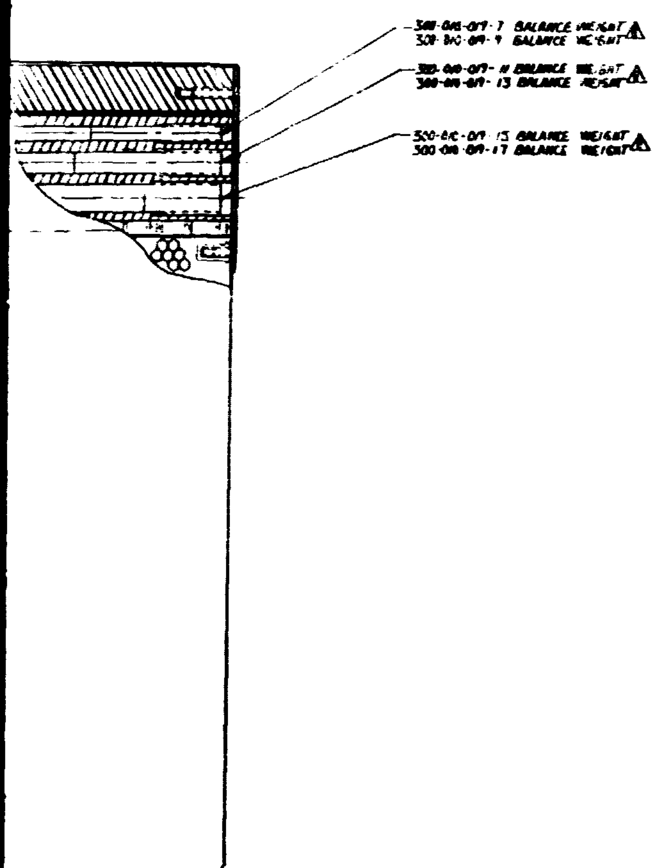

-4	-3	-2	-1	PART OR IDENTIFYING NO.	NOMENCLATURE OR DESCRIPTION
3	3			[illegible]	INNER RACE
		AR	AR	EPON 934	ADHESIVE
AR	AR			PRC	PRO SEAL
4	4			LCN12-820	NUT
		4	4	MS24665-[illegible]	PIN COTTER
AR	AR			MS20995-C[illegible]	LOCK WIRE
4	4			MS20002C[illegible]	WASHER
3	3			MS29513-[illegible]	O RING
3	3			MS29513-[illegible]	O RING
		3	3	MS24665-[illegible]	PIN COTTER
6	6			MS17825-4	NUT
4	4			MS20002-8	WASHER
4	4			MS21250-[illegible]	BOLT
		1	1	AN756-1	NAME PLATE
12	12			AN960-[illegible]	WASHER
18	18			AN960-[illegible]	WASHER
18	18			AN502-[illegible]	SCREW
6	6			AN175-21	BOLT
1	1			300-010-200-1	UNIVERSAL
3				-107-14	BRACKET
	3			-107-15	BRACKET
3	3			-107-13	SHIM
3	3			-107-9	RETAINER
3	3			-107-7	CLAMP
3	3			-107-5	RING
3	3			-107-1	SPACER
		3	3	-106-3	NUT
		3	3	-106-1	BOLT ASSY
3	3			-105-1	SEAL ASSY
3	3			-104-1	RACE
3	3			-103-5	STRAP ASSY
1	1			-101-1	YOKE ASSY
		AR	AR	-017-7	BALANCE
		AR	AR	-019-9	BALANCE
		AR	AR	-017-11	BALANCE
		AR	AR	-019-13	BALANCE
		AR	AR	-017-15	BALANCE
		AR	AR	-019-17	BALANCE
		3		[illegible]	BLADE ASSY
			3	[illegible]	BLADE ASSY
		1		[illegible]	HUB ASSY
			1	[illegible]	HUB ASSY
				[illegible]	PROPROTOR
				300-010-100-1	PROPROTOR

NOTES:

9. LOCK WIRE PER BPS FW 4043
8. CUT WEIGHT TO LENGTH AS REQUIRED FOR BALANCE; NO WEIGHT MAY BE CUT LESS THAN .50 LONG. BALANCE PROPROTOR ASSEMBLY USING MINIMUM WEIGHT IN EACH BLADE.
7. RETAINING NUT, TAB WASHER & LOCKWASHER, TO ADJUST END PLAY & TO CENTER HUB ASSY WITH UNIVERSAL JOINT CENTER WITH ADJUSTING SCREWS. CENTER WITHIN .002. TORQUE SCREWS TO [illegible] & REPLACE LOCKWASHER, TABWASHER & NUT. TORQUE NUT 50-100 FT-LB & LOCK.
6. FILL SPINDLE BORE & TRUNNION OIL CAVITIES WITH SAE [illegible] MIL-L-2104 OIL BY WORKING ALL AIR OUT AS OIL IS ADDED. FILL UNTIL RESERVOIRS ARE ½ FULL.
5. THIS PART IS INNER RACE OF 204-010-251-1 BEARING
4. BOND WITH EPON 934 PER FW 4535.
3. LOCKWIRE & COTTER PIN PER BPS FW 4043
2. TORQUE PER BPS FW 4[illegible] EXCEPT AS SHOWN
1. FOR HUB ASSY NO. & HUB SERIAL NO. MARK PER BPS FW 4050.

0 INCHES SCALE 10

FOLDOUT FRAME 3

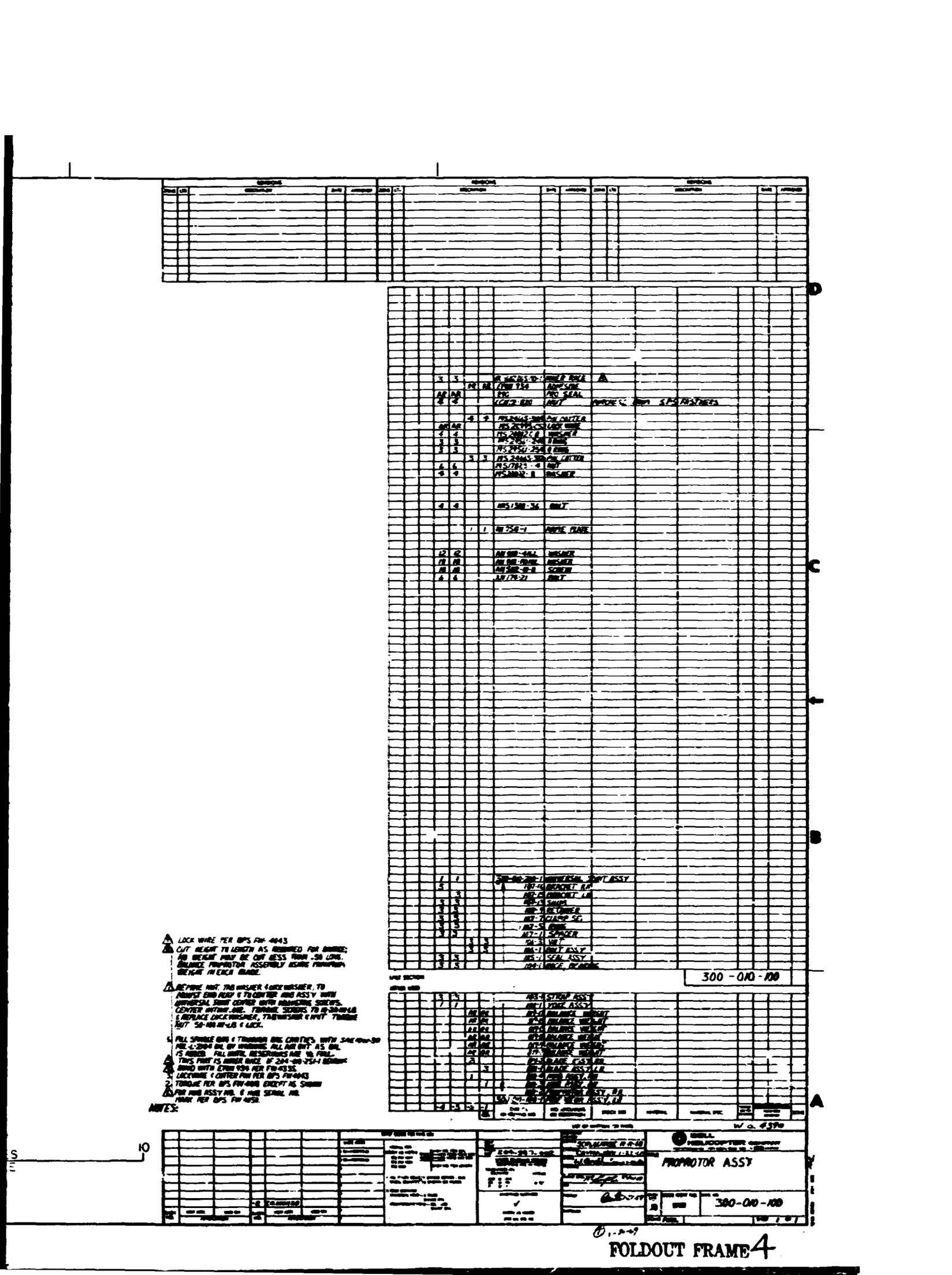

PROPROTOR ASSY

300-010-100

FOLDOUT FRAME 4

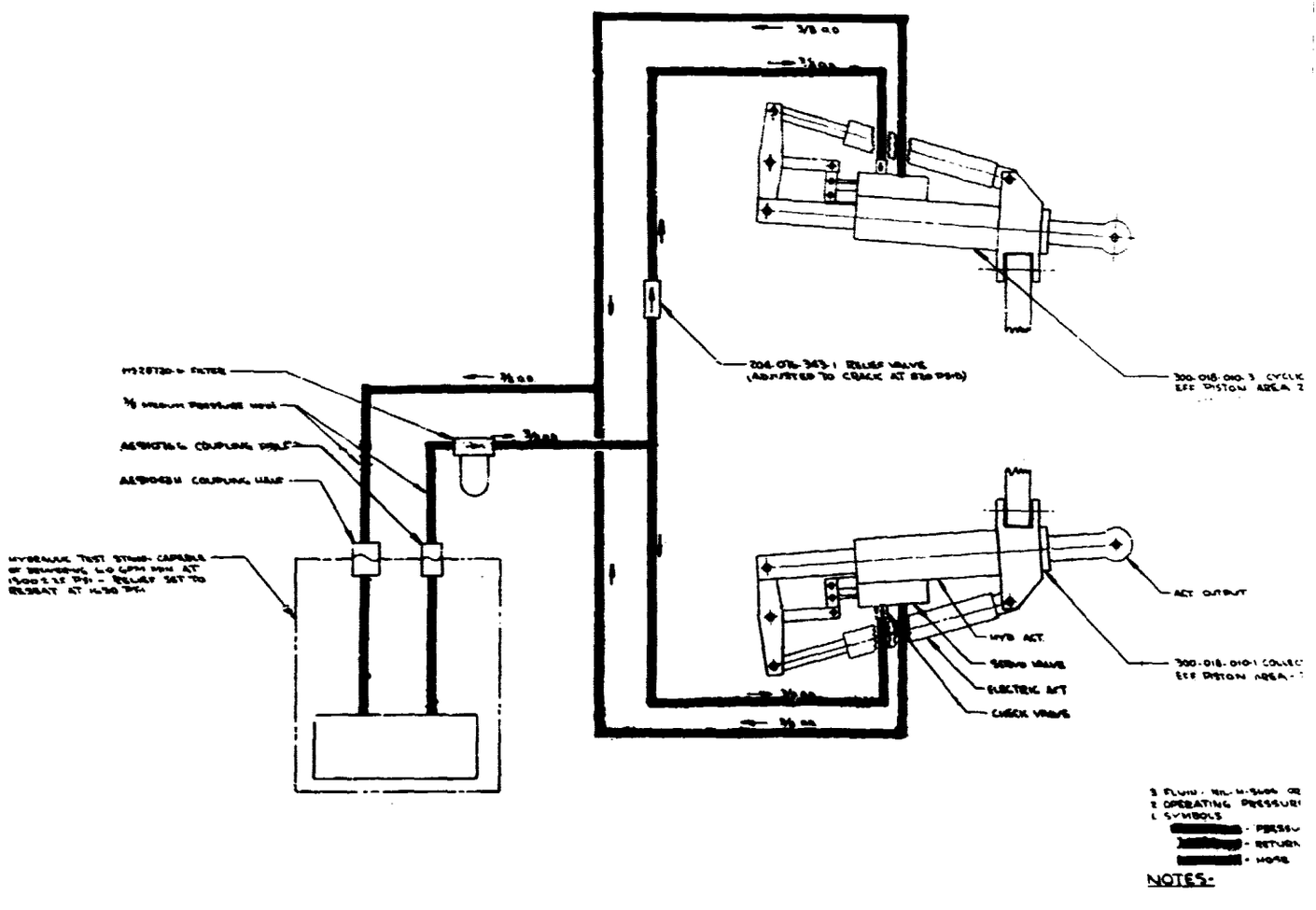

FOLDOUT FRAME

1

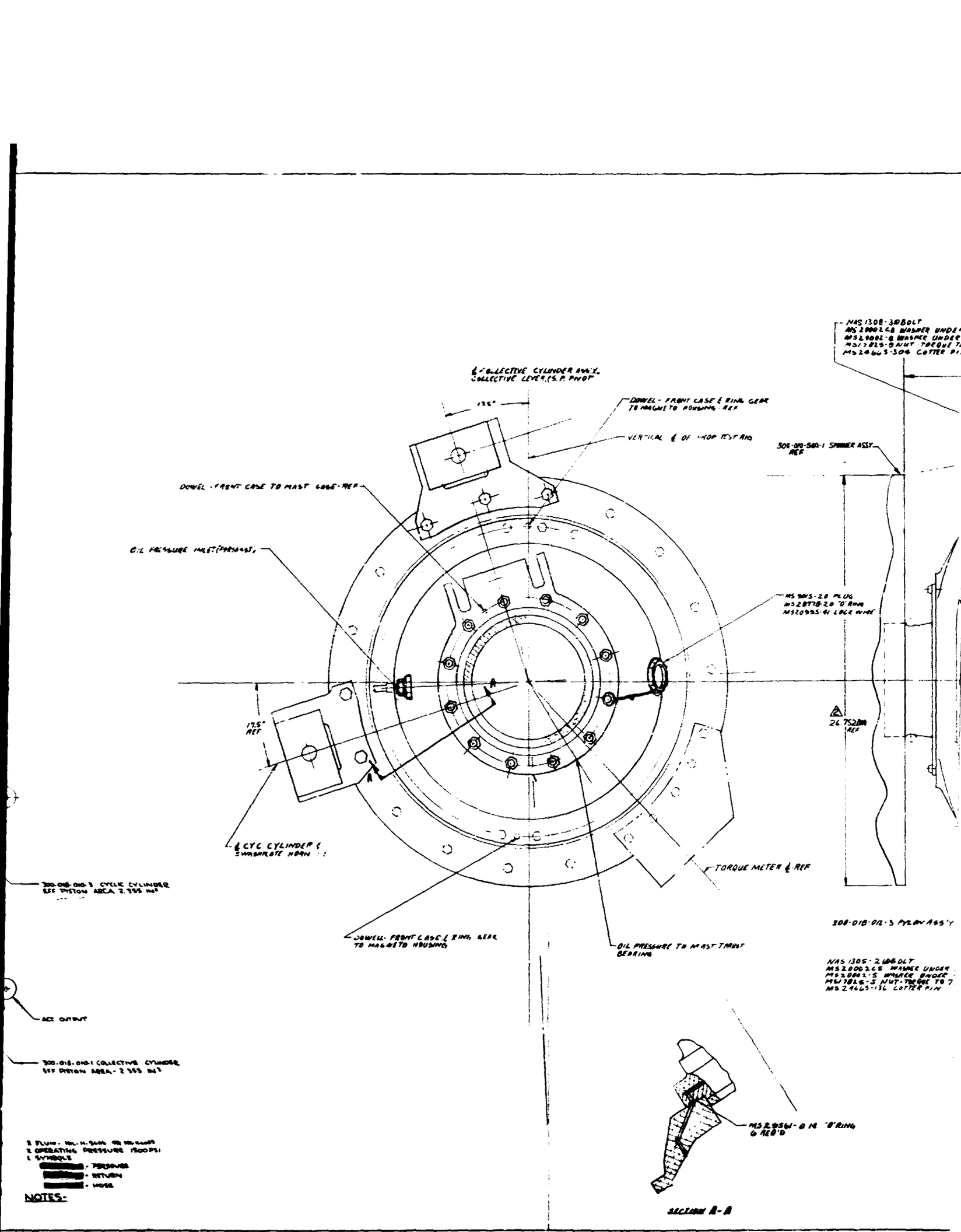

NOTES:-

1. SYMBOLS
   - PRESSURE
   - RETURN
   - HOSE
2. OPERATING PRESSURE 1500 PSI

FOLDOUT FRAME

2

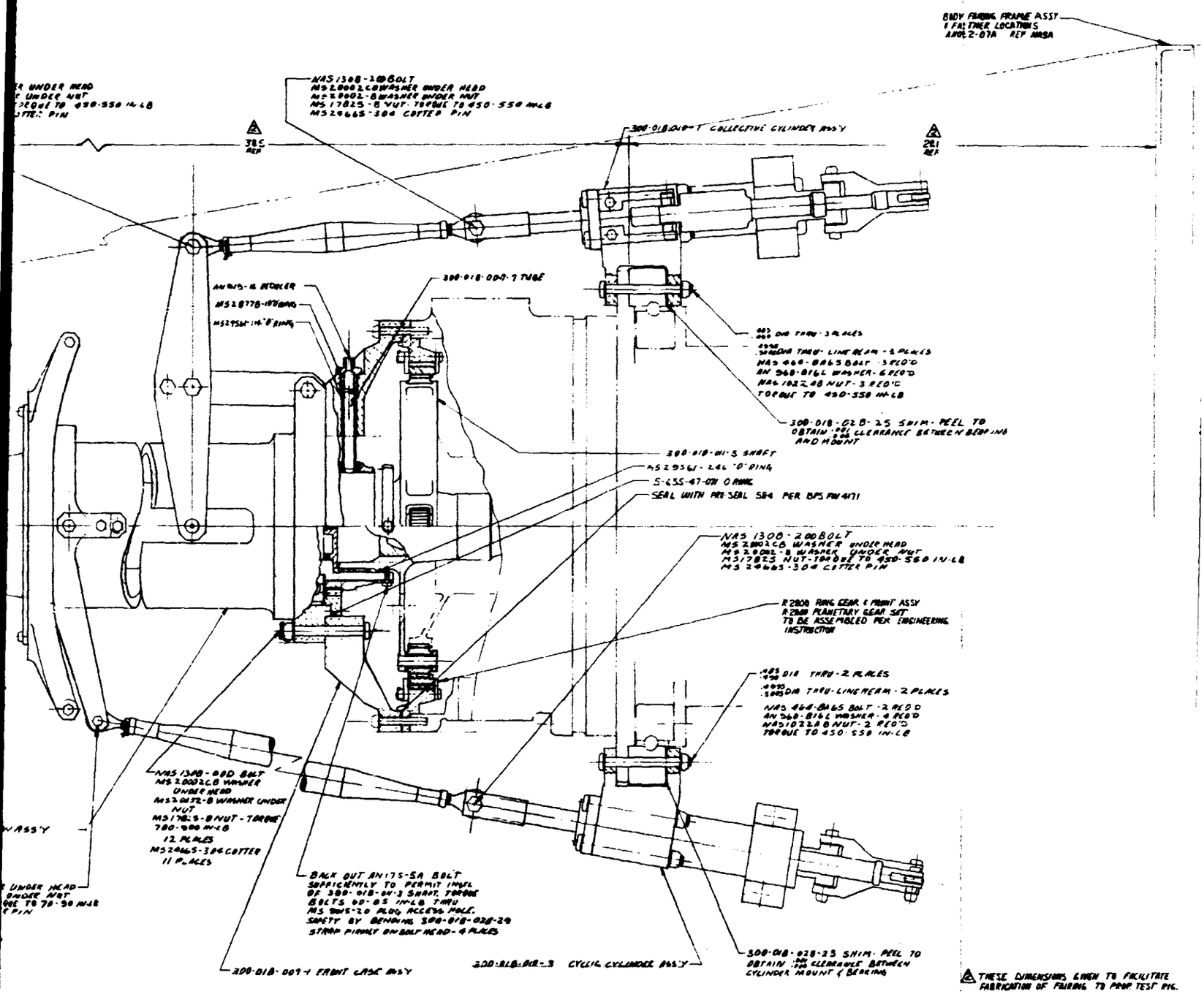

VIEW ROTATED FOR CLARITY

NOTES –

1. TORQUE PER BPS 4018 EXCEPT AS NOTED

△ THESE DIMENSIONS GIVEN TO FACILITATE FABRICATION OF FAIRING TO PROP TEST RIG.

FOLDOUT FRAME 3

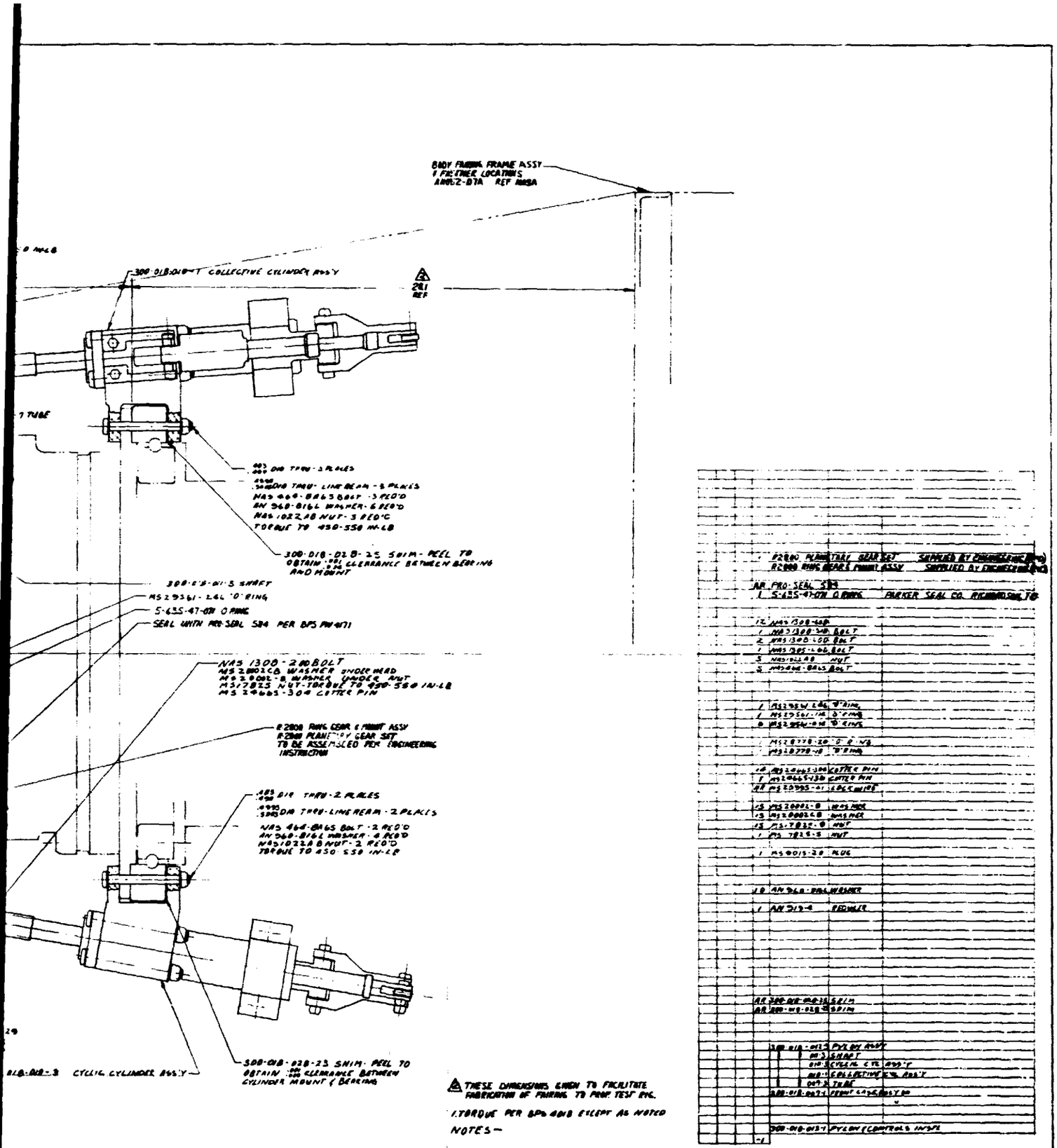

FOLDOUT FRAME
4

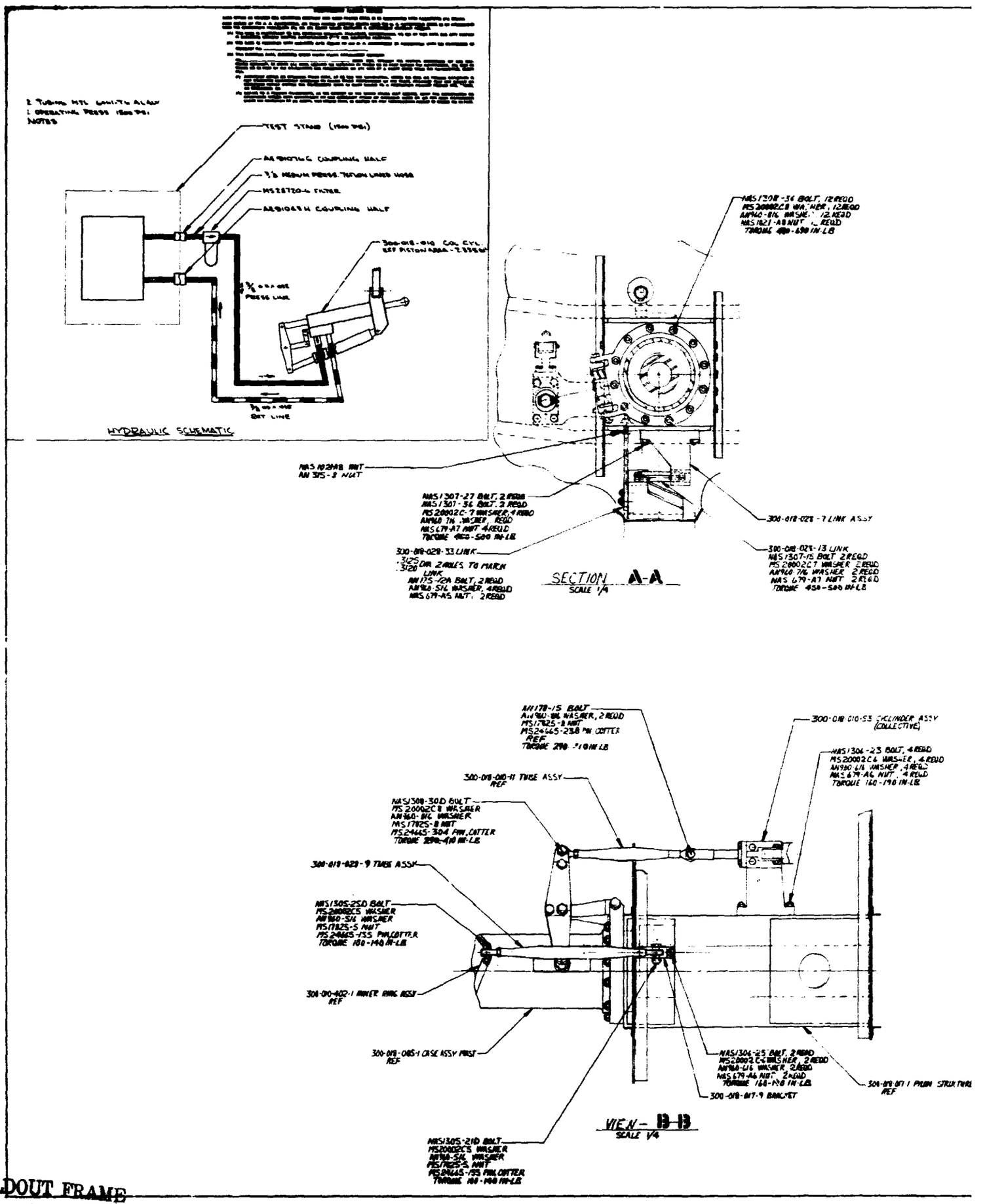

FOLDOUT FRAME 1

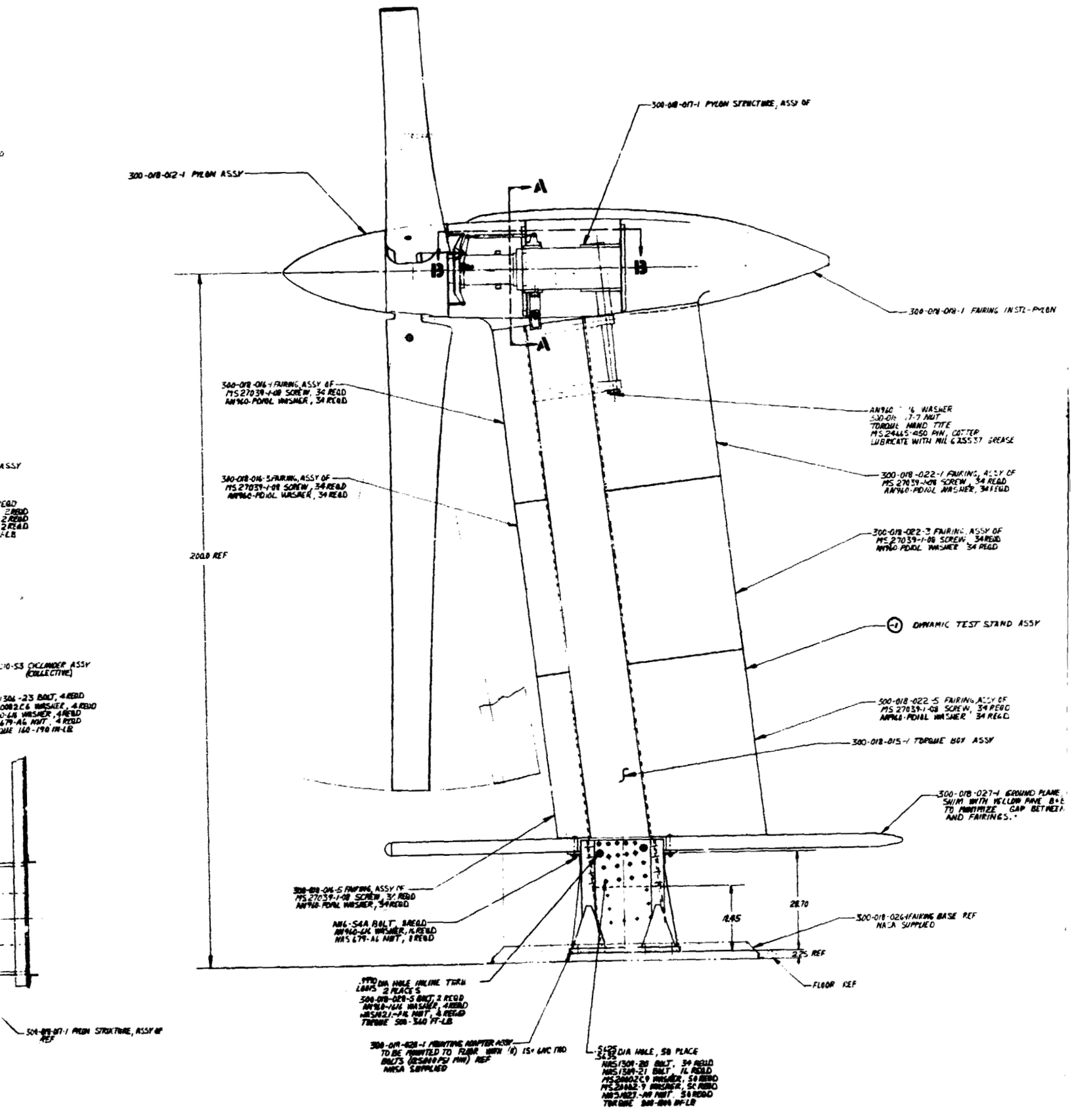

FOLDOUT FRAME 2

300-018-018-1 FAIRING INSTL

AN960-3616 WASHER
300-018-017-7 NUT
TORQUE MIND TITE
MS24665-450 PIN, COTTER
LUBRICATE WITH MIL G 25537 GREASE

300-018-022-1 FAIRING, ASSY OF
MS 27039-1-08 SCREW, 34 REQD
AN960-PD10L WASHER, 34 REQD

300-018-022-3 FAIRING, ASSY OF
MS 27039-1-08 SCREW, 34 REQD
AN960 PD10L WASHER 34 REQD

(-1) DYNAMIC TEST STAND ASSY

300-018-022-5 FAIRING ASSY OF
MS 27039-1-08 SCREW, 34 REQD
AN960-PD10L WASHER 34 REQD

300-018-015-1 TORQUE BOX ASSY

300-018-027-1 GROUND PLANE, ASSY OF
SHIM WITH YELLOW PIPE B+B AS REQD
TO MINIMIZE GAP BETWEEN GROUND PLANE
AND FAIRINGS.

300-018-026 FAIRING BASE REF
NASA SUPPLIED

NOTE:

1. TORQUE PER BPS-FW-4018 EXCEPT AS NOTED.

300-018-024-1 SPAR ASSY

(-3) DYNAMIC TEST STAND ASSY
V4 STIFFNESS
SAME AS -1 ASSY EXCEPT AS
SHOWN.

2.70

5.85

11.45°
13.75°

8.00

300-018-024-7 BEAM
REF

SHIM WITH YELLOW PIPE B+B AS
REQD TO MINIMIZE GAP BETWEEN GROUND
PLANE & FAIRINGS.

300-018-028-5 BOLT, 2 REQD
AN3-6-H4K WASHER, 4 REQD
NAS 1021-A4 NUT, 4 REQD
TORQUE 500-540 FT-LB

300-018-029-3 BOLT, 12 REQD
MS 20002-9 WASHER, 24 REQD
NAS 1021-A9 NUT, 24 REQD
TORQUE 800-1000 IN-LB

4	4	NAS 1304-23	BOLT
2	2	NAS 1304-25	BOLT
14	14	NAS 1309-21	BOLT
34	34	NAS 1309-20	BOLT
1	1	NAS 1308-30D	BOLT
1	1	NAS 1305-50	BOLT
1	1	NAS 1305-210	BOLT
4	4	NAS 1021-A6	NUT
34	50	NAS 1021 A9	NUT
13	13	NAS 1022-A8	NUT
4	4	AMS 679-A7	NUT
19	19	NAS 679-A6	NUT
2	2	NAS 679-A5	NUT
12	12	NAS 1308-36	BOLT
6	6	MS 20002C7	WASHER
6	6	MS 20002C6	WASHER
204	204	MS 27039-1-08	SCREW
1	1	MS 24665-450	PIN, COTTER
1	1	MS 24665-304	PIN, COTTER
2	2	MS 24665-55	PIN COTTER
34	34	MS 20002-9	WASHER
	50	MS 20002C9	WASHER
18	18	MS 20002C8	WASHER
2	2	MS 20002C5	WASHER
1	1	MS 17825-8	NUT
2	2	MS 17825-5	NUT
2	2	AN 175-12A	BOLT
1	1	AN 315-8	NUT
1	1	AN 960-3616	WASHER
19	19	AN 960-816	WASHER
4	4	AN 960-716	WASHER
22	22	AN 960-616	WASHER
6	6	AN 960-516	WASHER
204	204	AN 960-PD10L	WASHER
8	8	AN 5-5A	BOLT
2	2	NAS 1921-34	NUT
2	2	NAS 1304-27	BOLT
1	1	300-018-028-3	LINK
1	1	-7	LINK
1	1	-9	TUBE ASSY
1	1	-11	LINK ASSY
2	2	-5	BOLT
12		300-018-028-3	BOLT
	1	300-018-027-1	GROUND PLANE
	1	300-018-024-1	SPAR ASSY
	1	300-018-022-5	FAIRING ASSY
	1	-022-3	FAIRING ASSY
	1	300-018-022-1	FAIRING ASSY
	1	300-018-026-1	MOUNTING ASSY
	1	300-018-018-1	FAIRING INSTL
		-9	BRACKET
		-7	NUT
	1	300-018-017-1	PYLON STRUCTURE
		-5	FAIRING ASSY
		-3	FAIRING ASSY
	1	300-018-014-1	FAIRING ASSY
	1	300-018-015-1	TORQUE BOX
	1	300-018-012-1	PYLON ASSY
	1	300-018-010-5	CYLINDER ASS
		-3	CYLINDER TRU
		300-018-014-1	DYNAMIC TEST

FOLDOUT FRAME
3

ROUE PER BPS-FW4018 EXCEPT AS NOTED.

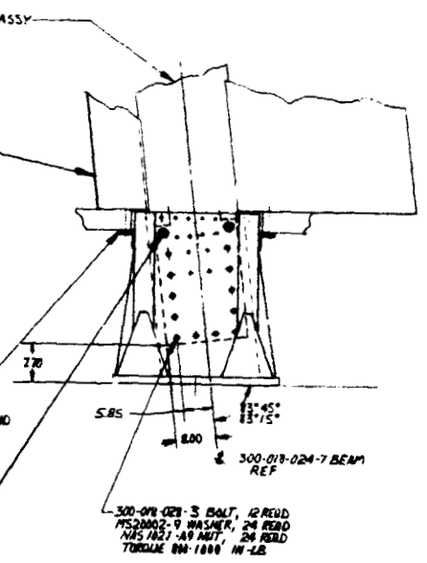

	4	4	NAS1306-23	BOLT
	2	2	NAS1306-25	BOLT
		14	NAS1309-21	BOLT
		34	NAS1309-20	BOLT
			NAS1308-30	BOLT
			NAS1305-50	BOLT
			NAS1305-210	BOLT
	4	4	NAS1021-N6	NUT
	24	50	NAS1021-A9	NUT
	13	13	NAS1021-A8	NUT
	4	4	NAS679-A7	NUT
	14	14	NAS679-A6	NUT
	2	2	NAS679-A5	NUT
	12	18	NAS1308-34	BOLT
	6	6	MS20002C7	WASHER
	4	4	MS20002C4	WASHER
	24	204	MS20002C9	WASHER
			MS24665-450	PIN COTTER
			MS24665-304	PIN COTTER
	2	2	MS24665-153	PIN COTTER
	24	58	MS20002-9	WASHER
		50	MS20002C7	WASHER
	18	18	MS20002C8	WASHER
	2	2	MS20002C5	WASHER
	1	1	MS17825-8	NUT
	2	2	MS17825-5	NUT
	2	2	AN175-12A	BOLT
	1	1	AN315-8	NUT
	1	1	AN960-5/16	WASHER
	19	19	AN960-816	WASHER
	4	4	AN960-716	WASHER
	22	22	AN960-616	WASHER
	6	6	AN960-516	WASHER
	204	204	AN960-10L16	WASHER
	8	8	AN6-54A	BOLT
	2	2	NAS1307-34	BOLT
	2	2	NAS1307-27	BOLT
			300-018-028-3	LUGS
			-7	ALIGN
			-9	TRUE ASSY
			-11	LINK ASSY
	2	2	-5	BOLT
	12		300-018-028-5	BOLT
			300-018-027-1	GROUND PLANE ASSY OF
			300-018-024	SPAR ASSY W/ STIFFNESS
			300-018-022-5	FAIRING ASSY OF
			-322-5	FAIRING ASSY OF
			300-018-022-1	FAIRING ASSY OF
			300-018-021-1	MOUNTING ADAPTER ASSY
			300-018-015-1	FAIRING INSTL, PYLON
			-9	BRACKET
			-7	NUT
			300-018-017-1	PYLON STRUCTURE ASSY OF
			-5	FAIRING ASSY
			-3	FAIRING ASSY
			300-018-016-1	FAIRING ASSY
			300-018-013-1	FAIRING ASSY
			300-018-012-1	PYLON ASSY
			300-018-014-1	CYLINDER ASSY (COLLECTIVE)
			-3	DYNAMIC TEST STAND ASSY & INSTALLATION (AS SCHEMATIC)
			300-018-014-1	DYNAMIC TEST STAND ASSY & INSTALLATION

BELL Helicopter CORP. FORT WORTH, TEXAS

FABRICATION LAYOUT

TITLE: DYNAMIC TEST STAND ASSY & INSTALLATION

SCALE: 1/10

MODEL: AS

DRAWING NO. 300-018-014

FOLDOUT FRAME 4